frontiers | Research Topics

Case reports in veterinary neurology and neurosurgery

Edited by
Koen Santifort, Bruno André Lopes, Simone Spinillo, Andrea Tipold, Joao Miguel De Frias and Susana Monforte

Published in
Frontiers in Veterinary Science

ISSN 1664-8714
ISBN 978-2-8325-6428-8
DOI 10.3389/978-2-8325-6428-8

About Frontiers

Frontiers is more than just an open access publisher of scholarly articles: it is a pioneering approach to the world of academia, radically improving the way scholarly research is managed. The grand vision of Frontiers is a world where all people have an equal opportunity to seek, share and generate knowledge. Frontiers provides immediate and permanent online open access to all its publications, but this alone is not enough to realize our grand goals.

Frontiers journal series

The Frontiers journal series is a multi-tier and interdisciplinary set of open-access, online journals, promising a paradigm shift from the current review, selection and dissemination processes in academic publishing. All Frontiers journals are driven by researchers for researchers; therefore, they constitute a service to the scholarly community. At the same time, the *Frontiers journal series* operates on a revolutionary invention, the tiered publishing system, initially addressing specific communities of scholars, and gradually climbing up to broader public understanding, thus serving the interests of the lay society, too.

Dedication to quality

Each Frontiers article is a landmark of the highest quality, thanks to genuinely collaborative interactions between authors and review editors, who include some of the world's best academicians. Research must be certified by peers before entering a stream of knowledge that may eventually reach the public - and shape society; therefore, Frontiers only applies the most rigorous and unbiased reviews. Frontiers revolutionizes research publishing by freely delivering the most outstanding research, evaluated with no bias from both the academic and social point of view. By applying the most advanced information technologies, Frontiers is catapulting scholarly publishing into a new generation.

What are Frontiers Research Topics?

Frontiers Research Topics are very popular trademarks of the *Frontiers journals series*: they are collections of at least ten articles, all centered on a particular subject. With their unique mix of varied contributions from Original Research to Review Articles, Frontiers Research Topics unify the most influential researchers, the latest key findings and historical advances in a hot research area.

Find out more on how to host your own Frontiers Research Topic or contribute to one as an author by contacting the Frontiers editorial office: frontiersin.org/about/contact

Case reports in veterinary neurology and neurosurgery

Topic editors

Koen Santifort — IVC Evidensia Small Animal Referral Hospital Arnhem, Neurology, Netherlands

Bruno André Lopes — Southfields Veterinary Specialists, United Kingdom

Simone Spinillo — ChesterGates Veterinary Specialists, United Kingdom

Andrea Tipold — University of Veterinary Medicine Hannover, Germany

Joao Miguel De Frias — University of Edinburgh, United Kingdom

Susana Monforte — University of Cambridge, United Kingdom

Citation

Santifort, K., Lopes, B. A., Spinillo, S., Tipold, A., De Frias, J. M., Monforte, S., eds. (2025). *Case reports in veterinary neurology and neurosurgery*. Lausanne: Frontiers Media SA. doi: 10.3389/978-2-8325-6428-8

Drs. Koen Santifort, Bruno A. Lopes, and Simone Spinillo are employed by private veterinary hospitals. All other Topic Editors declare no competing interests with regards to the Research Topic subject.

Table of contents

frontiers | Frontiers in Veterinary Science

TYPE Editorial
PUBLISHED 20 May 2025
DOI 10.3389/fvets.2025.1614212

OPEN ACCESS

EDITED AND REVIEWED BY
Andres M. Perez,
University of Minnesota Twin Cities,
United States

*CORRESPONDENCE
Koen M. Santifort
koen.santifort@evidensia.nl

RECEIVED 18 April 2025
ACCEPTED 29 April 2025
PUBLISHED 20 May 2025

CITATION
Santifort KM, De Frias JM, Spinillo S, Lopes BA, Monforte Monteiro S and Tipold A (2025) Editorial: Case reports in veterinary neurology and neurosurgery. *Front. Vet. Sci.* 12:1614212. doi: 10.3389/fvets.2025.1614212

Editorial: Case reports in veterinary neurology and neurosurgery

Koen M. Santifort [1,2]*, Joao Miguel De Frias [3], Simone Spinillo [4], Bruno A. Lopes [5,6], Susana Monforte Monteiro [6] and Andrea Tipold [7]

[1]IVC Evidensia Small Animal Referral Hospital Arnhem, Neurology, Arnhem, Netherlands, [2]IVC Evidensia Small Animal Referral Hospital Hart van Brabant, Neurology, Waalwijk, Netherlands, [3]Hospital for Small Animals, Royal (Dick) School of Veterinary Studies, The University of Edinburgh, Edinburgh, United Kingdom, [4]ChesterGates Veterinary Specialists, Chester, United Kingdom, [5]Southfields Veterinary Specialists, Linnaeus Veterinary Limited, Basildon, United Kingdom, [6]Department of Veterinary Medicine, University of Cambridge, Cambridge, United Kingdom, [7]Department of Small Animal Medicine and Surgery, University of Veterinary Medicine, Hannover, Germany

KEYWORDS

neurology, neuropathology, neurosurgery, neuro-oncology, case series

Editorial on the Research Topic
Case reports in veterinary neurology and neurosurgery

Case reports have long been instrumental in the progression of medical knowledge, offering detailed insights into unique clinical scenarios that enhance our understanding of disease processes, diagnostic challenges, and therapeutic strategies. In the realm of veterinary neurology and neurosurgery, such reports are invaluable for documenting rare conditions, innovative treatments, and unexpected outcomes across a diverse range of animal species. The aim of this "*Case reports in veterinary neurology and neurosurgery—volume I*" Research Topic was and that of the volumes to come remains to be to establish a lasting and prominently featured platform for the publication of case reports in veterinary neurology and neurosurgery, fostering a collaborative environment for knowledge sharing and professional development. By sharing case-based clinical experiences and outcomes, veterinarians contribute to a collective database of knowledge that benefits the entire profession. This collaborative effort can contribute to advances in the field of veterinary neurology as a whole. Case reports (single cases) as well as case series (multiple cases) are included in this Research Topic.

This first Volume of "*Case reports in veterinary neurology and neurosurgery*" contains 17 publications. Their strengths and learning points are highlighted and could contribute to clinical management and potentially spark future, larger prospective studies. The case reports of Volume 1 describe features in the elderly, but also in young dogs, from clinical phenomena to pathophysiology, and different neurosurgery techniques to neuropathology. Known and previously unknown genetic mutations and their clinical relevance, new aspects in inflammatory central nervous systems diseases, and insights for particular neoplastic disorders are discussed.

Exploring the genetic underpinnings of limb length variations in a family of Dachshunds, Sullivan et al. contributed to the understanding of chondrodysplasia and its genetic markers with their report titled "*FGF4L1 retrogene insertion is lacking in the tall dachshund phenotype*". This manuscript highlights how the limb length is important for this breed to maintain working ability, aiming to help in aspects of animal welfare protection as this breed has been banned recently from exhibition in Germany.

Eguchi et al. identified and documented a novel genetic mutation linked to hereditary myotonia in their case report titled "*A CLCN1 complex variant mutation in exon 15 in a mixed-breed dog with hereditary myotonia*", enhancing the genetic profiling of neuromuscular disorders in canines.

Kang et al., in their case report titled "*Ischemic brain infarction and cognitive dysfunction syndrome in an aged dog*", highlighted a possible correlation between ischemic brain infarction and cognitive dysfunction in geriatric canines, emphasizing the importance of considering vascular events in behavioral changes.

In a case report by Jackson et al., titled "*Presumed cerebral salt wasting syndrome in a 10-week-old German Shorthaired Pointer*", this particular syndrome following traumatic brain injury in a dog is described, enlightening the reader about this unusual condition, as well as describing a new diagnostic method that could be used in similar presentations.

The case report titled "*Positioning head tilt observed in a dog and four cats with bilateral peripheral vestibular dysfunction*" by Tamura et al. documented a unique clinical sign associated with bilateral vestibular dysfunction, aiding in the recognition and diagnosis of these conditions.

Yin et al. provided valuable insights into the clinical presentation, diagnostic challenges, histological characteristics, and management strategies for intraneural perineuriomas in canines in their report titled "*Intraneural perineurioma in dogs: a case series and brief literature review*".

Rancilio et al. have, in their report titled "*Suprasellar and trigeminal nerve oligodendroglioma with pseudoprogression after radiotherapy and serial MRI in a dog*", detailed the phenomenon of pseudoprogression and cranial nerve involvement in a canine oligodendroglioma. This phenomenon is well-described in the human counterpart, but its occurrence in dogs has been rarely reported, solidifying the use of canine patients as a good comparative model of human neuro-oncologic conditions.

A surgical approach for resecting a fourth ventricular meningioma in a dog is described by Jeong et al. in the case report titled "*Gross total resection of a primary fourth ventricular meningioma using the telovelar approach in a dog*", providing a reference for similar neurosurgical procedures.

Demonstrating the effectiveness of compartmental resection in treating malignant nerve sheath tumors, Smith et al. in their case report titled "*Resolution of lameness via compartmental resection of a malignant nerve sheath neoplasm of the median nerve in a dog*" highlighted the relevance of considering neurogenic causes in dogs presenting with lameness.

Hobert et al. in their case report titled "*One-stage craniectomy and cranioplasty digital workflow for three-dimensional printed polyetheretherketone implant for an extensive skull multilobular osteochondosarcoma in a dog*", showcased the application of 3D printing technology in creating custom implants for cranial reconstruction, advancing surgical techniques in veterinary oncology and neurosurgery.

The case report titled "*Intracranial epidermoid cyst in a cat*" by Terao et al. included information on the diagnosis and management of a rare diagnosis in a cat, contributing to the knowledge of diagnostic features of such a case.

The feasibility and outcomes of surgically removing rare intracranial dermoid cysts in a feline patient is demonstrated by the case report titled "*Successful surgical resection of an intracranial frontal lobe dermoid cyst in a cat*" by Nakano et al., contributing to surgical approaches in similar cases.

Shi et al. in their report titled "*Endoscope-assisted single-incision double-channel mini-open hemilaminectomy for the treatment of acute thoracolumbar intervertebral disc disease in 11 dogs*" described a minimally invasive surgical technique for thoracolumbar disc disease, emphasizing its efficacy and potential benefits over traditional methods.

In the report titled "*Surgical management of single-level thoracolumbar vertebral body segmentation and formation failure causing progressive thoracolumbar myelopathy in three adult large-breed dogs*", Couto et al. provided insights into surgical interventions for congenital vertebral malformations causing myelopathy, offering an innovative way to manage such anomalies.

In the report titled "*Double adjacent ventral slot in two medium-sized breed dogs*", Cojocaru highlighted a modified surgical technique addressing cervical disc disease, offering an approach for more extensive ventral decompression.

Santifort et al. in their case report titled "*Necrotizing leukomyelitis and meningitis in a Pomeranian*", presented a case of clinically severe inflammatory spinal cord disease of unknown etiology, underscoring the need for inclusion of this differential diagnosis, based on clinical findings as well as MRI findings.

Last but not least, in light of a well-known risk in human MRI studies, the report titled "*Radiofrequency-induced thermal burn injury in a dog after magnetic resonance imaging*" notified the veterinary profession of the possibility of this complication of veterinary MRI procedures, underscoring the need for caution and monitoring during and after imaging (Lichtenauer et al.).

In summary, all these case reports offered contributions to our collective knowledge concerning various topics, including surgical approaches and techniques, differential diagnosis, medical and alternative treatment, pathophysiology, genetics, clinical management, and clinical phenomenology. Through their respective contributions, we continue to learn from single case reports and case series, opening new avenues for research and generating clinically useful insights.

Author contributions

KS: Writing – original draft, Writing – review & editing. JD: Writing – review & editing. SS: Writing – review & editing. BL: Writing – review & editing. SM: Writing – review & editing. AT: Writing – review & editing.

Conflict of interest

The authors declare that the research was conducted in the absence of any commercial or financial relationships

that could be construed as a potential conflict of interest.

The author(s) declared that they were an editorial board member of Frontiers, at the time of submission. This had no impact on the peer review process and the final decision.

Generative AI statement

The author(s) declare that Gen AI was used in the creation of this manuscript. To check for and correct typographical and grammatical errors, ChatGPT (accessed online April 2025) was used.

Publisher's note

frontiers | Frontiers in Veterinary Science

TYPE Case Report
PUBLISHED 11 January 2024
DOI 10.3389/fvets.2023.1233230

OPEN ACCESS

EDITED BY
Sílvia Sisó,
AbbVie, United States

REVIEWED BY
Viktor Palus,
Neurovet, Slovakia
Koen Santifort,
IVC Evidensia Small Animal Referral Hospital Arnhem, Neurology, Netherlands

*CORRESPONDENCE
Maninder Sandey
✉ mzs0011@auburn.edu

†PRESENT ADDRESSES
Brittani Sexton,
Metropolitan Veterinary Hospital, Copley, OH, United States

Aline Rodrigues Hoffmann,
Department of Comparative, Diagnostic and Population Medicine, College of Veterinary Medicine, University of Florida, Gainesville, FL, United States

RECEIVED 01 June 2023
ACCEPTED 28 December 2023
PUBLISHED 11 January 2024

CITATION
Yin J-H, Sexton B, Jukier T, Yanke AB, Holland M, Miller AD, Stranahan L, Hoffmann AR and Sandey M (2024) Case report: Intraneural perineurioma in dogs: a case series and brief literature review. *Front. Vet. Sci.* 10:1233230. doi: 10.3389/fvets.2023.1233230

Case report: Intraneural perineurioma in dogs: a case series and brief literature review

Ji-Hang Yin[1], Brittani Sexton[2†], Tom Jukier[2], Amy B. Yanke[2], Merrilee Holland[2], Andrew D. Miller[3], Lauren Stranahan[4], Aline Rodrigues Hoffmann[4†] and Maninder Sandey[1*]

[1]Department of Pathobiology, College of Veterinary Medicine, Auburn University, Auburn, AL, United States, [2]Department of Clinical Sciences, College of Veterinary Medicine, Auburn University, Auburn, AL, United States, [3]Department of Population Medicine and Diagnostic Sciences, Section of Anatomic Pathology, College of Veterinary Medicine, Cornell University, Ithaca, NY, United States, [4]Department of Veterinary Pathobiology, Texas A&M School of Veterinary Medicine & Biomedical Sciences, Texas A&M University, College Station, TX, United States

Intraneural perineurioma is an exceptionally rare neoplasm in animals. This case study comprises a series of three cases and a brief literature review focusing on canine intraneural perineurioma. The pathological and immunohistochemical findings are documented, revealing that canine intraneural perineurioma frequently affects adult dogs aged between 3 and 10 years old, with a male predominance. Clinical signs associated with intraneural perineurioma in dogs include spinal pain, lameness, and paresis, resulting from the involvement of spinal nerve roots of the pelvic limbs, brachial plexus, or distal part of the median nerve. Most neoplasms had characteristic pseudo-onion bulb patterns on histopathology. Neoplastic perineurial cells, in most cases, expressed laminin and claudin-1, and NF200 consistently highlighted the central axon. While the immunohistochemical (IHC) profile of intraneural perineurioma in veterinary medicine remains incompletely characterized, the available IHC data from all reported cases suggest that a combination of laminin and claudin-1 immunomarkers, along with distinctive histological features, can assist in establishing a definitive diagnosis of intraneural perineurioma.

KEYWORDS

canine, spinal nerve roots, intraneural perineurioma, immunohistochemistry, brief literature review

Introduction

The World Health Organization (WHO) classification of tumors of the peripheral nerves includes Schwannoma, neurofibroma, perineurioma, and malignant peripheral nerve sheath tumors (1). Among these, perineurioma is rarely reported in the human literature and has limited cases documented in veterinary medicine (2–8).

Perineurioma is a benign and slow-growing neoplasm composed exclusively of perineurial cells (9, 10). In human medicine, two variants of perineuriomas are recognized: extraneural soft tissue tumor and intraneural variant (1). The extraneural soft tissue tumors are typically well-demarcated, unencapsulated masses that most commonly develop in subcutaneous tissues of the extremities or trunk and are rarely associated with an identifiable nerve (1, 11). Conversely, an intraneural perineurioma usually develops as a solitary nodular mass that commonly involves peripheral nerves or nerve roots of the cervical and lumbar spinal cord (1, 11).

Despite the distinct affected sites, both variants share immunohistochemical and ultrastructural features of neoplastic perineurial cells (1, 10). Histologically, intraneural perineurioma contains characteristic "pseudo-onion bulbs" structures composed of concentric layers of perineurial cells surrounding either myelinated or non-myelinated axons or endoneurial capillaries (1). Neoplastic perineurial cells are spindle-shaped cells with a fusiform to elongate nucleus and a scant amount of eosinophilic cytoplasm, histomorphologically resembling fibroblasts. Neoplastic perineurial cells can be distinguished from fibroblasts by electron microscopy. Ultrastructurally, normal and neoplastic perineurial cells have elongated, thin, and overlapping cytoplasmic processes, discontinuous basal lamina, and pinocytocytic vesicles (9). Some overlapping processes are connected by poorly formed desmosome-like junction complexes (5, 6, 9, 12).

In veterinary medicine, diagnosing various subtypes of benign peripheral nerve sheath tumors, such as Schwannoma, neurofibroma, and perineurioma, can be challenging due to shared morphological features. Schwannomas are benign and well-circumscribed tumors, consist of neoplastic Schwann cells arranged in diverse patterns like interwoven bundles, streams, herringbone, whorls, or Verocay bodies. In contrast, neurofibromas comprise a mixed population of neoplastic Schwann cells, perineurial cells, and fibroblasts, separated by abundant collagen. Intraneural perineuriomas typically exhibit perineurial cells organized in pseudo-onion bulb structures, as previously described (7).

Various immunomarkers have been investigated to differentiate among different subtypes of peripheral nerve tumors. For example, laminin is commonly utilized in diagnosing peripheral nerve sheath tumors, although it is expressed in both neoplastic Schwann and perineurial cells. Sox-10, which exhibits high expression in Schwann cells, demonstrates strong and diffuse immunoreactivity in Schwannomas (14). NF200 and Periaxin are two immunomarkers that can be used to highlight centrally entrapped axons in pseudo-onion bulbs in perineuriomas (7, 14). In human medicine, epithelial membrane antigen (EMA) is a widely used immunohistochemical marker for identifying perineuriomas (9, 10, 12, 13); however, its applicability in veterinary species is limited. Additionally, claudin-1 and glucose transporter 1 (GLUT-1) are routinely used as supportive markers for perineurioma (10). In this study, we present three cases involving canine intraneural perineurioma. We documented signalment, clinical history, and detailed pathological and immunohistochemical findings for these cases. Additionally, we conducted a comprehensive review of previously reported cases and offered a concise literature review on canine intraneural perineurioma.

Case 1

A 3-year-old male castrated beagle dog was referred to the Neurology and Neurosurgery Service at the Auburn University Veterinary Teaching Hospital due to chronic left pelvic limb lameness that had commenced 5 months before presentation.

Multiple magnetic resonance imaging (MRI) revealed a large, well-defined fusiform-shaped mass within the left caudal lumbar spinal canal. This mass extended from the caudal endplate of the L5 vertebra to the mid-vertebral body of L7, causing severe lateral displacement and compression of the L5-L7 spinal cord segments. These findings were consistent with neoplastic growth, including possible differentials such as meningioma, intradural peripheral nerve sheath tumor, and round cell neoplasia. Given the progression of the dog's clinical symptoms, the owner opted for humane euthanasia, and the dog underwent postmortem evaluation.

At necropsy, the left L5 spinal nerve root was enlarged, and a well-demarcated, unencapsulated, firm, tan, 2 x 0.5 x 0.5-cm mass that markedly compressed the adjacent L5-L7 spinal cord was identified (Figures 1A, B). Histologically, the mass was unencapsulated, mildly infiltrative, densely cellular, and composed of fusiform cells arranged in concentric lamellations that ensheathed a central axon or capillaries forming pseudo-onion bulbs structures (Figures 1C, D). Neoplastic cells had indistinct cell borders and a scant amount of eosinophilic cytoplasm. Nuclei were oval to elongate with finely stippled chromatin and 1-3 small nucleoli. The neoplastic cells had mild anisocytosis and anisokaryosis with four mitotic figures in ten standardized 400 x fields (2.37-mm^2). All the formalin-fixed paraffin-embedded tissues of canine perineuriomas were subjected to immunohistochemistry staining (Supplementary Table 2). Immunohistochemically, approximately 90% of the neoplastic perineurial cells had strong and diffuse cytoplasmic immunolabeling for vimentin (Figure 1E) and laminin (Figure 1F), while approximately 50% had claudin-1 immunolabeling (Figure 1G). S-100 (Figure 1H) and glial fibrillary acidic protein (GFAP) immunolabeling was only observed in the Schwann cells within the pseudo-onion bulbs, in which multiple ensheathed axons were immunolabeled with neurofilament 200 (NF200) (Figures 1I,J). Neoplastic cells lacked immunoreactivity for Periaxin (Figure 1K) and Sox-10 (Figure 1L) antigens. Similar to NF200, Periaxin immunolabeling was detected in axons. In addition, Schwann cells within the pseudo-onion bulbs were highlighted with Sox-10 antibody.

Case 2

A 10.7-year-old neutered male Labrador Retriever mix dog presented to a referral veterinary neurology clinic due to a two-week history of pelvic limb weakness. MRI scans revealed a strongly contrast-enhancing mass within the spinal cord extending along the right side of the spinal cord from C6-T1 and into the associated nerve roots. Clinical differentials included a malignant peripheral nerve sheath tumor or lymphoma. Due to the poor long-term prognosis, the patient was euthanized, and a postmortem examination was conducted.

During necropsy, a mass of approximately 0.7 cm in diameter effacing the right-side of the spinal cord was identified. The formalin-fixed spinal mass was submitted to Cornell University Animal Health Diagnostic Center for histopathologic diagnosis. Histologically, at the lateral to anterior funiculus level of the right-sided spinal cord at C6-T1, an unencapsulated, well-demarcated, and densely cellular neoplasm was observed, which multifocally compressed and invaded the adjacent spinal cord (Figure 2A). The neoplasm contained numerous pseudo-onion bulbs structures similar to those observed in

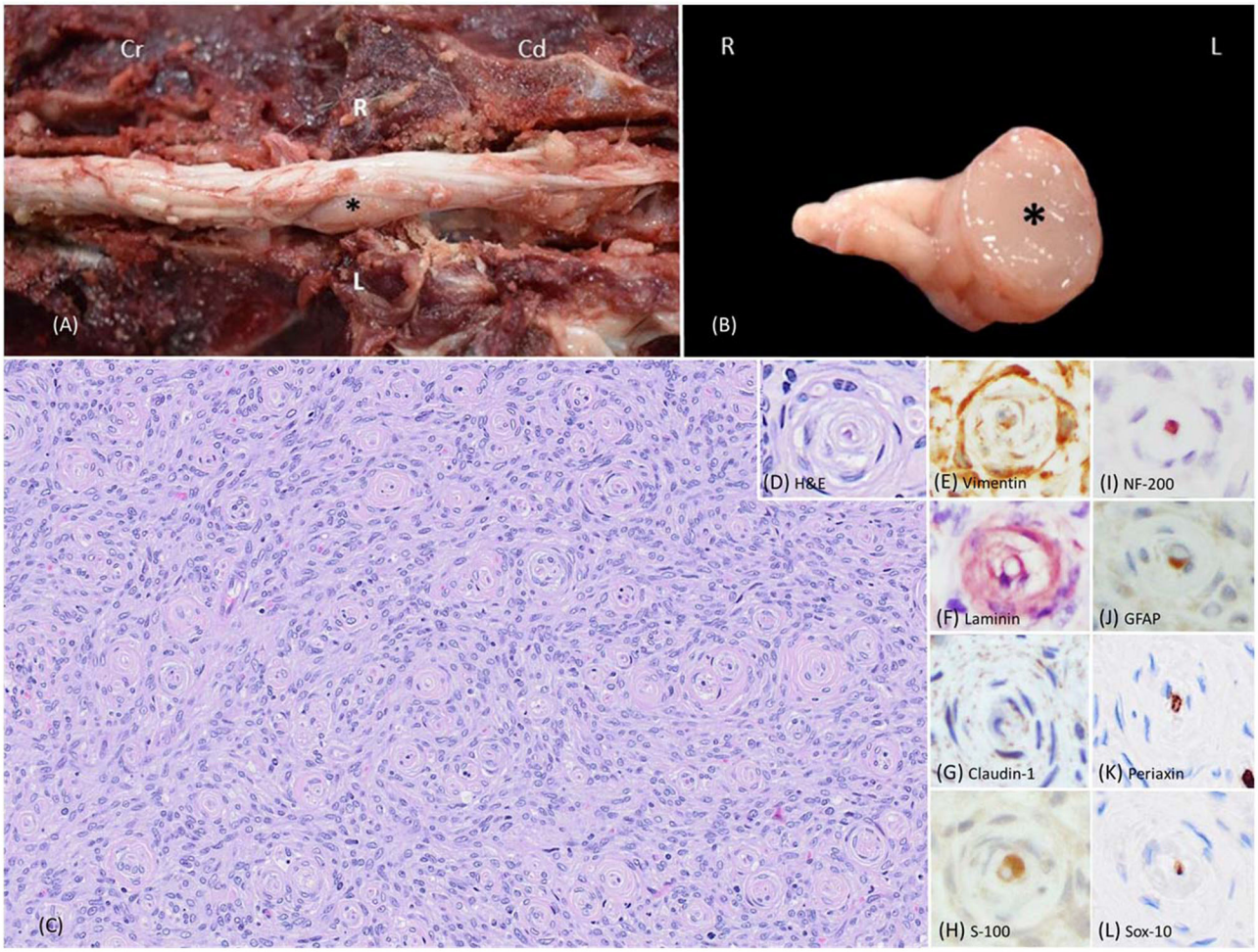

FIGURE 1
Images of intraneural-extramedullary perineurioma involving the left L5 spinal nerve roots in a beagle dog (case 1). **(A)** Gross photos show the spinal cord and an intraneural-extramedullary mass. The picture, taken post-dura opening, reveals an enlarged left spinal nerve root entrapped by a well-defined, unencapsulated, firm, tan mass measuring 2 cm x 0.5 cm x 0.5 cm (black star). Cr: Cranial; Cd: Caudal. L: left-sided; R: right-sided. **(B)** The cross-section of the intraneural-extramedullary mass (black star). L: left-sided; R: right-sided. **(C)** Histologically, the mass contained numerous pseudo-onion bulbs, characterized by neoplastic perineurial cells arranged in concentric lamellations wrapping a central myelinated or non-myelinated axon. Haematoxylin and eosin stain (H&E), 20X. **(D)** Higher magnification of the pseudo-onion bulbs of intraneural-extramedullary perineurioma. H&E, 40X. **(E)** Neoplastic perineurial cells had a strong cytoplasmic immunolabeling for vimentin antigen. Immunohistochemistry (IHC), DAB, 40X. **(F)** Neoplastic perineurial cells had a strong cytoplasmic immunolabeling for laminin antigen. IHC, Vector NovaRED, 40X. **(G)** Neoplastic perineurial cells had a strong cytoplasmic immunolabeling for claudin-1 antigen. IHC, DAB, 40X. **(H)** The Schwann cells were immunolabeled with S-100, while the neoplastic perineurial cells lacked immunoreactivity. IHC, DAB, 40X. **(I)** The central axon showed strong immunolabeling for the NF200 antigen. IHC, Vector NovaRED, 40X. **(J)** The Schwann cells were immunolabeled with GFAP, but the neoplastic perineurial cells lacked immunoreactivity. IHC, DAB, 40X. **(K)** The central axon showed immunolabeling for Periaxin antigen. Neoplastic perineurial cells lacked immunolabeling for Periaxin antigen. IHC, DAB, 40X. **(L)** The Schwann cells were immunolabeled with Sox-10 antigen. Neoplastic perineurial cells lacked immunolabeling for the Sox-10 antigen. IHC, DAB, 40X.

the first case (Figures 2B, C). Immunohistochemical profiling of the neoplasm revealed that approximately 90% of the neoplastic perineurial cells were immunolabeled for vimentin (Figure 2D) and laminin (Figure 2E). Similar to that described in case 1, approximately 20% of the neoplastic perineurial cells showed a fine punctate immunolabeling pattern for claudin-1 antigen (Figure 2F). Multiple pseudo-onion bulbs contained centrally located NF200 immunolabeled axons ensheathed by GFAP and S-100 positive Schwann cells (Figures 2G–I). No immunolabeling was observed in neoplastic perineurial cells for Periaxin (Figure 2J) and Sox-10 (Figure 2K) antigens with multiple pseudo-onion bulbs contain centrally located Periaxin immunolabeled.

Case 3

A 10-year-old spayed female Labrador Retriever dog presented to the Texas A&M Oncology Service with a four-month history of limping and lameness in the left thoracic limb. MRI revealed enlarged left spinal nerve roots at the C7-C8 as well as the right C8 nerve root. Clinical

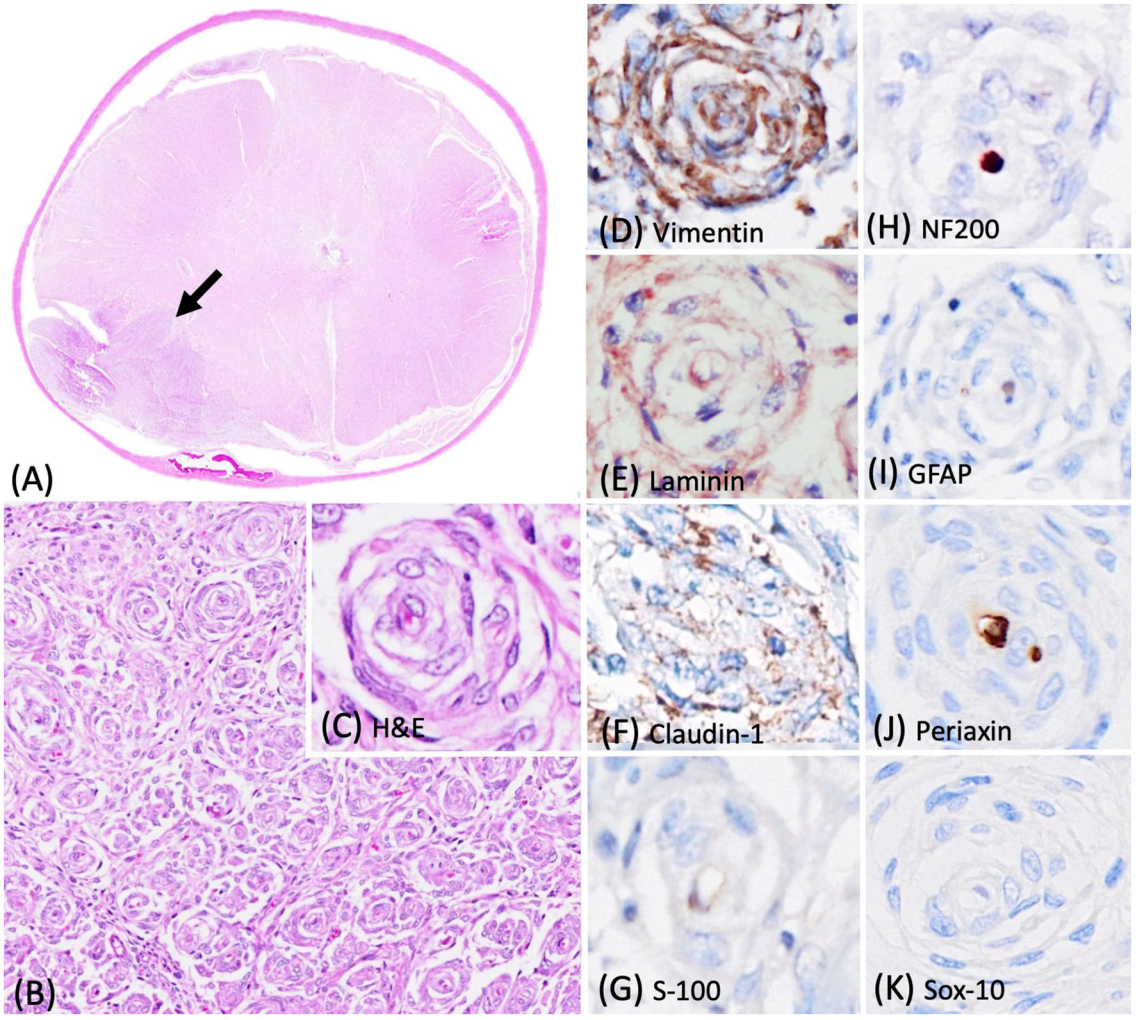

FIGURE 2
Photomicrographs of the intraneural-extramedullary perineurioma in a Labrador Retriever mix dog (case 2). **(A)** The lateral to anterior funiculus level of the right-sided spinal cord at C6-T1 contained a spinal mass with numerous pseudo-onion bulbs, characterized by neoplastic perineurial cells arranged in concentric lamellations wrapping a central myelinated or non-myelinated axon. Haematoxylin and eosin stain (H&E), 2X. **(B, C)** Higher magnification of the pseudo-onion bulbs of intraneural-extramedullary perineurioma. H&E, 20X and 40X. **(D)** Neoplastic perineurial cells had a strong cytoplasmic immunolabeling for vimentin antigen. Immunohistochemistry (IHC), DAB, 40X. **(E)** Neoplastic perineurial cells had a strong cytoplasmic immunolabeling for laminin antigen. IHC, Vector NovaRED, 40X. **(F)** Neoplastic perineurial cells had a fine punctate immunolabeling pattern for claudin-1 antigen. IHC, DAB, 40X. **(G)** The Schwann cells were immunolabeled with S-100, but the neoplastic perineurial cells lacked immunreactivity. IHC, DAB, 40X. **(H)** The central axon showed strong immunolabeling for the NF200 antigen. IHC, Vector NovaRED, 40X. **(I)** The Schwann cells were immunolabeled with GFAP, but the neoplastic perineurial cells lacked immunoreactivity. IHC, DAB, 40X. **(J)** The central axon showed immunolabeling for Periaxin antigen. Neoplastic perineurial cells lacked immunolabeling for Periaxin antigen. IHC, DAB, 40X. **(K)** Neoplastic perineurial cells lacked immunolabeling for the Sox-10 antigen. IHC, DAB, 40X.

differentials included peripheral nerve sheath tumors or neuritis. The left C7 spinal nerve root was surgically removed for histopathologic evaluation.

Histologically, the biopsied C7 spinal nerve root was mildly expanded by an unencapsulated, approximately 0.3 cm in diameter, densely cellular mass confined to the perineurium (Figure 3A). This mass contained a neoplastic population of spindle cells arranged in short, tight, haphazard streams, bundles, and whorls on the pre-existing stroma (Figures 3B, C). This pattern of the neoplastic proliferations closely resembled those of the previously reported canine perineuriomas (6). Approximately 90% of the neoplastic perineurial cells had immunolabeling for vimentin (Figure 3D) and laminin antigens (Figure 3E). Approximately 30–60% of the neoplastic perineurial cells showed fine punctate immunolabeling for claudin-1 antigen as that observed in case 1 (Figure 3F). Approximately 90% of the neoplastic perineurial cells in this case expressed S100 (Figure 3G). Multiple neoplastic whorls contained NF200 immunolabeled axons, often rimmed by GFAP labeled Schwann cells (Figures 3H, I). Similar to case 1 and 2, the neoplastic cells had negative immunolabeling for Periaxin (Figure 3J) and Sox-10 (Figure 3K) antigens.

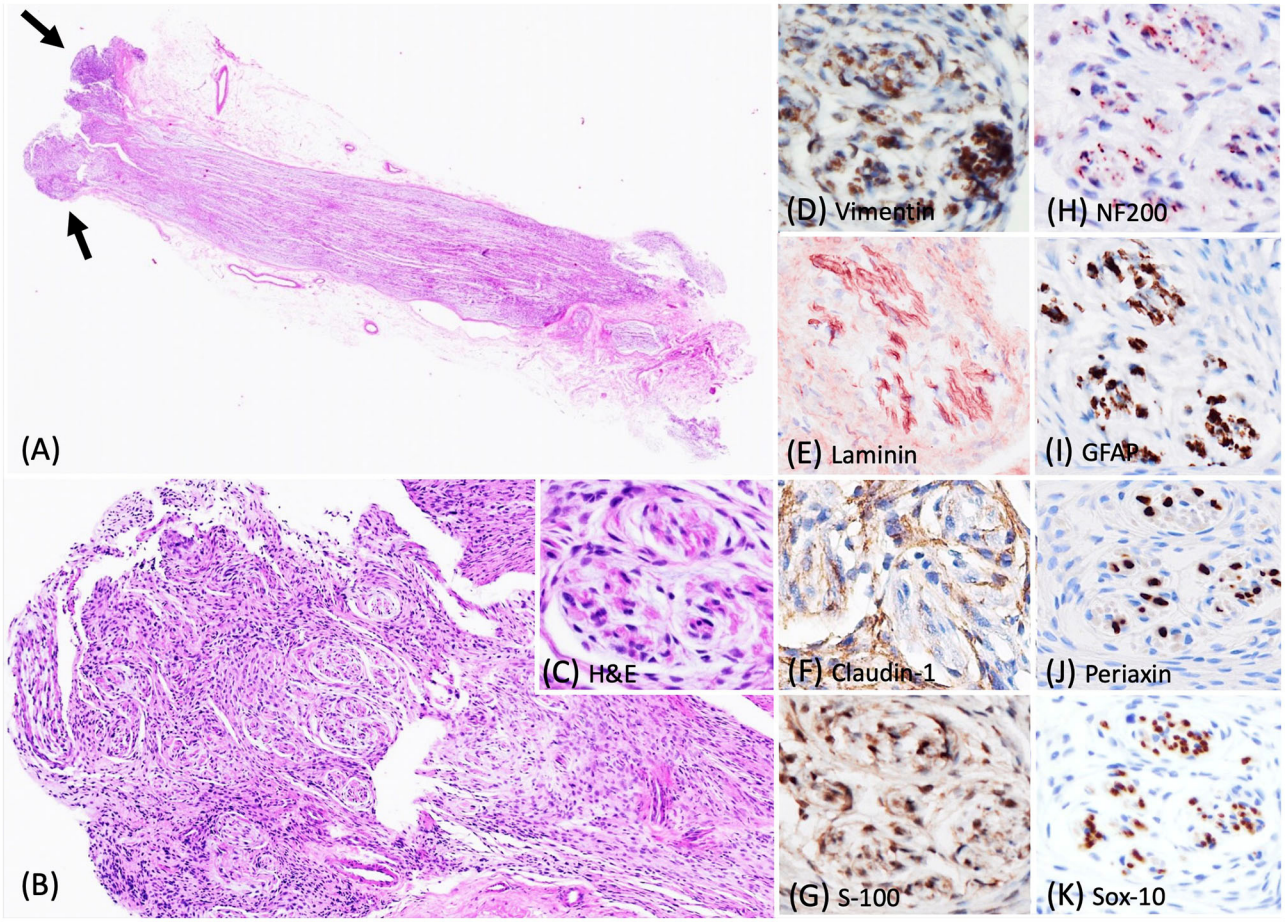

FIGURE 3
Photomicrographs of the intraneural-extramedullary perineurioma in a Labrador Retriever dog (case 3). **(A)** Histologically, the biopsied C7 spinal nerve root was mildly expanded by a unencapsulated mass, characterized by neoplastic perineurial cells arranged in concentric lamellations wrapping a central myelinated or non-myelinated axon (arrow). Haematoxylin and eosin stain (H&E), 2X. **(B, C)** Higher magnification of the pseudo-onion bulbs of intraneural-extramedullary perineurioma. H&E, 10X and 40X. **(D)** Neoplastic perineurial cells had a strong cytoplasmic immunolabeling for vimentin antigen. IHC, DAB, 40X. **(E)** Neoplastic perineurial cells had a strong cytoplasmic immunolabeling for laminin antigen. IHC, Vector NovaRED, 40X. **(F)** Neoplastic perineurial cells were immunolabeled with claudin-1 antigen. IHC, DAB, 40X. **(G)** Neoplastic perineurial cells had a strong cytoplasmic immunolabeling for S-100 antigen. IHC, DAB, 40X. **(H)** The central axon had a strong immunolabeling for the NF200 antigen. IHC, Vector NovaRED, 40X. **(I)** The Schwann cells were immunolabeled with GFAP, but the neoplastic perineurial cells lacked immunoreactivity. IHC, DAB, 40X. **(J)** The central axon showed immunolabeling for Periaxin antigen. Neoplastic perineurial cells lacked immunolabeling for Periaxin antigen. IHC, DAB, 40X. **(K)** The Schwann cells were immunolabeled with Sox-10 antigen. Neoplastic perineurial cells lacked immunolabeling for the Sox-10 antigen. IHC, DAB, 40X.

Discussion

In this case study, we described a case series of canine intraneural perineurioma and focused on the pathological and immunohistochemistry findings. Additionally, in our search across databases such as PubMed, CAB Direct, Web of Science, and Google Scholar, we found three previously reported cases of canine intraneural perineuriomas (Table 1). In summary, intraneural perineurioma commonly occurred in adult dogs, typically aged between 3 and 10 years in both small and large breeds. Most cases of canine perineurioma were observed in males (6/6). Clinical manifestations associated with intraneural perineurioma included symptoms such as spinal pain, lameness, and paresis, resulting from the involvement of spinal nerve roots or peripheral nerves. In all cases, large masses in the spinal canal or spinal roots were demonstrated in MRI and common gross findings included the presence of a cylindrical mass associated with nerve bundles. Histologically, most perineuriomas have neoplastic perineurial cells arranged in characteristic pseudo-onion bulb structures or whorls.

The expression of various immunomarkers in nerve sheath tumors exhibits marked overlap, and the diagnostic utility of immunohistochemistry has not been definitively established. Several immunomarkers have been frequently employed in an effort to identify perineurioma and distinguish them from other nerve sheath tumors in both human and veterinary medicine. Various immunomarkers, including claudin-1, collagen IV, epithelial membrane antigen (EMA), GFAP, GLUT-1, NF200, neurofilament, periaxin-1, Sox-10, and S-100 antibodies, were used in these cases. In our presented cases (case 1–3), the neoplastic perineurial cells were all immunolabeled for vimentin, laminin, and

TABLE 1 Signalment, clinical history, anatomic location, and gross findings of reported canine intraneural perineurioma.

Breed	Age (years)	Sex	Clinical signs	Location	Gross findings	References
Published cases						
German shepherd	6	MN	Progressive, nonpainful, left pelvic limb paresis	Left L5-L6 spinal nerve roots	Focally and cylindrically thickened nerve roots (twice the normal size)	(6)
Beagle	9	M	Progressive, cervicothoracic pain, tetraparesis	Left brachial plexus	Cylindrical enlargement (0.8-cm in diameter)	(8)
Leonberger	4	M	2-year history left thoracic limb lameness	Distal part of median nerve	Markedly thickened distal part of median nerve (1 cm in diameter)	(5)
N/A	N/A	N/A	N/A	Cervical nerve root	N/A	(14)
Rottweiler	9	MN	Progressive, mild ataxia in all limbs	Left C1-2 spinal nerve root	Contrast enhancing intradural extramedullary mass at nerve root	(14)
Labrador retriever N/A	5	FS	Intermitent, 6-month, thoracic limb lameness/tetraparesis, pain	Left C2 nerve root	Contrast enhancing intradural intramedullary mass at nerve root (2 cm in diameter)	(14)
Unpublished data						
Labrador retriever	10	MN	Non-progressive, non-painful, hind limb weakness	C6-T1 spinal nerve root	Unencapsulated mass (0.7-cm in diameter)	Cornell University, unpublished data
Mixed breed dog	10	FS	4-month history limping and lameness on left forelimb	C7 left spinal nerve	Unencapsulated mass (0.3-cm in diameter)	Texas A&M University, unpublished data
Beagle	3	MN	5-month progressive pelvic limb weakness, lumbar pain	Left spinal root containing the spinal nerves of L4-L6	Unencapsulated mass (0.5-cm in diameter)	Auburn University, unpublished data

L, Lumbar; M, Male; MN, Male neutered.

claudin-1. NF200 and Periaxin consistently highlighted the central axon in three cases. Only one case (case 2) had S-100 labeling in the neoplastic perineurial cells. Similar to the published cases, vimentin (2/2 cases), laminin (5/5 cases), and claudin-1(1/1 case) frequently labeled neoplastic perineurial cells. Previously, Sisó et al. (14) has shown positive expression of S-100, GFAP, Periaxin, and Sox-10 in canine perineuriomas.

The intermediate filament protein GFAP, primarily expressed in glial cells, exhibits variable expression in benign nerve sheath tumors (14). No GFAP expression was detected in the presented cases 1–3. Laminin proteins are expressed in the basement membrane and has been utilized to identify perineurial cells and Schwann cells (15–17). Neoplastic perineruial cells in all presented cases had positive immunoreactivity for laminin. Claudin-1, primarily found in the tight junctions of endothelial and epithelial cells, is also expressed in both normal and neoplastic human perineurial cells (5, 18). Notably, ∼92% of human perineuriomas have positive immunolabeling for claudin-1 (5). In dogs, claudin-1 is strongly expressed in both normal and neoplastic perineurial cells (5). Moreover, claudin-1 is absent in Schwann cells, making it a valuable tool for excluding other peripheral nerve neoplasms (5). In all cases, neoplastic perineurial cells had positive immunolabeling for claudin-1 in our study. Similarly, claudin-1 expression was also detected in a previously reported case of intraneural perineurioma in a 4-year-old male leonberger (5). However, claudin-1-poistive perineurial cells varied from 20 to 60% between neoplasms. Thus, it is necessary to examine multiple tumor sections to accurately detect the claudin-1 expression.

In conclusion, despite the rarity of reported cases in veterinary medicine, perineurioma should be considered as a potential differential diagnosis for masses associated with peripheral nerves. In cases of suspected canine intraneural perineuriomas, confirmation of the diagnosis can be achieved by identifying characteristic histologic pseudo-onion bulb structures and observing positive immunolabeling for laminin and claudin-1 in perineurial cells. The peculiar histomorphology of perineuriomas generally distinguishes them from other nerve sheath tumors, such as schwannomas. While both perineuriomas and schwannomas exhibit laminin expression, the application of claudin-1 and Sox-10 may aid additional specificity in identifying cell origin.

Data availability statement

The original contributions presented in the study are included in the article/Supplementary material, further inquiries can be directed to the corresponding author.

Ethics statement

Ethical approval was not required for the studies involving animals in accordance with the local legislation and institutional requirements because the dog was submitted for standard necropsy to the Department of Pathobiology and is not subject to animal ethic guideline. Written informed consent was obtained from the owners for the participation of their animals in this study. Written informed consent was obtained from the participant/patient(s) for the publication of this case report.

Author contributions

J-HY drafted the manuscript. BS, TJ, AY, and MH participated in the clinical management. BS, TJ, and AY performed neurologic examinations. MH interpreted the findings of diagnostic imaging and provided imaging figures. J-HY and MS performed postmortem examinations (gross and histopathology) and provided gross and histopathologic figures. AM, LS, and AH provided unpublished cases. BS, TJ, AY, MH, AM, LS, AH, and MS participated in the revision of the manuscript. All authors contributed to the article and approved the submitted version.

Acknowledgments

We thank Kreig Embriano (Department of Clinical Sciences, College of Veterinary Medicine, Auburn University) for the radiology service. We thank Cynthia Hutchinson and Lisa Jolly (Histology Laboratory, Pathobiology, College of Veterinary Medicine, Auburn University) for making histopathology slides. We thank Animal Disease Diagnostic Laboratory, College of Veterinary Medicine, Purdue University and Veterinary Diagnostic Laboratory, Michigan State University for claudin-1 immunohistochemistry stain. We thank Dr. Matti Kiupel at Michigan State University for helping us on claudin-1 immunohistochemistry images (case 2 and case 3). We thank Dr. Brian Porter at Texas A&M University for helping us search cases, ship slides, and contact with the pathologists.

Conflict of interest

The authors declare that the research was conducted in the absence of any commercial or financial relationships that could be construed as a potential conflict of interest.

Publisher's note

Supplementary material

The Supplementary Material for this article can be found online at: https://www.frontiersin.org/articles/10.3389/fvets.2023.1233230/full#supplementary-material

References

1. Kleihues P, Louis DN, Scheithauer BW, Rorke LB, Reifenberger G, Burger PC, et al. The WHO classification of tumors of the nervous system. *J Neuropathol Exp Neurol.* (2002) 61:215–25. doi: 10.1093/jnen/61.3.215

2. Toyoda T, Ochiai K, Ohashi K, Tomioka Y, Kimura T, Umemura T. Multiple perineuriomas in chicken (*Gallus gallus domesticus*). *Vet Pathol.* (2005) 42:176–83. doi: 10.1354/vp.42-2-176

3. Ochi A, Ochiai K, Hatai H, Umemura T. Naturally occurring multiple perineuriomas in a chicken (*Gallus domesticus*). *Vet Pathol.* (2008) 45:685–9. doi: 10.1354/vp.45-5-685

4. Cusack L, Blas-Machado U, Mayer J. Spontaneous spinal plexiform perineurioma in a juvenile chicken (*Gallus domesticus*). *J Vet Diagn Invest.* (2017) 29:557–60. doi: 10.1177/1040638717702936

5. Cornelis I, Chiers K, Maes S, Kramer M, Ducatelle R, De Decker S, et al. Claudin-1 and glucose transporter 1 immunolabelling in a canine intraneural perineurioma. *J Comp Pathol.* (2012) 147:186–90. doi: 10.1016/j.jcpa.2011.12.005

6. Higgins RJ, Dickinson PJ, Jimenez DF, Bollen AW, Lecouteur RA. Canine intraneural perineurioma. *Vet Pathol.* (2006) 43:50–4. doi: 10.1354/vp.43-1-50

7. Lanigan LG, Russell DS, Woolard KD, Pardo ID, Godfrey V, Jortner BS, et al. Comparative pathology of the peripheral nervous system. *Vet Pathol.* (2021) 58:10–33. doi: 10.1177/0300985820959231

8. Martins TB, Ramos AT. Viott AdM, Adeodato AG, Graça DL. Canine intraneural perineurioma Brazilian. *J Vet Pathol.* (2010) 3:66–9. Available online at: https://www.semanticscholar.org/paper/Canine-intraneural-perineurioma-Martins-Ramos/6e6d60d0bb6d9b4aea3a1934fb004b4b6223c34b#citing-papers

9. Boyanton Jr BL, Jones JK, Shenaq SM, Hicks MJ, Bhattacharjee MB. Intraneural perineurioma: a systematic review with illustrative cases. *Arch Pathol Lab Med.* (2007) 131:1382–92. doi: 10.5858/2007-131-1382-IPASRW

10. Rodriguez FJ, Folpe AL, Giannini C, Perry A. Pathology of peripheral nerve sheath tumors: diagnostic overview and update on selected diagnostic problems. *Acta Neuropathol.* (2012) 123:295–319. doi: 10.1007/s00401-012-0954-z

11. Sachanandani NS, Brown JM, Zaidman C, Brown SS, Mackinnon SE. Intraneural perineurioma of the median nerve: case report and literature review. *Hand.* (2010) 5:286–93. doi: 10.1007/s11552-009-9228-1

12. Emory TS, Scheithauer BW, Hirose T, Wood M, Onofrio BM, Jenkins RB. Intraneural perineurioma. a clonal neoplasm associated with abnormalities of chromosome 22. *Am J Clin Pathol.* (1995) 103:696–704. doi: 10.1093/ajcp/103.6.696

13. Theaker JM, Gatter KC, Puddle J. Epithelial membrane antigen expression by the perineurium of peripheral nerve and in peripheral nerve tumours. *Histopathology.* (1988) 13:171–9. doi: 10.1111/j.1365-2559.1988.tb02022.x

14. Sisó S, Marco-Salazar P, Roccabianca P, Avallone G, Higgins RJ, Affolter VK. Nerve fiber immunohistochemical panel discriminates between nerve sheath and perivascular wall tumors. *Vet Sci.* (2022) 10:1. doi: 10.3390/vetsci10010001

15. Court FA, Wrabetz L, Feltri ML. Basal lamina: schwann cells wrap to the rhythm of space-time. *Curr Opin Neurobiol.* (2006) 16:501–7. doi: 10.1016/j.conb.2006.08.005

16. Hill RE, Williams RE. A quantitative analysis of perineurial cell basement membrane collagen IV, laminin and fibronectin in diabetic and non-diabetic human sural nerve. *J Anat.* (2002) 201:185–92. doi: 10.1046/j.1469-7580.2002.00083.x

17. Jaakkola S, Savunen O, Halme T, Uitto J, Peltonen J. Basement membranes during development of human nerve: Schwann cells and perineurial cells display marked changes in their expression profiles for laminin subunits and beta 1 and beta 4 integrins. *J Neurocytol.* (1993) 22:215–30. doi: 10.1007/BF01246360

18. Folpe AL, Billings SD, McKenney JK, Walsh SV, Nusrat A, Weiss SW. Expression of claudin-1, a recently described tight junction-associated protein, distinguishes soft tissue perineurioma from potential mimics. *Am J Surg Pathol.* (2002) 26:1620–6. doi: 10.1097/00000478-200212000-00010

frontiers | Frontiers in Veterinary Science

TYPE Case Report
PUBLISHED 12 March 2024
DOI 10.3389/fvets.2024.1303084

OPEN ACCESS

EDITED BY
Sílvia Sisó,
AbbVie, United States

REVIEWED BY
Luciana Mandrioli,
University of Bologna, Italy
Thomas Cardy,
Cave Veterinary Specialists, United Kingdom

*CORRESPONDENCE
Koen M. Santifort
✉ koen.santifort@evidensia.nl

RECEIVED 27 September 2023
ACCEPTED 26 February 2024
PUBLISHED 12 March 2024

CITATION
Santifort KM, Garosi L and Weerts EAWS (2024) Case Report: Necrotizing leukomyelitis and meningitis in a Pomeranian.
Front. Vet. Sci. 11:1303084.
doi: 10.3389/fvets.2024.1303084

Case Report: Necrotizing leukomyelitis and meningitis in a Pomeranian

Koen M. Santifort[1,2]*, Laurent Garosi[3] and Erik A. W. S. Weerts[4]

[1]IVC Evidensia Small Animal Referral Hospital Arnhem, Neurology, Arnhem, Netherlands, [2]IVC Evidensia Small Animal Referral Hospital Hart van Brabant, Neurology, Waalwijk, Netherlands, [3]Vet Oracle Teleradiology, Norfolk, United Kingdom, [4]Division of Pathology, Department of Biomedical Health Sciences, Faculty of Veterinary Medicine, Utrecht University, Utrecht, Netherlands

A 2.5-year-old female entire Pomeranian dog was presented for acute paraparesis progressing within 2 days to paraplegia. General physical examination was unremarkable. Neurological examination showed paraplegia without nociception, a mass reflex upon testing perineal reflexes and withdrawal reflexes in the pelvic limbs and patellar hyperreflexia. Cutaneous trunci reflexes were absent caudal to the level of the 6th thoracic vertebra. Spinal hyperesthesia was present. Neuroanatomical localization was consistent with a T3-L3 myelopathy. Hematological and biochemical blood tests [including C-reactive protein (CRP)] were within reference ranges. MRI of the spinal cord from the level of the 1st thoracic vertebra to the sacrum revealed a patchy, ill-defined, moderate to marked T2W hyperintense, contrast enhancing intramedullary lesion extending from T1 to L4. Medical treatment based on a working diagnosis of meningomyelitis of unknown cause was initiated with corticosteroids and methadone based on pain scores. Prognosis was grave and after 3 days without return of nociception, the dog was euthanized according to the owners' wishes. Post-mortem histopathological examination of the brain and spinal cord yielded a morphological diagnosis of severe, segmental, bilateral and fairly symmetrical, necrotizing lymphohistiocytic leukomyelitis, with a non-suppurative angiocentric leptomeningitis. Some minor, focal, lymphocytic perivascular cuffing was found in the medulla oblongata as well, but otherwise there were no signs of brain involvement. No infectious causes were identified with ancillary tests. This case report underlines the importance of including meningomyelitis in the differential diagnosis list of dogs presented for acute progressive neurological signs referable to a myelopathy.

KEYWORDS

meningomyelitis, MUO, immune-mediated, small breed, dog, lymphohistiocytic

Introduction

Acute-onset canine myelopathies are fairly common in veterinary clinical neurology. The thoracolumbar spinal cord is most often affected, resulting in clinical presentations that vary from spinal hyperesthesia, to paresis, to paralysis with or without nociception and incontinence. The most common cause for acute-onset thoracolumbar myelopathy is intervertebral disc disease (IVDD) (1–5). Intervertebral disc extrusion (IVDE) of degenerated nucleus pulposus represents the largest subgroup of IVDD, but other subgroups such as acute non-compressive nucleus pulposus extrusion (ANNPE) and hydrated nucleus pulposus

extrusion (HNPE), with their own clinical and diagnostic imaging characteristics are differential diagnoses to consider (2).

Aside from IVDD, various other etiological categories with representative diseases included therein should be included in the differential diagnosis list of patients with acute-onset thoracolumbar myelopathies (1). These include trauma (e.g., vertebral fracture/luxation and resultant compression, tearing, shearing, laceration, and hemorrhage of/in the spinal cord), inflammatory disorders (e.g., discospondylitis and empyema, meningomyelitis infectious versus immune-mediated), toxicity or nutritional deficiency (rarely identified clinically in dogs, more common in farm animals), vascular disorders [hematomyelia, ischemic myelopathy (fibrocartilaginous embolic myelopathy, FCEM)], anomalies with acute complications (hamartoma, cavernous angioma), and (para)neoplastic disorders (e.g., multiple myeloma, lymphoma, primary spinal cord tumors). Each of these disorders could have primary or secondary necrotizing and inflammatory components that can be identified definitively by histopathological examination. Ascending-descending myelomalacia caused by a primary spinal cord insult due to IVDE is an example of severe, usually fatal, and often hemorrhagic, progressive necrosis of the spinal cord parenchyma (6–8).

To clinically differentiate between the different etiological categories, clinical reasoning as well as results of diagnostic tests are combined to yield the most likely or confirmed *in vivo* diagnosis. Diagnostic imaging is the mainstay for diagnosis of acute thoracolumbar myelopathies in dogs, complimented by ancillary tests such as blood work (hematology, biochemisty, c-reactive protein (CRP)), cerebrospinal fluid (CSF) analysis, and serology and polymerase chain reaction tests for infectious agents. Magnetic resonance imaging (MRI) is the gold standard for the diagnosis of most thoracolumbar myelopathies in dogs.

Imaging characteristics of various specific disease entities, including IVDD subtypes, infectious causes (e.g., discospondylitis), and vascular causes (e.g., FCE) have been described (9–13). Additionally, numerous reports include individual descriptions of findings on imaging studies for specific disorders, including infectious and non-infectious meningomyelitis. Combining transverse, dorsal, and sagittal planes of different types of sequences, differentiation between disorders preferentially affecting certain locations (e.g., focal/multifocal, grey/white matter/both, unilateral/bilateral) in the spinal cord may be achieved to a certain degree. Histopathological examination remains invaluable for more accurate description and certainty, however.

This case report details the clinical, diagnostic imaging, and histopathological findings in a small breed dog with an acute, symmetrical, progressive, painful, T3-L3 myelopathy with loss of nociception. The aim is to highlight the value, pitfalls, and importance of each, as well as to document detailed findings of this case to which the true etiology remains unknown.

Case description

A 2.5-year-old female entire Pomeranian dog was presented to the neurology department of IVC Evidensia Small Animal Hospital (Arnhem, The Netherlands) for acute paraparesis progressing within 2 days to paraplegia. The referring veterinarian had diagnosed bilateral patellar luxation and had prescribed rest and meloxicam (0.1 mg/kg *per os* q24h) 3 days earlier. Over the weekend, the dog deteriorated quickly and lost the ability to ambulate, urinate and defecate. General examination was unremarkable. Orthopedic examination revealed bilateral patellar luxation. Neurological examination showed paraplegia without nociception, a mass reflex upon testing perineal reflexes and withdrawal reflexes in the pelvic limbs and patellar hyperreflexia. Cutaneous trunci reflexes were absent caudal to the level of the 6th thoracic vertebra. Thoracolumbar (para)spinal hyperesthesia was present. The bladder was full and upon manual expression, urethral sphincter resistance was noted consistent with an upper motor neuron bladder. The rest of the examination, including evaluation of mental status and behavior, cranial nerve function tests and proprioceptive and reflex tests of the thoracic limbs, was unremarkable. A neuroanatomical localization of a T3-L3 myelopathy was concluded. Hematological and biochemical blood tests [including c-reactive protein (CRP; 6.1 mg/L, ref. range 0–10.0 mg/L)] were unremarkable.

The top differential diagnosis considered at this point was IVDD (IVDE, possibly with secondary myelomalacia). Other differential diagnoses that were considered at this point included unwitnessed trauma, vascular (hematomyelia), inflammatory (meningomyelitis of unknown origin, suspected immune-mediated), infectious (e.g., protozoal myelitis, canine distemper virus myelitis), anomalies with acute complications, and neoplastic (e.g., lymphoma) etiologies.

A high-field magnetic resonance imaging (MRI; 1.5 T Canon Vantage Elan) study of the thoracolumbar spinal cord from the level of the 1st thoracic vertebra to the sacrum was performed under general anesthesia. Premedication included 0.4 mg/kg methadone and 6 µg/kg dexmedetomidine, followed by 3 mg/kg propofol in boluses to effect for induction of anesthesia. Isoflurane 2–3% was used for maintenance of anesthetic plane. Performed sequences included: sagittal T2-weighted (T2W), sagittal short tau inversion recovery (STIR), sagittal T1W, dorsal STIR, transverse T2W, transverse T1W, transverse T2*, transverse post-contrast T1W, sagittal post-contrast 3D T1W and transverse post-contrast T1W with fat saturation. The MR images revealed no sign of intervertebral disc disease, nucleus pulposus signal of all imaged intervertebral discs being T2 hyperintense. There was a patchy ill-defined intramedullary lesion of variable extent, but seen from T1 to L4 (Figure 1). Both gray and white matter were affected. The entire cross-sectional area of the cord was affected at the level of T9. The lesion was heterogeneous, moderate to marked T2W hyperintense when compared to the rest of the cord and T1W isointense. The spinal cord parenchyma showed moderate, patchy, contrast enhancement from T7 to T12 and L1 to L3. The cord appeared swollen at those levels and the surrounding meninges were thickened and contrast enhancing, including enhancement along the ventral medial fissure at the level of T9. A lumbar CSF tap was unsuccessful.

The main differential diagnoses that were considered at this point included inflammatory (meningomyelitis of unknown origin, suspected immune-mediated), infectious (e.g., protozoal myelitis, canine distemper virus myelitis) and neoplastic (e.g., lymphoma) etiologies.

Medical treatment was initiated with dexamethasone (0.4 mg/kg once IV), prednisolone (1 mg/kg q12h *per os*), and methadone based on pain scores (0.2–0.5 mg/kg q4-8h). An indwelling urinary catheter was placed and intravenous fluid therapy initiated (Ringer's lactate solution 3–5 mL/kg/h). Prognosis was grave and after 3 days without

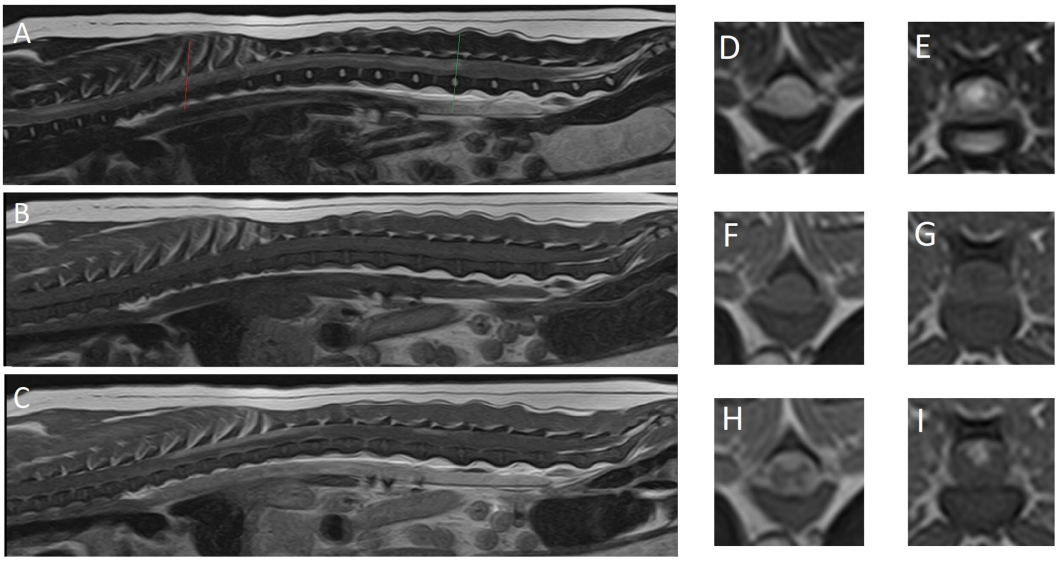

FIGURE 1
Magnetic resonance images of reported case. **(A)** Midsagittal plane, **(D)** transverse plane and **(E)** transverse plane are T2-weighted images. **(B)** Midsagittal plane, **(F)** transverse plane and **(G)** transverse plane are T1-weighted images. **(C)** Midsagittal plane, **(H)** transverse plane and **(I)** transverse plane are T1-weighted post-contrast images. **(D,F,H)** The level of T8 (red line). **(E,G,I)** The level of L3-4 intervertebral disc (green line).

return of nociception, the dog was euthanized (by intravenous administration of 140 mg/kg pentobarbital) according to the owners' wishes.

Post-mortem gross and histopathological examination of the brain and spinal cord was performed. Macroscopically, the thoracolumbar segments of the spinal cord were swollen and showed yellowish discoloration through intact dura mater. After fixation in 10% buffered formalin and sectioning of the affected thoracolumbar segments, malacic areas were identified in the dorsal and ventral funiculi.

Microscopic examination of five hematoxylin and eosin-stained T3-L3 spinal cord sections confirmed an inflammatory process mostly restricted to spinal cord white matter and leptomeninges (Figure 2). This process was characterized by a bilateral and fairly symmetrical, severe necrotizing leukoencephalitis (Figure 2A) with perivascular lymphocytic cuffs (Figure 2B). At the epicenter of the lesions, at segments T9-T12, both dorsal and ventromedial funiculi had marked pallor and were hypercellular. Large numbers of histiocytes infiltrated, compressed, and effaced nerve fibers at those locations totally effacing the spinal white matter architecture. Numerous axons were enlarged (spheroids), and there were empty myelin sheaths, and myelin breakdown accompanied by large macrophages, gitter cells found within dilated myelin sheaths that contain axonal debris, all admixed with a few lymphocytes and neutrophils (Figures 2C,D). Similar granulomatous inflammatory lesions also affected the most submeningeal and superficial white matter, circumferentially, which appear pale, edematous, and hypercellular. No such lesions were found in the gray matter of the spinal cord. At T9-T12, visualization of the meninges confirmed large lymphocytic infiltrates surrounding both the ventral and the dorsal spinal arteries as well as their vascular tree along the leptomeninges (Figures 2A,G,H). The central branch at the ventral median fissure was populated by a dense population of lymphocytes with a few monocytes and neutrophils that upon entry into the gray matter expanded a few Virchow-Robin spaces surrounding the central canal of the ventral horns. Similarly, branches of the dorsal spinal arteries resulted in perivascular lymphocytic cuffs and scattered lymphocytes in the neuropil of the dorsal horns. Neuronal necrosis was not observed in any section. There was no evidence of vasculitis, thrombosis, vascular necrosis, or thromboembolisms in any of the examined sections.

Cranial to but also at T9 (Figures 2A,E,F), spinal cord lateral funiculi multifocally showed evidence of axonal tract degeneration in the form of axonal spheroids and digestion chambers with reactive astrocytes and capillaries (Figures 2E,F). The inflammatory process in those rostral spinal cord sections was minimal and restricted to a few immune cells infiltrating some perivascular spaces.

Ancillary special stains to aid the detection of infectious agents, included a PAS (periodic acid-schiff), Grocott's methenamine silver stain and a Giemsa stain, and yielded a negative result. Immunohistochemistry for the detection of canine distemper virus, Toxoplasma gondii, *Neospora caninum* and canine parvovirus also provided negative results. Real-time polymerase chain reaction (PCR) tests on spinal cord tissue for *Bartonella* spp., canine distemper virus, *Cryptococcus neoformans*, *Neospora* spp., and *Toxoplasma gondii* were negative as well.

The final morphological diagnosis was a severe, segmental, bilateral and fairly symmetrical, necrotizing lymphohistiocytic leukomyelitis, with a non-suppurative angiocentric leptomeningitis. A specific etiology was not identified.

Discussion

Despite not being able to reach a specific etiological diagnosis in this case, we considered this case important to document for a number of reasons that we will discuss in the following paragraphs.

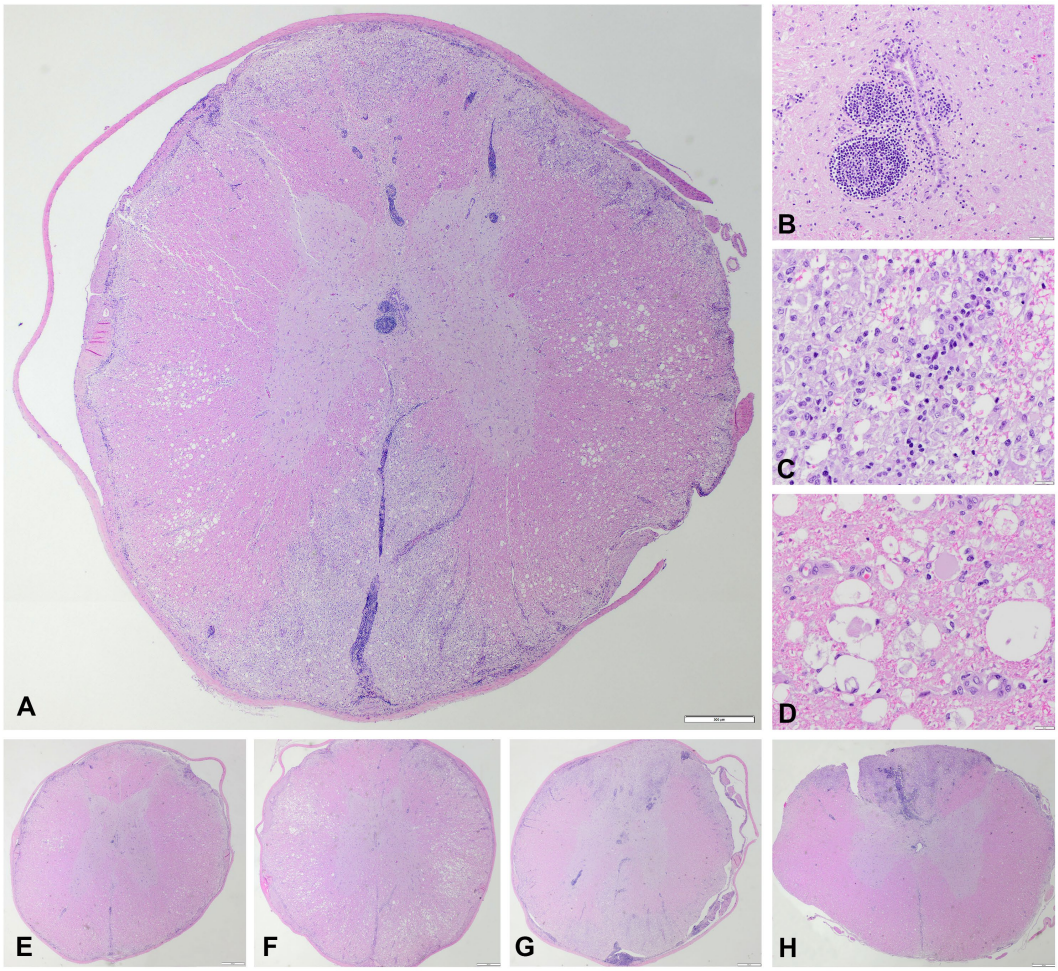

FIGURE 2
Microscopic images, hematoxylin and eosin. **(A)** Transversal section of the thoracic spinal cord at the level of T9 with bilateral fairly symmetrical necrotizing and lymphohistiocytic leukomyelitis of the dorsal, lateral, and ventral funiculi with a vascular pattern affecting the ventral spinal artery and dorsolateral arteries, and their main branches (vertical and sulcal), degenerative changes of the myelin sheaths and axons in the lateral funiculi, and non-necrotic gray matter with lymphocytic perivascular cuffing and multifocal lymphohistiocytic infiltration within the leptomeninges. Scale bar = 500 µm. **(B)** Lymphocytic perivascular cuffing in the grey matter adjacent to the central canal. Scale bar = 50 µm. **(C)** Detail of the dorsal and lateral funiculi, necrotizing and lymphohistiocytic leukomyelitis with presence of many gitter cells. Scale bar = 20 µm. **(D)** Detail of the lateral funiculi, myelin sheaths vacuolation with marked swelling of axons (spheroids). Scale bar = 20 µm. **(E)** Transversal section of the thoracic spinal cord at the level of T3. Scale bar = 500 µm. **(F)** Transversal section of the thoracic spinal cord at the level of T6. Scale bar = 500 µm. **(G)** Transversal section of the thoracic spinal cord at the level of T12. Scale bar = 500 µm. **(H)** Transversal section of the thoracic spinal cord at the level of L3/4. Scale bar = 500 µm. The craniocaudal extent of the lesions, with preferential involvement of the dorsal funiculi at the lumbar segment in **H**, is appreciated in **E–H**.

First, the value and pitfalls of using clinical reasoning to determine the most likely differential diagnosis are highlighted by the change in number and types of differential diagnoses considered in this case. The top differential considered after history taking and clinical examination was IVDD (IVDE). This would usually be a surgically treatable disorder. The only consistently prognostically valuable clinical parameter in dogs with thoracolumbar IVDE is the presence or absence of nociception; dogs without nociception in the pelvic limbs or tail have a worse prognosis for recovery (4). In one study (1), loss of nociception in canine spinal cord disease was noted in only 5–6% of cases, with listed causes including IVDE, ischemic myelopathy and acute non-compressive nucleus pulposus extrusion (ANNPE) (1). The grade of neurological disability, mainly the loss of nociception, has been identified as a risk factor for the development of ascending-descending myelomalacia. One large study determined that 14.5% of dogs without nociception developed this disastrous complication, while a smaller study found that 21.5% of dogs without nociception died as a consequence thereof despite routine surgery (6, 8). Extensive hemilaminectomy and durotomy were recently proposed and shown to decrease the rate of this complication in dogs (8, 14, 15). In our case, nociception was absent which prompted swift diagnostic imaging to accurately assess the if this dog could have benefitted from surgery. The diagnostic imaging results resulted in a much different plan. Therefore, whilst clinical reasoning is of great value to clinicians, uncommon or less expected diagnosis should not be discounted early on. This is most important when owner are informed ahead of diagnostic test results on the possible outcomes of either the tests themselves or, prematurely, of recommended procedures that follow on the results of those tests.

Second, the value and limitations of MRI in diagnosing or excluding differentials from the differential diagnosis list is reflected in this case report. MRI findings, while very suggestive, were not confirmatory of an inflammatory process. No IVDD was identified on the images and subsequently excluded from the differential diagnosis list. Since the CSF tap failed, no further clinical indications were available to corroborate the suspicion of inflammation or possibly identify neoplastic cells. The post-mortem histopathology confirmed the suspicions of inflammation, but also provided us with the opportunity to assess the similarities between the diagnostic imaging findings (Figure 1) with the histopathological findings (Figure 2). We would like for the reader to compare these alongside each other and appreciate the way the MRI findings largely reflect the histological findings, but also appreciate that the histopathological findings are even more extensive than can be seen on the MR images.

Third, the value and limitations of histopathological examination are highlighted by this case. The changes in the spinal cord parenchyma and meninges was detailed and confirmed that the pathological process was indeed severe as suspected based on the clinical characteristics and imaging findings, with necrosis of the affected tissue. Despite efforts to identify a specific etiology, none was found. Therefore, one may conclude that the term 'meningomyelitis of unknown origin' and more specifically since histologically characterizeable 'necrotizing leukomyelitis and meningitis of unknown origin'. The suffix '-of unknown origin' is often interpreted as 'likely immune-mediated'. This may be the case, but maybe not. As said in the introduction, a number of etiological categories may be characterized by primary or secondary necrotizing and inflammatory histopathological findings. We deliberately included in the descriptions the term 'fairly' for annotation to the "symmetrical" nature of the lesions. The most severely affected segments of the spinal cord were included for examination (segments T8–T10). At the level of these segments, the lesions were severe and fairly symmetrical. However, this is most likely not reflective of the nature of the underlying etiology (i.e., inflammatory process), but rather reflects the effect of the passing of time in an initially multifocal disease process. The authors suspect that the lesions were likely multifocal in nature at the start and that the passing of time led to confluence of the lesions. This, in combination with the restricted anatomy of the spinal cord (transversely at least), can account for the end-stage lesion aspects seen and described in this report. After deliberation with other veterinary (neuro)pathologists, concluded that the necrotizing changes are most likely secondary to a combination of the inflammatory processes as well as ischemia linked to pressure effects of the inflammation on the blood vessels of the spinal cord parenchyma. The distribution of the lesions in the regions of the larger blood vessels and the bilaterally fairly symmetrical pattern seemed to us suggestive thereof. Also, the extent of changes and damage in the grey matter were clearly surpassed by those in white matter. Necrotizing meningomyelitis may arguably be applicable to not limit the morphological diagnosis to the spinal cord white matter and include the abnormalities in grey matter. Still, the authors concluded that the severity of the lesions in white matter preferentially over grey matter merits the inclusion of the prefix leuko- in this case. Finally, although we performed a number of ancillary tests including IHC and PCR, we cannot exclude infectious causes of the identified pathological changes due to lack of testing for other agents as well as imperfect sensitivity and specificity of these tests. Recent reports on tick-born encephalitis in dogs revealed mostly bilateral and symmetrical brain changes with MRI (16, 17). Other etiologies more commonly linked to bilateral and symmetrical changes would include metabolic, toxic, nutritional, and degenerative etiologies, but none of these categories are associated with the changes identified in this case to the knowledge of the authors. Due to lack of identification of an infectious cause, we preferentially consider an auto-immune basis to the changes seen in this case, although we acknowledge the fact that we cannot be entirely certain. In this light, the term 'necrotizing leukomyelitis and myelitis of unknown origin' could be applied.

Meningomyelitis in dogs can be caused by an infection, but is suspected to occur alternatively also as suspectedly immune-mediated disease (18–21). Several studies looking for infectious causes of meningoencephalomyelitis or meningoencephalitis have not identified infectious agents, leading to the continued use of the suffix '-of unknown origin' or similar suffices (22, 23). Similar studies focusing on MUO of the spinal cord only have not been performed. Necrotizing meningomyelitis of unknown origin or necrotizing forms of meningoencephalitis of unknown origin (MUO) affecting only the spinal cord are reported rarely in dogs of various breeds, both small (including toy) and large (e.g., hound) (18, 19) and mostly young to middle aged dogs (18–20). Neurological signs are diverse, but general proprioceptive ataxia, paresis, and paraspinal hyperesthesia are the most commonly reported clinical signs (18, 19). The case reported here is unusual with regard to the severity of the clinical presentation, being presented with paraplegia without nociception and both urinary and fecal incontinence. In one study documenting MUO affecting the spinal cord only, not a single case was documented to be (tetra- or) paraplegic without nociception (18). Most cases had involvement of the cervical spinal cord segments. Urinary- and/or fecal incontinence is reported in a minority (10%) (18). In that study, a single case of a 3-year-old female neutered Yorkshire terrier presented with ambulatory tetraparesis was diagnosed with necrotizing meningoencephalomyelitis via histopathological examination (18). Additionally, a 2-year-old female neutered Weimaraner with acute necrohemorrhagic myelitis and vasculitis, that was presented at a veterinary clinic with ambulatory paraparesis progressing to non-ambulatory status, was published as case report (19). As for consistency of the underlying histopathological findings, signs of vasculitis and hemorrhage as reported in the Weimaraner case were not found in our case (19) and no detailed histopathological findings were given in the study on the Yorkshire terrier (18).

Specifically in regards to the case reported here, the authors would like to draw the readers' attention to some important considerations.

In our case, a lumbar CSF tap was unsuccessful and CSF analysis could not be performed. The added value of CSF analysis in cases of inflammatory myelopathies has been demonstrated (18, 19, 21, 24, 25). One study found a pleocytosis in CSF in 100% of cases of 'spinal-only' MUO. Total protein measurement was above reference values in 17/18 dogs (94%). In contrast, a leukocytosis in complete blood counts was only present in 2 dogs (10%) while lymphopenia was present in six dogs (29%). Lumbar CSF taps are reported to be unsuccessful in 13.9% of cases where it was attempted (26). In retrospect, cisternal CSF tap, though likely yielding a less representative sample for analysis in case of myelopathies (27, 28), might have been considered for the case reported here. General bloodwork including a complete blood count revealed no abnormalities and serum CRP was within reference range in our case. This finding is consistent with CRP being normal in

most cases of MUO as well (29). For MUO (not for spinal-only MUO or non-infectious meningomyelitis), numerous studies have focused on findings specific and reliable biomarkers (29). As this search continues, future studies could also focus on their value in the diagnosis of meningomyelitis of unknown origin in dogs.

MRI findings in our case consisted an extensive area of (likely confluent) multifocal T2W hyperintense lesions that were T1W isointense and showed parenchymal (spinal cord) as well as meningeal contrast enhancement. MRI features of meningomyelitis of unknown origin in dogs have been reported (18). These include: focal (71%), multifocal (19%) or no lesions (10%); ill-defined, intramedullary, hyperintense lesions on T2W images that are isointense on T1W images; parenchymal contrast enhancement (86%); and meningeal contrast enhancement (81%). Meningeal contrast enhancement could be the only finding (18). Concurrent brain lesions may be identified on MRI, which would suggest meningoencephalomyelitis that can be confirmed by histological examination (18). The extensive parenchymal and meningeal contrast enhancement seen on post-contrast studies as performed in our case provide valuable information to give preference to a diagnosis of meningomyelitis.

In the case reported here, treatment was limited to immunosuppressive treatment with dexamethasone and prednisolone. In a study including 21 dogs with "spinal-only MUO," medical treatment and the results thereof were reported (18). All dogs were treated with immunosuppressive doses of corticosteroids (dexamethasone 0.3–0.5 mg/kg/day or prednisolone 2–4 mg/kg/day). Fourteen dogs (67%) received additional treatment with cytosine arabinoside in various protocols. Three dogs (14%) showed deterioration despite treatment. There is no definitive proof that additional treatment (e.g., with cytosine arabinoside) to corticosteroids provides benefit in cases of MUO (30, 31). Future studies should provide more information on the possible benefits thereof (32).

Euthanasia was elected for the dog in this case report due to a grave prognosis based on the severity of initial clinical signs including absent nociception and incontinence, and no sign of improvement after initiation of treatment. Based on two larger studies of dogs with meningomyelitis (one including only a non-infectious etiology, the other including both infectious and non-infectious etiologies), approximately 50% of dogs with this diagnosis die (either by euthanasia or naturally) despite attempts at treatment (18, 19).

In the scope of comparative medicine or One Health, in human medical literature the term "(idiopathic) transverse myelitis" is used to describe an acute, bilateral inflammation of the spinal cord with either infectious or non-infectious (idiopathic) causes (33–39). Many patients in the most severely affected category will exhibit loss of sensation and incontinence. MRI findings largely overlap those reported for "spinal-only" MUO in dogs (18, 35, 36). The percentage of cross-sectional area of the spinal cord that is affected varies, but often exceeds two thirds (35). In our case, 100% of the cross-sectional area was affected at the level of the T9 vertebra. This feature does not necessarily correlate to clinical severity in humans (33, 35, 36). Specific MRI features can also be of value in determining the likelihood of idiopathic transverse myelitis versus infectious causes of transverse myelitis (36). Future studies may provide more insights on the value of MRI for the differentiation of infectious versus non-infectious (suspected immune mediated) causes of meningomyelitis. Still, it is clear also from human medical literature that *in vivo* diagnoses of (idiopathic) transverse myelitis cannot be regarded as definitive diagnoses (40); histopathological diagnoses may differ in a large number of suspected cases. In our case, the diagnosis of severe, multifocal, bilateral and fairly symmetrical, multifocal, lymphohistiocytic necrotizing leukomyelitis and meningitis with a vascular pattern affecting the ventral spinal artery and dorsolateral arteries, and their main branches (vertical and sulcal) was based on post-mortem histopathology of the entire central nervous system. This particular pattern of inflammatory lesions in the spinal cord has not been documented before in dogs to the knowledge of the authors.

In conclusion, this case report underlines the importance of including meningomyelitis in the differential diagnosis list of dogs presented for acute progressive neurological signs referable to a myelopathy. Clinical reasoning, diagnostic tests including diagnostic imaging, and histopathological examinations all have their own value and pitfalls or limitations to consider.

Data availability statement

The original contributions presented in the study are included in the article/supplementary material, further inquiries can be directed to the corresponding author.

Ethics statement

Ethical approval was not required for the studies involving animals in accordance with the local legislation and institutional requirements because the animal was treated in accordance with the local legislation and institutional requirements. Written informed consent was obtained from the owners for the participation of their animals in this study.

Author contributions

KS: Conceptualization, Data curation, Investigation, Visualization, Writing – original draft. LG: Investigation, Visualization, Writing – review & editing. EW: Investigation, Visualization, Writing – review & editing.

Funding

The author(s) declare financial support was received for the research, authorship, and/or publication of this article. The publication fee was covered by IVC Evidensia's fund for publication of peer-reviewed scientific articles.

Acknowledgments

The authors would like to thank Dr. Martí Pumarola (Barcelona) and the editor for his and her feedback on the final draft of the manuscript before submission and after peer-review. The authors

would like to thank and acknowledge IDEXX molecular diagnostics department for the performance of the PCR tests.

Conflict of interest

The authors declare that the research was conducted in the absence of any commercial or financial relationships that could be construed as a potential conflict of interest.

Publisher's note

References

1. Cardy TJ, De Decker S, Kenny PJ, Volk HA. Clinical reasoning in canine spinal disease: what combination of clinical information is useful? *Vet Rec*. (2015) 177:171. doi: 10.1136/vr.102988

2. Fenn J, Olby NJ. Canine spinal cord injury consortium (CANSORT-SCI). Classification of intervertebral disc disease. *Front Vet Sci*. (2020) 7:579025. doi: 10.3389/fvets.2020.579025

3. Olby NJ, da Costa RC, Levine JM, Stein VM. Canine spinal cord injury consortium (CANSORT SCI). Prognostic factors in canine acute intervertebral disc disease. *Front Vet Sci*. (2020) 7:596059. doi: 10.3389/fvets.2020.596059

4. Olby NJ, Moore SA, Brisson B, Fenn J, Flegel T, Kortz G, et al. ACVIM consensus statement on diagnosis and management of acute canine thoracolumbar intervertebral disc extrusion. *J Vet Intern Med*. (2022) 36:1570–96. doi: 10.1111/jvim.16480

5. Rossi G, Stachel A, Lynch AM, Olby NJ. Intervertebral disc disease and aortic thromboembolism are the most common causes of acute paralysis in dogs and cats presenting to an emergency clinic. *Vet Rec*. (2020) 187:e81. doi: 10.1136/vr.105844

6. Balducci F, Canal S, Contiero B, Bernardini M. Prevalence and risk factors for presumptive ascending/descending Myelomalacia in dogs after thoracolumbar intervertebral disk herniation. *J Vet Intern Med*. (2017) 31:498–504. doi: 10.1111/jvim.14656

7. Griffiths IR. The extensive myelopathy of intervertebral disc protrusions in dogs ('the ascending syndrome'). *J Small Anim Pract*. (1972) 13:425–37. doi: 10.1111/j.1748-5827.1972.tb06870.x

8. Takahashi F, Honnami A, Toki M, Dosaka A, Fujita Y, Hara Y, et al. Effect of durotomy in dogs with thoracolumbar disc herniation and without deep pain perception in the hind limbs. *Vet Surg*. (2020) 49:860–9. doi: 10.1111/vsu.13409

9. da Costa RC, De Decker S, Lewis MJ, Volk H. Canine spinal cord injury consortium (CANSORT-SCI). Diagnostic imaging in intervertebral disc disease. *Front Vet Sci*. (2020) 7:588338. doi: 10.3389/fvets.2020.588338

10. De Risio L, Adams V, Dennis R, McConnell F, Platt S. Magnetic resonance imaging findings and clinical associations in 52 dogs with suspected ischemic myelopathy. *J Vet Intern Med*. (2007) 21:1290–8. doi: 10.1892/06-273.1

11. Mai W. Reduced field-of-view diffusion-weighted MRI can identify restricted diffusion in the spinal cord of dogs and cats with presumptive clinical and high-field MRI diagnosis of acute ischemic myelopathy. *Vet Radiol Ultrasound*. (2020) 61:688–95. doi: 10.1111/vru.12907

12. Ruoff CM, Kerwin SC, Taylor AR. Diagnostic imaging of Discospondylitis. *Vet Clin North Am Small Anim Pract*. (2018) 48:85–94. doi: 10.1016/j.cvsm.2017.08.007

13. Specchi S, Johnson P, Beauchamp G, Masseau I, Pey P. Assessment of interobserver agreement and use of selected magnetic resonance imaging variables for differentiation of acute noncompressive nucleus pulposus extrusion and ischemic myelopathy in dogs. *J Am Vet Med Assoc*. (2016) 248:1013–21. doi: 10.2460/javma.248.9.1013

14. Jeffery ND, Mankin JM, Ito D, Boudreau CE, Kerwin SC, Levine JM, et al. Extended durotomy to treat severe spinal cord injury after acute thoracolumbar disc herniation in dogs. *Vet Surg*. (2020) 49:884–93. doi: 10.1111/vsu.13423

15. Nakamoto Y, Uemura T, Hasegawa H, Nakamoto M, Ozawa T. Outcomes of dogs with progressive myelomalacia treated with hemilaminectomy or with extensive hemilaminectomy and durotomy. *Vet Surg*. (2021) 50:81–8. doi: 10.1111/vsu.13514

16. Gonzalo-Nadal V, Kohl A, Rocchi M, Brennan B, Hughes J, Nichols J, et al. Suspected tick-borne flavivirus meningoencephalomyelitis in dogs from the UK: six cases (2021). *J Small Anim Pract*. (2024) 65:132–43. doi: 10.1111/jsap.13682

17. Kleeb C, Golini L, Beckmann K, Torgerson P, Steffen F. Canine tick-borne encephalitis: clinical features, survival rate and neurological sequelae: a retrospective study of 54 cases (1999-2016). *Front Vet Sci*. (2021) 8:782044. doi: 10.3389/fvets.2021.782044

18. Cornelis I, Volk HA, Van Ham L, De Decker S. Clinical presentation, diagnostic findings and outcome in dogs diagnosed with presumptive spinal-only meningoencephalomyelitis of unknown origin. *J Small Anim Pract*. (2017) 58:174–82. doi: 10.1111/jsap.12622

19. Parry AT, Penning VA, Smith KC, Kenny PJ, Lamb CR. Imaging diagnosis--necrotizing meningomyelitis and polyarthritis. *Vet Radiol Ultrasound*. (2009) 50:412–5. doi: 10.1111/j.1740-8261.2009.01558.x

20. Griffin JF, Levine JM, Levine GJ, Fosgate GT. Meningomyelitis in dogs: a retrospective review of 28 cases (1999 to 2007). *J Small Anim Pract*. (2008) 49:509–17. doi: 10.1111/j.1748-5827.2008.00588.x

21. Radaelli ST, Platt SR. Bacterial meningoencephalomyelitis in dogs: a retrospective study of 23 cases (1990-1999). *J Vet Intern Med*. (2002) 16:159–63. doi: 10.1892/0891-6640(2002)016<0159:bmidar>2.3.co;2

22. Barber RM, Porter BF, Li Q, May M, Claiborne MK, Allison AB, et al. Broadly reactive polymerase chain reaction for pathogen detection in canine granulomatous meningoencephalomyelitis and necrotizing meningoencephalitis. *J Vet Intern Med*. (2012) 26:962–8. doi: 10.1111/j.1939-1676.2012.00954.x

23. Hoon-Hanks LL, McGrath S, Tyler KL, Owen C, Stenglein MD. Metagenomic investigation of idiopathic Meningoencephalomyelitis in dogs. *J Vet Intern Med*. (2018) 32:324–30. doi: 10.1111/jvim.14877

24. Di Terlizzi R, Platt S. The function, composition and analysis of cerebrospinal fluid in companion animals: part I - function and composition. *Vet J*. (2006) 172:422–31. doi: 10.1016/j.tvjl.2005.07.021

25. Di Terlizzi R, Platt SR. The function, composition and analysis of cerebrospinal fluid in companion animals: part II - analysis. *Vet J*. (2009) 180:15–32. doi: 10.1016/j.tvjl.2007.11.024

26. Fentem R, Nagendran A, Marioni-Henry K, Madden M, Phillipps S, Cooper C, et al. Complications associated with cerebrospinal fluid collection in dogs. *Vet Rec*. (2023) 193:e2787. doi: 10.1002/vetr.2787

27. Early PJ, Munana KJ, Olby NR, Mariani CL. Comparison of cerebrospinal fluid parameters from the cerebellomedullary and lumbar cisterns in 54 dogs. *Can Vet J*. (2019) 60:885–8.

28. Lampe R, Foss KD, Vitale S, Hague DW, Barger AM. Comparison of cerebellomedullary and lumbar cerebrospinal fluid analysis in dogs with neurological disease. *J Vet Intern Med*. (2020) 34:838–43. doi: 10.1111/jvim.15700

29. Andersen-Ranberg E, Berendt M, Gredal H. Biomarkers of non-infectious inflammatory CNS diseases in dogs - where are we now? Part I: meningoencephalitis of unknown origin. *Vet J*. (2021) 273:105678. doi: 10.1016/j.tvjl.2021.105678

30. Barber R, Downey KL. Treatment with Cytarabine at initiation of therapy with cyclosporine and glucocorticoids for dogs with Meningoencephalomyelitis of unknown origin is not associated with improved outcomes. *Front Vet Sci*. (2022) 9:925774. doi: 10.3389/fvets.2022.925774

31. Jeffery N, Granger N. New insights into the treatment of meningoencephalomyelitis of unknown origin since 2009: a review of 671 cases. *Front. Vet. Sci*. (2023) 10:1114798. doi: 10.3389/fvets.2023.1114798

32. Lowrie M. In search of the best analysis regarding treatment for meningoencephalitis of unknown origin in dogs. *Front Vet Sci*. (2023) 9:1062114. doi: 10.3389/fvets.2022.1062114

33. Andronikou S, Albuquerque-Jonathan G, Wilmshurst J, Hewlett R. MRI findings in acute idiopathic transverse myelopathy in children. *Pediatr Radiol*. (2003) 33:624–9. doi: 10.1007/s00247-003-1004-8

34. Borchers AT, Gershwin ME. Transverse myelitis. *Autoimmun Rev*. (2012) 11:231–48. doi: 10.1016/j.autrev.2011.05.018

35. Choi KH, Lee KS, Chung SO, Park JM, Kim YJ, Kim HS, et al. Idiopathic transverse myelitis: MR characteristics. *AJNR Am J Neuroradiol*. (1996) 17:1151–60.

36. Goh C, Desmond PM, Phal PM. MRI in transverse myelitis. *J Magn Reson Imaging*. (2014) 40:1267–79. doi: 10.1002/jmri.24563

37. Krishnan C, Kerr DA. Idiopathic transverse myelitis. *Arch Neurol*. (2005) 62:1011–3. doi: 10.1001/archneur.62.6.1011

38. Transverse Myelitis Consortium Working Group. Proposed diagnostic criteria and nosology of acute transverse myelitis. *Neurology*. (2002) 59:499–505. doi: 10.1212/wnl.59.4.499

39. West TW, Hess C, Cree BA. Acute transverse myelitis: demyelinating, inflammatory, and infectious myelopathies. *Semin Neurol*. (2012) 32:097–113. doi: 10.1055/s-0032-1322586

40. Zalewski NL, Flanagan EP, Keegan BM. Evaluation of idiopathic transverse myelitis revealing specific myelopathy diagnoses. *Neurology*. (2018) 90:e96–e102. doi: 10.1212/WNL.0000000000004796

frontiers | Frontiers in Veterinary Science

TYPE Case Report
PUBLISHED 13 May 2024
DOI 10.3389/fvets.2024.1364635

OPEN ACCESS

EDITED BY
Andrea Tipold,
University of Veterinary Medicine
Hannover, Germany

REVIEWED BY
Hidetaka Nishida,
Azabu University, Japan
Aurelian-Sorin PASCA,
Iasi University of Life Sciences (IULS), Romania

*CORRESPONDENCE
Esther A. Lichtenauer
✉ esther.lichtenauer@evidensia.nl

†These authors have contributed equally to this work

RECEIVED 02 January 2024
ACCEPTED 29 April 2024
PUBLISHED 13 May 2024

CITATION
Lichtenauer EA, Santifort KM, Bergknut N, van Soens I, Beukers M and Carrera I (2024) Case report: Radiofrequency-induced thermal burn injury in a dog after magnetic resonance imaging. *Front. Vet. Sci.* 11:1364635. doi: 10.3389/fvets.2024.1364635

Case report: Radiofrequency-induced thermal burn injury in a dog after magnetic resonance imaging

Esther A. Lichtenauer[1*†], Koen M. Santifort[1,2†], Niklas Bergknut[1], Iris van Soens[1], Martijn Beukers[1] and Ines Carrera[3]

[1]IVC Evidensia Small Animal Referral Hospital Hart van Brabant, Neurology, Waalwijk, Netherlands, [2]IVC Evidensia Small Animal Referral Hospital Arnhem, Neurology, Arnhem, Netherlands, [3]Vet Oracle Teleradiology, Norfolk, United Kingdom

A 10-year-old male Shar-Pei was referred for lethargy and proprioceptive deficits of the left thoracic limb. An magnetic resonance imaging (MRI) examination of the cervical spinal column and the brain was performed. The MRI examination of the brain was normal. A left-sided C3-C4 intervertebral disc extrusion with spinal cord compression was diagnosed. Medical treatment was elected. Within a week after the MRI examination, the dog presented with deep partial-thickness skin burn wounds in both axillae. Since the specific absorption rate had not exceeded the safety limits during any of the scans and no other procedures or circumstances were identified that could possibly have resulted in burn injuries, the thermal burn injuries were diagnosed as radiofrequency (RF) burns. The wounds healed by secondary intent over the next month. RF burns are the most reported complication in humans undergoing MRI but have not been reported in veterinary patients. Clinicians and technicians should consider the potential risk for RF burns in veterinary patients and take precautions regarding positioning of the patient and take notice of any signs of burn injury when performing follow-up examinations.

KEYWORDS

skin folds, Shar-Pei, MRI complication, thermal injury, induction

Introduction

Magnetic resonance imaging (MRI) is deemed a relatively safe imaging modality. However, complications related to MRI examinations are reported more often in human patients than in veterinary patients. The most common complication, during MRI examinations, in human medicine is radiofrequency (RF) induced thermal burn injury.

Health agencies in the United Kingdom and the United States reported that RF burns account for ~50% of all MRI accidents (1, 2). These RF burns may be related to contact with conductive objects (e.g., specific clothing or ECG cables), skin-on-skin contact (e.g., skin folds or extremities in contact with the body) or contact with the bore (2). The reported severity of the burns varies from first degree (superficial-thickness) burns where only the epidermis is affected, to second degree (partial-thickness) burns where the epidermis and part of the dermis is affected, to third degree (full-thickness) burns where the epidermis and dermis are destroyed (2–5). By screening the patient prior to the MRI examination to identify conductive objects and by careful positioning of the patient during the MRI examination RF burns can be avoided (1).

FIGURE 1
Overall appearance of the dog.

Although technicians, neurologists and radiologists utilizing clinical MRI scans for veterinary patients may be aware of the complications reported in human medicine, there are, to our knowledge, no previous reports in veterinary medicine of MRI related RF burns in clinical cases. This case report documents the occurrence of RF burn injury in a Shar-Pei dog that underwent an MRI examination of the brain and cervical spinal cord.

Case description

A 10-year-old male entire Shar-Pei dog was presented with one-day history of lethargy and stumbling on the left thoracic limb. General clinical examination was unremarkable, apart from the dog being more lethargic than expected. Also of note and particularly relevant to this report is the presence of thick skin with prominent skin folds, as is typical for this breed (6). Figure 1 shows the overall appearance of the dog. Neurological examination showed proprioceptive deficits in the left thoracic limb but with intact spinal reflexes. Palpation of the neck including passive movements did not show clear signs of hyperesthesia.

Based on the results of the neurological examination, a C1-5 myelopathy (left-sided) was suspected. Intracranial disease was not completely ruled out due to the ambiguous lethargy. Hence, an MRI examination of the brain and cervical spinal cord was planned. Pre-anesthetic blood work, including hematology, biochemistry, electrolytes, C-reactive protein (CRP) and pre-prandial bile acids did not reveal any clinically significant abnormalities.

Anesthesia of the dog for the MRI examination included premedication with 0.2 mg/kg butorphanol IV and 0.1 mg/kg midazolam IV and induction with 6 mg/kg propofol IV. Maintenance of the anesthesia was achieved with inhalant isoflurane. The patient was monitored during the anesthesia with capnography and an MRI compatible esophageal stethoscope.

For the MRI scan (1.5T Canon Vantage Elan) the dog was placed in sternal recumbency, with the thoracic limbs positioned backwards next to the trunk (Figure 2). Two bottles of warm water wrapped in a blanket were placed next to the patient's abdomen and the patient was covered with a blanket. The following sequences were included for the study the brain: dorsal T1 weighted (W) inversion recovery (TR 2.4s, TE 18 ms, FOV 140 × 140 mm, slice thickness 3.0 mm, matrix 192 × 224, interslice gap 0.2 mm), sagittal T2W fast spin echo (FSE) (TR 5.5s, TE 120 ms, FOV 160 × 160 mm, slice thickness 3.0 mm, matrix 320 × 256, interslice gap 0.2 mm), axial T2W FSE (TR 5.9s, TE 90 ms, FOV 140 × 140 mm, slice thickness 3.0 mm, matrix 320 × 224, interslice gap 0.2 mm), T1W FSE (TR 0.4s, TE 10 ms, FOV 140 × 140 mm, slice thickness 3.0 mm, matrix 256 × 224, interslice gap 0.2 mm), susceptibility weighted imaging (TR 2,4s, TE 18 ms, FOV 200 × 200 mm, slice thickness 2.0 mm, matrix 320 × 304, interslice gap−1.0 mm), and diffusion-weighted imaging (TR 3,6s, TE 94 ms, FOV 200 × 225 mm, slice thickness 3.0 mm, matrix 160 × 256, interslice gap 1,5 mm) with apparent diffusion coefficient map. After intravenous contrast administration (gadolinium, 0.15 mmol/kg), axial T1W FSE (TR 0.4s, TE 10 ms, FOV 140 × 140 mm, slice thickness 3.0 mm, matrix 256 × 224, interslice gap 0.2 mm), T2W fluid attenuated inversion recovery (TR 8.0s, TE 120 ms, FOV 160 × 140 mm, slice thickness 3.0 mm, matrix 192 × 208, interslice gap 0.2 mm) and 3D T1W gradient echo (TR 10.4ms, TE 4.3 ms, FOV 180 × 160 mm, slice thickness 1.0 mm, matrix 180 × 160, interslice gap 0.0 mm) were acquired.

For the study of the cervical vertebral column the following sequences were included: dorsal short tau inversion recovery (TR 3.0s, TE 60 ms, FOV 200 × 300 mm, slice thickness 3.0 mm, matrix 192 × 288, interslice gap 0.3 mm), sagittal T2W FSE (TR 3495 ms, TE 110 ms, FOV 280 × 200 mm, slice thickness 2.5 mm, matrix 352 × 256, interslice gap 0.2 mm), T1W FSE (TR 663 ms, TE 10 ms, FOV 300 × 200 mm, slice thickness 2.5 mm, matrix 184 × 256 mm, interslice gap 0.2 mm), and axial T2W FSE (TR 5.6s, TE 115 ms, FOV 180 × 180 mm, slice thickness 2.5 mm, matrix 256 × 256, interslice gap 0.0 mm) and T1W FSE (TR 583 ms, TE 10 ms, FOV 180 × 180 mm, slice thickness 2.5 mm, matrix 192 × 192, interslice gap 0.0 mm) and 3D myelogram (TR 4s, TE 289 ms, FOV 220 × 220 mm, slice thickness 1.5 mm, matrix 224 × 272 mm, interslice gap 0.0 mm). Total scan time was ∼75 min. During our study, the maximum specific absorption rate (SAR) was 0.39 W/kg during a sequence with a duration of <6 min. The average SAR per sequence was 0.12 W/kg and the duration of all sequences was maximum 6 min. The body temperature before and after the MRI scan was respectively 37.1°C and 38.0°C.

MRI showed severe extradural spinal cord compression at the level of the C3-C4 intervertebral disc, lateralized to the left side of the spinal canal (Figure 3). A hydrated nucleus pulposus extrusion was diagnosed. In addition, a minor protrusion of the C4-C5 intervertebral disc was found, without compression of the spinal cord. The MRI examination of the brain was unremarkable.

The owners elected conservative treatment and the patient was recovered from anesthesia. Meloxicam was prescribed at 0.1 mg/kg q24h (after a single starting oral dose of 0.2 mg/kg), together with

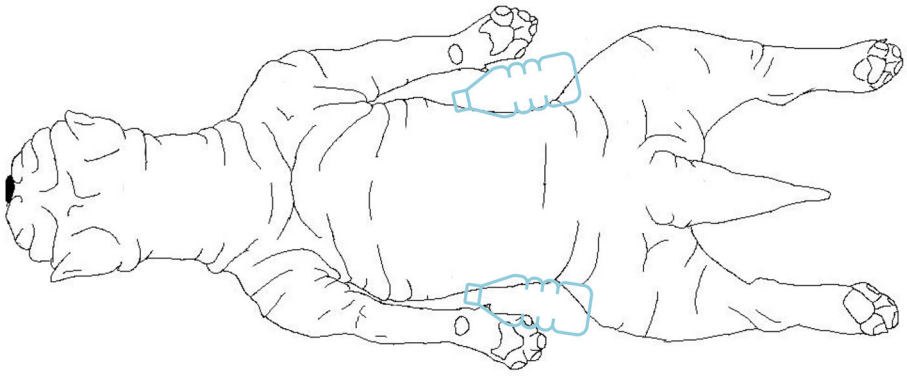

FIGURE 2
Drawing from a dorsal view of the positioning of the dog during the MRI examination. The dog was placed in sternal recumbency, with the thoracic limbs positioned backwards next to the trunk. Two bottles of warm water wrapped in a blanket were placed next to the patient's abdomen.

gabapentin 10 mg/kg q8h and in addition to rest and controlled physiotherapy for 3 weeks.

Several hours after the MRI the owner noticed a subcutaneous fluid filled pocket in the left axilla of the dog, which disappeared in the following days. Four days after the MRI the dog presented at the emergency service with a severe partial-thickness skin burn (Figure 4, week 1) and seven days after the MRI a second, but less severe, partial-thickness skin burn was noticed in the other axilla. The owner was questioned thoroughly and the procedures that had been performed were scrutinized. No other procedures or circumstances were identified that could possibly have resulted in burn injuries. Consequently, the thermal burn injuries were diagnosed as MRI related radiofrequency-induced burns.

After discussion with the owner about management options for the skin burns, conservative (non-surgical) treatment was elected. The burns were left to heal via secondary intention over the next few weeks, with regular revisits for bandaging and dressing with silver-sulfate (Figure 4). The owner still reported signs of pain despite the use of meloxicam and gabapentin. To improve the analgesia, tramadol was prescribed at 2 mg/kg q8h for 1 week in addition to the meloxicam and gabapentin. After 1 month both of the skin burns were almost healed and no further follow up was required. The meloxicam was discontinued and the gabapentin phased out over a course of 3 weeks. The amount of physical activity was slowly increased over a period of 1 month. At telephone follow-up 3 months after the initial consultation, no gait abnormalities, nor pain was reported by the owner, and the skin had almost completely healed.

Discussion

There are four main types of burn injury: thermal injury, radiation injury, chemical injury, and electrical injury (7). MRI-related burn injuries fall in the first category, but consideration may be given to use a sub-classification due to its specific nature, such as "radiofrequency-induced thermal burn injury." In our case, the owner was questioned to identify any other plausible causes of the burn injuries, including: circumstances at home; any procedures that might have been performed between the MRI and the presentation for the burn injuries; possible exposure to chemicals; contact with radiators; exposure to radiation or electrical appliances of any kind. None were identified. In any case, the sites where the burns occurred are not likely to have been exposed to other likely causes for burn injuries (such as contact with radiators). Finally, a causal relationship between the MRI and the burn injuries is supported by the time relationship between the MRI study and presentation for the burn injuries. All in all, we concluded that the burn injuries in our patient were MRI related radiofrequency-induced burns. To the authors' knowledge, this has not been documented before in veterinary medicine and is not reported in reviews on the subject (7, 8).

The thermal burn injury in the dog reported here may be classified as a local, partial-thickness burn injury. This type of burn injury may take 24–48 hours to become apparent for owners or veterinarians. Partial-thickness skin burns can heal within 1–3 weeks by re-epithelialization from hair follicles and sebaceous glands. A few days after the burn injury an eschar may be formed. Partial-thickness skin burns heal with minimal scar formation. Burn injuries can have serious local and systemic consequences for a patient and need to be addressed with care. Fortunately, the reported patient here did not experience any further significant complications during treatment of the wound (7–9).

MRI related thermal burn injuries are the most common reported adverse event in humans after an MRI scan (2) and numerous human cases have been reported in the literature (3–5, 10–15). Causes for thermal burn injuries during an MRI scan can be skin-to-skin contact, bore contact, contact with an object, not RF related or unclear (2).

Thermal burn injuries caused by radiofrequency pulses can occur when there is contact between skin and a conductive object or direct skin-to-skin contact. There are several proposed mechanisms for the occurrence of RF burns, such as inductive heating, heating of a resonant loop and the "antenna effect." With inductive heating the RF electromagnetic field causes currents to flow through a conductive object which will heat the object. This phenomenon is called ohmic heating. When these currents flow in a loop that is in a resonant condition, a resonant loop forms and the heating

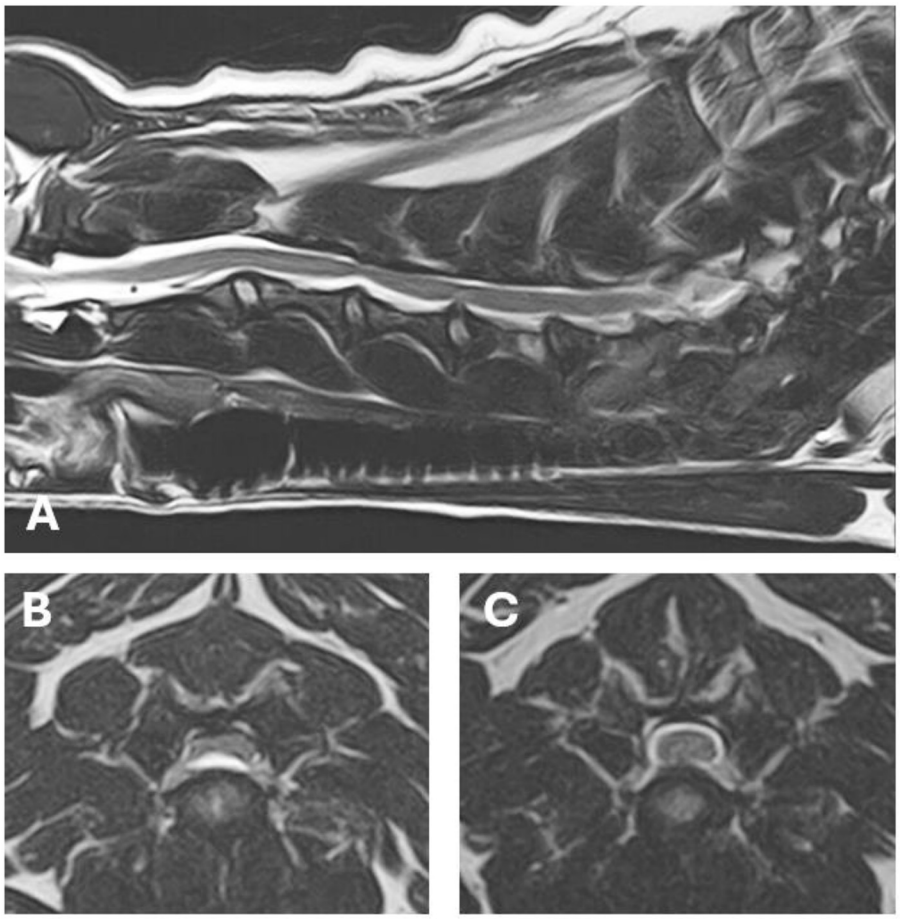

FIGURE 3
MRI images of the lesions found on MRI. **(A)** T2 weighted (W) sagittal image of the cervical spinal cord. **(B)** T2W axial image at the level of the C3–C4 hydrated nucleus pulposus extrusion with severe extradural spinal cord compression. **(C)** T2W axial image at the level of the minor C4–C5 intervertebral disc protrusion.

will become significant. With the "antenna effect" an elongated conductive object forms a resonant loop (13, 15, 16). Dempsey et al. have shown that the temperature of a conductive object can rise by 0.6°C with inductive heating, and by 61.1°C and 63.5°C with heating of a resonant loop or a resonant antenna, respectively (16).

RF heating increases with a stronger magnetic field. Theoretically, RF heating is proportional to the square of the static magnetic field (17). Now that the magnetic field strength of MRI devices are generally increasing, and 1.5T or 3.0T are becoming more commonly used in veterinary practice, there is a potentially increasing risk for RF burns.

Theoretical heating of the tissues of the patient caused by the RF pulses is evaluated by the SAR, which is depicted in watts per kilogram bodyweight. The SAR can be calculated taking into account the patients height, weight, and the scan settings such as for example RF pulse frequency and the angulation of the RF magnetic field (18). There are guidelines with upper allowable SAR values for safe MRI examinations in humans. The maximal SAR that is allowed is <4.0 W/kg over 6 min. With this SAR, the body temperature of the person will rise by 1°C maximum (1). For animals, no safety limits have been established for the SAR. During our study, the maximum SAR was 0.39 W/kg during a sequence with a duration of <6 min. The average SAR per sequence was 0.12 W/kg and the duration of all sequences was maximum 6 min. This could not have significantly contributed to the thermal burn injuries. However, when a resonant conductive loop was formed, focal overheating could have occurred in our patient, even when the SAR did not exceed the upper limit.

As is indicated with the SAR, the time of an MRI examination itself may be one of the factors involved in predicting the risk for thermal burn injuries in patients. In this case, the brain as well as the cervical spinal cord was scanned. Reducing scan time (e.g., by leaving out certain sequences that may not be necessary in every case), reduces the total energy 'transmitted' to the body of the patient. It has been shown that 'rapid' protocols for brain imaging yield comparable differential diagnoses compared to a "full" brain protocol (19). Both the occurrence and severity of burn injuries may be influenced by total scanning time.

In our case, the patient was of a dog breed known for its loose and thick skin with prominent skin folds (6). Also, the patient had thin fur in its axillae. The skin and fur characteristics, together with the positioning of the patient during the MRI examination

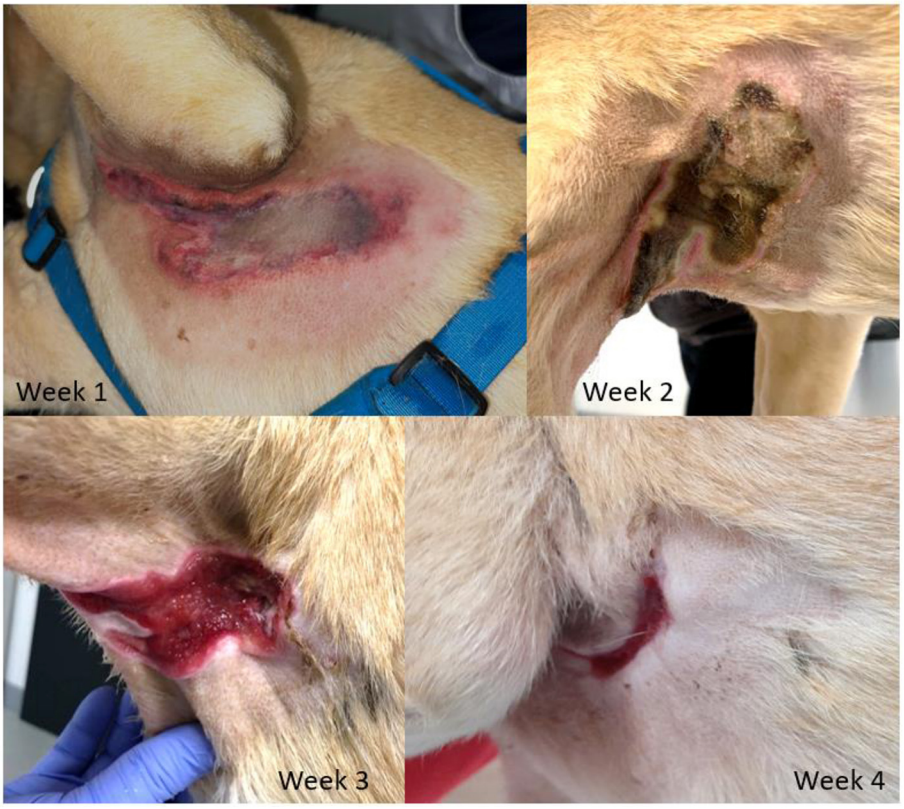

FIGURE 4
Photographical series of the burn wound in the left axillary region (sequence over a 4-week time span).

make it likely that skin-to-skin contact occurred between skin folds in the axillae. There was no contact between the dog and conductive objects or the bore. Even though the patient underwent an extensive MRI examination, the SAR had not been exceeded. Based on these data, we concluded that the thermal burn injuries reported in our patient must be RF thermal burn injuries by skin-to-skin contact. It is also possible that the thick skin of the Shar-Pei and its histological and molecular characteristics predispose this breed to RF thermal burn injury occurrence. Although this is merely a theory, we would propose to carefully monitor dogs of this breed undergoing MRI studies for RF thermal burn injuries and take precautionary measures as discussed below.

The fact that our patient was under general anesthesia and thus not able to report any pain may have contributed to the occurrence of the RF burns. Human patients that are conscious during the MRI examination can press the alarm-button when they feel pain or a hot sensation. This safety feature is unfortunately not possible in veterinary patients. During the monitoring of the anesthesia of our patient, a temporary increase in the heartrate was noticed. In retrospect we assume that this may have been caused by pain due to the occurrence of the RF burns.

Precautions must be taken to prevent RF burns. In human medicine MRI safety guidelines are available (1, 20). In these guidelines recommendations are made on how to prevent RF burns. No specific protocols exist for the veterinary patient. By extrapolation from the human safety guidelines we propose some considerations listed in Table 1 to prevent thermal burn injuries when performing MRI studies in veterinary patients.

TABLE 1 **Proposed considerations to reduce the risk of MRI-induced radiofrequency burns in veterinary patients.**

Screen patients	Screen patients for implants, devices and other metallic objects. Unknown objects should be assumed unsafe.
Screen objects	Screen objects in the scan room for MRI safety.
No wearables	Remove all leashes, collars, clothing, anti-parasitic collars, etcetera, from the patient
Positioning	Position the patient to avoid skin-to-skin contact
Padding	Place protective padding in between areas where there is a risk for skin-to-skin contact, contact with the bore, coils or cables.
Cables	Route cables out of the scanner in a straight line and don't let cables touch the patient
SAR	Follow the safety limits of the SAR and use the lowest SAR as possible.
Monitor patient	Monitor the patient; e.g., increases in respiratory rate or heart rate may indicate a painful sensation caused by a RF burn.

In conclusion, MRI related radiofrequency-induced thermal burn injuries can occur in dogs undergoing standard MRI examinations using a 1.5T scanner. Clinicians and technicians should be aware of the potential risk of this complication and 1/

take precautions to prevent its occurrence 2/ carefully inspect (at-risk) patients after MRI studies to take adequate measures in case of burn injuries.

Data availability statement

The raw data supporting the conclusions of this article will be made available by the authors, without undue reservation.

Ethics statement

Ethical approval was not required for the studies involving animals in accordance with the local legislation and institutional requirements because the data used in this case report was obtained during a medical consultation requested by the owner of the animal. Written informed consent was obtained from the owners for the participation of their animals in this study.

Author contributions

EL: Conceptualization, Funding acquisition, Investigation, Project administration, Visualization, Writing – original draft, Writing – review & editing. KS: Conceptualization, Supervision, Visualization, Writing – original draft, Writing – review & editing. NB: Conceptualization, Investigation, Supervision, Writing – review & editing. IS: Supervision, Writing – review & editing. MB: Visualization, Writing – review & editing. IC: Supervision, Visualization, Writing – review & editing.

Funding

The author(s) declare that financial support was received for the research, authorship, and/or publication of this article. The publication fee was covered by the IVC Evidensia.

Acknowledgments

The authors would like to thank Wendy Lichtenauer for creating Figure 2 and Jeanette Pijnenburg for assistance in processing the sequence information of the MRI studies.

Conflict of interest

IC was employed by the Vet Oracle Teleradiology.

The authors declare that the research was conducted in the absence of any commercial or financial relationships that could be construed as a potential conflict of interest.

Publisher's note

All claims expressed in this article are solely those of the authors and do not necessarily represent those of their affiliated organizations, or those of the publisher, the editors and the reviewers. Any product that may be evaluated in this article, or claim that may be made by its manufacturer, is not guaranteed or endorsed by the publisher.

References

1. Medicines and Healthcare products Regulatory *Agency. Safety Guidelines for Magnetic Resonance Imaging Equipment in Clinical Use.* (2021) Available online at: https://www.gov.uk/government/publications/safety-guidelines-for-magnetic-resonance-imaging-equipment-in-clinical-use (accessed September 8, 2023).

2. Delfino JG, Krainak DM, Flesher SA, Miller DL. MRI-related FDA adverse event reports: a 10-yr review. *Med Phys.* (2019) 46:5562–71. doi: 10.1002/mp.13768

3. Pietryga JA, Fonder MA, Rogg JM, North DL, Bercovitch LG. Invisible metallic microfiber in clothing presents unrecognized MRI risk for cutaneous burn. *AJNR Am J Neuroradiol.* (2013) 34:E47–50. doi: 10.3174/ajnr.A2827

4. Tokue H, Tokue A, Tsushima Y. Unexpected magnetic resonance imaging burn injuries from jogging pants. *Radiol Case Rep.* (2019) 14:1348–51. doi: 10.1016/j.radcr.2019.08.015

5. Ross JR, Matava MJ. Tattoo-induced skin "burn" during magnetic resonance imaging in a professional football player: a case report. *Sports Health.* (2011) 3:431–4. doi: 10.1177/1941738111411698

6. Zanna G, Fondevila D, Ferrer L, Espada Y. Evaluation of ultrasonography for measurement of skin thickness in Shar-Peis. *Am J Vet Res.* (2012) 73:220–6. doi: 10.2460/ajvr.73.2.220

7. Vaughn L, Beckel N. Severe burn injury, burn shock, and smoke inhalation injury in small animals. Part 1: burn classification and pathophysiology. *J Vet Emerg Crit Care.* (2012) 22:179–86. doi: 10.1111/j.1476-4431.2012.00727.x

8. Pavletic MM, Trout NJ. Bullet, bite, and burn wounds in dogs and cats. *Vet Clin North Am Small Anim Pract.* (2006) 36:873–93. doi: 10.1016/j.cvsm.2006.02.005

9. DeSanti L. Pathophysiology and current management of burn injury. *Adv Skin Wound Care.* (2005) 18:323–34. doi: 10.1097/00129334-200507000-00013

10. Dempsey MF, Condon B, Hadley DM. MRI safety review. *Semin Ultrasound CT MR.* (2002) 23:392–401. doi: 10.1016/S0887-2171(02)90010-7

11. Chaljub G, Kramer LA, Johnson III RF, Johnson Jr RF, Singh H, Crow WN, et al. Projectile cylinder accidents resulting from the presence of ferromagnetic nitrous oxide tanks in the MR suite. *AJR Am J Roentgenol.* (2001) 177:27–30. doi: 10.2214/ajr.177.1.1770027

12. Alsing KK, Johannesen HH, Hansen RH, Serup J. Tattoo complications and magnetic resonance imaging: a comprehensive review of the literature. *Acta Radiol.* (2020) 61:1695–700. doi: 10.1177/0284185120910427

13. Abdel-Rehim S, Bagirathan S, Al-Benna S, O'Boyle C. Burns from ECG leads in an MRI scanner: case series and discussion of mechanisms. *Ann Burns Fire Disasters.* (2014) 27:215–8.

14. Watari T, Tokuda Y, MRI. thermal burn injury: an unrecognized consequence of wearing novel, high-tech undergarments. *QJM.* (2018) 111:495–6. doi: 10.1093/qjmed/hcy064

15. Vister J, van Erling L, Steens SC, Meijer FJA. Brandwonden tijdens een MRI-scan ("Burn during an MRI scan"). *Ned Tijdschr Geneeskd.* (2014) 158:A7927.

16. Dempsey MF, Condon B, Hadley DM. Investigation of the factors responsible for burns during MRI. *J Magn Reson Imaging.* (2001) 13:627–31. doi: 10.1002/jmri.1088

17. Kim SJ, Kim KA. Safety issues and updates under MR environments. *Eur J Radiol.* (2017) 89:7–13. doi: 10.1016/j.ejrad.2017.01.010

18. Tang M, Yamamoto T. Progress in understanding radiofrequency heating and burn injuries for safer MR imaging. *Magn Reson Med Sci.* (2023) 22:7–25. doi: 10.2463/mrms.rev.2021-0047

19. Johnson KA, Sutherland-Smith J, Oura TJ, Sato AF, Barton B. Rapid brain MRI protocols result in comparable differential diagnoses versus a full brain protocol in most canine and feline cases. *Vet Radiol Ultrasound.* (2023) 64:86–94. doi: 10.1111/vru.13134

20. U.S. Food and Drug Administration. *MRI Safety Posters.* (2020) Available online at: https://www.fda.gov/radiation-emitting-products/mri-magnetic-resonance-imaging/mri-safety-posters (accessed March 19, 2024).

frontiers | Frontiers in Veterinary Science

TYPE Case Report
PUBLISHED 15 May 2024
DOI 10.3389/fvets.2024.1346816

OPEN ACCESS

EDITED BY
Andy Shores,
Mississippi State University, United States
Andrea Tipold,
University of Veterinary Medicine Hannover, Germany

REVIEWED BY
Gerardo Fatone,
University of Naples Federico II, Italy
Richard Shinn,
Virginia Tech, United States

*CORRESPONDENCE
Razvan Grigore Cojocaru
razvan_cojocaru91@yahoo.com
Cristina Gaspar
gasparcristina99@yahoo.com

†These authors have contributed equally to this work and share senior authorship

RECEIVED 30 November 2023
ACCEPTED 25 April 2024
PUBLISHED 15 May 2024

CITATION
Cojocaru RG, Sicoe B, Gaspar C, Grigoreanu A, Orghici G, Tibru I and Lacatus R (2024) Case report: Double adjacent ventral slot in two medium-sized breed dogs.
Front. Vet. Sci. 11:1346816.
doi: 10.3389/fvets.2024.1346816

Case report: Double adjacent ventral slot in two medium-sized breed dogs

Razvan Grigore Cojocaru[1]*, Bogdan Sicoe[1], Cristina Gaspar[1]*, Alexandra Grigoreanu[1], Gabriel Orghici[1], Ioan Tibru[1†] and Radu Lacatus[2†]

[1]Faculty of Veterinary Medicine, University of Life Sciences "King Mihai I", Timisoara, Romania, [2]Faculty of Veterinary Medicine, University of Agricultural Sciences and Veterinary Medicine, Cluj-Napoca, Romania

Two medium-sized, 7-year-old dogs, with no previous history of pain, presented with acute neurologic symptoms consistent with intervertebral disk disease. Both cases had CT, where cervical pathology was identified. In one dog, the diagnosis was singular extensive cervical disk herniation with possible epidural hemorrhage and in the other, the diagnosis was multiple-site cervical disk herniation. The first dog, a Shar-Pei, underwent treatment with two standard adjacent ventral slots between the C4–C5 and C5–C6 intervertebral disk spaces and a fenestration between the C3 and C4 intervertebral disk spaces. The second case, a beagle, underwent a double adjacent standard ventral slot between the C5–C6 and C6–C7 intervertebral disk spaces. Both dogs recovered uneventfully after the surgery and showed no signs of recurrence during a 2-year follow-up period. This is the first detailed report of the use of a double adjacent ventral slot as a treatment for spinal decompression in medium-sized dogs with multiple-site spinal cord compression.

KEYWORDS

double adjacent ventral slot, cervical disk disease, medium-sized dogs, IVDE, tetraplegia

Introduction

Intervertebral disk disease (IVDD) is one of the most common causes of spinal cord dysfunction in dogs that present acute neurologic deficits (1).

Clinical signs can vary depending on the type of herniation, the location, and the extent of the compression (2).

The most common location for disk herniation in dogs is in the thoracolumbar region of the vertebral canal, with 16 to 25% of cases reported in the cervical region (3). The majority of dogs with cervical disk herniation present with a nucleus pulposus extrusion rather than an annulus protrusion (1, 3–7).

The cervical disk extrusions are most commonly encountered in chondrodystrophic dogs and they usually have an acute onset (1, 8).

Traditionally, disk herniations were divided into two distinct types: Hansen Type 1 (IVD extrusion) and Hansen Type 2 (IVD protrusion). A third type was also described as an acute non-compressive or high-velocity low-volume disk disease (9–12).

More recently, Fenn et al. (4) suggested the need for more precise classification, considering the latest advances in veterinary diagnostic techniques (magnetic resonance imaging), proposing the following specific pathologies individually: Hansen type 1/acute

(IVD extrusion); Hansen type 2/chronic (IVD protrusion); acute IVD extrusion (HT1) with extensive hemorrhage; acute non-compressive nucleus pulposus extrusion (ANNPE); hydrated nucleus pulposus extrusion (HNPE); intradural/intramedullary IVD extrusion (IIVDE); traumatic IVD extrusion; and fibrocartilaginous embolic myelopathy (FCEM).

In the cervical region, the incidence rate of IVDE varies between 16 and 25% and is more commonly encountered in small breed dogs, where C3–C4 is the most commonly reported site. Hansen type 2 disk protrusion is more commonly found in large breed dogs between the C5 and C6 intervertebral disk spaces (3, 13).

Conservative treatment and surgical treatment have been described for canine patients with cervical disk extrusion, with the ventral approach to the cervical vertebrae being the most common choice of decompression treatment (14, 15).

The advantages of the ventral slot include minimal dissection to access the vertebral bodies to perform the slot and also a prophylactic fenestration to the adjacent disks. The main disadvantages reported for this technique include venous sinus hemorrhage, hypoventilation, respiratory distress, cardiac arrhythmias, instability/ subluxation of the vertebras, spinal cord trauma, and insufficient exposure to intraforaminal and lateral disk extrusion and postoperative infection (1, 16–18).

A double or even triple adjacent ventral slot has been described for multiple disk herniations or for lesions that have a longer extent but have not been reported in medium- and large-breed dogs (19, 20).

Case description

Two medium-sized (10–25 kg) (21), middle-aged dogs, namely, a Shar-Pei (case 1 - entire female, 18 kgs, 7 years and 10 months) and a Beagle (case 2—entire male, 25 kgs, 7 years and 5 months) were referred for having an acute onset of neurologic signs (ataxia and neurologic deficits).

The owners reported an acute onset of the neurologic signs, which started 24–48 h before the presentation. At the time of presentation, both dogs did not have any history of other health problems and did not show any signs of pain before the onset of the clinical signs. A general and neurologic examination was conducted and nothing abnormal was detected apart from the following clinical signs:

Case 1 was non-ambulatory, tetraplegic, and had a moderate pain reaction on the hyperextension and hyperflexion of the neck. The withdrawal reflex and patellar reflex were reduced in the right pelvic limb and deep pain perception was reduced in both pelvic limbs.

Case 2 was non-ambulatory, tetraplegic with spontaneous severe pain reaction at any attempt of hyperflexion of the neck. Withdrawal reflexes were reduced in both pelvic limbs and deep pain perception.

These findings were consistent with upper motor neuron deficit in the thoracic limbs and lower motor neuron deficit in the pelvic limbs.

For both cases, a blood sample was taken from the jugular vein and submitted to the laboratory for biochemistry and hematology analysis, and no abnormality was detected.

Following the blood analysis, the dogs were submitted for a CT scan of the cervical region for diagnosis purpose. The CT scan was performed under sedation as described: a 20 G IV catheter was placed in the right cephalic vein and a 0.1 mg/kg butorphanol with 0.01 mg/kg of medetomidine was administered intravenously. The positioning of the dog was in dorsal recumbency. The CT findings were as follows:

Case 1

The CT scan showed hyperattenuating material present in the vertebral canal at the level of C4–C5, with the intervertebral space at this level being visibly narrowed. The material was located ventral and left lateral to the spinal cord. Caudally, the mild hyperattenuating material extended to the caudal part of the C5 vertebral body. The material presented higher Hounsfield unit values (88–101 HU) compared to the medulla (29–44 HU) and occupied 47.8% of the vertebral canal diameter (Figures 1, 2). Ventral extradural material that was isoattenuating to the spinal cord was present at the level of the C5–C6 disk (Figure 3). The C3–C4 intervertebral space was visibly narrowed, with *in situ* mineralized material and no visible spinal cord compression (Figure 2). These findings were consistent with C4–C5 disk extrusion with moderate to severe compression and C5–C6 mild Hansen type 1 extrusion.

Case 2

The CT scan revealed hyperattenuating heterogeneous material present in the vertebral canal at the level of intervertebral disk space C5–C6, with caudal extension near the C6–C7 intervertebral disk space and minimal cranial extension. The material was located ventral and right lateral to the spinal cord, presented higher HU values (97–185) compared to the spinal cord (12–51), and occupied 45% of the vertebral canal diameter. The C5–C6 intervertebral disk space was markedly narrowed when compared to the adjacent intervertebral spaces (Figures 4–7). These findings were consistent with the Hansen type 1 disk extrusion with moderate spinal cord compression.

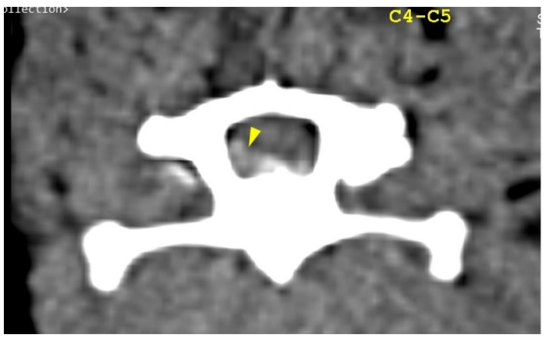

FIGURE 1
Transverse section of the C4–C5 intervertebral disk space. Yellow arrowhead highlights mild hyperattenuating extruded disk material and possible hemorrhage, located ventral and left lateral to the spinal cord.

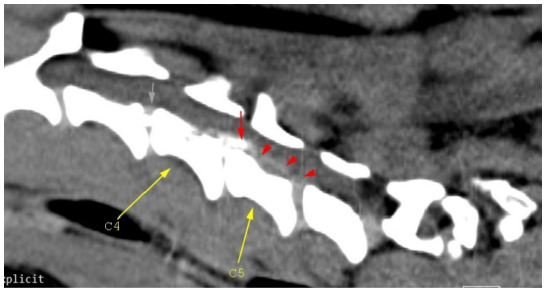

FIGURE 2
Mid-cervical sagittal view. The gray arrow depicts *in situ* C3–C4 disk mineralization; the red arrow highlights mineralized herniated disk material (C4–C5), and the red arrowheads highlight mild hyperattenuating disk material and possible hemorrhage. Malalignment of the cervical-thoracic segment is observed and this is due to the positioning of the dog.

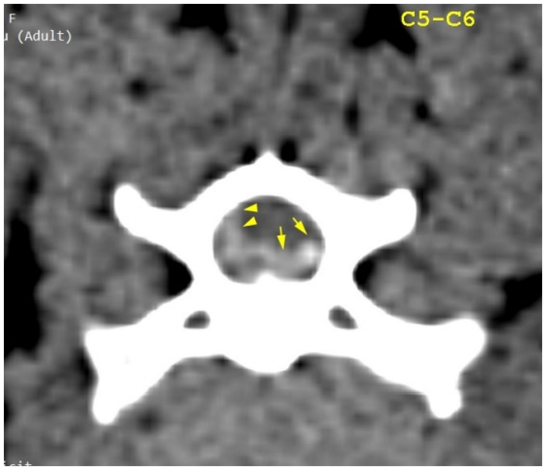

FIGURE 3
Transverse section of the C5–C6 intervertebral disk space. Yellow arrowheads highlight mild hyperattenuating herniated disk material and possible hemorrhage; yellow arrows highlight hyperattenuating disk material.

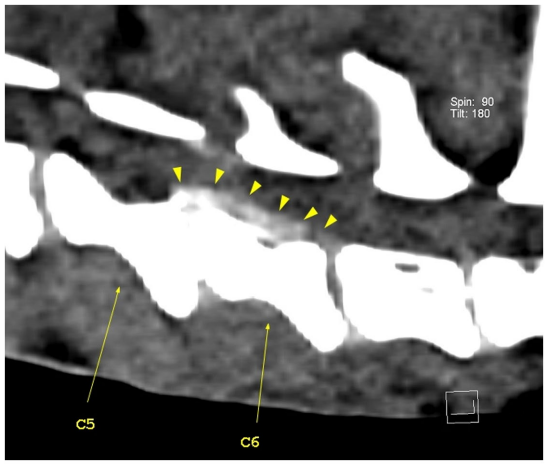

FIGURE 4
Sagittal view of the caudal cervical segment of the vertebral column. The C5–C6 intervertebral disk space is narrower than the adjacent ones, with visible heterogenous hyperattenuating herniated disk material (yellow arrowheads). The herniated disk material extends caudally to the caudal part of the C7 vertebral body.

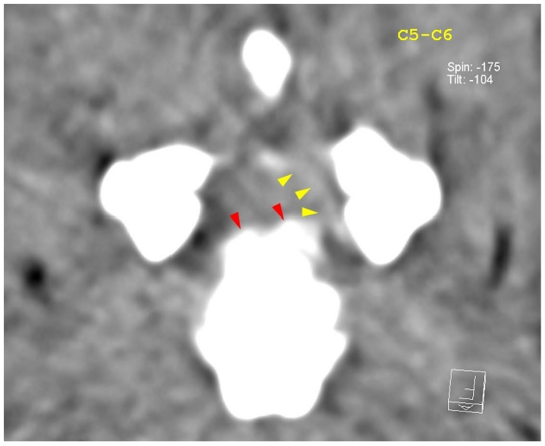

FIGURE 5
Transverse view at the level of the C5–C6 intervertebral disk space. Red arrowheads highlight the mineralized component of the herniated disk, while the yellow arrowheads highlight mild hyperattenuating disk material with possible hemorrhage.

Both dogs were tetraplegic with an upper motor neuron deficit in the thoracic limbs; this finding is suggestive of C1–C5 cervical spine pathology. Although both dogs had some degree of lower motor neuron deficit in the pelvic limbs, there was no abnormality detected at the level of the thoracolumbar spinal cord.

The CT findings were discussed with the owners, and the treatment chosen for both of the dogs was to surgically decompress the spinal cord by performing a double adjacent ventral slot. For the first case, a standard ventral slot was performed between the C4–C5 and C5–C6 intervertebral disk spaces, and a fenestration was performed between the C3 and C4 intervertebral disk spaces. For the second case, a standard ventral slot was performed between the C5–C6 and C6–C7 intervertebral disk spaces. Both patients were prepared immediately for the surgical procedure, as described by Platt & da Costa (22).

Fluid therapy was initiated using a balanced crystalloid solution of sodium chloride 0.9% at a rate of 10 mL/kg/h to maintain hydration and electrolyte balance. The premedication consisted of the administration of 0.3 mg/kg/IV of methadone and 0.01 mg/kg/IV of medetomidine, and the general anesthesia was induced with 0.5–1 mg/kg/IV of propofol. Both patients were intubated, and the anesthesia was maintained with isoflurane and oxygen. A dose of 22 mg/kg of cefuroxime was administered approximately 20 min prior to the skin incision, and it was repeated one more time after 90 min, during the surgical procedure. The total duration of the procedure for case 1 was 150 min and for case 2 was 170 min.

Both dogs were placed in dorsal recumbency and prepared for surgery and a single dose of 10 mg/kg/IV of paracetamol and 0.2 mg/kg/IV of meloxicam was administered in the preoperative period. Hemorrhage was controlled using bipolar cautery. A *Standard Ventral*

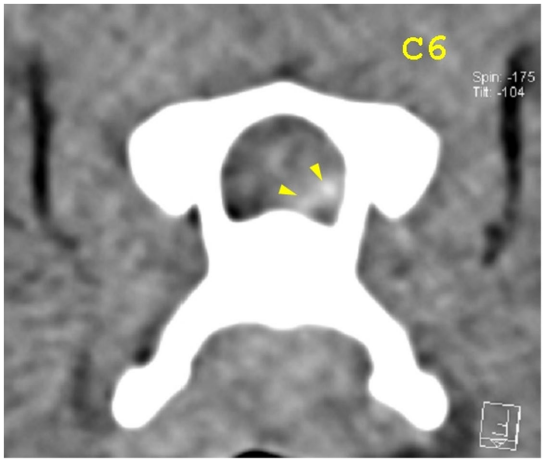

FIGURE 6
Transverse view at the caudal end of the C6 vertebra. Yellow arrowheads highlight mild hyperattenuating disk material with possible hemorrhage.

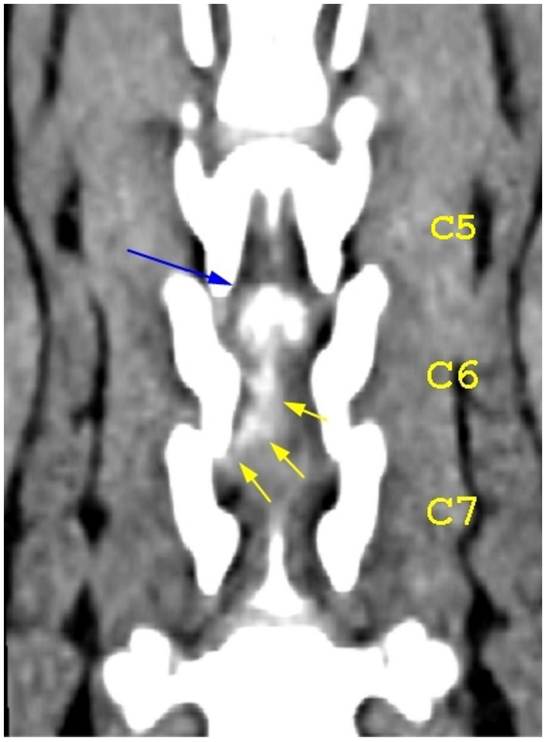

FIGURE 7
Dorsal view of the caudal cervical segment of the vertebral column. The blue arrow highlights the mineralized component of the herniated disk at the level of the C5–C6 intervertebral disk space; the yellow arrows highlight the caudal extension of the herniated disk material.

Slot was performed for both patients by using an electric drill and a combination between a 3 mm and a 4 mm burr. The size of the slot was 30% of the vertebral body length and approximately 50% of the vertebral width. For case 1, a prophylactic fenestration was performed between C3 and C4, using a no. 11 surgical blade and a curette, as mineralized material was present *in situ* at that level on the CT scan. The skin was closed in a routine fashion using 3/0 USP polydioxanone, and no attempt to place a drain was made as it was not considered necessary.

Both dogs recovered well from anesthesia, and no complication was noted during the procedure and the recovery time. Ice packing was performed for approximately 10–20 min every 4 h in the first 24 h after the surgery to prevent excessive swelling and seroma formation.

The postoperative treatment included the administration of meloxicam 0.1 mg/kg PO for 5 days, paracetamol 10 mg/kg PO for 2 days, and gabapentin 10–20 mg/kg/8 h PO for 7 days. A second dose of 0.3 mg/kg/IV of methadone was repeated at 4 h after the first administration. Only two doses of methadone were administrated for both patients as the pain score showed no necessity for supplementary analgesics. The modified Glasgow Composite Pain Scale was used for both patients for the time being hospitalized. Both patients were evaluated by the surgeon in the morning, using the composite pain scale, and the analgesic protocol was guided by the total pain score.

Both patients were hospitalized for 5 days postoperatively, and the diet regime during this period was made using resting energy requirement (RER) calculations. Both patients were ambulatory at the time of discharge, and the owners were advised to enforce strict rest for the next 21 days, and only short walks on a leash were permitted during this period. Follow-up examinations were performed 21 days postoperatively, and the modified Glasgow Composite Pain Scale showed no signs of pain at the surgical site or on the hyperflexion or hyperextension of the neck. The neurologic signs were completely restored, and the owners did not report any complications during this period.

Both dogs came for follow-up examinations at 3 months and 6 months after the surgery, and their owners reported normal activity with no signs of neurologic dysfunction.

Discussion

The ventral slot procedure is one of the most common neurosurgical procedures used to treat cervical intervertebral disk herniation in dogs (18). Many other procedures have been described for cervical decompression, including disk fenestration, dorsal laminectomy, hemilaminectomy, and the slanted ventral slot (23, 24). The standard ventral slot is the most commonly used procedure because the direction of the herniated disk usually occurs dorsomedially and also this technique provides access to the floor of the vertebral canal compared to other techniques (1, 18)..

Several complications have been associated with this procedure, such as hemorrhage from the venous sinus, vertebral subluxation, hypoventilation, and insufficient exposure to the lesions that are lateralized, which can lead to incomplete spinal cord decompression. Although other techniques seem more appropriate for lateralized disk material, other authors have reported good clinical outcomes by using a ventral slot even for lateralized disk material (16, 18, 25, 26).

In one of our cases (case 2—Beagle), it was reported that there was minimal bleeding from the venous sinus that resolved with lavage with sterile saline solution at 37°C in the slot and waiting for 5 min. Apart from this inconvenience, no other complication was noted in any of our cases.

In 2020, Kang et al. (27) described the advantages and limitations of the vertebral window provided by a standard ventral slot when compared with a slanted ventral slot, and the results showed that both techniques have limitations, especially in cases where the disk have migrated caudally. The modified slanted ventral slot provides good access to the herniated disk as long as the disk has not migrated caudally, with obvious limitations reported for C3–C4 and C5–C6 intervertebral disk spaces. Considering the location and the large amount of disks that need to be removed for both of our patients, a standard ventral slot procedure was used for both of them. The author recommends that rigorous presurgical planning based on CT imaging should help in the selection of the most appropriate surgical technique that will allow sufficient disk removal and a good clinical outcome.

In 2020, Guo et al. (28) conducted a retrospective study in which they compared the clinical outcome between two groups of canine patients who suffered from single- or multiple-site cervical disk herniation. A total of 123 dogs underwent a single standard ventral slot procedure and 62 dogs underwent multiple-site standard ventral slot procedures. From the total number of dogs that underwent multiple ventral slot decompression, none of the dogs were large breeds, and only two dogs were included in the medium breed category. The author also reported that two of the dogs from the multiple-site ventral slot category showed the following outcome: one of them died of possible cardiac arrest 3 days postoperatively and the other did not become ambulatory at day 4 postoperatively, and no data were reported after that. Considering that only 2 patients were of medium breed and there is currently no information about a double adjacent ventral slot in a large breed dog, it would have been helpful if the author had reported the category to which the two patients belonged.

Merbl et al. (19) reported in 2017 the outcome after performing a triple adjacent ventral slot in a toy breed (Pomeranian) suffering from severe extradural compression due to mineralized disk extrusions between C3–C4, C4–C5, and C5–C6. The author reports that the size and shape of the slot were modified to prevent any postoperative destabilization of the cervical spine, and a cervical splint was also used in the postoperative period to minimize neck movement. The planning of the slot was performed based on the CT findings in a way that will allow complete removal of the herniated disk material. The length of all the slots was approximately 25% smaller than a standard ventral slot, and the width was smaller in C4–C5 and C5–C6 when compared with C3–C4. We can presume that these changes in the width and the length of the ventral slot could have a significant contribution to the prevention of postoperative complications, such as vertebral subluxation, as mentioned in the literature (25). In this case presentation, the correlation between the CT findings and the intraoperative aspect of the retrieved disk material suggests that the disk extrusion between C3 and C4 was highly incriminating for the clinical signs. Overall, the clinical outcome for this particular case was good, with the author suggesting that although the patient improved significantly postoperatively, minor pelvic limb ataxia and proprioceptive deficits were present (19).

In 2022, Olender et al. (20) reported a good long-term prognosis in four small breed dogs (French bulldogs) suffering from extensive cervical IVDE that were treated with double adjacent ventral slots. In all four cases, the extruded material was located ventrolaterally, and the herniated content also had a hemorrhagic component. However, the author investigates the fact whether the hemorrhagic component of the extruded material does or does not require a surgical decompression or would resolve spontaneously over time. Considering that the origin and the amount of the hemorrhage can vary at that level and that in the absence of an MRI, it is hard to assess the extent of the intradural/intramedullary damage, and also the fact that hemorrhage is associated with high risks of tissue liquefication and increased intramedullary pressure, leading to myelomalacia (29), we recommend that any sort of compression at this level should be managed by surgical decompression.

We used a CT scan to evaluate our patients and found specific lesions that matched their neurolocalization. Although the literature suggests that a non-contrast CT scan is a good option to accurately evaluate canine patients with IVDD, especially if the lesion corresponds with the neurolocalization (30–32), we suggest that magnetic resonance imaging would have been a better option if intradural or intramedullary lesions were present.

An inverted cone technique is recommended as it involves less bone removal, resulting in lower risks of hemorrhage and vertebral subluxation (22, 33). In both of our cases, a standard ventral slot was performed, where the length of the slot was approximately 50% of the total length of the vertebra and its width was approximately 25–27% of the total width of the vertebra. In case 1, a triple ventral slot was considered for C3–C4 due to the presence of mineralized disk material; however, since there was no compression at that level, a prophylactic fenestration was performed instead.

Both our cases showed 100% clinical recovery, with no signs of recurrence during a 2-year follow-up period. We advised the owners to look out for any signs of neck pain that could be related to vertebral subluxation during this period, but no such signs were reported in the follow-up period. Even though both of our patients were 7-year-old, intact, medium-sized dogs, the small number of cases does not allow us to conclude the incidence of double adjacent disk herniation in these specific patients.

To date, data about the treatment of dogs with multiple adjacent cervical disk herniations are limited. Our case presentation shows good clinical outcomes following this procedure in two medium-sized dogs with multiple cervical disk herniations.

Data availability statement

The raw data supporting the conclusions of this article will be made available by the authors, without undue reservation.

Ethics statement

Ethical approval was not required for the studies involving animals in accordance with the local legislation and institutional requirements because the reason we did not require ethical approval is that the treatment that we applied was for patients who presented to the small animal hospital with pathologies that required a specific therapeutic surgical treatment that involved a combination of validated surgical procedures previously described. Written informed consent was obtained from the owners for the participation of their animals in this study.

Author contributions

RC: Conceptualization, Investigation, Methodology, Validation, Writing – original draft, Writing – review & editing. BS: Formal analysis, Investigation, Software, Writing – original draft, Writing – review & editing. CG: Conceptualization, Formal analysis, Writing – original draft, Writing – review & editing. AG: Formal analysis, Writing – original draft. GO: Investigation, Validation, Visualization, Software, Writing – review & editing. IT: Supervision, Validation, Writing – review & editing. RL: Supervision, Validation, Writing – review & editing.

Funding

The author(s) declare that no financial support was received for the research, authorship, and/or publication of this article.

Conflict of interest

The authors declare that the research was conducted in the absence of any commercial or financial relationships that could be construed as a potential conflict of interest.

Publisher's note

All claims expressed in this article are solely those of the authors and do not necessarily represent those of their affiliated organizations, or those of the publisher, the editors and the reviewers. Any product that may be evaluated in this article, or claim that may be made by its manufacturer, is not guaranteed or endorsed by the publisher.

References

1. Coates JR. Intervertebral disc disease. *Vet Clin North Am Small Anim Pract*. (2000) 30:77–110. doi: 10.1016/s0195-5616(00)50004-7

2. Webb AA, Ngan S, Fowler D. Spinal cord injury II: prognostic indicators, standards of care, and clinical trials. *Can Vet J*. (2010) 51:598–604.

3. Chang Y-P, Huang W-H, Lua W-Z, Wong W, Liu I-H, Liu C-H. Outcomes in dogs with multiple sites of cervical intervertebral disc disease treated with single ventral slot decompression. *Vet Sci*. (2023) 10:377. doi: 10.3390/vetsci10060377

4. Fenn J, Olby NJ. Canine spinal cord injury consortium (CANSORT-SCI). Classification of intervertebral disc disease. *Front Vet Sci*. (2020) 7:579025. doi: 10.3389/fvets.2020.579025

5. Gage ED. Incidence of clinical disc disease in the dog. *J Am Anim Hosp Assoc*. (1975) 11:135–8. doi: 10.2460/javma.240.11.1300

6. Goggin JE, Li AS, Franti CE. Canine intervertebral disc disease: characterization by age, sex, breed, and anatomic site of involvement. *Am J Vet Res*. (1970) 31:1687–92.

7. Shores A, Danel A (2023) Intervertebral disk disease in dogs. Today's veterinary Practice Available at: https://todaysveterinarypractice.com/neurology/intervertebral-disk-disease-in-dogs/

8. Fluehmann G, Doherr MG, Jaggy A. Canine neurological diseases in a referral hospital population between 1989 and 2000 in Switzerland. *J Small Anim Pract*. (2006) 47:582–7. doi: 10.1111/j.1748-5827.2006.00106.x

9. Gouveia D, Carvalho C, Cardoso A, Gamboa Ó, Almeida A, Ferreira A, et al. Early Locomotor training in Tetraplegic post-surgical dogs with cervical intervertebral disc disease. *Animals*. (2022) 12:2369. doi: 10.3390/ani12182369

10. Hansen HJ. A pathologic-anatomical study on disc degeneration in dog, with special reference to the so-called enchondrosis intervertebralis. *Acta Orthop Scand Suppl*. (1952) 11:1–117. doi: 10.3109/ort.1952.23.suppl-11.01

11. Jerram RM, Dewey CW. Acute thoracolumbar extrusion in dogs- part I. *Compend Contin Educ Pract Vet*. (1999) 21:922–30.

12. Toombs JP. Cervical intervertebral disc disease in dogs. *Compend Contin Educ Pract Vet*. (1992) 14:1477–86.

13. Cherrone KL, Dewey CW, Coates JR, Bergman RL. A retrospective comparison of cervical intervertebral disc disease in nonchondrodystrophic large dogs versus small dogs. *J Am Anim Hosp Assoc*. (2004) 40:316–20. doi: 10.5326/0400316

14. Levine JM, Levine GJ, Johnson SI, Kerwin SC, Hettlich BF, Fosgate GT. Evaluation of the success of medical management for presumptive cervical intervertebral disc herniation in dogs. *Vet Surg*. (2007) 36:492–9. doi: 10.1111/j.1532-950X.2007.00296.x

15. Olsson SE. On disc protrusion in dog (enchondrosis intervertebralis); a study with special reference to roentgen diagnosis and to the value of disc fenestration. *Acta Orthop Scand Suppl*. (1951) 8:1–95. doi: 10.3109/ort.1951.22.suppl-8.01

16. Andruzzi MN, Simon BT, Boudreau E. Subclinical hypoventilation in dogs undergoing ventral slot Decompressive surgery for cervical myelopathy due to intervertebral disc herniation. *Front. Vet. Sci*. (2021) 8:777052. doi: 10.3389/fvets.2021.777052

17. Gordon-Evans W. Ventral slot and fenestration In: D Griffon and A Hamaide, editors. *Complications in small animal surgery*. Hoboken, NJ: Wiley (2016)

18. Rossmeisl JH, White C, Pancotto TE, Bays A, Henao-Guerrero PN. Acute adverse events associated with ventral slot decompression in 546 dogs with cervical intervertebral disc disease. *Vet Surg*. (2013) 42:795–806. doi: 10.1111/j.1532-950X.2013.12039.x

19. Merbl Y, Shamir MH, Chamisha Y, Peeri D, Benzioni H, Chai O. Three consecutive ventral slots for the treatment of cervical intervertebral disc disease in a dog. *Isr J Vet Med*. (2017) 72:49–53.

20. Olender M, Couturier J, Couturier L, Gatel L, Brissot H. Double adjacent ventral slots in cervical disc extrusion with epidural haemorrhage in four French bulldogs. *VCOT Open*. (2022) 5:e106–10. doi: 10.1055/s-0042-1757348

21. Salt C, Morris PJ, German AJ, Wilson D, Lund EM, Cole TJ, et al. Growth standard charts for monitoring bodyweight in dogs of different sizes. *PLoS One*. (2017) 12:e0182064. doi: 10.1371/journal.pone.0182064

22. Platt SR, da Costa RC. Cervical vertebral column and spinal cord In: SA Johnston and KM Tobias, editors. *Veterinary surgery: Small animal. 2nd* ed. St. Louis: Elsevier (2018)

23. McCartney W. Comparison of recovery times and complication rates between a modified slanted slot and the standard ventral slot for the treatment of cervical disc disease in 20 dogs. *J Small Anim Pract*. (2007) 48:498–501. doi: 10.1111/j.1748-5827.2006.00309.x

24. Wheeler S.J., Sharp J.H. (2005) *Cervical disc disease, in small animal spinal disorders: Diagnosis and surgery* Edinburgh: Elsevier Mosby, 92–120.

25. Lemarié RJ, Kerwin SC, Partington BP, Hosgood G. Vertebral subluxation following ventral cervical decompression in the dog. *J Am Anim Hosp Assoc*. (2000) 36:348–58. doi: 10.5326/15473317-36-4-348

26. Schwab ML, Ferrarin DA, Ripplinger A, Herculano LFS, Colvero ACT, Wrzesinski MR, et al. Ventral slot in the clinical recovery of dogs with lateralized compression as a result of cervical intervertebral disc disease - 20 cases (2008-2018). *Cienc Rural*. (2020) 50:e20190242. doi: 10.1590/0103-8478cr20190242

27. Kang HY, Kang J, Lee H, Kim N, Heo S. Comparison of access window created by cervical ventral slot and modified slanted ventral slot in canine cadaver. *Korean J Vet Res*. (2020) 60:139–44. doi: 10.14405/kjvr.2020.60.3.139

28. Guo S, Lu D, Pfeiffer S, Pfeiffer DU. Non-ambulatory dogs with cervical intervertebral disc herniation: single versus multiple ventral slot decompression. *Aust Vet J*. (2020) 98:148–55. doi: 10.1111/avj.12908

29. Henke D, Gorgas D, Doherr MG, Howard J, Forterre F, Vandevelde M. Longitudinal extension of myelomalacia by intramedullary and subdural hemorrhage in a canine model of spinal cord injury. *Spine J*. (2016) 16:82–90. doi: 10.1016/j.spinee.2015.09.018

30. da Costa RC, De Decker S, Lewis MJ, Volk H. Canine spinal cord injury consortium (CANSORT-SCI). Diagnostic imaging in intervertebral disc disease. *Front. Vet. Sci*. (2020) 7:588338. doi: 10.3389/fvets.2020.588338

31. Emery L, Hecht S, Sun X. Investigation of parameters predicting the need for diagnostic imaging beyond computed tomography in the evaluation of dogs with thoracolumbar myelopathy: retrospective evaluation of 555 dogs. *Vet Radiol Ultrasound*. (2018) 59:147–54. doi: 10.1111/vru.12576

32. Lim C, Kweon OK, Choi MC, Choi J, Yoon J. Computed tomographic characteristics of acute thoracolumbar intervertebral disc disease in dogs. *J Vet Sci*. (2010) 11:73–9. doi: 10.4142/jvs.2010.11.1.73

33. Goring RL, Beale BS, Faulkner RF. The inverted cone decompression technique: a surgical treatment for cervical vertebral instability "wobbler syndrome" in Doberman pinschers. Part 1. *J Am Anim Hosp Assoc*. (1991) 27:403–9.

frontiers | Frontiers in Veterinary Science

TYPE Case Report
PUBLISHED 22 August 2024
DOI 10.3389/fvets.2024.1450332

OPEN ACCESS

EDITED BY
Theresa Elizabeth Pancotto,
Virginia Tech, United States

REVIEWED BY
Sam Long,
Veterinary Referral Hospital, Australia
Anita Shea,
Massey University, New Zealand

*CORRESPONDENCE
YoungJin Jeon
✉ orangee0115@gmail.com

†These authors have contributed equally to this work and share first authorship

RECEIVED 17 June 2024
ACCEPTED 05 August 2024
PUBLISHED 22 August 2024

CITATION
Jeong J, Lee H, Rho Y and Jeon Y (2024) Case report: Gross total resection of a primary fourth ventricular meningioma using the telovelar approach in a dog.
Front. Vet. Sci. 11:1450332.
doi: 10.3389/fvets.2024.1450332

Case report: Gross total resection of a primary fourth ventricular meningioma using the telovelar approach in a dog

Jaemin Jeong[1†], Haebeom Lee[1†], Yoonho Rho[2] and YoungJin Jeon[1*]

[1]Department of Veterinary Surgery, College of Veterinary Medicine, Chungnam National University, Daejeon, Republic of Korea, [2]Department of Veterinary Surgery, College of Veterinary Medicine, Gyeongsang National University, Jinju, Republic of Korea

An 11-year-old spayed female Maltese dog presented with a 2-month history of gait alterations, wide-based stance, and chronic vomiting. Neurological examination revealed cerebellovestibular signs, including head tilt, nystagmus, strabismus, intentional tremor, and hypermetric gait. MRI showed a mass with iso- to hypointensity on T1-weighted (T1W) images and heterogeneous hyperintensity on T2-weighted (T2W) images, with marked non-uniform contrast enhancement. The tumor was removed via a telovelar approach without intraoperative complications. Postoperatively, the dog developed non-ambulatory paraparesis with the rigidity of the pelvic limbs but recovered ambulation within 6 days. Preoperative neurological signs progressively improved, and the patient was discharged without complications 10 days after surgery. Histological examination revealed dense spindle cells with an abundant collagen matrix and oval-shaped nucleated cells with small whorls, leading to a diagnosis of transitional meningioma of the fourth ventricle. MRI follow-up at 8 months postoperatively showed no definitive evidence of recurrence. At the final follow-up, 15.4 months postoperatively, mild neurological signs, including a slight head tilt and subtle strabismus, remained, but the rest of the neurological examination was normal. This is the first reported case of a meningioma in the fourth ventricle of a dog successfully removed using the telovelar approach.

KEYWORDS

meningioma, fourth ventricle, fourth ventricular meningioma, telovelar approach, dog

1 Introduction

Primary ventricular tumors are relatively uncommon in veterinary medicine. The most common tumor located in the ventricular system is the choroid plexus tumor (CPT), which accounts for up to 7% of primary brain tumors and is the third most common type of primary intracranial tumor in dogs (1, 2). Other primary tumors, such as ependymoma, astrocytoma, and meningioma, can also occur within the ventricles, although reported cases are limited (3–9). The prevalence of primary fourth ventricular tumors is presumed to be less than 5% of all primary brain tumors. This estimation is based on the finding that 49% of CPT are located in the fourth ventricle, while other primary fourth ventricular tumors have been reported only rarely as single-case reports (7, 10). The clinical signs associated with fourth ventricle tumors are predominantly cerebellovestibular signs, including strabismus, head tilt, obtunded mental

status, and delayed postural reactions (7, 11). Additionally, an absent menace response has also been reported (11).

Meningiomas typically occur in the rostrotentorial region, accounting for 62.2 to 84.4% of all cases (12, 13). In contrast, intraventricular meningiomas are extremely rare; only two lateral ventricular meningiomas and one-fourth ventricular meningioma have been described (6, 7, 9). The single case of a fourth ventricular meningioma was diagnosed postmortem through histopathologic examination and classified as a microcystic subtype, which is a rare form of meningioma. In human medicine, intraventricular meningioma is similarly rare, constituting 0.7–3% of intracranial meningiomas, with only 6.6% of these occurring in the fourth ventricle (14, 15).

While a standard treatment protocol for fourth ventricular tumors has not been established in veterinary medicine, surgical removal is considered the first line of treatment in human medicine (16). The surgical approach to the fourth ventricle is particularly challenging due to its narrow anatomical location between the brain stem, specifically the medulla oblongata and the cerebellum (17). In the human literature, the transvermian and telovelar approach are well-described methods for accessing the fourth ventricle. The telovelar approach has been used to surgically resect a choroid plexus carcinoma (CPC) within the fourth ventricle in a dog (11). This technique offers several advantages over the transvermian approach, such as sparing the vermis and providing better exposure in craniocaudal and lateral directions (11, 18, 19).

The author found no existing literature describing the surgical removal of a fourth ventricular meningioma and its outcome in veterinary medicine. This case report aims to describe the neuroradiological findings, detailed surgical technique, and long-term outcome of a primary fourth ventricular meningioma, classified as the transitional subtype.

2 Case description

A client-owned, 11-year-old spayed female Maltese dog weighing 3.8 kg was referred with a 2-month history of falling episodes with gait alterations, wide-based stance, nausea, and vomiting. Nausea and vomiting could not be controlled by maropitant (1 mg/kg, orally, q24hr) at the primary veterinary clinic. The physical examination revealed a systolic murmur of grade 4/6 at the left heart apex, which was later evaluated as grade B1 myxomatous mitral valve disease; other findings were normal. Neurological examination revealed bright and alert mentation, an obvious left head tilt, positional, horizontal nystagmus with fast phase to the right, ventrolateral positional strabismus of left eye, intentional head tremor, and hypermetric gait. Concurrent vestibular and cerebellar signs indicated a lesion on the left central vestibular system and cerebellum. The lesion was thought to be a space-occupying mass, and differential diagnoses included neoplasia (CPT, glioma, meningioma, and lymphoma), cyst, or cyst-like lesion. Inflammatory diseases, anomalies, and degenerative diseases were thought to be less likely. Blood tests were within normal reference range, except for a mildly elevated liver panel. No abnormal findings were identified on the thoracic radiographs. MRI revealed a 10.4 × 11 × 16.2 mm sized, oval-shaped, and slightly left-sided intraventricular mass. The mass showed iso- to hypointensity on T1W images, heterogeneous hyperintensity on T2W images, hyperintensity on fluid-attenuated inversion recovery sequences (FLAIR), and marked non-uniform contrast enhancement (Figures 1A–D). The mass compressed and displaced the medulla oblongata ventrally and the cerebellum dorsally. Obstructive ventriculomegaly was observed rostral to the lesion. The neuroradiological findings corresponded with the symptoms. A presumptive diagnosis of an intraventricular tumor was made, with CPT considered the most likely differential diagnosis.

Surgical removal of the tumor using the telovelar approach was planned as described in a previous study (11). Prior to the anesthetic induction, maropitant (1 mg/kg, IV), dexamethasone (0.2 mg/kg, IV), and cefazoline (22 mg/kg, IV) were administered. The patient was premedicated with midazolam (0.2 mg/kg, IV) and administered propofol (4 mg/kg, IV) slowly, followed by intubation with a reinforced endotracheal tube to avoid kinking due to surgical position. The dog was maintained with 1–1.5% (vaporizer setting) isoflurane with a constant 100% O2 flow of 2 L/min. The patient was positioned with the neck flexed as much as possible, slightly over 90 degrees, to achieve the maximum opening of the foramen magnum, taking care not to compress the jugular vein. After the patient preparation, mannitol (0.25 g/kg, IV) was infused slowly over 15 min to achieve better brain relaxation and prevent reperfusion injury (20–22). During anesthesia, the monitoring parameters, including electrocardiogram, heart rate (HR), respiratory rate (RR), oxygen blood saturation (SpO2), rectal temperature, non-invasive blood pressure (NIBP), end-tidal CO2, tidal volume, airway pressure, and compliance, were within the normal range. Remifentanil was administered IV at a flow rate of 5–6ug/kg/h for analgesia.

The surgical approach to suboccipital craniectomy was performed routinely (11, 23). Suboccipital craniectomy was performed and additional partial dorsal laminectomy of the atlas was performed to expose the widest opening of the caudal fossa. Both procedures were conducted meticulously using a Kerrison rongeur. When the caudal fossa was sufficiently exposed, a neurosurgical microscope was used to magnify the surgical site and capture the image (Figure 2). Micro-bleeding from the dura mater was coagulated by bipolar electrocautery to maintain a clear surgical site. The dura mater was picked with a double-pronged tissue pick instrument and incised with a von Graefe knife without excessive tension. The incision was made from the level of the cerebellar uvula to the level of the atlas, longitudinally. The dura mater was retracted laterally without suturing. The tela choroidea was identified as the thin, avascular, membranous layer located between the uvula and the medulla oblongata. The tela choroidea was easily incised with a blunt-ended, 90°-angled Sisson nerve hook, and the tumor was identified through the incision. Neurosurgical lint-free sponges were packed around the tumor to visualize the tumor and retract the brain parenchyma. Visible blood vessels on the tumor were coagulated with a bipolar electrocautery. The hook probe, a micro-ring curette, and tumor forceps were used alternately to perform blunt dissection around the tumor with minimal traction. Meticulous maneuvering of the cerebellum dorsally with a semi-blunt Sachs nerve elevator through the sponge provided a wider surgical site. During the dissection, minor bleeding was controlled with sponges and ophthalmic triangular swabs. After the dissection, the mass was detached from the ventricle by grasping it with tumor forceps and removed as a single solitary piece. Minor bleeding after removal was controlled by attaching absorbable oxidized regenerated celluloses to the ventral surface of the ventricle and filling the ventricle with

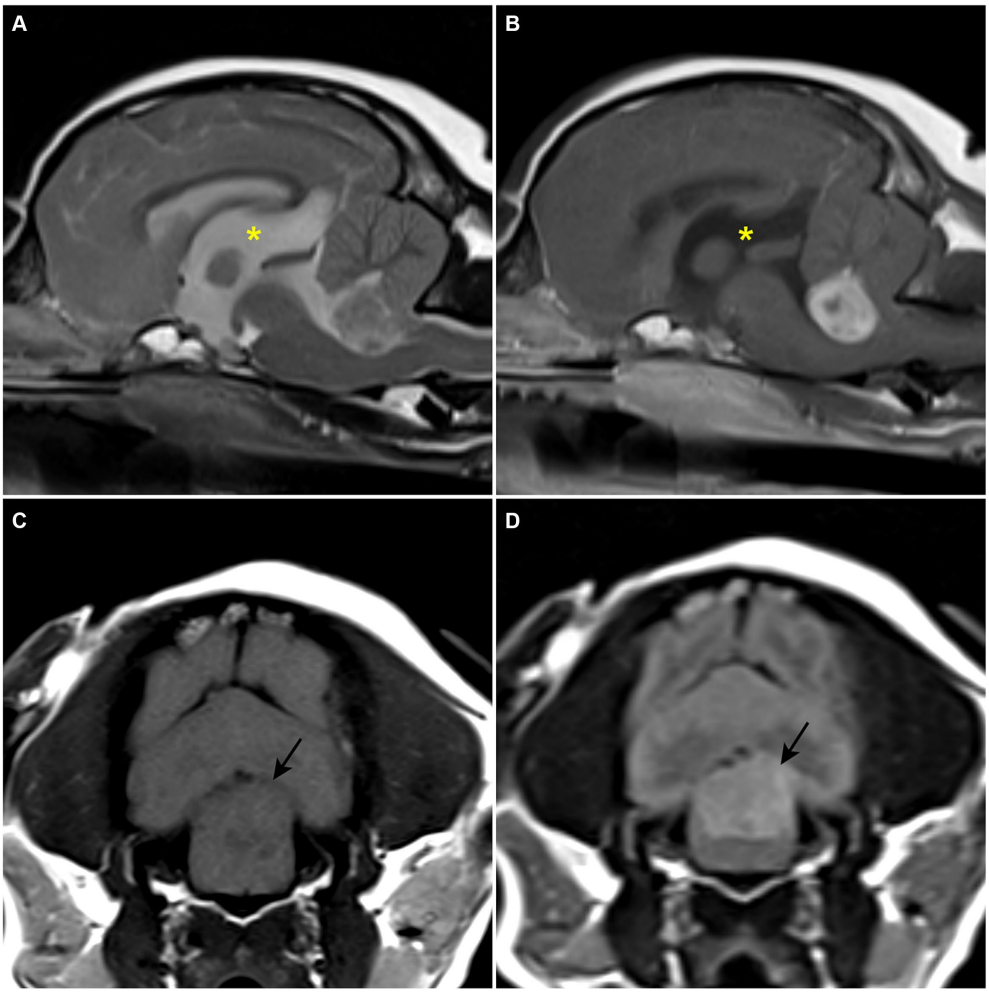

FIGURE 1
Preoperative MRI. **(A)** T2-weighted sagittal plane. A heterogenous hyperintense space-occupying the lesion is confirmed within the fourth ventricle. **(B)** T1-weighted post-contrast sagittal plane. A strong enhanced mass-like lesion is confirmed within the fourth ventricle. An enlarged third ventricle (asterisk) is revealed. **(C)** T1-weighted transverse plane. Hypo- to isointense lesion is confirmed. **(D)** T2 fluid-attenuated inversion recovery transverse plane. The lesion is revealed as a hyperintensive signal.

Hartmann's solution. Sponges were removed and generous irrigation was performed to confirm the absence of residual bleeding and to spare the ventricle space. A thin sheath, thought to be a residual tumor capsule, was confirmed on the caudodorsal surface of the medulla oblongata and partially removed with Castroviejo scissors. The tela choroidea remained open, and the dura mater was sutured with a synthetic dura substitute (ReDura, Medprin Biotech, Frankfurt, Germany) to maximize the space over the foramen magnum using 6/0 absorbable suture material (6/0 PDS II, Ethicon, Raritan, NJ) in a single interrupted pattern. Closure of the muscle layer and skin was performed routinely. The entire removed mass was submitted for histopathological examination.

The patient was moved for a postoperative MRI to confirm the surgical removal of the tumor. Immediate postoperative MRI revealed the removal of the tumor, but a strongly enhancing structure was confirmed ventral to the caudal cerebellar lobe on T1W with gadolinium images (Figures 3A,B). The tumor was white to gray, oval-shaped, 15.8 × 10.5 × 10 mm, and firm (Figure 4A). Histological examination revealed dense spindle cells with an abundant collagen matrix, the typical finding of the fibrous subtype, and oval-shaped nucleated cells with small whorls, the common finding of the meningothelial subtype (Figures 4B,C). The combination of the findings, including medical imaging, gross appearance, and histopathologic findings, led to a definitive diagnosis of primary fourth ventricular transitional meningioma.

The patient recovered smoothly from anesthesia. Vital signs were monitored and neurological examinations were performed at regular intervals throughout the convalescent period. There was no significant alteration of vital parameters, such as HR, PR, NIBP, and body temperature, during monitoring. On the day of the surgery, non-ambulatory paraparesis with hindlimb rigidity was observed but improved after a single infusion of mannitol (0.5 g/kg, IV, slowly over 15 min). A single event of mental dullness was observed 3 days after the surgery, but it soon recovered after a single administration of mannitol (0.5 g/kg, IV, slowly over 15 min). Preoperative signs, such as vomiting and vestibular signs, improved progressively, and ambulation recovered 6 days after the surgery. During hospitalization, amoxicillin-clavulanic acid (20 mg/kg, IV, q12hr), prednisolone

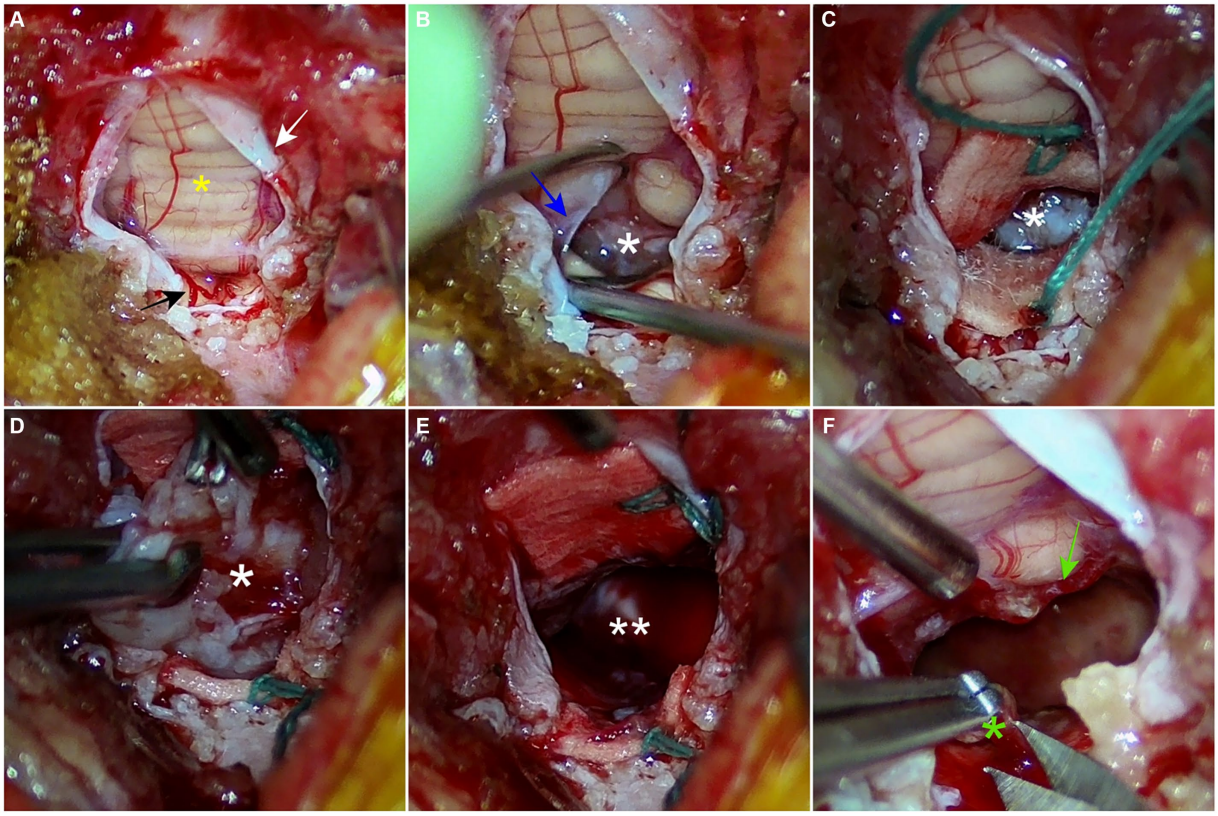

FIGURE 2
Intraoperative images from neurosurgical microscope. **(A)** A dural incision is made longitudinally from the level of the cerebellar uvula to the level of the atlas. The vermis and dura mater are indicated as a yellow asterisk and a white arrow, respectively. A branch of the caudal cerebral artery is highlighted with a black arrow. **(B)** An avascular tela choroidea (blue arrow) is incised with a nerve hook probe. The tumor (white asterisk) is confirmed through the incision. **(C)** Two green-stringed neurosurgical sponges are packed around the tumor to retract the brain parenchyma and secure the surgical field. **(D)** Through repeated meticulous maneuvers using tumor forceps, a hook probe, and a micro-ring curette, the tumor is bluntly dissected from the fourth ventricle **(E)** The tumor is removed, and the space (double white asterisks) of the fourth ventricle is confirmed. **(F)** The remaining suspected tumor capsule (green asterisk) is partially resected. The remaining choroid plexus is highlighted with a green arrow.

(0.5 mg/kg, PO, q12hr), levetiracetam (20 mg/kg, IV, q8hr), gabapentin (10 mg/kg, PO, q12hr), esomeprazole (1 mg/kg, IV, q12hr), and maropitant (1 mg/kg, IV, q24hr) were administered. Acetazolamide (10 mg/kg, PO, q8hr) was added after the event of mental dullness. Remifentanil was infused (6ug/kg/h, IV) for analgesia, gradually tapered according to the monitored pain response, and withdrawn at 3 days post-surgery. The patient was discharged 10 days after surgery with remaining neurological signs, including positional nystagmus, slight head tilt, and hypermetria. The antibiotic was discontinued and hydroxyurea (50 mg/kg, orally, every other day) was added to the medication upon discharge.

At the first follow-up, 43 days after surgery, the patient showed head tilt, positional nystagmus, and hypermetria, but other clinical signs had resolved. Medication was modified to exclude acetazolamide and reduce the dosage of prednisolone to 0.3 mg/kg, q12hr. At 6-month postoperative follow-up, neurologic signs recover to normal, except for a slight head tilt. Levetiracetam was discontinued, and prednisolone was reduced to 0.5 mg/kg, q24hr. Eight months after the surgery, a follow-up MRI was requested by the client to verify no recurrence of the tumor. The former contrast-enhanced structure had reduced significantly and appeared to be a membranous structure (Figures 3C,D). The size of the lateral ventricle returned to within the normal reference; preoperative ventricle/brain index: 0.61, 8-month postoperative ventricle/brain- index: 0.56 (24). There was no recurrence of the mass-like lesion in the fourth ventricle. At the final follow-up at 15.4 months postoperatively, the patient showed a slight head tilt and subtle positional strabismus. The client was satisfied with the outcome. Throughout the follow-up, regular blood work, including complete blood count, total protein, globulin, alanine aminotransferase (ALT), alkaline phosphatase (ALP), aspartate aminotransferase and gamma-glutamyl transferase, was performed every 2 months to monitor the effect of the medication, especially prednisolone and hydroxyurea. Mild anemia and elevated ALT and ALP were observed throughout the medication but without further deterioration. Based on the MRI findings and the absence of further deterioration in neurological signs, it was presumed that there was no recurrence of the tumor.

3 Discussion

This case report describes the first successful surgical removal of a primary fourth ventricular transitional meningioma in a dog, providing a detailed account of MRI findings, surgical technique,

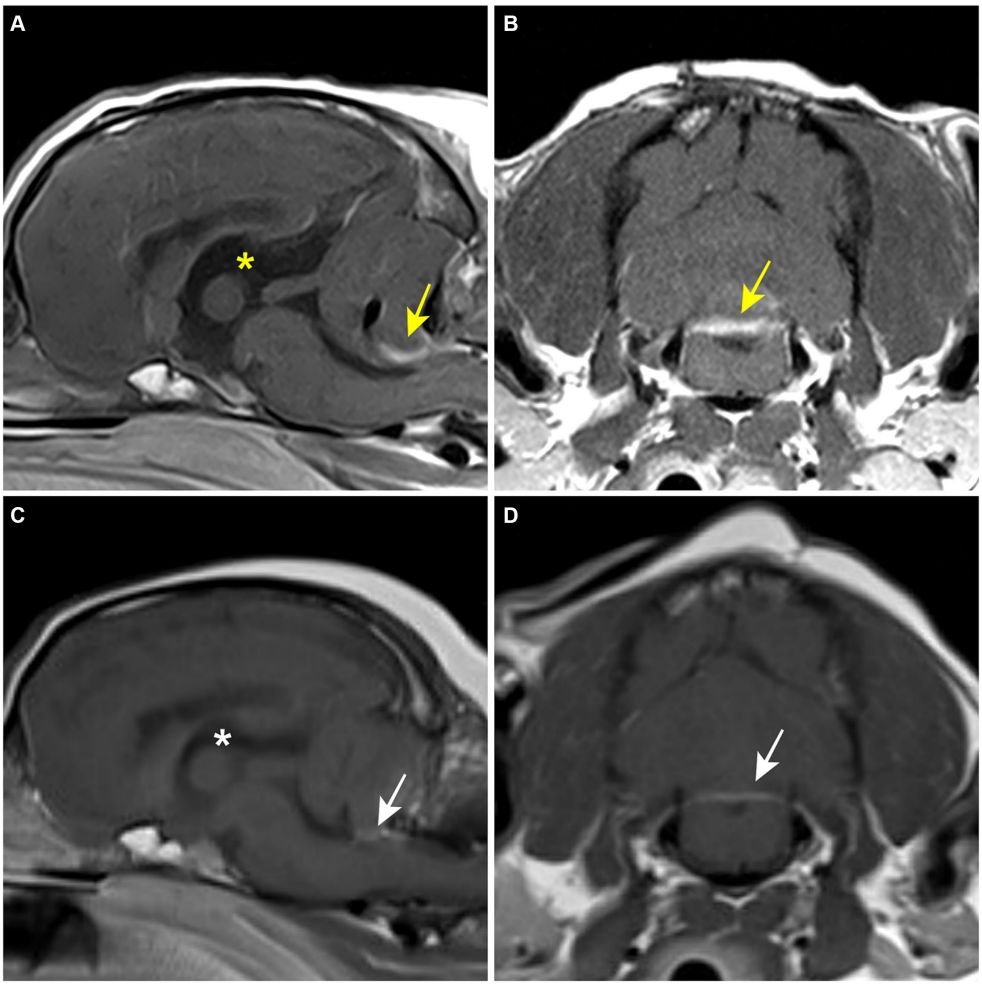

FIGURE 3
Postoperative MRI. **(A,B)** Immediate postoperative T1-weighted post-contrast MRI. A contrast-enhanced lesion (yellow arrow) is revealed on the caudoventral aspect of the cerebellum. The third ventricle (yellow asterisk) is still enlarged. **(C,D)** 8-month postoperative T1-weighted post-contrast MRI. Contrast-enhanced lesion (white arrow) and the third ventricle (white asterisk) are reduced compared to the former MRI findings.

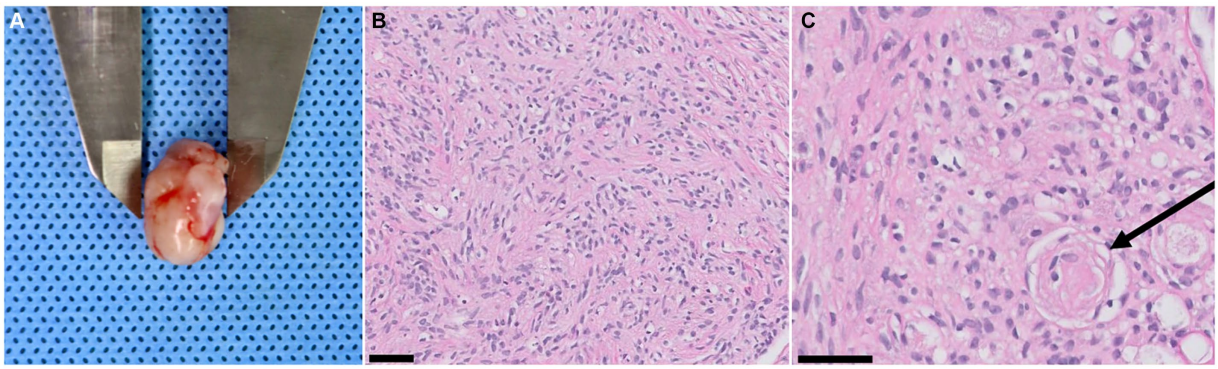

FIGURE 4
Tumor gross appearance and biopsy results. **(A)** A resected fourth ventricular tumor. The gross appearance is white to gray (relatively low vascularization), oval-shaped, 15.8 × 10.5 × 10 mm in size, and has a firm texture. **(B)** Dense spindle cells with an abundant collagen matrix are confirmed. These findings are typical findings of the fibrous subtype of meningioma (magnification ×20, black 50 μm scale bar, hematoxylin and eosin stain). **(C)** Oval-shaped nucleated cells with small whorls (black arrow) are revealed, indicating the meningothelial subtype meningioma. (magnification ×40, black 50 μm scale bar, hematoxylin and eosin stain).

postoperative care, and outcome. Despite the uncommon occurrence of intraventricular meningiomas in dogs, it is essential to consider meningioma in the differential diagnosis for fourth ventricular masses due to their differing characteristics from CPTs.

The recurrence of the brain tumor is closely related to the completeness of the resection. Although there are limited cases of surgical treatment of fourth ventricle tumors, meningiomas are thought to be more feasible to resect totally in a gross manner than CPT. In our case, the tumor was well-encapsulated and relatively less vascularized. Therefore, it was able to be removed en bloc without piecemeal maneuvering and with minimal bleeding. A previous study described that a CPT was removed in three pieces and the figures showed that the sponge was notably red, indicating more bleeding from the tumor resection compared to our case (11). Another report, describing the removal of lateral ventricular CPT in a dog, reported bleeding as the main intraoperative complication (25). Additionally, human literature indicates that uncontrollable hemorrhage during CPT resection is associated with perioperative mortality, which can range up to 30% (26). Although it is difficult to draw definitive conclusions from a single case, these characteristics can impact surgical outcomes. Therefore, further research through a larger number of case studies on a fourth ventricular meningioma is necessary to better understand the prognosis related to surgery.

Preoperatively, CPT was the primary consideration due to its neuroanatomical prevalence and histological origin. The choroid plexus consists of pia, ependyma, and proliferated capillaries and is found within the ventricular system (17). CPTs, including choroid plexus papilloma (CPP) and carcinoma (CPC), originate from the choroid plexus epithelium (10, 27). In contrast, meningiomas typically arise from arachnoid cap cells (1). To date, only four cases of intraventricular meningiomas have been reported in the veterinary literature, including one case of primary fourth ventricular microcystic meningioma, two cases of lateral ventricular meningioma, and the current case (6, 7, 9). Although studies on the origin of intraventricular meningiomas in veterinary medicine are limited, human literature suggests they may arise from the stroma of the choroid plexus or tela choroidea (28). The diagnosis of meningioma in our case adds further evidence that meningiomas can indeed occur in this location within the ventricular system of dogs.

MRI is considered the gold standard for diagnosing brain diseases. However, differentiating between CPC and intraventricular meningioma using MRI is challenging. Some pathological differences may be reflected in MRI findings (29). CPCs are highly vascular, with abundant microvasculature, making them more likely to appear hypointense on T1W, hyperintense on T2W, and exhibit signal voids on FLAIR (30). Additionally, their gross appearance can be indicated by an irregular margin on MRI images (31). According to previous veterinary studies, these MRI features of CPT align with the pathological hypotheses (1, 10, 13, 32–34). In our case, the tumor showed iso- to hypointensity on T1W, heterogeneous hyperintensity on T2W, hyperintensity on FLAIR, and strong enhancement after gadolinium infusion. However, the few reported intraventricular meningioma cases, including our case, showed significant variation in MRI findings (6, 7, 9). Therefore, MRI alone is not reliable for differentiating between CPTs and intraventricular meningiomas. Further studies are needed to correlate MRI findings with histological characteristics to improve diagnostic accuracy.

In our case, postoperative MRI sequences confirmed that the tumor was removed and showed no signs of recurrence at 8 months postoperatively. An initial contrast-enhanced lesion observed on the immediate postoperative MRI was found to have reduced in size on the 8-month postoperative MRI. Differential diagnoses for this lesion included residual choroid plexus, inflammation, and remaining tumor tissue. The choroid plexus was considered the most likely due to the surgical findings, the lesion's size reduction, and prolonged use of prednisolone. The choroid plexus, located beneath the caudal lobe of the cerebellum and extending into the lumen of the fourth ventricle, can enhance with contrast due to its rich blood supply and lack of a blood–brain barrier (17, 35). Furthermore, a residual sheath, presumed to be the tumor capsule, was identified on the caudodorsal surface of the brainstem, which did not correspond to the lesion's location. However, there remains a possibility of residual neoplastic cells in the choroid plexus since intraventricular meningiomas can originate from it. Thus, regular follow-ups to monitor neurological status and two postoperative MRI scans have been implemented.

The temporary deterioration of neurological signs observed post-surgery, including non-ambulatory paraparesis and mental dullness, may be attributed to retraction and maneuvering during the procedure, as well as to reperfusion damage and subsequent edema following decompression Additionally, it could be a result of acute postoperative hydrocephalus. According to human literature, residual hemostatic material is known to be a risk factor for acute postoperative hydrocephalus since it can cause occlusion of cerebrospinal fluid flow (36, 37). The interaction between cerebrospinal fluid, blood, and foreign bodies tends to promote coagulation (38). Predictive factors for acute hydrocephalus following lateral ventricular tumor resection include preoperative hydrocephalus and the presence of intraventricular hemostatic agents, both of which were relevant in our case (39). Therefore, meticulous handling and protection of the parenchyma during surgery, along with generous irrigation with warm fluid, are crucial for preventing complications after the fourth ventricular tumor resection (36). Additionally, careful monitoring and immediate treatment are essential for managing postoperative complications (40).

This case report has several limitations. First, it is based on a single case, thus further studies are needed to verify MRI findings for diagnosing intraventricular tumors and to evaluate the prognosis of surgically resected intraventricular meningiomas. Additionally, the pathomechanism of mental dullness observed 3 days after the surgery could not be explained, as MRI or CT images were not taken at the time. Finally, although there was no evidence of recurrence according to neurological examination and MRI at the final follow-up, the risk of recurrence remains. Therefore, further investigation of the long-term outcomes is necessary.

In conclusion, this case report presents the first instance of a surgically treated primary fourth ventricular meningioma in a dog, providing a detailed account of MRI findings, surgical technique, postoperative care, and its satisfactory outcome. This case highlights the importance of including meningioma in the differential diagnoses for fourth ventricular masses, despite the rarity of intraventricular meningiomas in dogs.

Data availability statement

The raw data supporting the conclusions of this article will be made available by the authors, without undue reservation.

Ethic statement

Ethical approval was not required for the studies involving animals in accordance with the local legislation and institutional requirements because we report a case study of a veterinary hospital. We have the consent of both the owner and veterinarian that this dog (underwent the listed examinations and surgical intervention) was treated not for experimental but for medical reasons. Written informed consent was obtained from the owners for the participation of their animals in this study.

Author contributions

JJ: Conceptualization, Data curation, Investigation, Methodology, Resources, Software, Supervision, Validation, Visualization, Writing – original draft, Writing – review & editing. HL: Conceptualization, Data curation, Formal analysis, Funding acquisition, Investigation, Methodology, Resources, Supervision, Validation, Visualization, Writing – original draft, Writing – review & editing. YR: Formal analysis, Investigation, Methodology, Supervision, Validation, Writing – review & editing. YJ: Conceptualization, Data curation, Investigation, Methodology, Project administration, Supervision, Validation, Visualization, Writing – original draft, Writing – review & editing.

Funding

The author(s) declare that financial support was received for the research, authorship, and/or publication of this article. This research was supported by a basic science research program through the National Research Foundation of Korea (NRF) funded by the Ministry of Education (RS-2023-00247989).

Conflict of interest

The authors declare that the research was conducted in the absence of any commercial or financial relationships that could be construed as a potential conflict of interest.

Publisher's note

All claims expressed in this article are solely those of the authors and do not necessarily represent those of their affiliated organizations, or those of the publisher, the editors and the reviewers. Any product that may be evaluated in this article, or claim that may be made by its manufacturer, is not guaranteed or endorsed by the publisher.

References

1. Miller AD, Miller CR, Rossmeisl JH. Canine primary intracranial Cancer: a Clinicopathologic and comparative review of glioma, meningioma, and choroid plexus tumors. *Front Oncol*. (2019) 9:1151. doi: 10.3389/fonc.2019.01151

2. Rossmeisl JH, Pancotto TE. Tumors of the nervous system In: DM Vail, DH Thamm and JM Liptak, editors. Withrow & Macewen's small animal clinical oncology. *6th* ed. St. Louis, MI: Elsevier Health Sciences (2019). 657–74.

3. Miller AD, Koehler JW, Donovan TA, Stewart JE, Porter BF, Rissi DR, et al. Canine Ependymoma: diagnostic criteria and common pitfalls. *Vet Pathol*. (2019) 56:860–7. doi: 10.1177/0300985819859872

4. Lehner L, Czeibert K, Csébi P, Diószegi K, Nagy G. Case report: intraventricular tumor removal using Transcallosal approach and follow-up in three dogs. *Front Vet Sci*. (2023) 10:1240934. doi: 10.3389/fvets.2023.1240934

5. Rissi DR, Levine JM, Eden KB, Watson VE, Griffin JF IV, Edwards JF, et al. Cerebral Oligodendroglioma mimicking intraventricular neoplasia in three dogs. *J Vet Diagn Invest*. (2015) 27:396–400. doi: 10.1177/1040638715584619

6. Ortiz-Nisa S, de la Fuente C, Sant'Ana F, Pumarola M, Añor S. Clinical, imaging and histopathological characteristics of a malignant intracranial meningioma with pulmonary metastasis in a dog. *Vet Rec Case Rep*. (2022) 10:e365. doi: 10.1002/vrc2.365

7. Salvadori C, Pintore MD, Ricci E, Konar M, Tartarelli CL, Gasparinetti N, et al. Microcystic meningioma of the fourth ventricle in a dog. *J Vet Med Sci*. (2011) 73:367–70. doi: 10.1292/jvms.10-0337

8. Hansen KS, Li CF, Théon AP, Kent MS. Stereotactic radiotherapy outcomes for intraventricular brain Tumours in 11 dogs. *Vet Comp Oncol*. (2023) 21:665–72. doi: 10.1111/vco.12929

9. Ijiri A, Yoshiki K, Tsuboi S, Shimazaki H, Akiyoshi H, Nakade T. Surgical resection of twenty-three cases of brain meningioma. *J Vet Med Sci*. (2014) 76:331–8. doi: 10.1292/jvms.12-0373

10. Westworth D, Dickinson P, Vernau W, Johnson E, Bollen A, Kass P, et al. Choroid plexus tumors in 56 dogs (1985–2007). *J Vet Intern Med*. (2008) 22:1157–65. doi: 10.1111/j.1939-1676.2008.0170.x

11. Antonakakis MG, Carletti BE, Anselmi C, McGrath S, Minguez JJ. Use of a Telovelar approach for complete resection of a choroid plexus tumor in a dog. *Vet Surg*. (2022) 51:1273–9. doi: 10.1111/vsu.13859

12. Minato S, Cherubini GB, Della Santa D, Salvadori S, Baroni M. Incidence and type of brain herniation associated with intracranial meningioma in dogs and cats. *J Vet Med Sci*. (2021) 83:267–73. doi: 10.1292/jvms.20-0111

13. Snyder JM, Shofer FS, Van Winkle TJ, Massicotte C. Canine intracranial primary neoplasia: 173 cases (1986–2003). *J Vet Intern Med*. (2006) 20:669–75. doi: 10.1111/j.1939-1676.2006.tb02913.x

14. Nakamura M, Roser F, Bundschuh O, Vorkapic P, Samii M. Intraventricular Meningiomas: a review of 16 cases with reference to the literature. *Surg Neurol*. (2003) 59:490–503. doi: 10.1016/S0090-3019(03)00082-X

15. Lyngdoh BT, Giri PJ, Behari S, Banerji D, Chhabra DK, Jain VK. Intraventricular Meningiomas: a surgical challenge. *J Clin Neurosci*. (2007) 14:442–8. doi: 10.1016/j.jocn.2006.01.005

16. Sufianov R, Pitskhelauri D, Bykanov A. Fourth ventricle tumors: a review of series treated with microsurgical technique. *Front Surg*. (2022) 9:915253. doi: 10.3389/fsurg.2022.915253

17. de Lahunta A, Glass E, Kent M. Neuroanatomy gross description and atlas of transverse sections and magnetic resonance images In: De Lahunta's veterinary neuroanatomy and clinical neurology. Philadelphia, PA: Elsevier (2021). 6–44.

18. Deshmukh VR, Figueiredo EG, Deshmukh P, Crawford NR, Preul MC, Spetzler RF. Quantification and comparison of Telovelar and Transvermian approaches to the fourth ventricle. *Oper Neurosurg*. (2006) 58:ONS-202–7. doi: 10.1227/01.NEU.0000207373.26614.BF

19. Ebrahim KS, Toubar AF. Telovelar approach versus Transvermian approach in management of fourth ventricular tumors. *Egypt J Neurosurg*. (2019) 34:1–10. doi: 10.1186/s41984-019-0036-9

20. Zhang W, Neal J, Lin L, Dai F, Hersey DP, McDonagh DL, et al. Mannitol in critical care and surgery over 50+ years: a systematic review of randomized controlled trials and complications with Meta-analysis. *J Neurosurg Anesthesiol*. (2019) 31:273–84. doi: 10.1097/ANA.0000000000000520

21. Shan R, Zhou H, Liu X, Su G, Liu G, Zhang X, et al. Neuroprotective Effects of Four Different Fluids on Cerebral Ischaemia/Reperfusion Injury in Rats through Stabilization of the Blood–Brain Barrier. *Eur J Neurosci*. (2021) 54:5586–600. doi: 10.1111/ejn.15385

22. Grana IL, Mariné AF, MPI B, Feliu-Pascual AL. Successful surgical resection of an ependymal cyst in the fourth ventricle of a dog. *J Am Anim Hosp Assoc*. (2024) 60:25–30. doi: 10.5326/JAAHA-MS-7373

23. Akin EY, Shores A. Suboccipital Craniectomy/foramen magnum decompression In: A Shores and BA Brisson, editors. Current techniques in canine and feline neurosurgery. Hoboken, NJ: John Wiley and Sons (2017). 115–20.

24. Laubner S, Ondreka N, Failing K, Kramer M, Schmidt MJ. Magnetic resonance imaging signs of high intraventricular pressure-comparison of findings in dogs with clinically relevant internal hydrocephalus and asymptomatic dogs with Ventriculomegaly. *BMC Vet Res*. (2015) 11:1–11. doi: 10.1186/s12917-015-0479-5

25. Lehner L, Czeibert K, Benczik J, Jakab C, Nagy G. Transcallosal removal of a choroid plexus tumor from the lateral ventricle in a dog Case Report. *Front Vet Sci*. (2020) 7:536. doi: 10.3389/fvets.2020.00536

26. Asmaro K, Pawloski J, Skoch J. Giant choroid plexus papilloma resection utilizing a Transcollation system. *Oper Neurosurg*. (2020) 18:47–51. doi: 10.1093/ons/opz096

27. Higgins RJ, Bollen AW, Dickinson PJ, Sisó-Llonch S. Tumors of the nervous system In: DJ Meuten, editor. Tumors in domestic animals. *5th* ed. Ames, Iowa: John Wiley and Sons (2017). 834–91.

28. Osborn A. Meningiomas and other nonglial neoplasms In: A Patterson, editor. Diagn Neuroradiol. St. Louis, MI: Mosby-Year Book (1994). 620–2.

29. Takeuchi S, Sugawara T, Masaoka H, Takasato Y. Fourth ventricular meningioma: a case report and literature review. *Acta Neurol Belg*. (2012) 112:97–100. doi: 10.1007/s13760-012-0040-2

30. Nakano S, Uehara H, Wakisaka S, Kinoshita K. Meningioma of the fourth ventricle—case report—. *Neurol Med-Chir*. (1989) 29:52–4. doi: 10.2176/nmc.29.52

31. Alver I, Abuzayed B, Kafadar AM, Muhammedrezai S, Sanus GZ, Ziya A. Primary fourth ventricular meningioma: case report and review of the literature. *Turk Neurosurg*. (2011) 21:249–53. doi: 10.5137/1019-5149.jtn.2869-09.0

32. Ródenas S, Pumarola M, Gaitero L, Zamora À, Añor S. Magnetic resonance imaging findings in 40 dogs with histologically confirmed intracranial Tumours. *Vet J*. (2011) 187:85–91. doi: 10.1016/j.tvjl.2009.10.011

33. Wisner ER, Dickinson PJ, Higgins RJ. Magnetic resonance imaging features of canine intracranial neoplasia. *Vet Radiol Ultrasound*. (2011) 52:S52–61. doi: 10.1111/j.1740-8261.2010.01785.x

34. Bentley RT. Magnetic resonance imaging diagnosis of brain tumors in dogs. *Vet J*. (2015) 205:204–16. doi: 10.1016/j.tvjl.2015.01.025

35. McKinney AM. Choroid plexus: Normal locations and appearances In: Atlas of Normal imaging variations of the brain, skull, and Craniocervical vasculature. Cham, Switzerland: Springer (2017). 177–237.

36. Hendricks BK. Principles of intraventricular surgery: neurosurgical atlas. (2016). Available at: https://www.neurosurgicalatlas.com/volumes/brain-tumors/intraventricular-tumors/principles-of-intraventricular-surgery.

37. Ktari O, Frassanito P, Gessi M, Bianchi F, Tamburrini G, Massimi L. Gelfoam migration: a potential cause of recurrent hydrocephalus. *World Neurosurg*. (2020) 142:212–7. doi: 10.1016/j.wneu.2020.06.214

38. Vandersteene J, Baert E, Planckaert GM, Van Den Berghe T, Van Roost D, Dewaele F, et al. The influence of cerebrospinal fluid on blood coagulation and the implications for Ventriculovenous shunting. *J Neurosurg*. (2018) 130:1244–51. doi: 10.3171/2017.11.jns171510

39. Zhang C, Ge L, Li Z, Zhang T, Chen J. Single-center retrospective analysis of risk factors for hydrocephalus after lateral ventricular tumor resection. *Front Surg*. (2022) 9:886472. doi: 10.3389/fsurg.2022.886472

40. Panda NB, Mahajan S, Chauhan R. Management of Postoperative Neurosurgical Patients. *J Neuroanaesth Crit Care*. (2019) 6:080–6. doi: 10.1055/s-0039-1689055

frontiers | Frontiers in Veterinary Science

TYPE Case Report
PUBLISHED 29 August 2024
DOI 10.3389/fvets.2024.1459272

OPEN ACCESS

EDITED BY
John Henry Rossmeisl,
Virginia Tech, United States

REVIEWED BY
Shinji Tamura,
Tamura Animal Clinic, Japan
Yael Merbl,
Cornell University, United States

*CORRESPONDENCE
Julien Guevar
✉ Julien.guevar@anicura.ch

†These authors have contributed equally to this work and share first authorship

‡These authors have contributed equally to this work and share last authorship

RECEIVED 03 July 2024
ACCEPTED 25 July 2024
PUBLISHED 29 August 2024

CITATION
Hobert M, Sharma N, Benzimra C, Hinden S, Oevermann A, Maintz M, Beyer M, Thieringer F and Guevar J (2024) Case report: One-stage craniectomy and cranioplasty digital workflow for three-dimensional printed polyetheretherketone implant for an extensive skull multilobular osteochondosarcoma in a dog.
Front. Vet. Sci. 11:1459272.
doi: 10.3389/fvets.2024.1459272

Case report: One-stage craniectomy and cranioplasty digital workflow for three-dimensional printed polyetheretherketone implant for an extensive skull multilobular osteochondosarcoma in a dog

Marc Hobert[1†], Neha Sharma[2,3†], Caroline Benzimra[4], Sandro Hinden[1], Anna Oevermann[5], Michaela Maintz[2,3,6], Michel Beyer[2,3], Florian Thieringer[2,3‡] and Julien Guevar[1*‡]

[1]AniCura Tierklinik Thun, Thun, Switzerland, [2]Oral and Cranio-Maxillofacial Surgery, University Hospital Basel, Basel, Switzerland, [3]Medical Additive Manufacturing Research Group (Swiss MAM), Department of Biomedical Engineering, University of Basel, Allschwil, Switzerland, [4]Vetpixel SAS, Kochersberg, France, [5]Division of Neurological Sciences, DCR-VPH, Vetsuisse Faculty, University of Bern, Bern, Switzerland, [6]Institute for Medical Engineering and Medical Informatics IM², University of Applied Sciences and Arts Northwestern Switzerland, Muttenz, Switzerland

Objective: To report a digital workflow for use and long-term outcome of cranioplasty with a 3D-printed patient-specific Polyetheretherketone (PEEK) implant in a 12-y-old German Shepherd dog after surgical removal of an extensive occipital bone multilobular osteochondrosarcoma (MLO).

Study design: Retrospective case report.

Animal: A 12-year-old neutered Female German Shepherd dog was presented with facial deformity, blindness, tetraparesis, and ataxia. Magnetic resonance imaging (MRI) and computed tomography (CT) identified a large skull-based mass extending extra-and intracranially with severe compression of the cerebellum and occipital lobes of the cerebrum.

Methods: One-stage decompressive craniectomy using virtual surgical planned 3D-printed craniotomy cutting guides and the Misonix BoneScalpel® and reconstruction with a patient-specific 3D-printed PEEK cranial implant.

Results: 3D-printed craniectomy cutting guides allowed an adequate fit of the cranial implant to the original skull. Misonix BoneScalpel® allowed performing a safe and extensive craniectomy. Postoperative CT (8 weeks after surgery) confirmed the PEEK cranial implant to be in place and without implant rejection. Clinically, the neurological examination identified only a right-hind limb delay in proprioception 8 weeks postoperatively, which remained unchanged at 18 months after surgery. Adjunctive treatment included metronomic chemotherapy. Eighteen months after surgery the dog passed away for reasons unrelated to the MLO, no implant-related complications were reported.

Conclusion: 3D-printed craniectomy cutting guides, patient-specific PEEK cranial implant, and metronomic chemotherapy can lead to a successful long-term outcome in dogs with extensive skull MLO.

Clinical significance: PEEK is an alternative biomaterial that can be used successfully for skull reconstruction.

KEYWORDS

craniotomy, craniectomy, PEEK-polyether ether ketone, multilobular osteochondroma, dog

Introduction

Multilobular osteochondrosarcoma (MLO) is a prevalent and aggressive primary bone tumor affecting the flat bones of the canine skull. Characterized by rapid growth and local invasion, MLO often presents with facial asymmetry and neurological deficits due to significant mass effects on the underlying brain parenchyma. Diagnosis relies on advanced imaging techniques like computed tomography (CT) and magnetic resonance imaging (MRI) (1), often supplemented by fine-needle aspiration or biopsy.

Surgical intervention remains the mainstay of MLO treatment (2), aiming for complete tumor resection to maximize long-term survival and minimize recurrence risk. Additionally, decompressive craniectomy is frequently employed to alleviate intracranial pressure (ICP) and mitigate neurological complications associated with MLO's rapid expansion. Following extensive tumor removal, substantial cranial defects necessitate cranioplasty for cranial reconstruction and brain protection. Various reconstruction techniques have been used for dogs (3–10).

This case report describes the successful management of MLO in a canine patient implementing a digital workflow utilizing two innovative surgical techniques: virtual surgical planning (VSP) and medical 3D printing. VSP allows for meticulous preoperative planning, facilitating precise tumor resection and minimizing the risk of iatrogenic complications. Furthermore, medical 3D printing enables the creation of patient-specific cutting guides and implants, tailored to the individual anatomy of the patient (11–13).

The use of 3D-printed cutting guides offers enhanced surgical precision, ensuring accurate execution of the preoperative plan and reducing intraoperative variability (14). Additionally, a 3D-printed patient-specific polyetheretherketone (PEEK) cranial implant was utilized in this case. PEEK, a biocompatible material, presents several advantages for cranioplasty, including excellent biocompatibility, radiolucency (adequate for MRI), compatibility with radiation therapy and mechanical properties resembling cortical bone (15, 16).

To the author's knowledge, this is the first case report in the scientific literature regarding the digital workflow for PEEK 3D printing for cranioplasty in veterinary medicine. By incorporating these advancements, this case report contributes to the growing body of evidence supporting the utilization of advanced surgical techniques in improving MLO management and enhancing patient outcomes in veterinary oncology. This approach can improve surgical precision, optimize implant fit, and potentially reduce complication rates compared to conventional methods.

Clinical report

History, clinical evaluation, and findings

A 12 year old, neutered Female German Shepherd dog was presented with a chronic, progressively worsening history of decreased alertness, stumbling on all four limbs, and blindness. Physical examination revealed a facial deformity with a bilobed mass in the occipital region. The neurological evaluation identified diminished alertness and awareness, with absent menace responses bilaterally. Gait analysis demonstrated hypermetria with tetraparesis and ataxia affecting all four limbs. All spinal reflexes, including the cutaneous trunci muscle reflex, were normal. Vertebral column manipulation and palpation were unremarkable. No head tilt, nystagmus, or wide-based stance were observed. Complete blood count and serum biochemistry results fell within normal reference ranges. A multifocal neurological disorder affecting the cerebellum and forebrain was suspected.

MRI and CT imaging datasets of the brain were performed using a 0.25 Tesla magnet (VET MR Grande, Esaote, Genova, Italy) and a 16-slice CT scanner (Somatom Emotion, Siemens, Switzerland), respectively. Imaging revealed a large, multilobular, mineralized osteodestructive mass measuring 5 cm × 6 cm × 8 cm, arising from the occipital and parietal bones of the skull. The mass exhibited a coarse, granular appearance and caused significant mass effect, displacing and effacing most of the cerebellum and occipital lobes. Transtentorial herniation and brain edema were also evident. Additionally, MRI findings suggestive of secondary spinal cord edema were observed in the cranial cervical spine. Based on the comprehensive imaging features, multilobular osteochondrosarcoma was considered the most likely diagnosis.

To assess for metastasis, CT scans of the thorax and abdomen were performed, revealing no evidence of distant spread. Notably, careful evaluation of post contrast imaging focused on the skull presence/absence of contrast enhancement within large venous sinuses and their patency. These images demonstrated compression of the caudal portion of the dorsal sagittal sinus by the mass.

Preoperative virtual surgical planning

The patient's CT scans were exported as Digital Imaging and Communications in Medicine (DICOM) format and imported into a medical imaging software (Materialize Mimics Innovation Suite, version 24.0, Materialize NV, Leuven, Belgium), where the skull bones and the tumor extension were demarcated. After the segmentation process, the bone and tumor surface geometry was saved as a Standard Tessellation Language (STL) file. Subsequently, the patient-specific

cutting guides and the cranial implants were designed using computer-aided design modeling software (Geomagic Freeform, version 2021, 3D Systems, Rock Hill, South Carolina, United States).

Bilateral cutting guides, tailored for both the right and left sides of the cranial tumor extent, were meticulously designed. These guides were planned with specific features to accommodate the resection procedure effectively, integrating craniotomy grove to fit the Misonix BoneScalpel® (MBS) blade and fixation screw placements. The left and right cutting guides possessed a V-shaped interlocking feature to facilitate easier assembly, ensuring accurate and effective guidance during the surgical procedure. For the skull-specific craniotomy guide, the craniotomy line was first drawn 5 mm away from the skull tumor margins on the CAD software in order to balance the likelihood of clear margins and preservation of important anatomical landmarks (such as the occipital condyles). On each side of that line, two guiding walls were then designed. This led to a guide composed of two walls and a craniotomy groove in which the blade of the bone scalpel would slide in. In order to secure the guide to the skull, holes for fixation screws were added in the design (Figures 1A,E). These cutting guides were subsequently fabricated through Stereolithography (SLA) 3D printing technology utilizing biocompatible materials (BioMed Clear, Formlabs, Ohio, United States). In addition, a 3D model of the dog's occipital skull template was fabricated using a material-extrusion 3D printer [MakerBot PLA Filament (true white), MakerBot Replicator+, MakerBot Industries, Brooklyn, New York, United States]. This step evaluated the fit of the surgical cutting guide and the cranial implant. By utilizing this template model, the surgical team could assess the precise alignment and positioning of the guide and implant in relation to the patient's skull anatomy, ensuring optimal surgical outcomes.

To produce the 3D-printed PEEK patient-specific cranial implant, a material extrusion-based 3D printer (Kumovis R1.2, Kumovis GmbH, Munich, Germany) was employed. The STL file of the cranial implant design was imported into the 3D printer's slicing software (Simplify3D 4.1.1, Cincinnati, United States), where specific printing parameters for PEEK were chosen. Utilizing a 1.75 mm PEEK filament (Evonik Vestakeep®i4 3DF, Evonik Industries AG, Essen, Germany), the printer fabricated the cranial implant, with the sliced G-code file subsequently transferred to the printer (Figure 1C). After printing the cranial implant, the raft and support structures were manually removed using rotary tools, with no additional post-processing steps. Following fabrication, the PEEK cranial implant underwent autoclave sterilization, while the guide and skull template were sterilized with H_2O_2 according to standard protocols.

Surgical management

For the pre-operative management, a two-week course of corticosteroids (prednisolone, 1 mg/kg/day, PO) was administered pre-operatively to reduce brain edema. Figure 1 shows the pre-and post-surgery planning with the cutting guides and prosthesis.

The surgery was performed under general anesthesia with the patient in sternal recumbency. Following aseptic preparation, a midline skin incision was made between the orbits to the caudal

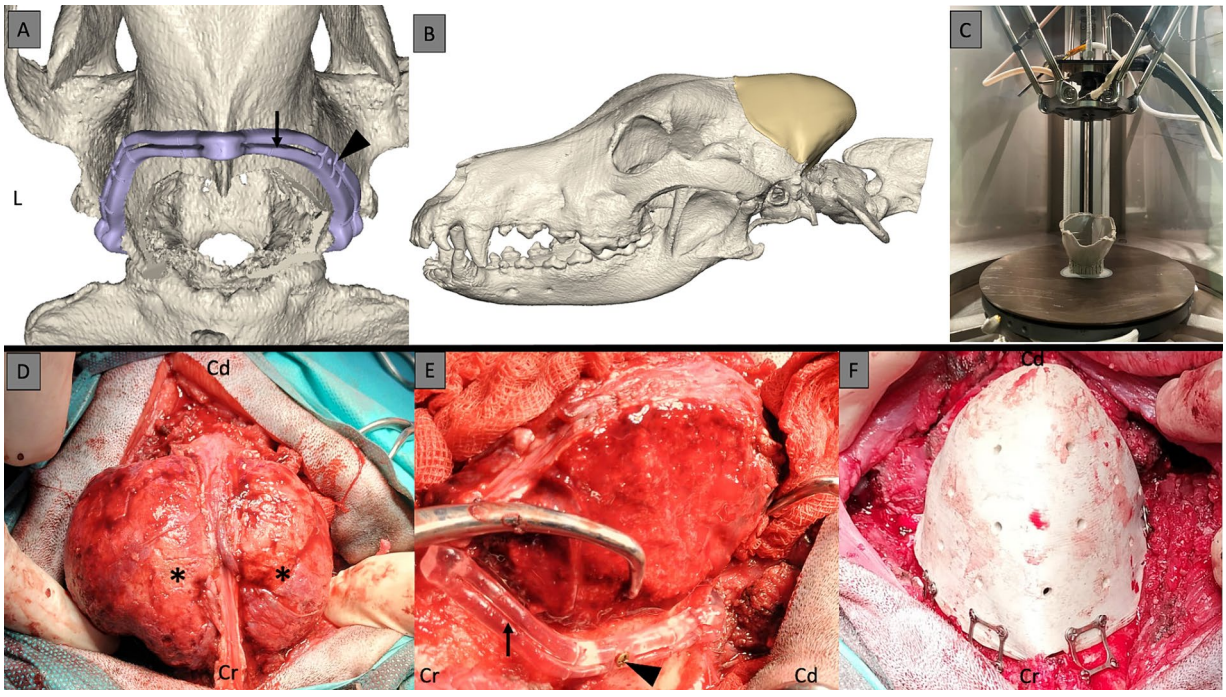

FIGURE 1
3D surgical planning of the cutting guides with the groove (black arrow) for the blade of the bone scalpel and the holes for the fixation screws (black arrowhead) **(A)**. 3D surgical planning with the skull prosthesis in place to fit exactly the craniotomy line **(B)**. 3D printing of the PEEK implant **(C)**. Multilobular osteochondrosarcoma (MLO) intraoperatively with a bilobed shape (black asterisks) **(D)**. MLO stripped of its masses to allow for placement of the cutting guides with craniotomy grove (black arrow) and the fixation screws (black arrowhead) **(E)**. 3D-printed PEEK skull implant after craniectomy and attached to the skull with screws and plates **(F)**. Cr, cranial; Cd, caudal; L, left.

portion of C2. The temporalis muscles were reflected bilaterally to expose the skull. In the occipital region, the superficial and deep cervical musculature were dissected to elevate the musculature from the occipital bone, C1 dorsal arch, and C2 spinous process. Wet gauze covered and moistened the exposed musculature throughout the surgery. The entire skull was exposed from one zygomatic arch to the other and caudally to the C1 transverse processes. The 3D-printed skull template and cutting guides guided the extent of exposure.

A Misonix BoneScalpel® (MBS) with 3D-printed cutting guides facilitated the craniotomy. After clearing residual soft tissue from the contact points, the guides were secured with 3 mm self-cutting skull screws. The bilobed MLO necessitated initial excision of its outer portion before guide placement. The MBS with a 20 mm Blade Blunt (MXB-20) facilitated near-bloodless tumor resection. Following this, a lateral craniotomy was performed using the cutting guides. Full-thickness osteotomy was achieved, except near the dorsal sagittal and transverse sinuses, where a Ø4.4 Diamond Shaver (MXB-S3) was utilized to prevent their transection. The lateral craniotomy was extended dorsally, caudally, and ventrally to achieve a lateral osteotomy while preserving the midline and caudal vascular regions. Bone flaps were carefully elevated from the dura mater bilaterally using a Freer periosteal elevator. Bipolar cautery on low settings controlled bleeding (10 Watt maximum, ICC 350, ERBE, Tubingen Germany) Tactile feedback aided in identifying the inner cortical layer during bone removal with the MBS and blade blunt. The diamond shaver connected the two lateral craniectomies at their cranial and caudal contact points over the dorsal sagittal and transverse sinuses, respectively. With complete craniotomy achieved, the intracranial MLO was gradually elevated dorsally and caudally using hand traction and a Freer periosteal elevator to detach the dura mater safely from the abnormal bone. Moderate hemorrhage from the left transverse sinus was controlled with obliteration with bone wax.

The 3D-printed patient-specific PEEK cranial implant was positioned over the craniectomy defect and secured with 3.0 mm self-drilling screws and skull plates (Matrix Neuro Plates, 0.4 mm thickness, Synthes, Zuchwil, Switzerland). While the fit was deemed satisfactory, a slight imperfection was noted in the most caudal portion of the occiput due to friable bone.

Polypropylene mesh (Prolene, Ethicon, Somerville, NJ) was used for neck muscle reconstruction. The mesh was left intact in the cervical portion but divided medially to allow expansion over each skull side. The mesh was cut to the deeper cervical musculature dorsally and covered with the superficial muscle layer. The mesh was then attached to the bilateral masseter muscle fascia using polydioxanone sutures (PDS II, Ethicon, Somerville, NJ). The mesh was not attached to the skull implant to prevent traction. Dead space between muscle layers was closed with interrupted sutures. Subcutaneous tissue and skin were closed with absorbable sutures and skin staples, respectively. Figure 2 shows pre- and post-operative CT.

Intraoperatively, the patient received cefazolin (22 mg/kg, IV), methylprednisolone succinate (10 mg/kg, IV), and mannitol (1 g/kg IV over 20 min). The surgical procedure lasted 4 h. Postoperative pain management included buprenorphine for 3 days, followed by a combination of prednisolone (1 mg/kg/day, PO), cefalexin (20 mg/kg, twice daily, PO), and gabapentin (10 mg/kg three times per day, PO) for 3 weeks. The dog was discharged on postoperative day 3 with neurological signs unchanged from pre-surgery. Histopathological examination of the resected bone confirmed a Grade I MLO according to the Dernell classification (2). Although the margins were free of tumor, potential recurrence was acknowledged due to the tumor's proximity to the resection margins.

Follow-Up

Regular telephone consultations were conducted to monitor the dog's clinical and neurological status. The eight-week follow-up revealed that the dog had a residual right pelvic limb proprioceptive deficit, while other neurological examination results had returned to normal. The owner observed marked improvements in the dog's gait, vision, behavior, and mentation within the first 3 weeks after the surgery. A computed tomography (CT) scan carried out 8 weeks post-surgery revealed a periosteal reaction at the cranial interface between the skull and the prosthesis and on the ventral aspect of the occipital craniectomy. There were no signs of implant rejection. The dog commenced chemotherapy 10 weeks following the surgery, with a regimen including Cyclophosphamide at 12.5 mg/day PO, Furosemide at 20 mg/day PO, Thalidomide at 50 mg/day PO, and Piroxicam at 15 mg/day PO as needed.

At 53 weeks post-surgery, the dog exhibited symptoms of apathy and hematochezia, but an abdominal ultrasound did not reveal any abnormalities. The dog received symptomatic inpatient treatment for 3 days, and chemotherapy was halted for 4 weeks due to suspected gastrointestinal adverse effects from the medication.

Seventy-nine weeks after the surgery, the dog developed coughing and vomiting, leading to a diagnosis of aspiration pneumonia and megaesophagus. Tests for Acetylcholine receptor antibodies, TSH, T4, and cortisol levels were all within normal limits. The dog was treated symptomatically with antibiotics for 3 days as an inpatient and was then discharged with a suspicion diagnosis of acquired idiopathic megaesophagus. Regrettably, the dog died at home. Ultimately, the dog's post-surgical survival time was 18 months.

Discussion

This case report demonstrates the successful application of a patient-specific 3D-printed polyetheretherketone (PEEK) cranial implant for cranioplasty following extensive tumor resection in a dog.

The selection of PEEK offered many reported advantages, including its robustness, lightweight nature and comfort for the animal. Moreover, PEEK implants are known for their biocompatibility and compatibility with imaging studies, thus ensuring diagnostic accuracy. Notably, they can withstand sterilization procedures while maintaining their structural integrity (17). Furthermore, PEEK cranial implants demonstrate sufficient dimensional accuracy and possess mechanical properties similar to cortical bone, essential for ensuring effective reconstruction and safeguarding anatomical cranial structures (18, 19). Nevertheless, it is essential to acknowledge the limitations associated with PEEK cranial implants. While 3D-printed PEEK cranial implants offer numerous benefits, these tend to be more costly compared to standard stock implants. Additionally, PEEK lacks osteointegration capabilities, hindering its ability to seamlessly integrate with surrounding bone tissue (20).

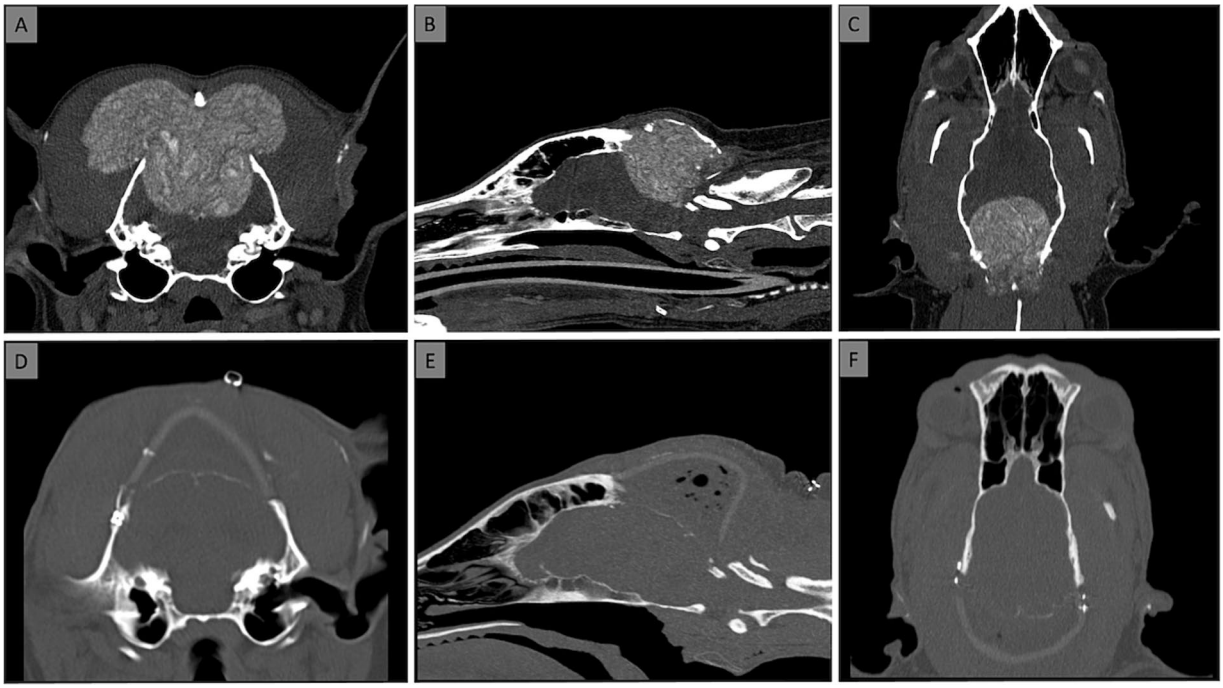

FIGURE 2
Computed Tomography [CT; transverse **(A,D)**, sagittal **(B,E)**, dorsal **(C,F)** views] at the time of diagnosis **(A–C)** and after placement of the prosthesis **(D–F)**. No dorsal sagittal sinus was visible at the level of the MLO on post contrast CT and MRI.

Conversely, other biomaterials commonly used in cranioplasty present their own set of advantages and drawbacks. For instance, polymethyl methacrylate (PMMA), although cost-effective and readily available, poses challenges in molding and adapting to complex cranial defects, potentially prolonging surgery time and increasing infection risks (21).Titanium mesh, known for its excellent biocompatibility and favorable mechanical strength, is prone to infection rates and deformation under trauma and can cause significant imaging artifacts (22). Recent studies also suggest a higher risk of implant failure with other biomaterials compared to PEEK cranial implants (23). Hydroxyapatite, while promoting bone growth, is brittle and may lead to fractures before complete integration (24), particularly in adult animals.

This case report highlights the potential advantages of using 3D-printed technology for cranioplasty: (1) improved accuracy and efficiency: Patient-specific implants ensure a precise fit, minimizing the risk of margin errors and facilitating reconstruction. (2) Enhanced visualization and planning: 3D-printed models of the skull and tumor can aid preoperative planning and improve intraoperative decision-making. (3) Reduced surgery time and potential complications: Precise cutting guides can streamline the craniotomy process, potentially reducing surgical time and associated risks.

Limitations and future directions: while this report demonstrates the successful application of this technology in a single case, further research is needed to evaluate its broader efficacy and long-term outcomes in a larger population. Additionally, considerations regarding cost-effectiveness and accessibility of 3D printing technology need to be addressed for wider adoption in veterinary medicine.

Overall, this case report contributes to the growing body of evidence supporting the potential benefits of 3D-printed patient-specific implants and cutting guides for cranioplasty in veterinary patients.

Data availability statement

The original contributions presented in the study are included in the article/supplementary material, further inquiries can be directed to the corresponding author.

Ethics statement

Ethical approval was not required for the studies involving animals in accordance with the local legislation and institutional requirements because this is a retrospective case report based on clinical and imaging findings. Owner did give verbal consent for use of CT and surgery data for publication. Written informed consent was not obtained from the owners for the participation of their animals in this study because this is a retrospective case report based on clinical and imaging findings.

Author contributions

MH: Writing – original draft, Writing – review & editing, Conceptualization. NS: Writing – original draft, Writing – review & editing, Conceptualization, Methodology, Software, Supervision,

Validation, Visualization. CB: Writing – original draft, Writing – review & editing, Investigation, Validation. SH: Writing – original draft, Writing – review & editing, Investigation, Supervision, Validation. AO: Writing – original draft, Writing – review & editing, Formal analysis, Supervision, Validation. MM: Writing – original draft, Writing – review & editing, Investigation, Methodology, Software. MB: Writing – original draft, Writing – review & editing, Investigation, Methodology, Software. FT: Writing – original draft, Writing – review & editing, Supervision, Validation. JG: Writing – original draft, Writing – review & editing, Conceptualization, Formal analysis, Investigation, Methodology, Project administration, Resources, Supervision, Validation, Visualization.

Funding

The author(s) declare that financial support was received for the research, authorship, and/or publication of this article. This work was funded by the Innovation Focus Regenerative Surgery of the University Hospital Basel and by the Werner Siemens Foundation through the Minimally Invasive Robot-Assisted Computer-guided LaserosteotomE II (MIRACLE II) project.

Conflict of interest

CB was employed by Vetpixel SAS.

The remaining authors declare that the research was conducted in the absence of any commercial or financial relationships that could be construed as a potential conflict of interest.

Publisher's note

References

1. Wisner ER, Zwingenberger AL. Atlas of small animal CT and MRI, section 1: Head and neck, chapter 1.4: Skull. Ames, Iowa, USA: Wiley Blackwell; (2015). p. 55–68.

2. Dernell WS, Straw RC, Cooper MF, Powers BE, LaRue SM, Withrow SJ. Multilobular osteochondrosarcoma in 39 dogs: 1979-1993. *J Am Anim Hosp Assoc*. (1998) 34:11–8. doi: 10.5326/15473317-34-1-11

3. Piazza AM, McAnulty JF, Early P, Guevar J. Craniectomies for dogs with skull multilobular Osteochondrosarcoma using the Misonix bone scalpel: cadaveric evaluation and retrospective case series. *Top Companion Anim Med*. (2023) 53-54:100772. doi: 10.1016/j.tcam.2023.100772

4. Hayes GM, Demeter EA, Choi E, Oblak M. Single-stage craniectomy and cranioplasty for multilobular osteochondrosarcoma managed with a custom additive manufactured titanium plate in a dog. *Case Rep Vet Med*. (2019) 2019:6383591. doi: 10.1155/2019/6383591

5. Sheahan DE, Gillian TD. Reconstructive cranioplasty using a porcine small intestinal submucosal graft. *J Small Anim Pract*. (2008) 49:257–9. doi: 10.1111/j.1748-5827.2007.00515.x

6. Bryant KJ, Steinberg H, McAnulty MF. Cranioplasty by means of molded polymethylmethacrylate prosthetic reconstruction after radical excision of neoplasms of the skull in two dogs. *J Am Vet Med Assoc*. (2003) 223:67–72. doi: 10.2460/javma.2003.223.67

7. Salyer KE, Bardach J, Squier CA, Gendler E, Kelly KM. Cranioplasty in the growing canine skull using demineralized perforated bone. *Plast Reconstr Surg*. (1995) 96:770–9. doi: 10.1097/00006534-199509001-00002

8. Igawa K, Mochizuki M, Sugimori O, Shimizu K, Yamazaki M, Nomoto S, et al. Tailor-made, tricalcium phosphate bone implant directly fabricated by 3-dimensional inkjet printer. *J Artif Organs*. (2006) 9:234–40. doi: 10.1007/s10047-006-0347-y

9. Shores A, Brisson BA. Advanced techniques in canine and feline neurosurgery chapter 21 surgical management and intraoperative strategies for Tumors of the skull. Hoboken, NJ: Wiley. (2023).

10. Rosselli DD, Platt SR, Freeman C, O'Neill J, Kent M, Holmes SP. Cranioplasty using titanium mesh after skull tumor resection in five dogs. *Vet Surg*. (2017) 46:67–74. doi: 10.1111/vsu.12577

11. Thieringer FM, Honigmann P, Sharma N. Medical additive manufacturing in surgery: translating innovation to the point of care In: S Ehsani, P Glauner, P Plugmann and FM Thieringer, editors. The future circle of healthcare. Future of business and finance. Cham: Springer (2022)

12. Wegmüller L, Halbeisen F, Sharma N, Kühl S, Thieringer FM. Consumer vs. high-end 3D printers for guided implant surgery-an in vitro accuracy assessment study of different 3D printing technologies. *J Clin Med*. (2021) 10:4894. doi: 10.3390/jcm10214894

13. Modgill V, Balas B, Chi M, Honigmann P, Thieringer FM, Sharma N. Knowledge domain and innovation trends concerning medical 3D printing for craniomaxillofacial surgery applications: a 30-year bibliometric and visualized analysis. *Craniomaxillofac Res Innov*. (2023) 8:27528464231170964. doi: 10.1177/27528464231170964

14. Murtezani I, Sharma N, Thieringer FM. Medical 3D printing with a focus on point-of-Care in Cranio-and Maxillofacial Surgery. A systematic review of literature. *Ann 3D Printed Med*. (2022) 6:100059. doi: 10.1016/j.stlm.2022.100059

15. Honigmann P, Sharma N, Okolo B, Popp U, Msallem B, Thieringer FM. Patient-specific surgical implants made of 3D printed PEEK: material, technology, and scope of surgical application. *Biomed Res Int*. (2018) 2018:4520636. doi: 10.1155/2018/4520636

16. Sharma N, Aghlmandi S, Cao S, Kunz C, Honigmann P, Thieringer FM. Quality characteristics and clinical relevance of in-house 3D-printed customized Polyetheretherketone (PEEK) implants for craniofacial reconstruction. *J Clin Med*. (2020) 9:2818. doi: 10.3390/jcm9092818

17. Sharma N, Zubizarreta-Oteiza J, Tourbier C, Thieringer FM. Can steam sterilization affect the accuracy of point-of-care 3D printed Polyetheretherketone (PEEK) customized cranial implants? An investigative analysis. *J Clin Med*. (2023) 12:2495. doi: 10.3390/jcm12072495

18. Sharma N, Honigmann P, Cao S, Thieringer F. Dimensional characteristics of FDM 3D printed PEEK implant for craniofacial reconstructions. *Trans Addit Manuf Meets Med*. (2020) 2:1. doi: 10.18416/AMMM.2020.2009009

19. Sharma N, Aghlmandi S, Dalcanale F, Seiler D, Zeilhofer HF, Honigmann P, et al. Quantitative assessment of point-of-care 3D-printed patient-specific Polyetheretherketone (PEEK) cranial implants. *Int J Mol Sci*. (2021) 22:8521. doi: 10.3390/ijms22168521

20. Yao S, Zhang Q, Mai Y, Yang H, Li Y, Zhang M, et al. Outcome and risk factors of complications after cranioplasty with polyetheretherketone and titanium mesh: a single-center retrospective study. *Front Neurol*. (2022) 13:926436. doi: 10.3389/fneur.2022.926436

21. Matsuno A, Tanaka H, Iwamuro H, Takanashi S, Miyawaki S, Nakashima M, et al. Analyses of the factors influencing bone graft infection after delayed cranioplasty. *Acta Neurochir*. (2006) 148:535–40. doi: 10.1007/s00701-006-0740-6

22. Kwiecien GJ, Rueda S, Couto RA, Hashem A, Nagel S, Schwarz GS, et al. Long-term outcomes of Cranioplasty: titanium mesh is not a long-term solution in high-risk patients. *Ann Plast Surg*. (2018) 81:416–22. doi: 10.1097/SAP.0000000000001559

23. Henry J, Amoo M, Taylor J, O'Brien DP. Complications of Cranioplasty in relation to material: systematic review, network meta-analysis and meta-regression. *Neurosurgery*. (2021) 89:383–94. doi: 10.1093/neuros/nyab180

24. Alkhaibary A, Alharbi A, Alnefaie N, Oqalaa Almubarak A, Aloraidi A, Khairy S. Cranioplasty: a comprehensive review of the history, materials, surgical aspects, and complications. *World Neurosurg*. (2020) 139:445–52. doi: 10.1016/j.wneu.2020.04.211

frontiers | Frontiers in Veterinary Science

TYPE Case Report
PUBLISHED 23 September 2024
DOI 10.3389/fvets.2024.1426421

OPEN ACCESS

EDITED BY
Theresa Elizabeth Pancotto,
Virginia Tech, United States

REVIEWED BY
Koen Santifort,
IVC Evidensia Small Animal Referral Hospital Arnhem, Netherlands
Maria Teresa Mandara,
University of Perugia, Italy

*CORRESPONDENCE
Hiroaki Kamishina
✉ kamishina@kyotoar.com

RECEIVED 01 May 2024
ACCEPTED 13 August 2024
PUBLISHED 23 September 2024

CITATION
Terao M, Uemura T, Hasegawa H, Ashida C, Ehara I, Ozawa T and Kamishina H (2024) Case report: Intracranial epidermoid cyst in a cat. *Front. Vet. Sci.* 11:1426421. doi: 10.3389/fvets.2024.1426421

Case report: Intracranial epidermoid cyst in a cat

Masashi Terao[1], Takashi Uemura[1], Hiroki Hasegawa[1], China Ashida[2], Ikuya Ehara[2], Tsuyoshi Ozawa[1] and Hiroaki Kamishina[1]*

[1]KyotoAR Animal Referral Medical Center, Kumiyama, Japan, [2]St. Luke's Animal Medical Center, Toyonaka, Japan

A 9-year-old American Shorthair, castrated male, weighing 4.3 kg was presented to our hospital because of intermittent ataxia and tetraparesis for 6 weeks. On presentation, the cat was in a stupor and on recumbency, and had vertical nystagmus in both eyes. These clinical signs suggested a brainstem disorder. MRI showed a mass lesion in the caudal aspect of the fourth ventricle with hyperintensity on T2-weighted and FLAIR imaging, low-intensity on T1-weighted imaging, and enhanced margins on post-contrast T1-weighted imaging. The mass compressed the fourth ventricle, causing obstructive hydrocephalus. A second cystic lesion was found rostral to the cerebellum. After MRI, the cat experienced respiratory difficulties and the mass was removed by emergency craniectomy. Although the mass including the cyst wall was successfully removed, the cat was euthanized because spontaneous breathing did not return. The mass was histopathologically diagnosed as epidermoid cyst. A biopsy to the rostral cystic lesion had not been performed and therefore the etiology of this lesion remained unclear. This is the first case of feline intracranial epidermoid cyst in which MRI and surgical excision were performed. MRI findings were similar to those in humans and dogs, suggesting that imaging studies are useful in cats for the diagnosis of intercranial epidermoid cyst.

KEYWORDS

brain, cholesteatoma, craniectomy, epidermoid cyst, feline, fourth ventricle, intracranial cyst, MRI

Introduction

Epidermoid cysts are benign cystic lesions in which epidermal cells ectopically migrate during development (1–3). They form cysts lined by stratified squamous epithelium, inside which exfoliated keratinized material accumulates and gradually enlarges. It is also called a cholesteatoma because of its macroscopic features (3, 4).

Intracranial epidermoid cysts often develop in the cerebellopontine angle and fourth ventricle. As they gradually enlarge, they compress the cerebellum and medulla, causing neurological signs, such as central vestibular disorders (2, 4). These lesions have been reported in humans, horses, dogs, and rats (2, 5–7), and only one case has been reported in a cat (8). In this report, no imaging or surgery was performed and the patient was euthanized and the diagnosis was made at necropsy.

In the present case, we had an opportunity to surgically remove an epidermoid cyst that developed caudal to the fourth ventricle of a cat. To the best of our knowledge, there have been no previous reports of surgical removal or magnetic resonance imaging (MRI) of intracranial epidermoid cysts in cats.

FIGURE 1
T2-weighted **(A)** and contrast-enhanced T1-weighted **(B)** sagittal MRI of the brain. An extra-axial cystic mass (white arrows) is observed caudal to the fourth ventricle and is compressing the fourth ventricle and medulla severely. A dilation of a second cystic lesion was also observed rostral to the cerebellum (*), which was considered an arachnoid diverticulum.

Case presentation

The case was a 9-year-old American Shorthair, neutered male, weighing 4.3 kg. For 6 weeks the cat had displayed intermittent tetraparesis and proprioceptive ataxia. The cat had no other clinical signs, with normal activity and appetite. No abnormalities were found in physical examination, complete blood count (CBC), blood biochemical test, and cardiac ultrasonography at the primary care clinic. No treatment was instituted at this time. However, abnormal gait continued intermittently and the cat fell down the stairs once. A few days after falling, the cat visited the emergency hospital following collapse and respiratory distress. Chest and abdominal radiography revealed no abnormalities. The patient was referred to the neurology department of our hospital.

At presentation, the cat was in a stupor state with a recumbent posture. It showed tachycardia (200 bpm) and hyperthermia (39.3°C). The cat was non-ambulatory tetraparetic, and showed absent postural reactions, mildly increased spinal reflexes, and decreased superficial pain perception in all limbs. Vertical nystagmus in both eyes was noted, which was exacerbated by placing the cat in dorsal-recumbency. The resting pupillary diameter of both eyes was mid-range, but both direct and indirect pupillary light reflexes were decreased. CBC and blood biochemical tests were unremarkable. Neurological examination was consistent with a brainstem disorder, and MRI of the brain was indicated.

The patient was premedicated with midazolam (Dormicum, Maruishi Pharmaceutical Co., Osaka, Japan; 0.2 mg/kg IV) and anesthetized with propofol (PropoFlo28, Zoetis Japan, Tokyo, Japan) injection to effect. After endotracheal intubation, general anesthesia was maintained with 2% sevoflurane (SEVOFLO, Maruishi Pharmaceutical Co., Osaka, Japan). MRI was performed using 0.3T AIRIS Vento (Hitachi, Tokyo, Japan) with sagittal, transverse and dorsal planes on T2-weighted (TR/TE = 4,000/100) imaging; transverse planes on T1-weighted (TR/TE = 380/15) imaging; and fluid-attenuated inversion recovery (FLAIR; TR/TE = 9,000/100) imaging. Sagittal, transverse and dorsal planes of T1-weighted imaging after IV injection of gadolinium (OMNISCAN 32%, GE HealthCare Pharma Co., Tokyo, Japan; 64 mg/kg IV) were also performed. MRI revealed an extra-axial mass lesion at the dorsal medulla and the caudal fourth ventricle, compressing the medulla ventrally and the cerebellum dorsally (Figure 1). The mass was high-intensity on T2-weighted and FLAIR imaging, low-intensity on T1-weighted imaging (higher than the signal of cerebrospinal fluid) and was enhanced in the margins on post-contrast T1-weighted imaging (Figure 2). The third ventricle, lateral ventricles, and olfactory ventricle were enlarged, and the sulci were obscured throughout. Based on these findings, we suspected that the patient had obstructive hydrocephalus secondary to a mass lesion caudal to the fourth ventricle. Epidermoid cysts, arachnoid diverticula, abscesses and neoplasms (e.g., meningioma, lymphoma and ependymoma) were differential diagnoses for the mass (8–11). A histopathological examination was considered necessary for diagnosis. A second cystic lesion was found between the tectum and the cerebellum, dorsal to the quadrigeminal cistern. This lesion showed the same signal pattern as cerebrospinal fluid: high intensity on T2-weighted imaging, low intensity on T1-weighted imaging and FLAIR imaging and no contrast enhancement. This concurrent lesion was suspected to be an arachnoid diverticulum, but the clinical significance of the lesion was unclear.

Although recovery was delayed after MRI, the patient was extubated temporarily after administration of concentrated glycerin (GLYCEOL, TAIYO Pharma Co., Tokyo, Japan; 1 g/kg slow IV), prednisolone (Prednisolone, Kyoritsu Seiyaku Co., Tokyo, Japan; 1 mg/kg SC), furosemide (Flosemide injection, Nichi-Iko Pharmaceutical Co., Toyama, Japan; 1 mg/kg IV). However, we reintubated when the patient stopped breathing and spontaneous respiration did not resume after which emergency craniectomy was performed.

A midline incision was made for an occipital approach to the dorsal medulla. After dural incision, a slightly glossy white mass was observed on the ventral side of the caudal border of the cerebellum (Figure 3). The mass was firmer than the brain parenchyma and had a cystic structure. Intraoperative imprint cytology of the contents of the cyst with Diff-Quick staining (SYSMEX Co., Kobe, Japan) revealed denucleated keratinocytes. No bacterial pathogens were observed. After internal decompression by excising the contents of the cyst, the cyst wall was excised. The brain parenchyma did not relocate and remained depressed after mass removal. We covered the craniectomy defect with a free flap of temporalis fascia and applied fibrin glue (Beriplast P Combi-Set Tissue adhesion, CSL Behring K.K., Tokyo, Japan). The wound was

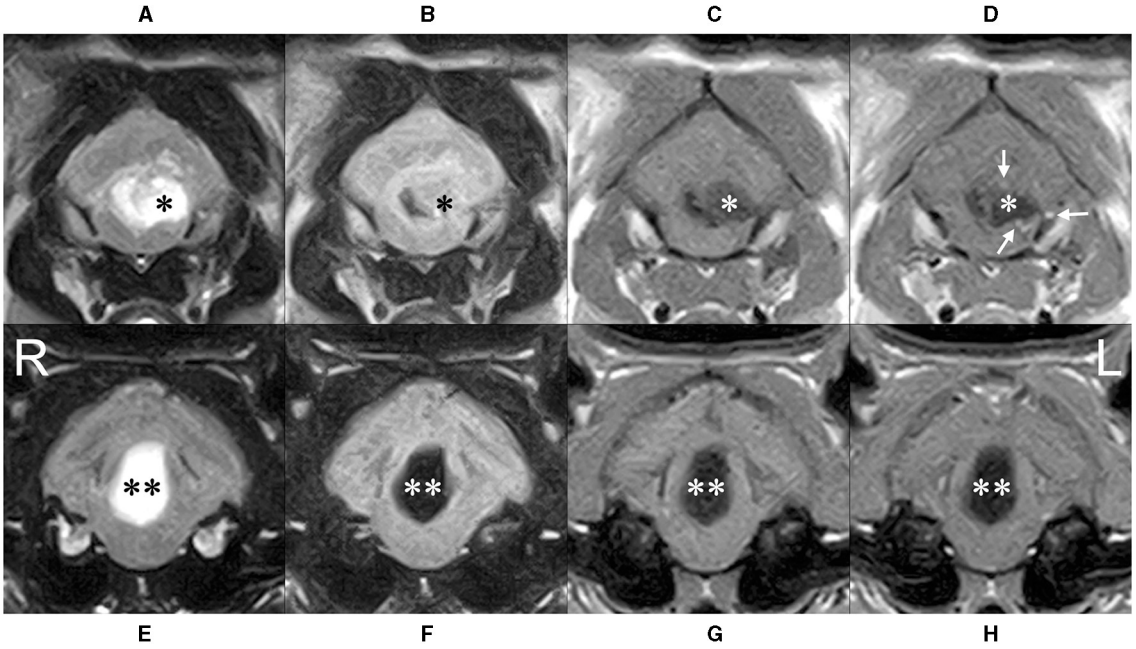

FIGURE 2
Transverse MRI at caudal **(A–D)** and rostral **(E–H)** level of the cerebellum. The cyst (*) severely compressed the fourth ventricle to the right, the medulla ventrally, and the cerebellum dorsally. High intensity on T2-weighted **(A)** and FLAIR **(B)** imaging, low intensity on T1-weighted imaging **(C)** (higher than cerebrospinal fluid) was observed, and contrast-enhanced T1-weighted imaging **(D)** showed a ring-shaped enhancement of the limbus (white arrows). The rostral cystic lesion (**) showed high intensity on T2-wighted imaging **(E)**, lower intensity than that of cerebrospinal fluid on FLAIR imaging **(F)** and low intensity on T1-wighted imaging **(G)** without any contrast enhancement **(H)**.

closed by a standard method. The excised lesions were fixed in 10% formalin solution. No cultural examination was performed.

Fentanyl (DAIICHI SANKYO Co., Tokyo, Japan; 3 μg/kg/h constant rate infusion) for analgesia and cefazolin (Sefazolin sodium, KOA ISEI Co., Yamagata, Japan; 20 mg/kg IV) as antibiotic were administered during surgery with crystalloid fluid infusion. Post-operatively, the patient did not resume spontaneous respiration and was euthanized after 22 h of ventilator management. Necropsy was not performed.

Histopathological examination of the submitted tissue was consistent with intracranial epidermoid cyst (Figure 4). The cyst wall was composed of inwardly keratinized stratified squamous epithelium, and the cyst cavity contained keratinized materials. Multinucleated giant cells and macrophages infiltrated in the surrounding cerebellar white matter, in which multilayered keratinization was seen with fibrogliosis.

Discussion

Previously, there is only one report of intracranial epidermoid cyst in a cat (8). In this report, all results were based on necropsy evaluation. In present case, we performed MRI and surgical treatment and this is the first report for this lesion in a cat. In both cases, the lesions were located adjacent to the fourth ventricle. Similarly, intracranial epidermoid cysts are likely to develop in cerebellopontine angles in humans and dogs (4, 12). While purebred dogs with intracranial epidermoid cysts have been sporadically reported (6, 13), there are no reports suggesting a genetic predisposition. There are currently too few feline cases to comment on breed or genetic predispositions. In dogs, intracranial epidermoid cysts usually occur in adulthood aged 7 years or younger (6, 13, 14). It takes time for these lesions to develop and expand despite a suspected congenital pathology. In humans, they are reported to occur often in middle age as 30–40 years old (3), and in another report they range widely from 16 to 78 years (15). Both feline cases were young to middle aged, consistent with reports in humans and dogs.

In our case, the cyst was depicted on MRI as a well-defined oval cyst beside the fourth ventricle. The inside of the cyst showed high intensity on T2-weighted and FLAIR imaging, low intensity on T1-weighted imaging, and the cyst wall was slightly enhanced by contrast medium in a ring-like pattern. A similar signal pattern has been reported in canine epidermoid cysts, suggesting that such imaging findings may be common in cats and dogs (1, 4). There is very little information when considering the differential diagnosis of cystic lesions in the fourth ventricle in cats because only abscesses and arachnoid diverticula have been reported thus far (10). In dogs, dermoid cysts, choroid plexus cysts and ependymal cysts are other cystic lesions in the fourth ventricle, and can be differentiated from epidermoid cysts by MRI (1, 4, 16, 17). In contrast-enhanced T1W imaging, abscesses show thicker ring-like lesion than epidermoid cysts and choroid plexus cysts show strong and homogeneous contrast enhancement (10, 16). Arachnoid diverticula and ependymal cysts show low intensity on FLAIR imaging (1, 17). Dermoid cysts are similar to epidermoid cysts in that they contain stratified squamous epithelium, but they are distinguished histologically by the presence

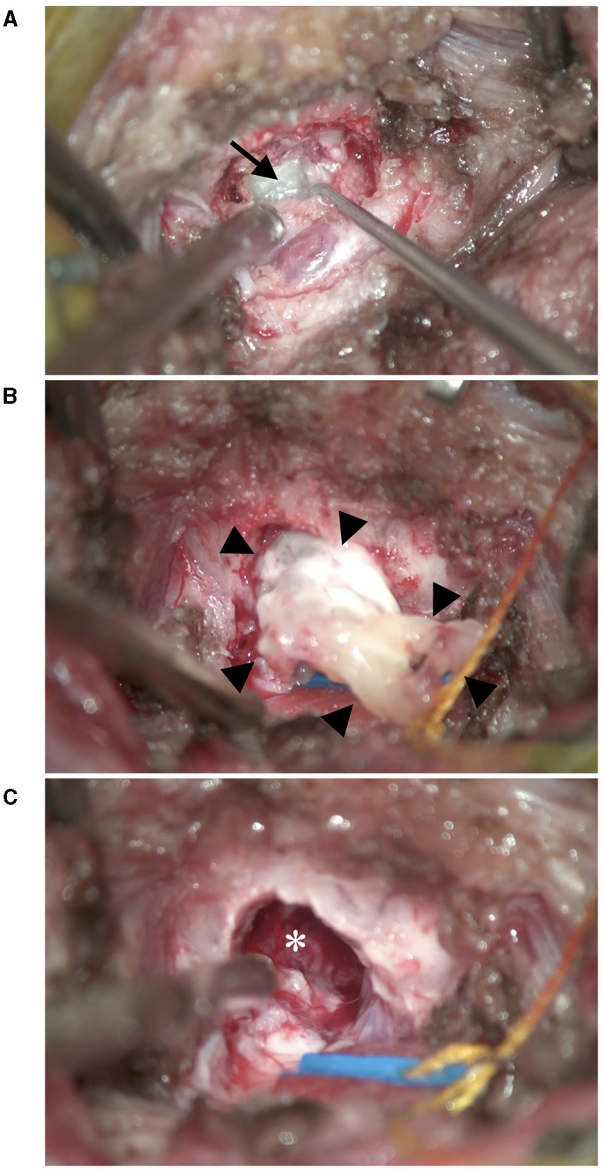

FIGURE 3
Intraoperative photographs. **(A)** After incision of the dura, a glossy white mass (black arrow) was revealed ventral to the cerebellum. **(B)** After removal of the contents of the mass, the cyst wall (black arrow heads) was excised. **(C)** After removal of the mass, the brain parenchyma did not relocate and remained depressed (*).

of organs that make up hair follicles, such as hair, sweat glands, and sebaceous glands in dermoid cysts. That is why dermoid cysts often show heterogeneous high intensity on T1-weighted MRI due to the presence of lipids whereas epidermoid cysts often show low intensity (1, 4). Other mass lesions, not necessarily cystic, that may occur in the fourth ventricle in cats are tumors, including meningioma, lymphoma, ependymoma, and metastatic tumors (11, 18, 19). These tumors often show moderate to fine contrast-enhancement (11, 20) whereas epidermoid cysts usually show slight ring-enhancement. Although definitive diagnosis requires pathological evaluation, MRI findings in our case support a diagnosis of an epidermoid cyst and are comparable to reports in other species.

MRI revealed a second cystic lesion rostral to the cerebellum. This lesion was adjacent to the quadrigeminal cistern and had the same signal pattern as cerebrospinal fluid, consistent with an arachnoid diverticulum. Although few cases in cats with arachnoid diverticulum have been previously reported, they are common in dogs and are incidental findings in more than half cases (21). The cerebellar compression rate in our case was ∼30%, which was higher than reported canine cases. However, no significant relationship between the cerebellar compression rate and clinical signs has been demonstrated in dogs (21). Therefore, the clinical contributions of this concurrent lesion compressing the medulla or cerebellum in our case were unknown. Other differentials for this lesion included true cystic lesions such as choroid plexus cysts (22), cystic tumors like meningiomas and replacement by cerebrospinal fluid after cerebellar atrophy. Histopathological examinations are needed to confirm its nature.

In humans, surgical removal of intracranial epidermoid cysts is the treatment of choice, and complete removal of the lesion is expected to result in a good prognosis (2, 15). In the present case, the epidermoid cyst was removed by an occipital approach, but the patient did not regain spontaneous respiration after surgery. This patient was already in respiratory arrest before surgery, suggesting severe medulla injury prior to surgery, but it is unknown if surgery contributed to the lack of improvement or if we simply intervened too late. In dogs, an epidermoid cyst in the fourth ventricle was surgically treated previously, and clinical signs similarly deteriorated after surgery (13). It is difficult to conclude whether surgery is recommended in dogs and cats based on these two reports. In cats, the lateral approach to meningiomas in the cerebellar fossa has been reported, in which no complication was observed (23). This approach is a surgical technique that manipulates the caudal fossa between the tentorium ossium and the nuchal crest from the lateral aspect and is considered to have the advantage of causing less damage to brain parenchyma such as the medulla. This technique may have improved the clinical course of the present case. However, because epidermoid cysts were often located ventral to the cerebellum and covered by cerebellar hemispheres, it may have been difficult to observe the lesions grossly by the lateral approach alone.

In human intracranial epidermoid cysts, incomplete resection of the squamous epithelium composing the cystic wall leads to recurrence, then the prognosis depends on whether complete surgical resection is achieved (2). In dogs, cases of suspected postoperative recurrence have been reported in intracranial and spinal cord epidermoid cysts (13, 24). There are few studies of surgical outcomes and prognosis in animals, and further studies are required to determine the best timing and approach for the surgical treatment of epidermoid cysts.

There are several limitations to the case we reported here. First, the clinical contributions of the rostral cystic-like lesion were still unclear. Any histopathological examination of this lesion was not performed while the excised lesion was diagnosed as an

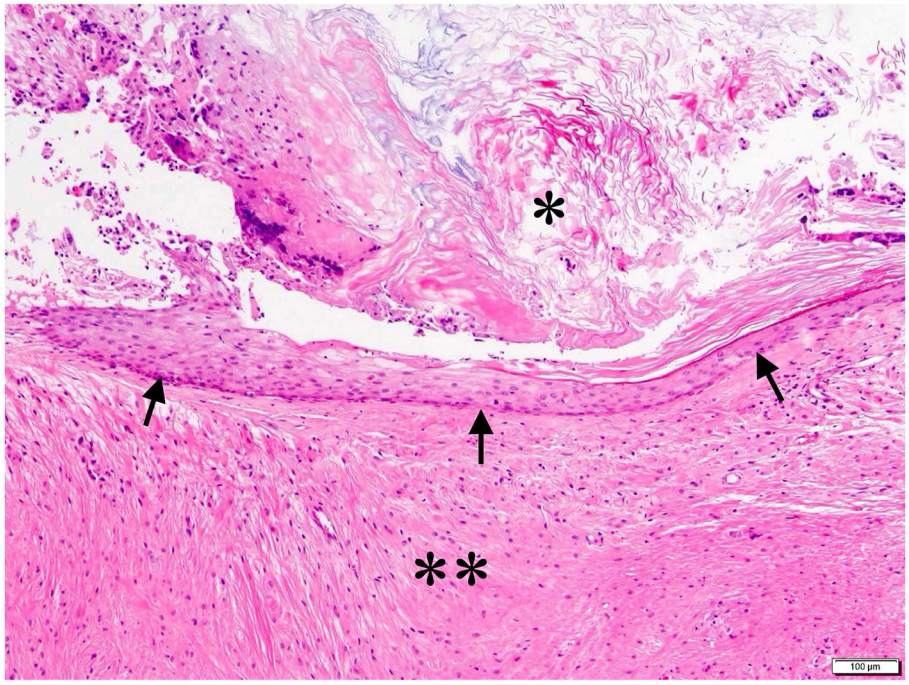

FIGURE 4
Histopathological image of the cyst. The keratinized stratified squamous epithelium formed the cyst wall (black arrow), and keratin accumulated in the cyst cavity (*). Multinucleated giant cells and macrophage infiltration and fibrous gliosis were observed in the surrounding cerebellar white matter with multilayered keratinization (**). HE stain; bar = 100 µm.

epidermoid cyst. There was a possibility that the cat failed to recover spontaneous respiration due to not only the epidermoid cyst but also the concurrent lesion. Another limitation to our description is the use of a low-field MRI. However, MR imaging in this case are similar to the images in canine case that were also performed with low-field MRI (6). Other reports using high-field MRI showed a slight heterogeneity in the epidermoid cysts (13), which differs in some respects from the images of the present case. Third, the information of the clinical course was limited. The presentation to our department was about 6 weeks after the onset of the disease, and details during this time were lacking. Moreover, we were not able to gain the information on the long-term postoperative course of this case because the patient died after surgery. In order to demonstrate that the surgery may be the standard therapy of intracranial epidermoid cysts in cats, it is necessary to experience a number of successful cases with long-term survival.

In summary, feline intracranial epidermoid cysts are considered histologically benign masses that cause central vestibular disorders due to their anatomic features of predominance around the fourth ventricle. Surgical resection may be necessary for treatment; however, the prognosis is still unclear.

Data availability statement

The original contributions presented in the study are included in the article/supplementary material, further inquiries can be directed to the corresponding author.

Ethics statement

Ethical approval was not required for the studies involving animals in accordance with the local legislation and institutional requirements because the cat was treated as a clinical case. Written informed consent was obtained from the owners for the participation of their animals in this study. Written informed consent was obtained from the owners of the animals for the publication of this case report.

Author contributions

MT: Writing – original draft, Conceptualization, Data curation, Formal analysis. TU: Data curation, Writing – review & editing. HH: Visualization, Writing – review & editing, Data curation. CA: Data curation, Writing – review & editing. IE: Writing – review & editing, Data curation. TO: Writing – review & editing, Data curation. HK: Supervision, Writing – review & editing.

Funding

The author(s) declare that no financial support was received for the research, authorship, and/or publication of this article.

Conflict of interest

The authors declare that the research was conducted in the absence of any commercial or financial relationships that could be construed as a potential conflict of interest.

Publisher's note

References

1. MacKillop E. Magnetic resonance imaging of intracranial malformations in dogs and cats. *Vet Radiol Ultrasound.* (2011) 52(1Suppl.1):S42–51. doi: 10.1111/j.1740-8261.2010.01784.x

2. Kumar S, Sahana D, Rathore L, Sahu RK, Jain A, Borde P, et al. Fourth ventricular epidermoid cyst - case series, systematic review and analysis. *Asian J Neurosurg.* (2021) 16:470–82. doi: 10.4103/ajns.AJNS_539_20

3. Hoang VT, Trinh CT, Nguyen CH, Chansomphou V, Tran TTT. Overview of epidermoid cyst. *Eur J Radiol Open.* (2019) 6:291–301. doi: 10.1016/j.ejro.2019.08.003

4. Platt S, Hicks J, Matiasek L. Intracranial intra-arachnoid diverticula and cyst-like abnormalities of the brain. *Vet Clin North Am Small Anim Pract.* (2016) 46:253–63. doi: 10.1016/j.cvsm.2015.10.004

5. Peters M, Brandt K, Wohlsein P. Intracranial epidermoid cyst in a horse. *J Comp Pathol.* (2003) 129:89–92. doi: 10.1016/S0021-9975(02)00169-X

6. Steinberg T, Matiasek K, Brühschwein A, Fischer A. Imaging diagnosis–intracranial epidermoid cyst in a Doberman Pinscher. *Vet Radiol Ultrasound.* (2007) 48:250–3. doi: 10.1111/j.1740-8261.2007.00238.x

7. Sugimoto T, Misawa Y, Niki R. An intracranial epidermal cyst in a Sprague-Dawley rat. *J Vet Med Sci.* (1994) 56:577–9. doi: 10.1292/jvms.56.577

8. Mazaro RD, Lorenzetti DM, Paz MC, Fighera RA. Intracranial epidermoid cyst in a cat. *Ciência Rural.* (2021) 51:e20200754. doi: 10.1590/0103-8478cr20200754

9. Reed S, Cho DY, Paulsen D. Quadrigeminal arachnoid cysts in a kitten and a dog. *J Vet Diagn Invest.* (2009) 21:707–10. doi: 10.1177/104063870902100519

10. Sturges BK, Dickinson PJ, Kortz GD, Berry WL, Vernau KM, Wisner ER, et al. Clinical signs, magnetic resonance imaging features, and outcome after surgical and medical treatment of otogenic intracranial infection in 11 cats and 4 dogs. *J Vet Intern Med.* (2006) 20:648–56. doi: 10.1111/j.1939-1676.2006.tb02910.x

11. Troxel MT, Vite CH, Massicotte C, McLear RC, Van Winkle TJ, Glass EN, et al. Magnetic resonance imaging features of feline intracranial neoplasia: retrospective analysis of 46 cats. *J Vet Intern Med.* (2004) 18:176–89. doi: 10.1111/j.1939-1676.2004.tb00158.x

12. Nagasawa D, Yew A, Safaee M, Fong B, Gopen Q, Parsa AT, et al. Clinical characteristics and diagnostic imaging of epidermoid tumors. *J Clin Neurosci.* (2011) 18:1158–62. doi: 10.1016/j.jocn.2011.02.008

13. De Decker S, Davies E, Benigni L, Wilson H, Pelligand L, Rayner EL, et al. Surgical treatment of an intracranial epidermoid cyst in a dog. *Vet Surg.* (2012) 41:766–71. doi: 10.1111/j.1532-950X.2012.01010.x

14. Platt SR, Graham J, Chrisman CL, Adjiri-Awere A, Clemmons RM. Canine intracranial epidermoid cyst. *Vet Radiol Ultrasound.* (1999) 40:454–8. doi: 10.1111/j.1740-8261.1999.tb00374.x

15. Hasegawa H, Vakharia K, Carlstrom LP, Van Gompel JJ, Driscoll CLW, Carlson ML, et al. Long-term surgical outcomes of intracranial epidermoid tumors: impact of extent of resection on recurrence and functional outcomes in 63 patients. *J Neurosurg.* (2021) 2021:1–9. doi: 10.3171/2021.5.JNS21650

16. Brewer DM, Cerda-Gonzalez S, Dewey CW, Coates JR. Diagnosis and surgical resection of a choroid plexus cyst in a dog. *J Small Anim Pract.* (2010) 51:169–72. doi: 10.1111/j.1748-5827.2009.00855.x

17. Wyss-Fluehmann G, Konar M, Jaggy A, Vandevelde M, Oevermann A. Cerebellar ependymal cyst in a dog. *Vet Pathol.* (2008) 45:910–3. doi: 10.1354/vp.45-6-910

18. Troxel MT, Vite CH, Van Winkle TJ, Newton AL, Tiches D, Dayrell-Hart B, et al. Feline intracranial neoplasia: retrospective review of 160 cases (1985–2001). *J Vet Intern Med.* (2003) 17:850–9. doi: 10.1111/j.1939-1676.2003.tb02525.x

19. Woolford L, de Lahunta A, Baiker K, Dobson E, Summers BA. Ventricular and extraventricular ependymal tumors in 18 cats. *Vet Pathol.* (2013) 50:243–51. doi: 10.1177/0300985812452580

20. Durand A, Keenihan E, Schweizer D, Maiolini A, Guevar J, Oevermann A, et al. Clinical and magnetic resonance imaging features of lymphoma involving the nervous system in cats. *J Vet Intern Med.* (2022) 36:679–93. doi: 10.1111/jvim.16350

21. Matiasek LA, Platt SR, Shaw S, Dennis R. Clinical and magnetic resonance imaging characteristics of quadrigeminal cysts in dogs. *J Vet Intern Med.* (2007) 21:1021–6. doi: 10.1111/j.1939-1676.2007.tb03059.x

22. Debreuque M, Ducerveau MN, Valin I, de Fornel P, Manassero M, Thibaud JL. Symptomatic lateral ventricular cystic lesion in a young cat. *JFMS Open Rep.* (2020) 6:2055116920930181. doi: 10.1177/2055116920930181

23. Kent M, Glass EN, Schachar J. A lateral approach to the feline cerebellar fossa: case report and identification of an external landmark for the tentorium ossium. *J Feline Med Surg.* (2020) 22:358–65. doi: 10.1177/1098612X19869699

24. Devathasan D, Murakami M, Miller MA, Thomovsky SA, Lewis MJ. Case report: recurrence of an extradural spinal epidermoid cyst following surgical excision in a dog. *Front Vet Sci.* (2022) 9:871023. doi: 10.3389/fvets.2022.871023

frontiers | Frontiers in Veterinary Science

TYPE Case Report
PUBLISHED 04 November 2024
DOI 10.3389/fvets.2024.1485454

OPEN ACCESS

EDITED BY
Edward E. Patterson,
University of Minnesota Twin Cities,
United States

REVIEWED BY
Anita Shea,
Massey University, New Zealand
Rell Lin Parker,
Virginia Tech, United States

*CORRESPONDENCE
Mariana Isa Poci Palumbo
✉ mariana.palumbo@ufms.br

RECEIVED 23 August 2024
ACCEPTED 24 September 2024
PUBLISHED 04 November 2024

CITATION
Eguchi GU, Palumbo MIP, Cerri FM, Basso RM, Oliveira-Filho JPd, Caramalac SM and Borges AS (2024) Case report: A *CLCN1* complex variant mutation in exon 15 in a mixed-breed dog with hereditary myotonia. *Front. Vet. Sci.* 11:1485454. doi: 10.3389/fvets.2024.1485454

Case report: A *CLCN1* complex variant mutation in exon 15 in a mixed-breed dog with hereditary myotonia

Gabriel Utida Eguchi[1], Mariana Isa Poci Palumbo[1]*, Fabrício Moreira Cerri[2], Roberta Martins Basso[2], José Paes de Oliveira-Filho[2], Silvana Marques Caramalac[1] and Alexandre Secorun Borges[2]

[1]Faculty of Veterinary Medicine and Animal Science, Federal University of Mato Grosso do Sul (UFMS), Campo Grande, MS, Brazil, [2]Department of Veterinary Clinical Science, School of Veterinary Medicine and Animal Science, São Paulo State University (Unesp), Botucatu, SP, Brazil

At 4 months of age, a male dog was presented with a complaint of a stiff gait following a startle response. Neurological examination revealed no deficits, but clinical myotonia was easily induced upon requesting the patient to jump. Additionally, myotonia of the upper lip muscles was observed upon manipulation. Hereditary myotonia was suspected, and electromyography confirmed the presence of myotonic potentials. Genetic testing of the myotonic patient identified a complex of mutations, including c.[1636_1639 delins AACGGG] and c.[1644 A>T], both located in exon 15 of the *CLCN1* gene leading to the formation of a premature stop codon. Genetic investigations of the mother and four littermates revealed that, except for one littermate who was wild type, all others carried a copy of the mutated gene. To the best of the authors' knowledge, these mutations have not been previously reported.

KEYWORDS

chloride channel, neuromuscular disorder, hereditary disease, electroneuromyography, congenital myotonia

Introduction

Myotonia, defined as a delayed relaxation of muscles after contraction, is the prominent sign of hereditary myotonia (1). In animals, non-dystrophic hereditary myotonia associated with abnormal chloride channel 1 has been previously described in many species, including goats (2), dogs (3–15), cats (16–18), pigs (19), and buffaloes (20). These species have been confirmed to be affected. In dogs, it was previously associated with purebred dogs (3–11). Only one study illustrates the genetic mutation associated with hereditary myotonia in a family of mixed-breed dogs (12).

The knowledge of the mutations involved in the *CLCN1* gene could prevent the propagation of the defect, consequently reducing the incidence of dogs suffering from the condition. *CLCN1* gene mutations exhibit complex heterogeneity with different mutations found across various dog lineages (5–8, 10–12). As more mutations are discovered, more comprehensive genetic screening for suspected dogs can be developed.

Here, we describe a recessive form of hereditary myotonia in a mixed-breed dog including the clinical presentation, electrophysiological abnormalities, and genetic characterization of a novel complex exon 15 mutation of the *CLCN1* gene, along with the genetic investigation of its relatives.

Case presentation

A 4-month-old male dog was referred with the main complaint of a stiff gait when startled or during any sudden movement initiation. This transient motor difficulty had been present since the first months of life. Otherwise, there were no other disclosed abnormalities, and the patient was reported as a normal puppy regarding growth and behavior. During the clinical evaluation, general physical parameters and neurological examination were all within normal limits. The dog had generalized muscular hypertrophy. Myotonia was easily induced, most prominently when the patient was requested to jump high steps. Additionally, due to the dog's defensive behavior, picking him up caused him to growl, and upper lip myotonia was also observed. The "warm-up phenomenon" (improvement in muscle stiffness and the ease of movement that occurs after repeated use of the affected muscles) was also present (Supplementary Video 1). The owners did not perceive the myotonic episodes as having a significant impact on the animal's overall quality of life. They noted that during the episodes, the patient might be in discomfort, but no signs of vocalization or pain behavior were described.

Considering the clinical myotonia, warm-up phenomenon, muscle hypertrophy, and absence of weakness, non-dystrophic hereditary myotonia associated with abnormal chloride channel 1 was suspected. Therefore, electromyography (EMG) was performed, and whole blood was sent for genetic investigation. Additional blood tests, including a complete blood count, creatinine, urea, alanine aminotransferase, alkaline phosphatase, total protein, and creatine kinase enzyme, were also conducted.

Blood samples were also collected from the mother and four littermates for genetic analysis. Unfortunately, no neurological examination was possible for these animals. However, no similar clinical signs were reported, and based on videos, photos,

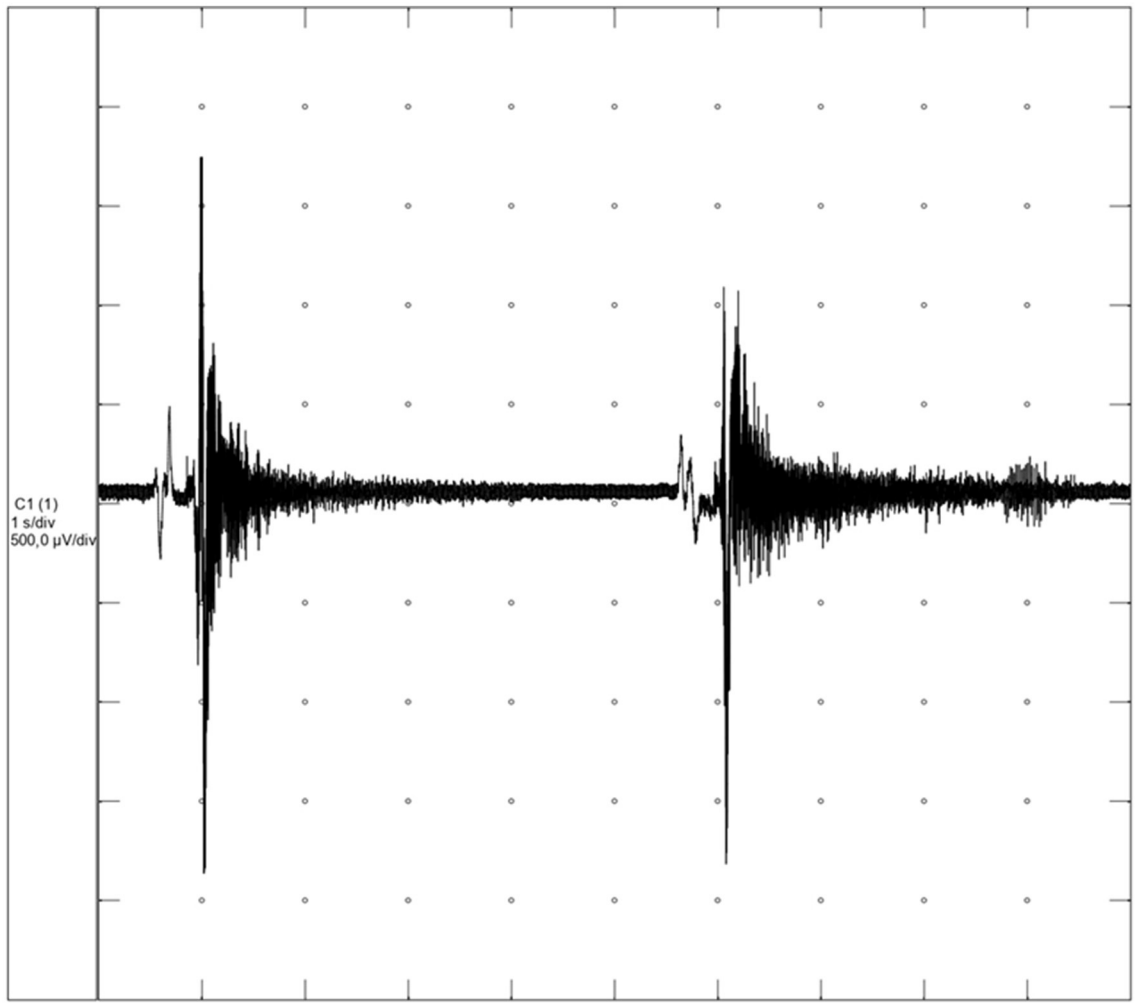

FIGURE 1
Myotonic discharges from the dog with hereditary myotonia (Neurotec Neuromap® EQPE041; 500 µV/division sensitivity and 1 s/division).

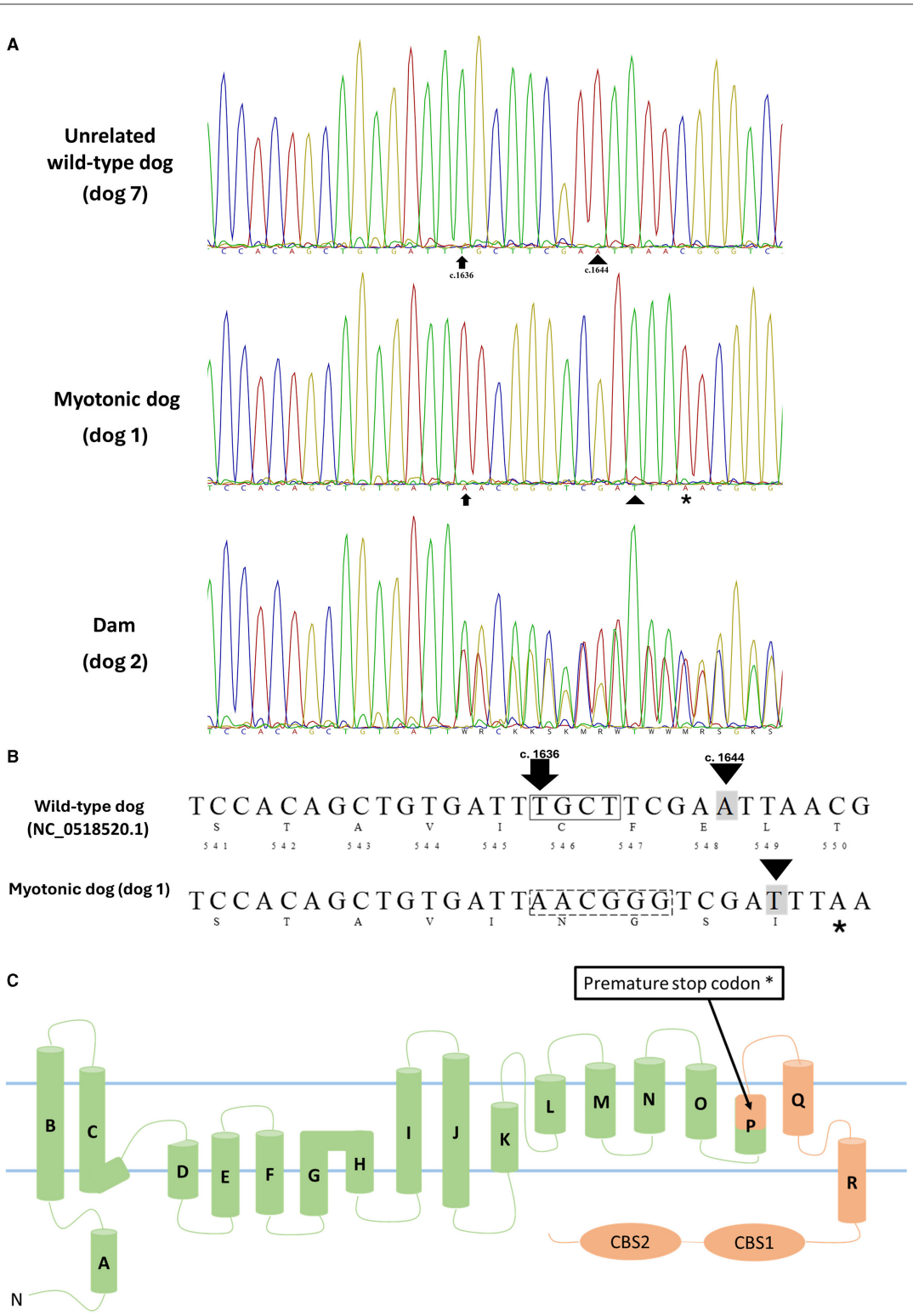

FIGURE 2
(A) Partial capillary sequencing chromatogram for exon 15 of *CLCN1* in an unrelated wild-type dog (dog 7), a myotonic dog (dog 1), and the dam (dog 2). The arrow indicates the start of the mutation (c.1636-1639delinsAACGGG), and the arrowhead indicates the second observed mutation (c.1644 A>T). **(B)** Schematic representation of nucleotide and amino acid sequences of the wild-type dog (top, NC_0518520.1) and the myotonic dog (bottom) with the corresponding nucleotide numbers and amino acids. The box representing four nucleotides in the wild-type sequence indicates the amino acids deleted in the myotonic animal (c.1636-1639del TGCT), while the hatched (- - -) box in the myotonic dog sequence (AACGGG) results from the insertion of 6 nucleotides (c.1636_1639delins AACGGG). The described complex mutation results in a frameshift and the formation of a premature stop codon. Nucleotide highlighted in gray indicates the observed substitution (c.1644 A>T). *Indicates a premature stop codon (TAA - c.1646-1648). **(C)** Membrane topology model of the human skeletal muscle chloride channel monomer, ClC-1 [modified from Brenes et al. (25)], representing the premature stop codon formation and compromising the structure of α-helices P (encompassing amino acids 541-551), Q and R as well as the CBS1 and 2 domains in addition to the P-Q and Q-R loops and the C-terminal, all of which play key roles in the proper functioning of this channel. In green are the structures that are preserved, and in orange are the structures that are absent in the dog with myotonia.

and a general physical examination performed by a generalist veterinarian at the time of blood collection, no abnormalities were found.

Diagnostic assessment

EMG was performed (Neurotec Neuromap® EQPE041) without any anesthetic medications. The band-pass filter was set between 30 and 10,000 Hz, and display settings were configured to 100 μV/division sensitivity and 10 ms/division sweep speed. The electrode was a concentric needle (Neurotecnologia® D039035408 40 mm, 28 G), and the grounding was a surface electrode with an alligator clip placed on the inguinal skin.

Myotonic potentials were present and myotonia was also characterized by its "wax and wane" sound in the tibialis cranialis, gastrocnemius, biceps femoris, and extensor carpi radialis muscles (Figure 1; Supplementary Video 2). Ancillary blood analysis showed no abnormalities.

Blood samples obtained from the myotonic dog (dog 1), its mother (dog 2), littermates (dogs 3–6), and an unrelated wild-type dog (dog 7, sourced from the DNA bank of the Veterinary Molecular Biology Laboratory of the Department of Veterinary Clinical Science of the FMVZ-Unesp) underwent genomic DNA extraction and purification using the DNeasy Blood & Tissue kit (Qiagen) following the manufacturer's instructions. DNA concentration was then measured using spectrophotometry (Nanodrop® 2000—Thermo Scientific™).

The primers used to amplify the 23 exons (coding sequence) of the canine *CLCN1* gene (Supplementary Table 1), along with the PCR conditions and thermocycling, were previously described (12). The amplicons were analyzed by 1.5% agarose gel electrophoresis, purified with magnetic beads, and sequenced via Sanger sequencing. The electropherograms were examined using Geneious Prime® 2019.1.3 software. The obtained sequences were compared to the reference of the *CLCN1* gene from Canis lupus familiaris (GenBank NP_001003124.1).

The alignment of sequences from the myotonic dog (dog 1), its mother (dog 2), littermates (dogs 3–6), and a wild-type dog (dog 7), along with the GenBank reference sequence (NP_001003124.1), revealed a complex of mutations c.[1636_1639delinsAACGGG] and c.[1644A>T], both in exon 15. This second mutation, c.[1644A>T], resulted in the modification of the amino acid sequence p.Glu548Asp. The chloride channel in the mutated animal has the initial 545 amino acids preserved, followed by the generation of four different amino acids (546–549). The variant complex c.[1636_1639delinsAACGGG] caused the formation of a premature stop codon in exon 15 (positions c.1646-1648). This results in a truncated protein with ~400 fewer amino acids compared to the normal CLC protein (NP_001003124.1), which has 976 amino acids in the dog (Figure 2).

Dog 4 had no alterations in the region of the observed mutation (wild type). Dogs 3, 5, and 6 each presented a copy of the mutated gene. The mother (dog 2) also showed the presence of a copy of the mutated sequence. Dogs 2, 3, 5, and 6 were considered heterozygous for the described mutations.

No treatment was instituted as the condition didn't seem to impact the patient's quality of life. Nonetheless, owner education was emphasized as a crucial aspect of managing this condition. Educating the owners about the nature of clinical myotonia is important because the episodes can cause psychological distress for some people who may mistakenly believe the dog is in active pain during these events. Additionally, owners were advised to remove all affected relatives from breeding programs to prevent the propagation of the genetic mutation.

Outcome and follow-up

Two years after the initial evaluation, the patient showed no worsening of the condition in terms of frequency and severity. The dog exhibited normal growth and behavior, and despite some visible generalized muscle hypertrophy (Supplementary Video 1), no other clinical abnormalities were found.

Discussion

Delayed relaxation of skeletal muscles after onset of movements or startle, muscle hypertrophy, and the "warm-up" phenomenon are highly indicative of hereditary myotonia related to chloride channel 1 abnormalities. The "warm-up" phenomenon serves as a valuable clinical tool in diagnostic criteria for hereditary myotonia (HC), distinguishing myotonic events from paradoxical myotonia, where muscle rigidity typically worsens with exercise (12, 21). Myotonia in domestic animals can also occur with sodium channel abnormalities, but these are usually associated with weakness, which was not observed in this dog.

While myotonia caused by mutations in *CLCN1* has been well-documented in purebred dogs (3–11), reports and genetic investigations in mixed-breed dogs remain limited but have been described (12). To the best of our investigation, no pure-breed ancestors could be identified in our patient.

Clinical myotonia was confirmed through EMG evaluation, which detected myotonic discharges [frequencies may range from 20 to 150 Hz, potential amplitudes range from 10 to 1,000 mV and last 500 ms or longer (22, 23)] resulting in a characteristic sound and distinguishes them from cases of pseudomyotonia, where clinical myotonia is present without myotonic potentials (1, 21). A limitation of this study is the lack of histological analysis of the musculature, as the biopsy was not authorized by the owner. This analysis is important to rule out cases of dystrophic myotonia, which was not the initial suspicion for this dog. In cases of hereditary myotonia, the muscle is usually only characterized by variation in the diameter of the fibers (15, 16).

Mutations in the *CLCN1* gene responsible for hereditary myotonia have been documented in various dog breeds, including Miniature Schnauzers (6), Australian Cattle Dogs (8), Labrador Retrievers (10), American Bulldogs (11). However, in the dog with myotonia from the present study, none of the previously reported mutations in the *CLCN1* gene associated with myotonia in dogs

or other domestic animals were identified. Only one study has reported a mutation in the *CLCN1* gene in a family of mixed-breed dogs, and that mutation was a complex variant in exon 6, different from the variant found in our study, which is located in exon 15 (12). Several mutations have been described in humans in exon 15, but not at the same position as the complex variant found in our study (3, 14, 24). The complex mutation observed in this patient resulting in a premature stop codon affected the structure of α-helices P (encompassing amino acids 541–551), Q (555–571), and R (576–585), as well as the 2 intracellular C-terminal cystathionin-β-synthase (CBS) segments (609–876), in addition to the P-Q and Q-R and the C-terminal loops, all of which play key roles in the proper functioning of *CLCN1*. This importance is underscored by ∼110 mutations located in this region that have been reported in humans, where amino acid alterations have led to congenital myotonia (25). Further supporting the significance of these α-helices (P, Q, and R) and CBS domains, congenital myotonia has also been described in animals, with point mutations in this region reported in a horse (26), cat (16), dogs (8–10), and goats (27). To highlight the importance of this region of the *CLCN1* gene in cases of myotonia in animals, we can mention goats, which were the first domesticated species described with myotonia and the responsible mutation is a single nucleotide change that results in the substitution of proline for a conserved alanine residue in the CBS (27). Therefore, it is reasonable to consider that, even in the absence of patch-clamp studies, the truncated *CLCN1* (∼400 aa shorter than the normal chloride channel 1) observed in the dog from the present study is responsible for the clinical myotonia. Considering the distribution of findings in the studied family and the sequencing results, it is concluded that this is an autosomal recessive form of the disease, similar to all other cases of hereditary myotonia associated with chloride channel mutations described in domestic animals to date.

Despite being a disease that typically does not severely compromise the quality of life of affected dogs, myotonia can still cause some limitations and predispose patients to accidental falls. In some cases, myotonic episodes may be frequent enough to hinder normal daily activities and require treatment attempts (10). Hereditary myotonia does not seem to reduce the life expectancy of affected individuals. Patients are often diagnosed as adults (7, 8, 10, 12) and typically experience no severe decline in quality of life or developmental issues. The patient described in our study had a follow-up period of 2 years, during which no deterioration in condition was observed. Nevertheless, from an owner's perspective, these episodes may resemble completely different physiological conditions, such as cramping syndromes, and thus owners may extrapolate the discomfort from any muscle cramp they have experienced themselves. Therefore, owner education is crucial regarding the nature of this condition and any available treatment options. When treatment is chosen, details such as type of medication, dosage, and expected outcomes have been previously reported.

Moreover, it is essential not to overlook owner education regarding the hereditary nature of this disease, and preventing mating and breeding of affected individuals should be strongly advised.

Data availability statement

The original contributions presented in the study are included in the article/Supplementary material, further inquiries can be directed to the corresponding author.

Ethics statement

The animal described in this study were received as clinical patient in the Veterinary Hospital of Universidade Federal de Mato Grosso do Sul—UFMS (Animal Ethics Committee protocol number 1.281/2023). The studies were conducted in accordance with the local legislation and institutional requirements. Written informed consent was obtained from the owners of the animals for the publication of this case report.

Author contributions

GE: Data curation, Investigation, Writing – original draft, Writing – review & editing. MP: Conceptualization, Data curation, Investigation, Writing – original draft, Writing – review & editing. FC: Data curation, Writing – original draft, Writing – review & editing. RB: Data curation, Writing – original draft, Writing – review & editing. JO-F: Writing – original draft, Writing – review & editing. SC: Writing – review & editing. AB: Data curation, Writing – original draft, Writing – review & editing.

Funding

The author(s) declare financial support was received for the research, authorship, and/or publication of this article. This study was financed in part by the Universidade Federal de Mato Grosso do Sul—UFMS/MEC - Brazil.

Conflict of interest

The authors declare that the research was conducted in the absence of any commercial or financial relationships that could be construed as a potential conflict of interest.

Publisher's note

All claims expressed in this article are solely those of the authors and do not necessarily represent those of their affiliated organizations, or those of the publisher, the editors and the

reviewers. Any product that may be evaluated in this article, or claim that may be made by its manufacturer, is not guaranteed or endorsed by the publisher.

Supplementary material

The Supplementary Material for this article can be found online at: https://www.frontiersin.org/articles/10.3389/fvets.2024.1485454/full#supplementary-material

SUPPLEMENTARY VIDEO 1
Dog with hereditary myotonia at first presentation with 4 months old and at 2-years follow-up; clinical myotonia episodes and "warm-up" phenomenon are observed. Note the muscle hypertrophy and upper lip myotonia (2-years).

SUPPLEMENTARY VIDEO 2
EMG evaluation of the dog with hereditary myotonia (Neurotec Neuromap® EQPE041; band pass filter, 30 to 10,000 Hz; display settings, 100 μV/division sensitivity and 10 ms/division sweep speed; sixty Hz filter "on"). Note myotonic discharges that wax and wane and characteristic sound.

SUPPLEMENTARY TABLE 1
Primers for PCR amplification.

References

1. Vite CH. Myotonia and disorders of altered muscle cell membrane excitability. *Vet Clin North Am Small Anim Pract.* (2002) 32:169–87. doi: 10.1016/S0195-5616(03)00084-6

2. Bryant SH. Myotonia in the goat. *Ann N Y Acad Sci.* (1979) 317:314–25. doi: 10.1111/j.1749-6632.1979.tb37355.x

3. Farrow BRH, Malik R. Hereditary myotonia in the Chow Chow. *J Small Anim Practc.* (1981) 22:451–65. doi: 10.1111/j.1748-5827.1981.tb00629.x

4. Hill SL, Shelton GD, Lenehan TM. Myotonia in a cocker spaniel. *JAAHA.* (1995) 31:506–9. doi: 10.5326/15473317-31-6-506

5. Rhodes TH, Vite CH, Giger U, Patterson DF, Fahlke C, George Jr AL, et al. missense mutation in canine ClC-1 causes recessive myotonia congenita in the dog. *FEBS Lett.* (1999) 456:54–8. doi: 10.1016/S0014-5793(99)00926-6

6. Vite CH, Melniczek J, Patterson D, Giger U. Congenital myotonic myopathy in the Miniature Schnauzer: an autosomal recessive trait. *J Hered.* (1999) 90:578–80. doi: 10.1093/jhered/90.5.578

7. Bhalerao DP, Rajpurohit Y, Vite CH, Giger U. Detection of a genetic mutation for myotonia congenita among Miniature Schnauzers and identification of a common carrier ancestor. *Am J Vet Res.* (2002) 63:1443–7. doi: 10.2460/ajvr.2002.63.1443

8. Finnigan DF, Hanna WJB, Poma R, Bendall AJ. A novel mutation of the *CLCN1* gene associated with myotonia hereditaria in an Australian cattle dog. *J Vet Intern Med.* (2007) 21:458–63. doi: 10.1111/j.1939-1676.2007.tb02990.x

9. Lobetti RG. Myotonia congenita in a Jack Russell terrier. *J S Afr Vet Assoc.* (2009) 80:106–7. doi: 10.4102/jsava.v80i2.181

10. Quitt PR, Hytönen MK, Matiasek K, Rosati M, Fischer A, Lohi H. Myotonia congenita in a Labrador Retriever with truncated CLCN1. *Neuromuscul Disord.* (2018) 28:597–605. doi: 10.1016/j.nmd.2018.05.002

11. Rodrigues DDJ, Damasceno AD, Araújo CETD, Torelli SR, Fonseca LGH, Delfiol DJZ, et al. Hereditary myotonia in American Bulldog associated with a novel frameshift mutation in the CLCN1 gene. *Neuromuscul Disord.* (2020) 30:991–8. doi: 10.1016/j.nmd.2020.10.007

12. Chimenes ND, Caramalac SM, Caramalac SM, Fernandes TD, Basso RM, Cerri FM, et al. A complex *CLCN1* variant associated with hereditary myotonia in a mixed-breed dog. *J Vet Diagn Invest.* (2023) 35:414–7. doi: 10.1177/10406387231176736

13. Mazón MJ, Barros F De la Pena P, Quesada JF, Escudero A, Cobo AM, Pascual-Pascual SI, et al. Screening for mutations in Spanish families with myotonia functional analysis of novel mutations in CLCN1 gene. *Neuromuscul Disord.* (2012) 22:231–43. doi: 10.1016/j.nmd.2011.10.013

14. Palma Milla C, Prior De Castro C, Gómez-González C, Martínez-Montero PI, Pascual Pascual S, Molano Mateos J. Myotonia congenita: mutation spectrum of CLCN1 in Spanish patients. *J Genet.* (2019) 98:1–10. doi: 10.1007/s12041-019-1115-0

15. Shelton GD, Mickelson JR, Friedenberg SG, Cullen JN, Graham K, Carpentier MC, et al. Variants in CLCN1 and PDE4C associated with muscle hypertrophy, dysphagia, and gait abnormalities in young French bulldogs. *Animals.* (2024) 14:722. doi: 10.3390/ani14050722

16. Gandolfi B, Daniel RJ, O'Brien DP, Guo LT, Youngs MD, Leach SB, et al. A novel mutation in CLCN1 associated with feline myotonia congenita. *PLoS ONE.* (2014) 9:e109926. doi: 10.1371/journal.pone.0109926

17. Corrêa S, Basso RMB, Cerri FM, Oliveira-Filho JP, Araújo Jr JP, Torelli SR, et al. Hereditary myotonia in cats associated with a new homozygous missense variant pAla331Pro in the muscle chloride channel ClC-1. *J Vet Intern Med.* (2023) 37:2498–503. doi: 10.1111/jvim.16837

18. Woelfel C, Meurs K, Friedenberg S, DeBruyne N, Olby NJ, A. novel mutation of the CLCN1 gene in a cat with myotonia congenita: diagnosis and treatment. *J Vet Int Med.* (2022) 36:1454. doi: 10.1111/jvim.16471

19. Araújo CET, Oliveira CMC, Barbosa JD, Oliveira-Filho JP, Resende LAL, Badial PR, et al. A large intragenic deletion in the CLCN1 gene causes hereditary myotonia in pigs. *Sci Rep.* (2019) 9:15632. doi: 10.1038/s41598-019-51286-7

20. Borges AS, Barbosa JD, Resende LAL, Mota LSLS, Amorim RM, Carvalho TL, et al. Clinical and molecular study of a new form of hereditary myotonia in Murrah water buffalo. *Neuromuscul Disord.* (2013) 23:206–13. doi: 10.1016/j.nmd.2012.11.008

21. Stee K, Van Poucke M, Peelman L, Lowrie M. Paradoxical pseudomyotonia in English Springer and Cocker Spaniels. *J Vet Intern Med.* (2020) 34:253–7. doi: 10.1111/jvim.15660

22. Kimura J. *Electrodiagnosis in Diseases of Nerve and Muscle: Principles and Practice.* 3rd ed. New York, NY: Oxford University Press (2001). p. 991.

23. Heatwole CR, Moxley RT. The nondystrophic myotonias. *Neurotherapeutics.* (2007) 4:238–51. doi: 10.1016/j.nurt.2007.01.012

24. Ivanova EA, Dadali EL, Fedotov VP, Kurbatov SA, Rudenskaya GE, Proskokova TN, et al. The spectrum of CLCN1 gene mutations in patients with nondystrophic Thomsen's and Becker's myotonias. *Genetika.* (2012) 48:952–61. doi: 10.1134/S1022795412090049

25. Brenes O, Pusch M, Morales F. ClC-1 chloride channel: inputs on the structure-function relationship of myotonia congenita-causing mutations. *Biomedicines.* (2023) 11:2622. doi: 10.3390/biomedicines11102622

26. Wijnberg ID, Owczarek-Lipska M, Sacchetto R, Mascarello F, Pascoli F, Grünberg W, et al. A missense mutation in the skeletal muscle chloride channel 1 (CLCN1) as candidate causal mutation for congenital myotonia in a New Forest pony. *Neuromusc Disord.* (2012) 22:361–7. doi: 10.1016/j.nmd.2011.10.001

27. Beck CL, Fahlke C, George AL Jr. Molecular basis for decreased muscle chloride conductance in the myotonic goat. *Proc Natl Acad Sci USA.* (1996) 93:11248–52. doi: 10.1073/pnas.93.20.11248

frontiers | Frontiers in Veterinary Science

TYPE Case Report
PUBLISHED 18 November 2024
DOI 10.3389/fvets.2024.1495807

OPEN ACCESS

EDITED BY
Andrea Tipold,
University of Veterinary Medicine Hannover, Germany

REVIEWED BY
Dakir Polidoro,
AniCura, Belgium
Fabio Stabile,
Wear Referrals Veterinary Specialist & Emergency Hospital, United Kingdom

*CORRESPONDENCE
Shinji Tamura
✉ cqx03426@ms8.megaegg.ne.jp

RECEIVED 13 September 2024
ACCEPTED 25 October 2024
PUBLISHED 18 November 2024

CITATION
Tamura S, Nakamoto Y, Santifort KM and Tamura Y (2024) Case report: Positioning head tilt observed in a dog and four cats with bilateral peripheral vestibular dysfunction. *Front. Vet. Sci.* 11:1495807. doi: 10.3389/fvets.2024.1495807

Case report: Positioning head tilt observed in a dog and four cats with bilateral peripheral vestibular dysfunction

Shinji Tamura[1]*, Yuya Nakamoto[2], Koen M. Santifort[3,4] and Yumiko Tamura[1]

[1]Tamura Animal Clinic, Hiroshima, Japan, [2]Neuro Vets Animal Neurology Clinic, Kyoto, Japan, [3]IVC Evidensia Referral Hospital Arnhem, Arnhem, Netherlands, [4]IVC Evidensia Referral Hospital Hart van Brabant, Waalwijk, Netherlands

Positioning head tilt (PHT) is a dynamic neurologic sign that occurs when the head tilts in the opposite side of a voluntary lateral turn of the head. Notably, a head tilt is absent when the head is held stationary or when the animal is moving forward. PHT is thought to be caused by a lack of inhibitory input to the vestibular nuclei due to dysfunction of the cerebellar nodulus and uvula (NU). NU dysfunction is proposed to not only be caused by pathologies that affect the NU itself, but also by reduced input of proprioceptive information from the spindles of cervical muscles. As an example of the former, it has been noted in dogs with hypoplasia of the cerebellar nodulus and uvula (NU), dogs with lysosomal storage diseases, and in a dog with a cerebellar tumor. As an example of the latter, it has been observed in feline cases of hypokalemic myopathy and myasthenia gravis. In this study, we describe and discuss our observations of PHT in one dog and four cats with lesions affecting the peripheral vestibular apparatus bilaterally.

KEYWORDS

positioning head tilt, dog, cat, bilateral vestibular, peripheral, otitis interna, idiopathic vestibular disease

1 Introduction

Positioning head tilt (PHT) in veterinary neurology is a clinical sign that occurs when the head tilts in the opposite side of a voluntary lateral turn of the head (e.g., tilting to the left when the head moves to the right and vice versa) (1, 2). Notably, a head tilt is absent when the head is held stationary or when the animal is moving forward. PHT has been documented in various cases, including three dogs with cerebellar hypoplasia [specifically of the nodulus and uvula (NU)] (1), a dog with a tumor invading the NU (3–5), and nine dogs with lysosomal disease (6). In the latter, the entire brain including the NU was atrophic. The PHT is thought to be caused by a lack of inhibitory input to the vestibular nuclei due to NU dysfunction. Additionally, PHT has been reported in 14 cats with hypokalemic myopathy (7) and 2 cats with myasthenia gravis (8). In these cases, the mechanism of PHT is believed to involve altered function of muscle spindles in the rectus and obliquus capitis muscles. This alteration possibly leads to disrupted proprioceptive information from the spindles to the NU, hindering the NU's ability to inhibit the excitation of rostral, medial, and caudal vestibular nuclei induced by head movement (7, 8).

Bilateral peripheral vestibular diseases occur occasionally in dogs and more frequently in cats, often resulting from bilateral otitis interna or idiopathic vestibular disease (9). Affected animals typically crouch low to the ground, walk tentatively, and may fall to both sides (9). Unlike unilateral vestibular conditions, these animals do not exhibit head tilt or pathological nystagmus and lack vestibulo-ocular reflexes. Instead, they often display wide lateral head excursions, interpreted as attempts to stabilize the visual field in the absence of physiological nystagmus (9).

In this study, we describe the cases of one dog and four cats with bilateral peripheral vestibular diseases presenting with PHT. The mechanism of PHT in these animals is discussed.

2 Case description

2.1 Case 1

A 14-year-and-8-month-old female neutered domestic short-haired (DSH) cat was referred to Tamura Animal Clinic for detailed examination of ataxia and wide lateral head excursions which had been present for an unknown period of time. The cat had been treated with steroids (details unknown) for unilateral head tilt (side unknown) during the previous 2 months at another hospital. When wide lateral head excursions were observed, PHT was observed concurrently (Supplementary Video 1). Neurological examination revealed vestibular ataxia, loss of vestibulo-ocular reflexes, and unresponsiveness to sound. The neuroanatomical lesion localization was: peripheral vestibulocochlear apparatus, bilaterally. The complete blood count (CBC) revealed no abnormalities. Serum biochemistry revealed increased alanine transaminase activity [132 IU/L; reference interval (RI) 18–51 IU/L]. MRI findings were consistent with bilateral otitis media/interna (0.3T Hitachi Airis II comfort) (9–11) (Figure 1). Cerebrospinal fluid (CSF) was not collected due to financial constraints. Medical treatment with cefovecin sodium (8 mg/kg s.c., once every 2 weeks) and marbofloxacin (8.5 mg/kg, p.o., sid) was prescribed for 10 weeks, but the signs did not change at the end of treatment.

2.2 Case 2

An 8-year-old female neutered DSH cat was referred to Tamura Animal Clinic with signs of horizontal nystagmus with fast phase to the right and lateral head excursions that had been observed for 10 days before referral. The cat had a subcutaneous ureteral bypass system which had been implanted for treatment of ureteral calculus 3 years earlier by the referring veterinarians. Additionally, polyarthritis had been diagnosed 4 months prior and prednisolone was administered since (dose at time of referral: 1.5 mg/kg once daily). Two and a half months before presentation, the cat had started showing signs consistent with a unilateral vestibular disorder. Specifically, signs reported in medical files and by the owner included a spontaneous pathological nystagmus, head tilt, wide-based stance, and vestibular ataxia. Details on the side of the abnormalities were not noted in the files. Thereafter, the vestibular signs had gradually improved. When the current signs were noticed, 10 days before referral, the prednisolone was reduced to 0.8 mg/kg once daily. At the time of arrival at Tamura Animal Clinic, although a detailed neurological examination could not be performed due to the aggressive nature of the cat, neither pathological nor physiological nystagmus was observed. PHT was observed during head excursions (Supplementary Video 1). The neuroanatomical lesion localization was: peripheral vestibular apparatus, bilaterally. CBC and serum biochemistry revealed no abnormalities. MRI revealed no abnormalities in the brain, middle ear, or inner ear (0.3T Hitachi Airis II comfort). CSF was not collected due to financial constraints. A diagnosis of bilateral idiopathic vestibular disease was made. No specific treatment was given. Vestibular ataxia improved, but there was no change in head movement. Four months later, the cat died as a consequence of progressive anemia of unknown cause.

2.3 Case 3

A 12-year-and-5-month-old female neutered DSH cat presented with a right-sided head tilt and horizontal nystagmus with fast phase to the right that had been present for the last 3 months. The patient was treated with steroids (details unknown) at another hospital. Two months after onset, the head tilt was less noticeable but persistent. The cat was referred to Neuro Vets Animal Neurology Clinic with signs of vestibular ataxia most prominently noticeable in the pelvic limbs and wide lateral excursions of the head that had been noticed for 2 weeks before. When the cat walked, mild PHT was observed (Supplementary Video 2). Neurological examination revealed bilateral, but slightly asymmetrical vestibular ataxia (tendency of leaning to the left with the pelvic limbs and caudal trunk), loss of vestibulo-ocular reflexes, and unresponsiveness to sound. The neuroanatomical lesion localization was: peripheral vestibulocochlear apparatus, bilaterally. CBC and serum biochemistry revealed no abnormalities. MRI findings were consistent with bilateral otitis media/interna (0.4T Hitachi APERT Lucent) (9–11) (Figure 1). CSF was not collected due to financial constraints. Medical treatment with amoxicillin clavulanate (30 mg/kg, p.o., bid) was initiated for 8 weeks. The neurologic signs did not resolve but were less severe over the course of treatment and after treatment at the 8-week follow-up.

2.4 Case 4

A 15-year-old female neutered DSH cat was presumptively diagnosed with bilateral otitis media/interna 1 week prior, directly after topical medication (Neptra, Elanco) had been applied in both ears for a diagnosis of otitis externa (based on otoscopic findings) bilaterally at another hospital. Tympanic membrane integrity or rupture was not reported in the medical files. Directly after topical medical treatment, cat showed severe bilaterally symmetrical vestibular ataxia, drooling, and bilateral Horner syndrome (miosis, enophthalmos, ptosis, and protrusion of the third eyelid), and had become unresponsive to sound. Directly afterwards, the ears were flushed and prednisolone (1 mg/kg, p.o., sid) and metoclopramide (0.2 mg/kg, p.o., tid)

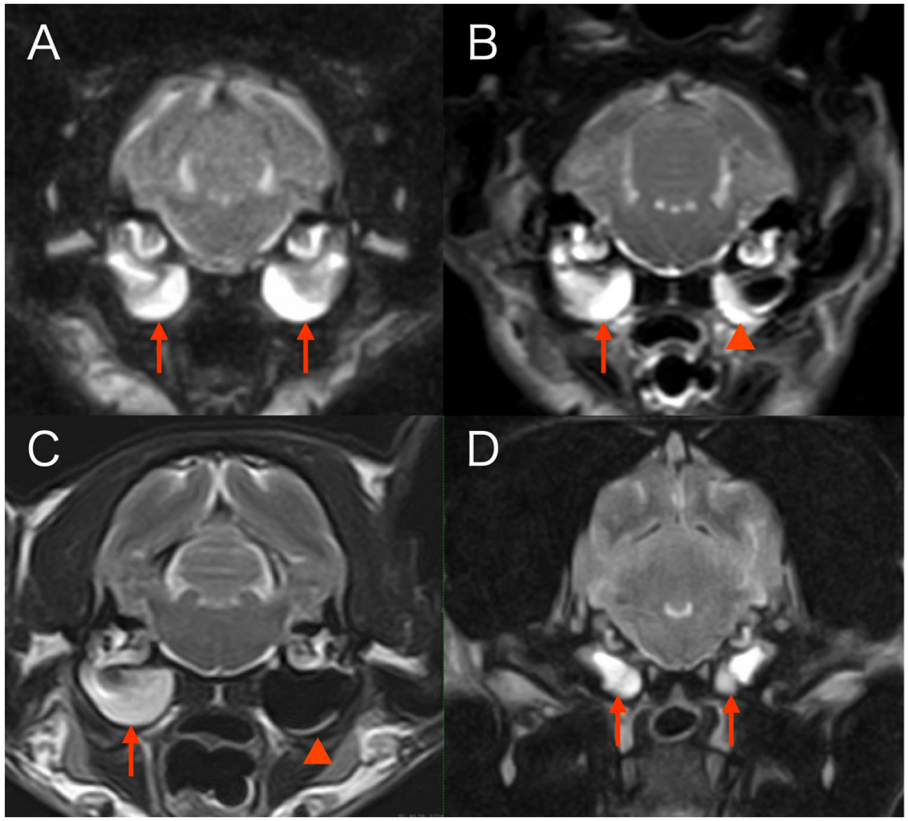

FIGURE 1
Transverse T2-weighted magnetic resonance images at the level of tympanic bullae. **(A)** Case 1. Both tympanic cavities are almost completely filled with fairly homogenous material hyperintense to gray matter (arrows). **(B)** Case 3. The right tympanic cavity is almost completely filled with fairly homogenous material hyperintense to gray matter (arrow). Material of similar signal intensity adheres along the walls of the left tympanic cavity (arrowhead). **(C)** Case 4. The right tympanic cavity is completely filled with fairly homogenous material hyperintense to gray matter (arrow). A faint crescent of material of similar signal intensity is present along the ventral border of the left tympanic cavity (arrowhead). **(D)** Case 5. Both tympanic cavities are completely filled with fairly homogenous material hyperintense to gray matter (arrows).

were administered by the referring veterinarian. The ataxia gradually improved but other signs persisted and the cat was referred to the neurology department of IVC Evidensia Referral Hospital Arnhem. Neurological examination revealed bilaterally symmetrical vestibular ataxia, wide lateral head excursions, PHT (Supplementary Video 1), bilaterally mildly decreased palpebral reflexes, bilateral Horner syndrome, loss of vestibulo-ocular reflexes, and unresponsiveness to sound. The neuroanatomical lesion localization was: peripheral vestibulocochlear apparatus, bilaterally. CBC and serum biochemistry revealed no abnormalities. MRI (1.5T Canon Vantage Elan), otoscopy findings, and clinical history were consistent with a diagnosis of bilateral tympanic membrane disruption, ototoxicity, and (suspectedly sterile) otitis media/interna (Figure 1) (9–11). CSF was not collected. After flushing of the tympanic cavities, the patient was treated medically with topical auricular medication every other day (honey ear drops, Dermiel®, AST Farma B.V., The Netherlands, and triamcinolone acetonide 0,1%), topical ear cleaner once every 2 weeks (VetSoothe Clear®), and oral dexamethasone (0.08 mg/kg, p.o., sid) for 1 week. Topical auricular medications were tapered and stopped after 2 months. At 4-month follow-up, persistent bilaterally symmetrical vestibular ataxia was still noticed and the cat remained unresponsive to sound. Signs of Horner syndrome were less apparent (mild ptosis, miosis, and protrusion of the third eyelid were still present).

2.5 Case 5

A 3-year-and-8-month-old female French bulldog was referred to Tamura Animal Clinic for sudden onset of vomiting, rotatory nystagmus, and abnormal head and trunk movements that had started 2 days before referral. The dog had difficulty standing up, and repeatedly and rapidly rolled the head from side to side with the abdomen on the floor. The trunk also rolled from side to side (Supplementary Video 3). Neurological examination revealed severe bilaterally symmetrical vestibular ataxia, head shaking, loss of vestibulo-ocular reflexes, and unresponsiveness to sound. The neuroanatomical lesion localization was: peripheral vestibulocochlear apparatus, bilaterally. CBC and serum biochemistry revealed elevated C-reactive protein (CRP) concentration (>7.0 mg/dL; RI<0.3). MRI findings were consistent with bilateral otitis media/interna (Figure 1) (9–11), inflammatory changes around the bulla tympanica on the right, and focal meningitis in the area of the right brain stem (0.3T Hitachi Airis II comfort). CSF was not collected due to financial constraints.

Medical treatment with maropitant citrate monohydrate (1 mg/kg, s.c. sid), cefovecin sodium (8 mg/kg s.c.), orbifloxacin (5 mg/kg s.c. sid), and subcutaneous fluid (for 6 days) until the dog had a satisfactory oral fluid and food intake. One week after the start of treatment, the patient was able to walk, but head excursions and PHT were observed (Video 3). CRP concentration had dropped to within RI. Additional cefovecin sodium (8 mg/kg s.c. once every 2 weeks) and marbofloxacin (6.9 mg/kg, p.o., sid) were administered for 8 weeks. Eight weeks later, residual neurological deficits were present, consisting of mild bilaterally symmetrical vestibular ataxia, head excursions, and PHT. At reevaluation 4 years later, mild bilaterally symmetrical vestibular ataxia remained, but head excursions and PHT had disappeared. It is unclear when the PHT had disappeared.

3 Discussion

The neural pathway for the maintenance of head equilibrium is described as follows. In a resting animal, the left and right otoliths receive symmetrical gravitational stimulation. This stimulation is transmitted through the vestibular nerve to the left and right lateral vestibular nuclei, which maintain head equilibrium by equally contracting the oblique and rectus capitis muscles, the antigravity muscles of the head, on both sides through the ipsilateral lateral vestibular spinal tract. When the head moves to the left, the rostral, medial, and caudal vestibular nuclei detect the shift in the center of gravity to the left, mainly through the input from the left and right semicircular canals. To maintain equilibrium, the left side of the body through the medial vestibulospinal tract increases the tone of the left-sided antigravity muscle groups and the right side decreases it, thereby preventing the body from falling to the left (12). Additionally, the responses of vestibular neurons are influenced by the current behavior and motor function of the animal. Vestibular neuron activity is modulated not only by input from the peripheral vestibular apparatus but also by proprioceptive receptive afferents and efferent signals from the motor nuclei and cortex during active movements (13).

When the head moves laterally to the left, the NU compares the input from the vestibular apparatus through the vestibulocerebellar tract with the input from the muscle spindles of the neck muscles through the spino-cuneocerebellar tract. This comparison provides relative positional information between the head and the trunk. The NU then outputs signals to inhibit the overexcitation of the left-sided reflexive rostral, medial, and caudal vestibular nuclei. Dysfunction of the NU can cause a head tilt to the right due to an excessively high tension of the left-sided antigravity muscles (1). This phenomenon highlights the importance of the NU receiving input from both the vestibular apparatus and the muscle spindles of the cervical muscles for its inhibitory function (12). In conditions like hypokalemic myopathy and myasthenia gravis in cats, reduced input from the cervical muscle spindles due to muscle spindle dysfunction can result in PHT (7, 8). In the five cases presented here, none of the patients were considered to have a dysfunction of NU or a muscular disease. In cases with bilateral peripheral vestibular dysfunction, head movement is detected by cervical muscle spindles. Stimulation of the medial vestibulospinal tract increases the tension of the oblique and rectus capitis muscles on the side toward which the head turns (1). However, the NU does not produce an inhibitory output because the input from the vestibular apparatus to the NU is lost, resulting in the PHT (7, 8). Interestingly, PHT in Case 5 disappeared at reevaluation 4 years later. Similarly, in a canine case of cerebellar hypoplasia, PHT also resolved, which was postulated to be due to "compensation" (1). Bilateral vestibular signs are known to be compensated over time (14, 15), suggesting that some form of cerebello-vestibular system compensation might explain the disappearance of the PHT in Case 5.

We postulate that in our five reported cases, it was the lack of input from the peripheral components of the vestibular system (i.e., the inner ear structures and vestibulocochlear nerve) that lead to NU dysfunction and the clinical signs of PHT. For two of the five patients (cases 2 and 5), we consider it unlikely that both peripheral vestibular systems were affected at the same time. We propose that the unilateral vestibular involvement first resulted in unilateral peripheral vestibular signs and then the other, previously normally functioning vestibular system was affected culminating in bilateral peripheral vestibular dysfunction. These cases showed pathological nystagmus at the second occasion. We hypothesize that some degree of compensation had occurred after the initial onset of unilateral vestibular dysfunction. When the unilateral peripheral vestibular system is damaged, input from that side of the peripheral vestibular system is absent. Signal transmission to the vestibular nuclei neurons on the damaged side is markedly reduced to absent. Vestibular compensation is thought to occur due to the release of inhibition through commissural fibers from the vestibular nuclei of the healthy side to the affected side, resulting in an increase in spontaneous firing, and also input of rotational information from the semicircular canal of the healthy side (16). Up to the time of loss of peripheral vestibular input from the previously healthy side, bilateral vestibular nuclei were active once again (the function of the nuclei on the affected side "compensated"). Loss of peripheral vestibular input from the previously healthy side then results in a new imbalance of activity in both vestibular nuclei and pathological, spontaneous nystagmus. The eventual disappearance of pathological nystagmus afterwards could then be explained by another "round" of compensation.

The repeated and rapid rolling of the head and trunk to the left and right with the abdomen on the floor observed on the second day in Case 5 has not been previously reported. However, similar signs have been described in laboratory cats within 0–2 days following bilateral labyrinthectomy (14, 15). In these studies, cats were able to sit up 1–2 days post-operation, and head oscillations, referred to as "excursions" in the literature, were noted (14, 15). These head oscillations included a slight rolling component, although the side was not described. The PHT observed in the present study may correspond to the rolling component these authors referred to (14, 15). The period from the 2nd to 7th day post-operation was marked by rapid recovery, with standing and walking abilities being restored. Weeks 2–6 represented the slow recovery phase, during which most functions returned, aside from persistent mild ataxia. Four months after the operation, oscillations of the head were no longer apparent in those experimentally lesioned cats (14, 15).

This study has some limitations, including the small number of cases. A more detailed observation of clinical signs and progression in a larger cohort with similar characteristics is warranted. Another limitation is that the diagnosis and treatments of bilateral otitis interna in three cats and one dog was based solely on the history, clinical findings, and MRI findings. Culture and sensitivity testing of middle ear content or flushes was not performed in those cases. Although a diagnosis of infectious otitis interna is not formally confirmed (which would require either rigorous sampling or histopathology), the presence of clinical signs such as loss of physiological nystagmus and unresponsiveness to sound supported the diagnosis of bilateral vestibulocochlear dysfunction. Together with the MRI findings, the diagnoses of otitis media/interna in this report align with those in other reports and that are accepted within the veterinary neurology community (9, 10, 17, 18). Antibiotic treatment for otitis media/interna should, when possibly, be based on sensitivity testing (17). However, unfortunately, even when cultures are performed they are often negative even though a bacterial cause is still highly suspected (9, 11, 17, 18). Empirical choices, clinician preferences, and generally broad-spectrum antibiotics therefore come into play when treating cases of (suspected) bacterial otitis media/interna.

In conclusion, this report identified a third lesion site (bilateral peripheral vestibular apparatus) capable of producing PHT, in addition to the previously reported NU and bilateral cervical muscle spindles. Although hypothetical, all of these lesion sites are part of the system that maintains head equilibrium during head movement and any lesion affecting these structures might result in PHT. These hypotheses may be strengthened through further observation of clinical cases.

Data availability statement

The original contributions presented in the study are included in the article/supplementary material, further inquiries can be directed to the corresponding author.

Ethics statement

Ethical approval was not required for the studies involving animals in accordance with the local legislation and institutional requirements because this is a retrospective observational descriptive study. Therefore, live animals were not used in this study, and the ethical approval is not required due to its nature. Written informed consent was obtained from the owners for the participation of their animals in this study.

Author contributions

ST: Conceptualization, Data curation, Writing – original draft, Writing – review & editing. YN: Data curation, Writing – review & editing. KS: Data curation, Writing – review & editing. YT: Writing – review & editing.

Funding

The author(s) declare that no financial support was received for the research, authorship, and/or publication of this article.

Acknowledgments

The authors thank the following for referring the clinical cases: Yuji Takenaga, DVM, KAITA animal hospital (Case 1); Chisako Kamio, DVM, Animal Medical Center ALOHA (Case 2), (Case 3); Yojiro Tamura, DVM, Ohno Chuou Momiji Animal Hospital (Case 5). The authors thank Laurent Garosi, Vet Oracle Telefariology, DVM, FRCVS, Dip ECVN for help in the interpretation of the magnetic resonance imaging study (Case 4). The authors thank all participating veterinarians and other staff who contributed to the clinical management of these patients. A part of this case study was presented as an oral presentation at the annual congress of the Japanese Society of Veterinary Neurology in Naha, Japan, in June 2024.

Conflict of interest

The authors declare that the research was conducted in the absence of any commercial or financial relationships that could be construed as a potential conflict of interest.

Publisher's note

Supplementary material

The Supplementary Material for this article can be found online at: https://www.frontiersin.org/articles/10.3389/fvets.2024.1495807/full#supplementary-material

SUPPLEMENTARY VIDEO 1
Cases 1, 2, and 4-Positioning head tilt (the head tilts in the opposite side of a voluntary lateral turn of the head).

SUPPLEMENTARY VIDEO 2
Case 3-Mild positioning head tilt (the head tilts in the opposite side of a voluntary lateral turn of the head).

SUPPLEMENTARY VIDEO 3
Case 5-Head tilting from side to side and trunk twisting from side to side, and positioning head tilt (head tilts in the opposite side of a voluntary lateral turn of the head).

References

1. Tamura S, Nakamoto Y, Uemura T, Tamura Y. Head tilting elicited by head turning in three dogs with hypoplasic cerebellar nodulus and ventral uvula. *Front Vet Sci.* (2016) 3:104. doi: 10.3389/fvets.2016.00104

2. Tamura S. Commentary: Transient postural vestibulo-cerebellar syndrome in three dogs with presumed cerebellar hypoplasia. *Front Vet Sci.* (2021) 8:613521. doi: 10.3389/fvets.2021.613521

3. Liatis T, Hammond D, Chapman GE, Cloquell Miro A, Stalin C, Gutierrez-Quintana R. MRI findings in a young dog with gliomatosis cerebri. *J Small Anim Pract.* (2022) 63:83. doi: 10.1111/jsap.13394

4. Tamura S. Was the "alternating head tilt" a "positioning head tilt"? *J Small Anim Pract.* (2022) 63:84. doi: 10.1111/jsap.13447

5. Liatis T, Gutierrez-Quintana R. Response to: was the "alternating head tilt" "positioning head tilt"? *J Small Anim Pract.* (2022) 63:85. doi: 10.1111/jsap.13427

6. Tamura S, Tamura Y, Nakamoto Y, Hasegawa D, Tsuboi M, Uchida K, et al. Positioning head tilt in canine lysosomal storage disease: a retrospective observational descriptive study. *Front Vet Sci.* (2021) 8:80266. doi: 10.3389/fvets.2021.802668

7. Tamura S, Nakamoto Y, Tamura Y. Reversible positioning head tilt observed in 14 cats with hypokalaemic myopathy. *J Feline Med S surg.* (2023) 25:6. doi: 10.1177/1098612X231175761

8. Tamura S, Nakamoto Y, Sozu Y, Tamura Y. Positioning head tilt observed in two cats with myasthenia gravis. *J Feline Med S surg Op Rep.* (2024) 10:1. doi: 10.1177/20551169231224534

9. Rossmeisl JH. Vestibular disease in dogs and cats. *Vet Clin Small Anim.* (2010) 40:81–100. doi: 10.1016/j.cvsm.2009.09.007

10. Castillo G, Parmentier T, Monteith G, Gaitero L. Inner ear fluid-attenuated inversion recovery MRI signal intensity in dogs with vestibular disease. *Vet Radiol Ultrasound.* (2020) 61:531–9. doi: 10.1111/vru.12876

11. Dutil GF, Guevar J, Schweizer D, Roosje P, Kajin F, Volk HA, et al. Otitis media and interna with or without polyps in cats: association between meningeal enhancement on postcontrast MRI, cerebrospinal fluid abnormalities, and clinician treatment choice and outcome. *J Feline Med Surg.* (2022) 24:e481–9. doi: 10.1177/1098612X221125573

12. Thomson C and Hahn C. Vestibular system. In: Thomson C, Hahn C editors *Veterinary Neuroanatomy: a Clinical Approach*. St Louis, MO: Elsevier (2012). p. 75–83.

13. Cullen KE, and oy JE. Signal processing in the vestibular system during active versus passive head movements. *J Neurophysiol.* (2004) 91:1919–1933. doi: 10.1152/jn.00988.2003

14. Money KE, Scott JW. Functions of separate sensory receptors of nonauditory labyrinth of the cat. *Am J Physiol.* (1962) 202:1211–20. doi: 10.1152/ajplegacy.1962.202.6.1211

15. Thomson DB, Inglis JT, Schor RH, Macpherson JM. Bilateral labyrinthectomy in the cat: motor behavior and quiet stance parameters. *Exp Brain Res.* (1991) 85:364–72. doi: 10.1007/BF00229414

16. Curthoys IS, Halmagyi GM. Vestibular compensation. *Adv Otorhinolafyngol.* (1999) 55:82–110. doi: 10.1159/000059059

17. Gotthelf LN. Diagnosis and treatment of otitis media. *Vet Clin Small Anim.* (2004) 34:469–87. doi: 10.1016/j.cvsm.2003.10.007

18. Jacobson LS, Janke KJ, Kennedy SK, Lockwood GA, Mackenzie SD, Porter CD, et al. A Pandora's box in feline medicine: presenting signs and surgical outcomes in 58 previously hoarded cats with chronic otitis media-interna. *J Feline Med Surg.* (2023) 25:1098612X231197089. doi: 10.1177/1098612X231197089

frontiers | Frontiers in Veterinary Science

TYPE Case Report
PUBLISHED 03 January 2025
DOI 10.3389/fvets.2024.1522745

OPEN ACCESS

EDITED BY
Bruno André Lopes,
Southfields Veterinary Specialists,
United Kingdom

REVIEWED BY
Sam Long,
Veterinary Referral Hospital, Australia
Virginia Crespo,
Southfields Veterinary Specialists,
United Kingdom
Cathryn Mellersh,
University of Cambridge, United Kingdom

*CORRESPONDENCE
Stacey Sullivan
✉ Sas0241@auburn.edu

RECEIVED 04 November 2024
ACCEPTED 11 December 2024
PUBLISHED 03 January 2025

CITATION
Sullivan S, Szeremeta KJ and Kutzler M (2025) Case report: FGF4L1 retrogene insertion is lacking in the tall dachshund phenotype. *Front. Vet. Sci.* 11:1522745. doi: 10.3389/fvets.2024.1522745

Case report: FGF4L1 retrogene insertion is lacking in the tall dachshund phenotype

Stacey Sullivan[1]*, Katarzyna Julia Szeremeta[2] and Michelle Kutzler[3]

[1]College of Veterinary Medicine, Auburn University, Auburn, AL, United States, [2]The International Working Teckel, Mannheim, Germany, [3]Department of Animal and Rangeland Sciences, Oregon State University, Corvallis, OR, United States

Two retrogene insertions, FGF4L1 (formerly 18-FGF4, colloquially CDPA) and FGF4L2 (formerly 12-FGF4, colloquially CDDY), have recently been discovered as determinants of short leg phenotype in dogs. This case study is comprised of a family of standard wirehaired dachshunds in which the dogs lacking the FGF4L1 gene exhibit a tall phenotype. The tall phenotype in the dachshunds of this report precludes the dog's working function of den work. The data presented in this report provide information as to how FGF4L1 status could be used in making breeding decisions in dachshunds to maintain working ability without compromising animal health.

KEYWORDS

case report, CDDY, CDPA, chondrodystrophy, chondrodysplasia, FGF4L1, FGF4L2, limb-length

Introduction

Canine morphology exhibits the widest variation of any mammal (1, 2) and in many breeds, morphology relates to working function. In dachshunds, a short leg phenotype was intentionally selected to enable the dog to work optimally in its historic hunting specialization: the pursuit of badger within dens, a function for which dachshunds are still used today (3). Dachshund literally translated from German means "badger dog." With their shorter legs compared to terriers, dachshunds working underground can dig and pull prey more easily, illustrating that their body morphology serves a functional purpose (3).

Two retrogene insertions, FGF4L1 (formerly 18-FGF4, colloquially CDPA) and FGF4L2 (formerly 12-FGF4, colloquially CDDY), are associated with a short leg phenotype in most dog breeds (4, 5). The insertions are reported to behave in a dominant manner with a gene dose effect, meaning that one copy of either gene is sufficient to shorten limb length in dogs but that two copies have a more pronounced effect (5). FGF4L1 has a greater impact on limb length than does FGF4L2, with two copies of FGF4L1 reducing antebrachial length by 25%, while two copies of FGF4L2 reduces antebrachial length by only 10% (5, 6). It has been reported that some dog breeds such as beagles exhibit short leg phenotype due to FGF4L2 only, while other dog breeds such as dachshunds exhibit a shorter leg phenotype due to both FGF4L1 and FGF4L2 (5). A few dog breeds such as miniature pinschers exhibit short leg phenotype without either retrogene insertion. In addition to affecting limb length, FGF4L1 is associated with carpal valgus in dogs (5, 7) and FGF4L2 is associated with early disk degeneration (6, 8–10). In 697 dachshunds, allele frequency for FGF4L1 and FGF4L2 was reported to be 0.98 and 0.95, respectively, meaning that 96% of the dachshunds tested had 2 copies of FGF4L1 and 90% had 2 copies of FGF4L2 (11). Thus, most dachshunds are homozygous for both FGF4 retrogene insertions.

We report here a case of an FGF4L1 zero-copy standard dachshund with a tall phenotype (48 cm height at withers) that falls outside the upper limit (40 cm) (12) suitable for den work in earth dog breeds. We also report an FGF4L1 zero-copy sibling with a similar tall phenotype, and FGF4L1 one-copy sire, dam, and littermate with the typical dachshund short phenotype. Our findings suggest that at least one FGF4L1 copy is necessary in dachshunds to maintain a phenotype capable of the dog's below-ground den hunting specialization (Figure 1).

Timeline

June 15, 2024

Tall dachshund identified in response to social media request.

August 6, 2024

Height/weight data, and genotype (FGF4L1 and FGF4L2) obtained from case dog.

August 10, 2024

Genotype (FGF4L1 and FGF4L2) data obtained from sire, dam and female littermate of case dog.

October 23, 2024

Genotype (FGF4L1 and FGF4L2) obtained from male littermate of case dog.

Narrative

A 5-year-old male intact standard wirehaired dachshund registered with the Deutscher Teckelklub was identified by one of the authors (KS) in response to a social media request for photographs of dachshunds of known FGF4 genotype for a book chapter on body morphology in working dachshunds. The dog was observed to lack the breed-typical short leg phenotype and was not immediately recognizable as a dachshund but was otherwise healthy. Height at withers was 48 cm, and weight was 17.5 kg (both approximately twice what is typical for a standard dachshund). Review of genotype data revealed the dog to have 0 copies of FGF4L1 and 1 copy of FGF4L2. The breeder of the dog was interviewed. The breeder had maintained ownership of the sire, dam, and a female littermate of the tall dachshund. It was reported that the sire and dam had been paired twice, and in each litter, multiple puppies of typical short leg phenotype were produced, along with one or two puppies of tall phenotype. The owner of a second tall dachshund, a male littermate to the case dog, was contacted. Height at withers for this second tall dachshund was 41 cm and weight was 11.7 kg. Each dachshund owner provided photographs of their dog(s) and FGF4L1 and FGF4L2 genotype data. Genotype and phenotype data are summarized in Table 1. Each phenotype group (short and tall) contained dogs with 1 or 2 FGF4L2 copies. However, no tall dachshund had the FGF4L1 insertion, while all of the short dachshunds had the FGF4L1 insertion. All of the dogs described in this report were healthy and no diagnostic tests or therapeutics were indicated.

Discussion

To our knowledge, this is the first report describing the phenotype of dachshunds lacking a copy of the FGF4L1 gene. The dachshunds presented in this report illustrate that a genotype

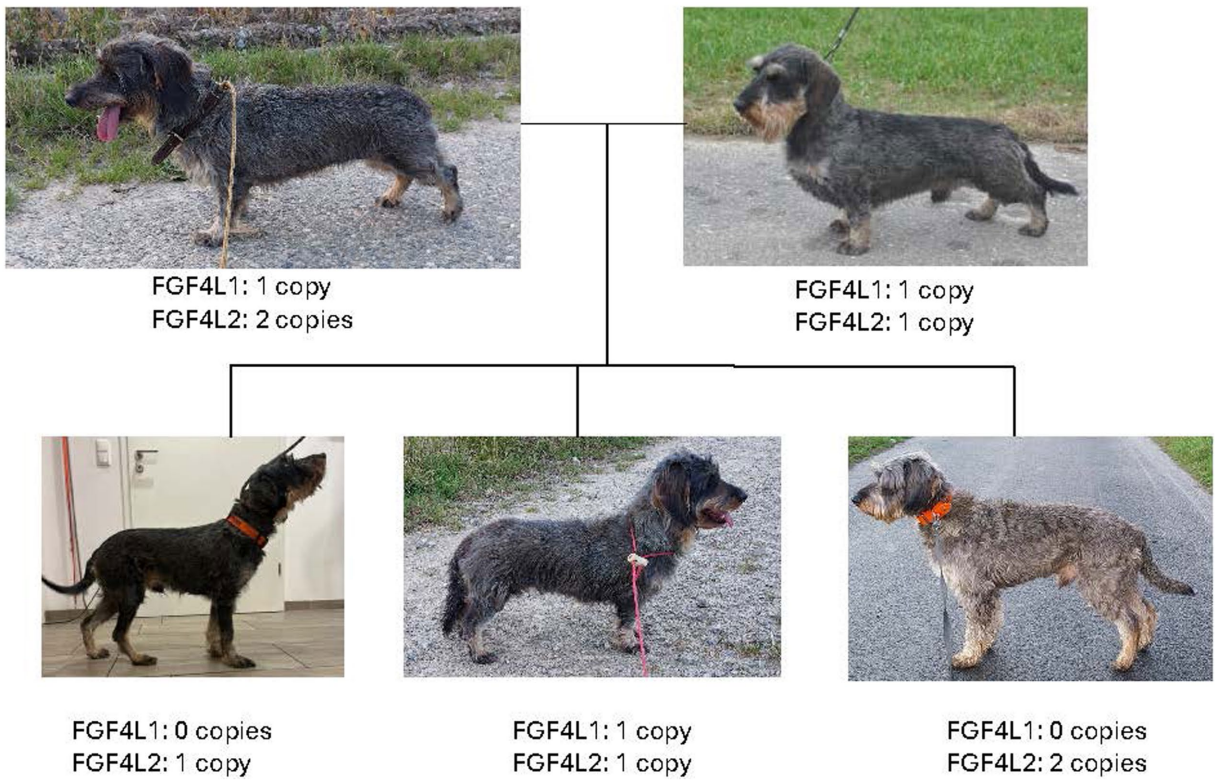

FIGURE 1
Family tree of the dachshunds including genotypes.

TABLE 1 Phenotype and FGF4L1 & FGF4L2 Genotype for the Dachshund Family.

Dog	Phenotype (height)	Genotype	Genotype
		FGF4L1 Copies	FGF4L2 Copies
Case	Tall (48 cm)	0	1
Male littermate	Tall (41 cm)	0	2
Sire	Short	1	1
Dam	Short	1	2
Female littermate	Short	1	1

lacking FGF4L1 may result in a tall phenotype unsuitable for den work. It is not known if this tall phenotype could result in musculoskeletal disorders later in life. Interestingly, the smaller of the two reported tall dachshunds carried two FGF4L2 copies and the taller individual carried only one FGF4L2 copy. This is consistent with the previously reported gene dose effect for limb length for these insertions (5), which predicts that a dog with four doses of these retrogene insertions (two copies of both FGF4L1 and FGF4L2, the typical dachshund pattern) would be shorter than a dog with two doses (zero FGF4L1 + two FGF4L2, the typical beagle pattern). Of the dachshunds in this report, one had the typical beagle pattern (zero FGF4L1 + two FGF4L2) and was of similar height (41 cm) to a 15-inch (38 cm) beagle.

It has also been reported that FGF4L1 has a more profound effect on limb length than FGF4L2 (5). The morphology of the dachshunds in our report supports that claim. The dachshunds with two doses of these retrogene insertions in the pattern one FGF4L1 + one FGF4L2 were short, but the dachshund with two doses in the pattern zero FGF4L1 + two FGF4L2 was tall. It is noteworthy that the short dachshund with three doses of these retrogene insertions in the pattern one FGF4L1 + two FGF4L2 was not readily distinguishable from the other short dachshunds. Thus, the dogs of our report suggest that FGF4L1 in at least one copy is necessary to the breed-defining short leg phenotype of dachshunds. Additionally, these dogs suggest that, provided FGF4L1 is present, FGF4L2 copy number is a less important determinant of limb length in dachshunds and may even be unnecessary to produce a short leg phenotype. In contrast, FGF4L2 might be necessary for breed-defining short leg phenotype in breeds lacking FGF4L1 such as the beagle.

Although the zero-copy FGF4L1 genotype in dachshunds is rare, the description of the dogs in this report is particularly timely, given the fact that in October 2024, the German government banned the exhibition of dogs with one or two FGF4L2 copies, and possibly one or two FGF4L1 copies (13). In 2021, the Animal Welfare Dog Regulations (Tierschutz-Hunderverordung) (14) were revised in Germany to prohibit exhibition of dogs that are the product of so-called "torture breeding" (qualzucht), which is the breeding of dogs with any inherited defect. In October 2024, implementation guidelines for the law were made public. The guidelines, which are intended to clarify the expectations for implementation by state veterinarians, list both FGF4L1 and FGF4L2 as "torture breeding traits" (qualzuchtmerkmale). It is unclear whether the guidelines ban dogs with one or two copies of both insertions, or only the FGF4L2 insertion. Regardless, the guidelines amount to a ban of many short leg dogs, including most dogs of breeds (such as dachshunds) with a high FGF4L2 gene frequency. Banned dogs are excluded from breed shows, working trials or any activity that has a competitive character or attracts an audience. Some of these activities are necessary Deutscher Teckelklub prerequisites for breeding in dachshunds.

A short leg phenotype itself, however, is not a defect, as illustrated by its common occurrence in nature in various species of animals such as the badger, weasel, otter, skink, turtles, and most rodents, where it conveys an adaptive advantage in moving through burrows, climbing, and swimming, and by lowering the animal's center of gravity (15, 16). Carpal valgus, although associated with FGF4L1 genotype, is uncommonly a clinical problem in dachshunds and is considered a fault according to the breed standard (17, 18). In 30 dachshunds, thoracic limb angular limb deformity was noted upon radiographic evaluation, but lameness, elbow incongruity, and osteoarthritis were uncommonly present (19), suggesting that thoracic limb shape may differ in dachshunds compared to other breeds without causing welfare concerns.

In contrast to FGF4L1 which is of questionable health significance in dachshunds, a genotype comprised of one or two FGF4L2 copies poses greater welfare concerns due to the association with intervertebral disk disease (IVDD) risk. However, the association between FGF4L2 and IVDD risk is a recent discovery (6) and the science on the subject is rapidly evolving. Within the last 2 years, evidence for a gene dose effect for FGF4L2-associated IVDD risk has been reported (10, 20). The gene dose evidence suggests stakeholders of breeds with high FGF4L2 allele frequency could adopt a strategy of initially breeding for FGF4L2 heterozygosity to reduce incidence of symptomatic disk disease and avoid genetic bottleneck, and then breed for zero copies once the frequency of the wild type allele increases. The dogs of our report suggest that lack of FGF4L2 may not preclude breed-defining short leg phenotype in dachshunds, provided FGF4L1 is present. The dachshund is a healthy breed other than FGF4L2-associated IVDD risk, with a longer life expectancy than most breeds of dogs, including mixed breeds and non-chondrodystrophic breeds (21–25). For this reason, it seems prudent to allow breed clubs time to adopt spinal health breeding schemes based on recent scientific advancements.

Conclusion

The dachshunds described in this report demonstrate that lack of FGF4L1 retrogene insertions may result in a tall phenotype that renders the dogs unsuitable for den work, the hunting niche for which the breed was developed. The scientific literature does not support a dachshund breed ban based on FGF4L1 genotype, since evidence for significant adverse health consequence of one or two FGF4L1 copies is lacking.

Data availability statement

The original contributions presented in the study are included in the article/supplementary material, further inquiries can be directed to the corresponding author.

Ethics statement

The requirement of ethical approval was waived by Institutional Animal Care and Use Committee, Auburn University for the studies involving animals because this case report did not involve animal manipulations for the purpose of answering a scientific question. The studies were conducted in accordance with the local legislation and institutional requirements. Written informed consent was obtained from the owners for the participation of their animals in this study.

Author contributions

SS: Conceptualization, Investigation, Visualization, Writing – original draft, Writing – review & editing. KS: Conceptualization, Investigation, Resources, Visualization, Writing – review & editing. MK: Writing – review & editing.

Funding

The author(s) declare that financial support was received for the research, authorship, and/or publication of this article. The authors thank Auburn University Department of Clinical Sciences for their financial support of publishing costs.

Acknowledgments

The authors thank the owners of the dogs described in this report for their cooperation in providing the data presented.

Conflict of interest

Each of the authors breeds and exhibits dachshunds. KS has authored three books on working dachshunds and is currently writing a fourth.

Generative AI statement

The authors declare that no Generative AI was used in the creation of this manuscript.

Publisher's note

References

1. Shearin AL, Ostrander EA. Canine morphology: hunting for genes and tracking mutations. *PLoS Biol*. (2010) 8:e1000310. doi: 10.1371/journal.pbio.1000310

2. Bannasch DL, Baes CF, Leeb T. Genetic variants affecting skeletal morphology in domestic dogs. *Trends Genet*. (2020) 36:598–609. doi: 10.1016/j.tig.2020.05.005

3. Bashniak VSJ. What is a dachshund? In Warriors under earth and sky: basics of the working dachshund and practical hunting. Lublin, Poland: Self (2023).

4. Parker HG, VonHoldt B, Quignon P, Margulies EH, Shao S, Mosher DS, et al. An expressed fgf4 retrogene is associated with breed-defining chondrodysplasia in domestic dogs. *Science*. (2009) 325:995–8. doi: 10.1126/science.1173275

5. Bannasch D, Batcher K, Leuthard F, Bannasch M, Hug P, Marcellin-Little DJ, et al. The effects of FGF4 Retrogenes on canine morphology. *Genes*. (2022) 13:325. doi: 10.3390/genes13020325

6. Brown EA, Dickinson PJ, Mansour T, Sturges BK, Aguilar M, Young AE, et al. FGF4 retrogene on CFA12 is responsible for chondrodystrophy and intervertebral disc disease in dogs. *Proc Natl Acad Sci USA*. (2017) 114:11476–81. doi: 10.1073/pnas.1709082114

7. Bellamy KKL, Lingaas F. Short and sweet: foreleg abnormalities in Havanese and the role of the FGF4 retrogene. *Canine Med Genet*. (2020) 7:19. doi: 10.1186/s40575-020-00097-5

8. Mogensen MS, et al. Validation of genome-wide intervertebral disk calcification associations in dachshund and further investigation of the chromosome 12 susceptibility locus. *Front Genet*. (2012) 3:225. doi: 10.3389/fgene.2012.00225

9. Batcher K, Dickinson P, Giuffrida M, Sturges B, Vernau K, Knipe M, et al. Phenotypic effects of FGF4 Retrogenes on intervertebral disc disease in dogs. *Genes*. (2019) 10:435. doi: 10.3390/genes10060435

10. Bianchi CA, Marcellin-Little DJ, Dickinson PJ, Garcia TC, Li CF, Batcher K, et al. FGF4L2 retrogene copy number is associated with intervertebral disc calcification and vertebral geometry in Nova Scotia duck tolling retrievers. *Am J Vet Res*. (2023) 84:1–10. doi: 10.2460/ajvr.22.09.0167

11. Embersics C, Bannasch D, Batcher K, Boudreau EC, Church M, Miller A, et al. Association of the FGF4L2 retrogene with fibrocartilaginous embolic myelopathy in dogs. *J Vet Intern Med*. (2024) 38:258–67. doi: 10.1111/jvim.16925

12. FCI Standard. (2024). Deutscher Jagd Terrier. Available at: https://www.fci.be/nomenclature/Standards/103g03-en.pdf (Accessed 11 April, 2024).

13. Deutscher Verband der Gebrauchshundsportvereine. (2024). Guidelines for the interpretation and enforcement of the exhibition ban. Available at: https://www.dvg-hundesport.de/file/dc4dbeaa91898f00019275c4f9f102cf.de.0/02_leitlinien_der_agt_zu_auslegung_und_vollzug_von___10_tierschhuv.pdf (Accessed 11 April, 2024).

14. Federal Law Gazette. (2024). Tierschutz-Hundeverordnung-Animal welfare dog regulations. Available at: https://www.gesetze-im-internet.de/tierschhuv/BJNR083800001.html (Accessed 11 April, 2024).

15. Maher AE, Burin G, Cox PG, Maddox TW, Maidment SCR, Cooper N, et al. Body size, shape and ecology in tetrapods. *Nat Commun*. (2022) 13:4340. doi: 10.1038/s41467-022-32028-2

16. Law CJ, Slater GJ, Mehta RS. Shared extremes by ectotherms and endotherms: body elongation in mustelids is associated with small size and reduced limbs. *Evolution*. (2019) 73:735–49. doi: 10.1111/evo.13702

17. AKC. (2024). Official Standard of Dachshund. Available at: https://images.akc.org/pdf/breeds/standards/Official_Standard_Dachshund.pdf (Accessed 11 April, 2024).

18. FCI. (2024). Standard Dachshund. Available at: https://www.fci.be/nomenclature/Standards/148g04-en.pdf (Accessed 11 April, 2024).

19. Lappalainen AK, et al. Breed-typical front limb angular deformity is associated with clinical findings in three chondrodysplastic dog breeds. *Front Vet Sci*. (2022) 9:1099903. doi: 10.3389/fvets.2022.1099903

20. Sullivan S, et al. The relationship between radiographic disc calcification score and FGF4L2 genotype in dachshunds. *J Vet Intern Med*. (2024) 10:96.

21. Proschowsky HF, Rugbjerg H, Ersboll AK. Mortality of purebred and mixed-breed dogs in Denmark. *Prev Vet Med*. (2003) 58:63–74. doi: 10.1016/S0167-5877(03)00010-2

22. McMillan KM, Bielby J, Williams CL, Upjohn MM, Casey RA, Christley RM. Longevity of companion dog breeds: those at risk from early death. *Sci Rep*. (2024) 14:531. doi: 10.1038/s41598-023-50458-w

23. O'Neill DG, Church DB, McGreevy P, Thomson PC, Brodbelt DC. Longevity and mortality of owned dogs in England. *Vet J*. (2013) 198:638–43. doi: 10.1016/j.tvjl.2013.09.020

24. Michell AR. Longevity of British breeds of dog and its relationships with sex, size, cardiovascular variables and disease. *Vet Rec*. (1999) 145:625–9.

25. Adams VJ, Evans KM, Sampson J, Wood JLN. Methods and mortality results of a health survey of purebred dogs in the UK. *J Small Anim Pract*. (2010) 51:512–24. doi: 10.1111/j.1748-5827.2010.00974.x

frontiers | Frontiers in Veterinary Science

TYPE Clinical Trial
PUBLISHED 07 January 2025
DOI 10.3389/fvets.2024.1504477

OPEN ACCESS

EDITED BY
Joao Miguel De Frias,
University of Edinburgh, United Kingdom

REVIEWED BY
Shinji Tamura,
Tamura Animal Clinic, Japan
Filipa Lourinho,
Southern Counties Veterinary Specialists, United Kingdom

*CORRESPONDENCE
Francisca Couto
✉ franciscacouto.vet@gmail.com

RECEIVED 30 September 2024
ACCEPTED 11 December 2024
PUBLISHED 07 January 2025

CITATION
Couto F, Tabanez J, Rose J and Driver C (2025) Surgical management of single-level thoracolumbar vertebral body segmentation and formation failure causing progressive thoracolumbar myelopathy in three adult large-breed dogs.
Front. Vet. Sci. 11:1504477.
doi: 10.3389/fvets.2024.1504477

Surgical management of single-level thoracolumbar vertebral body segmentation and formation failure causing progressive thoracolumbar myelopathy in three adult large-breed dogs

Francisca Couto*, Joana Tabanez, Jeremy Rose and Colin Driver

Lumbry Park Veterinary Specialists, Hampshire, United Kingdom

Objective: This study aimed to evaluate the medium-term outcome following spinal cord decompression and instrumented fixation of single-level congenital thoracolumbar vertebral malformations, characterized by combined failures of segmentation and formation, causing thoracolumbar myelopathy in three large-breed dogs.

Study design: This was a retrospective clinical study.

Animals: The animals involved in the study were three large-breed dogs.

Methods: Electronic patient records were retrospectively reviewed for adult large-breed dogs (>1 year) (>25 kg) with thoracolumbar myelopathy and a radiologic diagnosis of spinal cord compression associated with thoracolumbar vertebral malformation. The examination, diagnostic imaging, surgical management, and outcomes are described. The medium-term outcome was determined based on the neurological examination and follow-up imaging studies conducted up to 12 months post-operation.

Results: Three large-breed dogs were identified, presenting with progressive, non-painful T3–L3 spinal cord segment disease. Diagnosis was made using MRI and CT, which revealed single-level complex congenital vertebral malformation with combined failures of segmentation and formation in the T8–L1 region. Surgical management consisted of ventral cord decompression by bilateral mini-hemilaminectomy and partial corpectomy and vertebral fixation. Temporary postoperative neurological deterioration was observed in two cases. Follow-up was conducted at 6 weeks (examination) and 3 (examination), 6, and 12 months (examination and CT) postoperatively, and improved neurological function was confirmed, with all cases being ambulatory with persistent, mild paraparesis.

Conclusion: This retrospective study demonstrates the successful medium-term outcome following surgical management of complex thoracolumbar vertebral malformations in large-breed dogs.

KEYWORDS

vertebral stabilization, veterinary spinal surgery, thoracic malformations, corpectomy, congenital diseases vertebral stabilization, thoracicolumbar vertebral malformations, congenital diseases

1 Introduction

Congenital anomalies of the vertebral column are commonly identified in the thoracic spine of small-breed dogs, with French Bulldogs, English Bulldogs, Pug dogs, and Boston Terriers being overrepresented (1–5). These anomalies are less often observed in large-breed dogs, with limited case reports in puppies (2). Although the appropriate terminology has been debated, congenital thoracic vertebral malformations (CTVM) can be classified by failure of vertebral body segmentation (such as block vertebrae) and/or formation (such as hemivertebrae, wedge-shaped vertebrae, and "butterfly" vertebrae) (6, 7). This condition may predispose to abnormal angulation of the vertebral column (kyphosis, lordosis, or scoliosis), vertebral instability, canal stenosis, and spinal cord compression. Some deformations are common incidental findings in 'at-risk' breeds and are not commonly associated with clinical signs; others can develop neurological dysfunction with progressive, non-painful, pelvic limb ataxia, paraparesis, and incontinence. In these cases, non-surgical treatment is expected to result in a poor outcome (8). Different surgical techniques have been described with the aim of relieving spinal cord compression and stabilising the abnormal region (9, 10). In large-breed puppies, only two cases have been reported with a successful outcome following surgical treatment (1, 2). To the best of our knowledge, this is the first retrospective case series that evaluates medium-term outcomes following decompression fixation of complex thoracolumbar vertebral malformations, characterized by combined failures of segmentation and formation, in three adult large-breed dogs.

2 Materials and methods

2.1 Animals

Electronic patient records were retrospectively reviewed for adult (>1 year) large-breed dogs (>25 kg) with a radiologic diagnosis of spinal cord compression associated with thoracolumbar vertebral malformation. Three young adult (2–4 years old), intact female large-breed dogs (Rottweiler, Bloodhound, and Irish Water Spaniel) were identified (Table 1). All presented with a chronic, several-week history of progressive gait abnormalities, without apparent signs of discomfort. Cases 1 and 3 were ambulatory paraparetic with asymmetric pelvic limb ataxia (worse on the right and left, respectively) and abnormal pelvic limb postural reactions. Case 2 was non-ambulatory paraparetic with absent pelvic limb postural reactions and a cutaneous trunci cutoff at the level of T10. All three dogs were bright, alert, and responsive on initial examination. Segmental spinal reflexes and cranial nerve examination were normal. The remainder of the physical examination was unremarkable. In all dogs, complete blood count and serum biochemical profile were within normal limits. All cases had a T3–L3 spinal cord segment neuroanatomic localization. Given the progressive and non-painful history, congenital malformation, infectious/inflammatory processes, degenerative conditions, and neoplasia (e.g., intramedullary tumors) were considered most likely.

2.2 Preoperative imaging

Diagnostic imaging, including magnetic resonance imaging (MRI) and computed tomography (CT), was reviewed by at least one board-certified neurologist. MRI was acquired under general anesthesia using a 1.5 Tesla scanner (Siemens Symphony Tim System). Standard spin-echo T2-weighted (T2W) sagittal, transverse, and dorsal short tau inversion recovery (STIR) sequences were obtained through the thoracolumbar spine. CT images were obtained either under sedation or general anesthesia using a 160-slice scanner (Aquilion PRIME Toshiba, Canon Medical Systems USA, Inc., United States) with a 0.5-mm slice thickness in the transverse plane and a 1-mm reconstructed slice thickness in the sagittal and dorsal planes. CT images were used to evaluate the osseous structure for anomalous or traumatic lesions for surgical planning and postoperative follow-up. The images were evaluated using multi-planar reconstruction in a bone window using commercially available DICOM imaging software (OsiriX)[1]. ROI tools were used for linear measurements.

In case 1 (Figure 1), the T13 and L1 vertebral bodies were abnormally shaped and were non-segmented but had separate vertebral arches (pedicles, dorsal lamina, and spinous process). This caused a severe focal kyphotic deformity with secondary vertebral canal stenosis and ventral spinal cord compression. On T2W images in transverse view, within the cranial segment, the spinal cord diameter measured 5 × 5 mm, whereas at the apex of the malformation, it measured 4.5 × 3.7 mm. In addition, there were adjacent intervertebral disc degeneration and vertebral endplate sclerosis at T12. Case 2 had similar incomplete formation and segmentation of the T8 and T9 vertebral bodies (Figure 2), again causing significant kyphoscoliosis and spinal cord compression. Cranially, the spinal cord diameter was 5 mm, progressively decreasing to 1.8 mm and 3.5 mm above T8 and T9, respectively. In case 3 (Figure 3), there was incomplete ventral formation and segmentation of the T10 and T11 vertebral bodies. This formed one "mushroom-shaped" vertebral body, with adjacent intervertebral disc degeneration and protrusion (T9–T10 and T11–T12). In all cases, there was an increase in T2-weighted signal intensity within the spinal cord at the apex of the deformity, corresponding to the greatest degree of spinal cord compression, presumably reflecting oedema, inflammation, and/or gliosis.

2.3 Surgical procedures

All three cases were premedicated with methadone (0.2–0.3 mg/kg) and dexmedetomidine (3–5 mcg/kg), administered intravenously or intramuscularly. General anesthesia was then induced with propofol (4–6 mg/kg) to effect and maintained with isoflurane. Prophylactic antibiotics were given intravenously at induction

1 www.osirix-viewer.com

(cefuroxime 20 mg/kg) and subsequently repeated every 90 min during this procedure. Perioperative analgesia was achieved with methadone (0.1–0.2 mg/kg every 4 h) and continuous rate infusion (CRI) of ketamine (5–10 mcg/kg/min).

The dogs were positioned in sternal recumbency (as close as possible to preoperative imaging). A dorsal approach to the thoracolumbar spine was performed in all patients for a combination of ventral spinal cord decompression (via bilateral mini-hemilaminectomy and partial lateral corpectomy) and vertebral fixation with varying instrumentation. In case 1 (Figure 4), pedicle screw–rod fixation was performed using 4.0-mm diameter titanium alloy polyaxial screws (Fitzbionic Ltd., Surrey, UK) and 5.0-mm diameter interconnecting rods. In cases 2 (Figure 5) and 3, pins (2.4-mm diameter stainless steel threaded interface pins, Imex

TABLE 1 Signalment and clinical summary.

Signalment	Onset	Neurological examination	Neuroanatomical localization
Dog: case 1 2 years and 9 months Rottweiler Female intact 35 kg	4–6 weeks	Ambulatory paraparesis with pelvic limb ataxia (worse on the right). Reduced paw placement and hopping on both pelvic limbs (worse on the right).	T3–L3 spinal cord segments
Dog: case 2 4 years and 5 months Bloodhound Female intact 30 kg	Since being born	Non-ambulatory paraparesis. Absent paw placement on both pelvic limbs. Cutaneous trunci around T10.	T3–L3 spinal cord segments
Dog: case 3 4 years Irish Water Spaniel Female intact 20 kg	Since 12 weeks of age	Ambulatory paraparesis with pelvic limb ataxia (worse on the left). Reduced paw placement and hopping on both pelvic limbs (worse on the left). Cutaneous trunci present around the thoracolumbar junction.	T3–L3 spinal cord segments

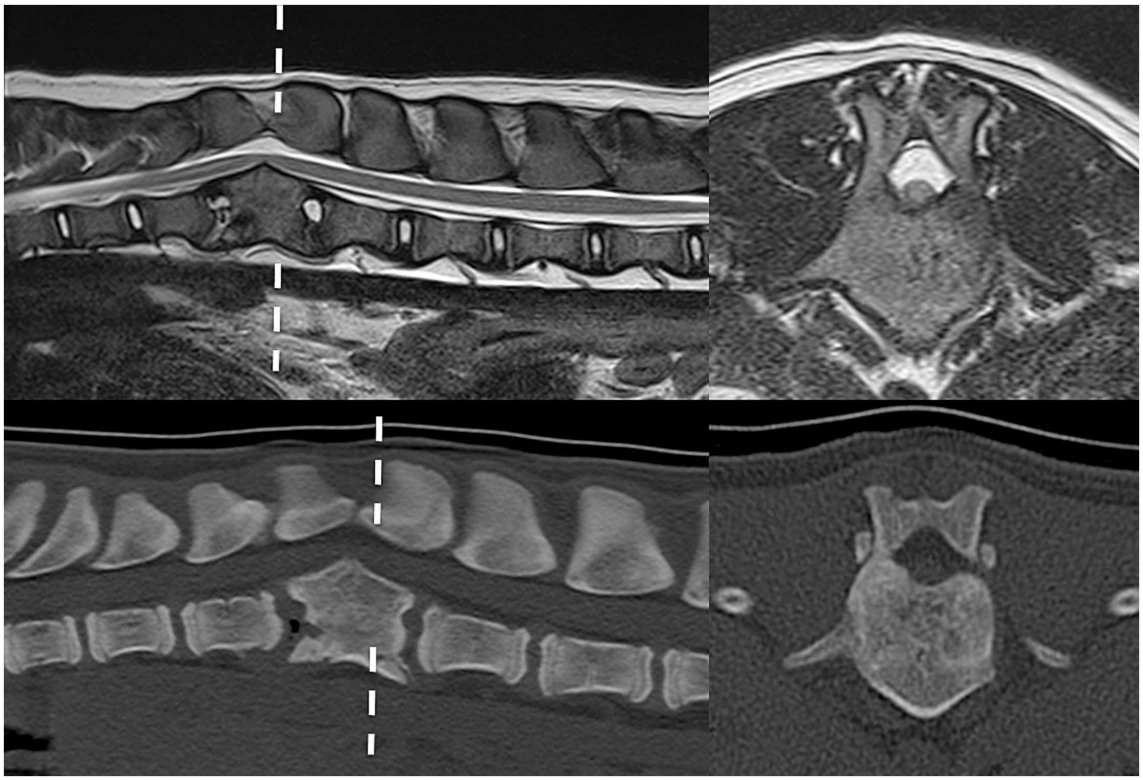

FIGURE 1
Preoperative imaging of case 1. T2W MRI (top row) and CT (bottom row) in sagittal (left) and transverse (right) planes at the level of incompletely formed and segmented T13 and L1 (dashed line represents transverse level).

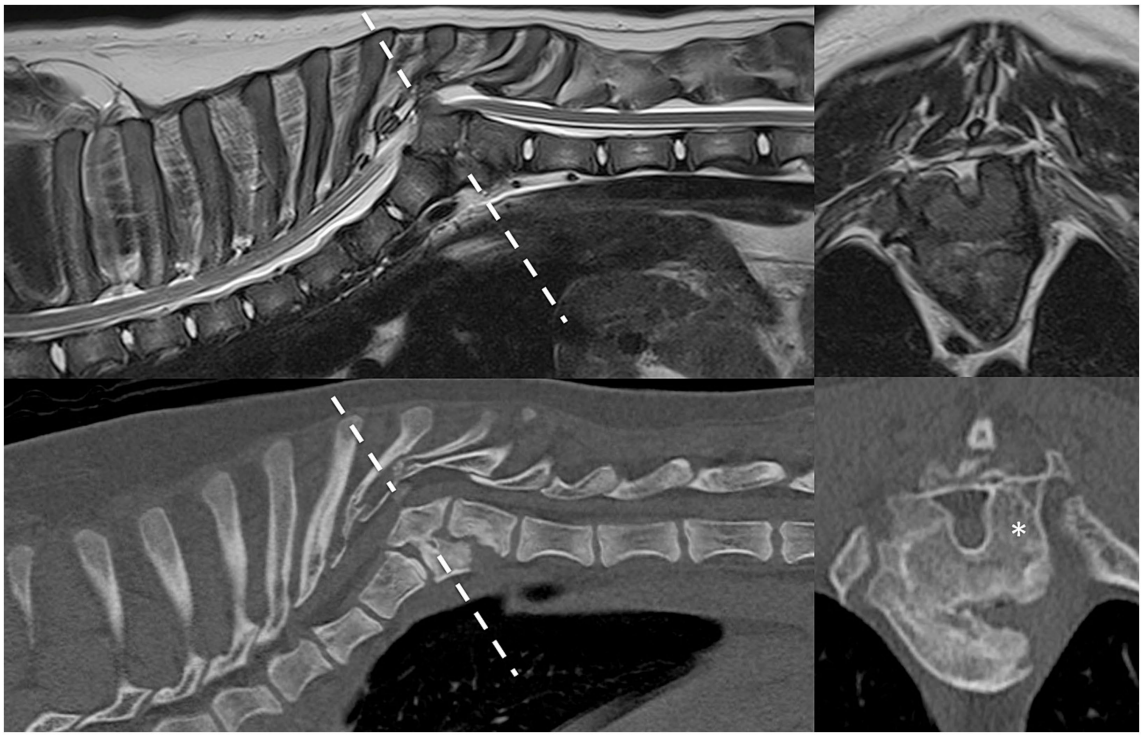

FIGURE 2
Preoperative imaging of case 2. T2W MRI (top row) and CT (bottom row) in sagittal (left) and transverse (right) planes at the level of incompletely formed and segmented T8 and T9 (dashed line represents transverse level). Asterisk = malformed left pedicle of T9 removed during surgery.

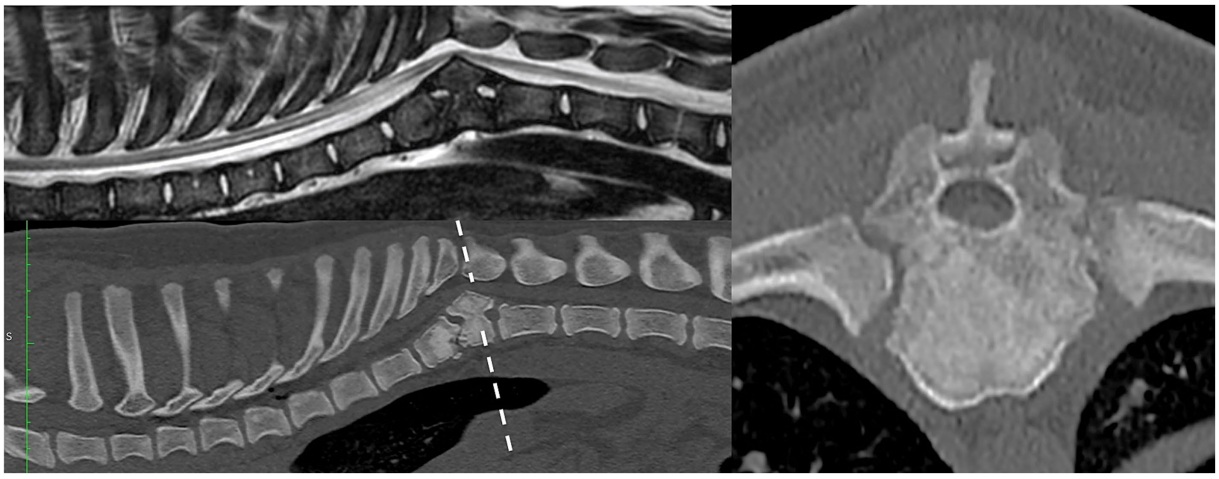

FIGURE 3
Preoperative imaging of case 3. T2W MRI (top row) and CT (bottom and right) in sagittal (left) and transverse (right) planes at the level of incompletely formed and segmented T10 and T11 (dashed line represents transverse level).

Veterinary Inc., Movora, Texas, USA) and bone cement (gentamicin-impregnated polymethylmethacrylate, PMMA, Stryker, Michigan, USA) were used. Vertebral pedicle and body implants were placed in a bi-cortical fashion using a free-hand technique along trajectories and depths determined from preoperative planning CT. In case 3 (Figure 6), a bilateral laminoplasty was subsequently performed using a contoured titanium alloy mesh (Veterinary Instrumentation, Sheffield, UK) anchored to a rib head with 2.0-mm self-tapping self-drilling screws and bone cement. A postoperative CT scan, taken immediately after the surgery, showed satisfactory ventral spinal cord decompression. In addition, implant placement was considered satisfactory because there was no evidence of vertebral canal breaches at any level, and the implants purchased satisfactory volumes of the vertebral pedicle and/or body according to the preoperative *in silico* plans.

Postoperatively, all dogs were prescribed intravenous analgesia with methadone (0.1–0.2 mg/kg every 4–6 h) and continuous rate infusion (CRI) of ketamine (2–5 mcg/kg/min), according to pain scores. In addition, they were treated with oral gabapentin (10 mg/kg

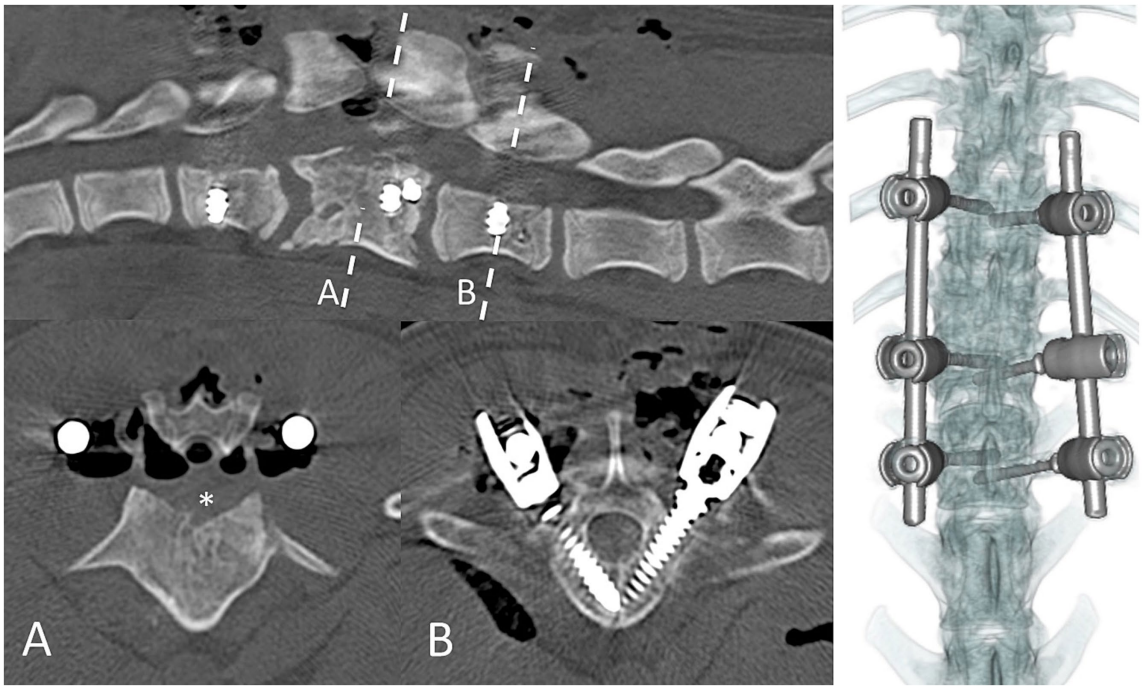

FIGURE 4
Immediate postoperative CT scan imaging of case 1. Dashed lines represent transverse levels. A = bilateral partial lateral corpectomy; asterisk denotes the region of bone removed to ventrally decompress the spinal cord. B = 4.5-mm pedicle–body screws in L2.

twice daily), paracetamol (10 mg/kg three times daily), and non-steroidal anti-inflammatory drugs such as meloxicam (0.1 mg/kg) or robenacoxib (1–2 mg/kg), once daily.

3 Results

3.1 Clinical outcome and follow-up

In two dogs (cases 1 and 2), transient neurological deterioration was evident, with both dogs suffering significant diminishment of voluntary motor function but with intact deep pain sensation. In addition, the dog in case 2 revealed spinal hyperesthesia associated with the incision site. In both cases, the following day, revision surgery revealed large compressive epidural hematomas, which were aspirated. The duration of hospitalization was 19 and 22 days for cases 1 and 2, respectively. Both dogs were discharged as non-ambulatory paraparetic but were ambulatory at the 6-week follow-up. Case 3 did not deteriorate postoperatively and was discharged after 9 days of hospitalization with ambulatory paraparesis. Preoperative and postoperative urinary and fecal incontinence was not perceived in these patients. Postoperative recommendations included restricted rest, with a gradual increase in the length of controlled lead walks, and physiotherapy by a certified canine rehabilitation therapist. Follow-up by a neurologist included repeated neurological examination at 6 weeks, and at 3, 6, and 12 months after surgery. Improvement was observed in all three dogs, with persistent but improved ambulatory paraparesis, fewer mistakes in paw placement, and better coordination. Two cases underwent follow-up CT scans at 6 and 12 months, which revealed unchanged vertebral canal volume and implants from the postoperative period.

4 Discussion

Congenital thoracic vertebral malformations are believed to be caused by the failure of vertebral ossification centers to form, fuse properly, or both, during embryonic or fetal development (4, 11). A variety of thoracic malformations have been reported in small-breed dogs with kyphosis, including wedge-shaped thoracic "hemivertebrae" and "butterfly" vertebrae, which are commonly observed in the mid to caudal thoracic vertebral region, between T6 and T9. Despite being rarely reported in large-breed dogs, congenital thoracic vertebral malformations in small animals can result in progressive kyphotic deformation of the vertebral column, with spinal cord compression and vertebral canal stenosis typically manifesting in young dogs (4, 9, 10, 12–14). In this retrospective study, a complex combined failure of vertebral formation and segmentation between T8 and L1 was associated with focal but marked kyphosis of the vertebral column at a single level in adult large-breed dogs.

Progression of clinical signs and poor outcomes have been reported in multiple studies after non-surgical treatment (8, 9, 14). Surgical techniques include fixation with or without spinal cord decompression and decompression without fixation (2, 9). Different surgical techniques for spinal decompression have been described (including dorsal laminectomy, hemilaminectomy, and/or corpectomy), and several strategies for spinal fixation (13). Two previous reports in large-breed dogs have demonstrated successful outcomes with surgical spinal decompression and fixation (1, 2). One report described a partial ventral corpectomy and fusion with pins and cement (1). Another described unilateral hemilaminectomy and lateral corpectomy, followed by bilateral stabilization with pins and PMMA bars (2). Although spinal fixation is not always considered

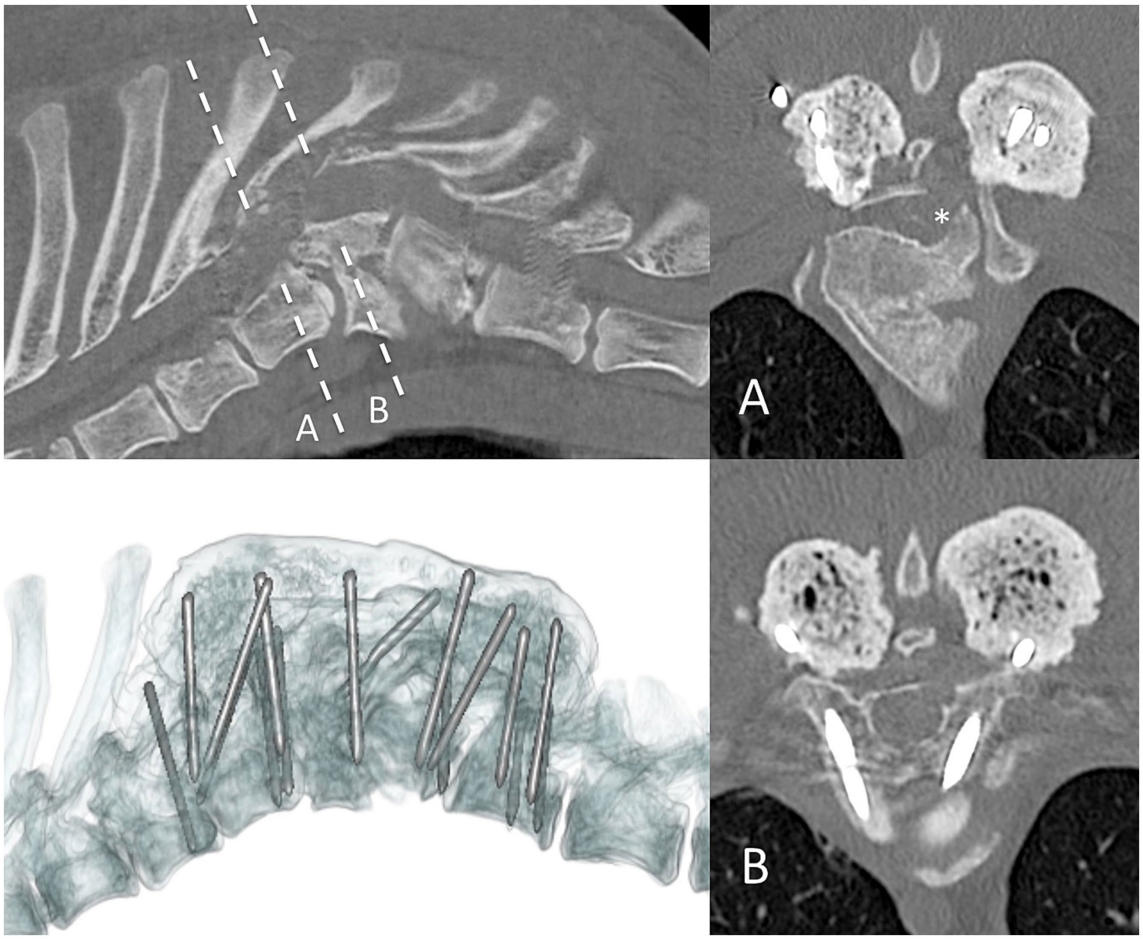

FIGURE 5
Postoperative CT scan imaging of case 2. Sagittal (top left), transverse (right column), and three-dimensional (bottom left) reconstructions. Dashed line represents the transverse level imaged. Asterisk denotes the region of bone removed from the left pedicle and dorsal aspect of the body of the T9 vertebra.

necessary, the decision to proceed with it should take into consideration multiple factors, including the extent of the surgical technique used for spinal cord decompression (such as bilateral hemilaminectomy over multiple vertebrae, partial corpectomy, radical dorsal laminectomy, or hemilaminectomy with corpectomy), the three-compartment concept of spinal stability (i.e., if two or more compartments are compromised, the vertebral column should be considered unstable), disease chronicity, and imaging findings suggestive of instability (13, 15). In the current case series, given the ventral spinal cord compression, decompression with a bilateral mini-hemilaminectomy followed by a partial lateral corpectomy was considered necessary. In addition, different strategies for spinal fixation have been reported, and the most commonly used instrumentation includes screws and plates, screws/pins, and PMMA (5, 13, 15). Furthermore, surgical experience, anatomical considerations, and the type of spinal fixation required help with the implant selection (15). Polyaxial pedicle screws and rods were used in case 1 due to implant availability and ease of application in the thoracolumbar region. Cases 2 and 3 were managed with threaded pins and PMMA due to appropriate implant sizing and ease of use.

Similar to previous reports in large-breed dogs treated surgically (1, 2), two of the three dogs in the present study demonstrated an immediate postoperative neurological deterioration. Postoperative CT scan and revision surgery confirmed the presence of epidural hematoma formation. Although considered unlikely, we cannot rule out the possibility of an underlying coagulopathy being the cause of the hematoma in cases 1 and 2. Further tests, such as a coagulation profile, were not performed in all three cases. Other complications, following surgical treatment, have been previously reported, such as iatrogenic injury to the spinal cord, nerve roots, intervertebral discs, and vascular structures, as well as invasion of the thoracic cavity, abnormal positioning of the implant, implant failure, or infection (9, 13, 15). Given the deterioration in both cases 1 and 2, in case 3, bilateral laminoplasty was performed to help limit the risk of postoperative spinal cord compression related to hematoma and dependent oedema formation, which was thought to be more of a risk in large-breed dogs due to the depth of the surgical wound and extent of muscle dissection. It is unclear whether this attempt was successful, but it may be beneficial in future cases.

Although all dogs in the present study gradually improved at 6 weeks, and at 3, 6, and 12 months after surgery, they remained with a mild residual ataxic gait. This incomplete recovery has also been reported in previous studies and may be associated with the chronicity and irreversible damage to the spinal cord before surgery (9).

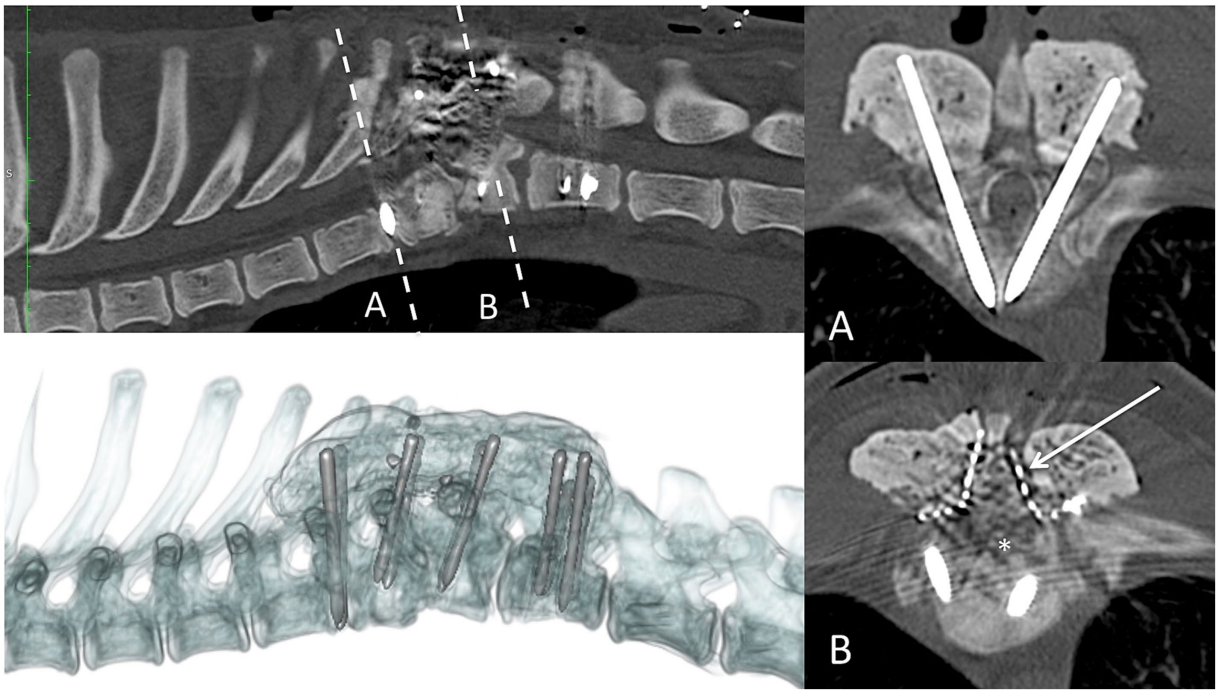

FIGURE 6
Postoperative CT scan imaging of case 3. Sagittal (top left), transverse (right column), and three-dimensional (bottom left) reconstructions. Dashed line represents the transverse level imaged. Asterisk = region of bone removed from bilateral partial lateral corpectomy. A titanium mesh laminoplasty was used to limit postoperative haematoma formation within the vertebral canal (arrow).

The limitations of this study include its retrospective nature and the small study population. A recent study discussing a congenital malformation in a large-breed dog treated with corpectomy and stabilization, reported a good prognosis with a long-term outcome of 34 months. This patient displayed a persistent, mild paraparesis (2). In addition, another study in brachycephalic dogs, investigating surgically managed malformations, reported chronic complications in 58% of the cases. A long-term follow-up was documented between 2006 and 2020 (14). This retrospective case series suggests that successful medium-term outcomes are possible in the surgical management of large-breed dogs with complex thoracolumbar vertebral malformations suffering from myelopathy. However, long-term evaluation should be considered in order to further evaluate potential chronic complications associated with surgery.

Data availability statement

The raw data supporting the conclusions of this article will be made available by the authors, without undue reservation.

Ethics statement

Ethical approval was not required for studies involving animals in accordance with the local legislation and institutional requirements because to our institution, there is no need to obtain an ethical approval for retrospective studies. We have the consent of the owners that these dogs were treated for medical reasons and verbal consent was used for imaging findings and surgery data for publication. Written informed consent was not obtained from the owners for the participation of their animals in this study because this is a retrospective study.

Author contributions

FC: Writing – original draft, Writing – review & editing. JT: Data curation, Investigation, Supervision, Writing – review & editing. JR: Conceptualization, Data curation, Investigation, Methodology, Supervision, Validation, Writing – review & editing. CD: Conceptualization, Data curation, Investigation, Methodology, Supervision, Validation, Writing – review & editing.

Funding

The author(s) declare that no financial support was received for the research, authorship, and/or publication of this article.

Conflict of interest

The authors declare that the research was conducted in the absence of any commercial or financial relationships that could be construed as a potential conflict of interest.

Generative AI statement

The authors declare that no Gen AI was used in the creation of this manuscript.

Publisher's note

References

1. Meheust P, Robert R. Surgical treatment of a hemivertebra by partial ventral corpectomy and fusion in a Labrador puppy. *Vet Comp Orthop Traumatol*. (2010) 23:262–5. doi: 10.3415/VCOT-09-04-0053

2. Musser C, Windsor R, Wininger F. Corpectomy and spinal stabilization using a 3D-printed spine model and custom jigs to address severe spinal deformities from T9-11 and L2-4 in a 6-month-old German shepherd puppy. *Clin Case Rep*. (2021) 9:e05229–7. doi: 10.1002/ccr3.5229

3. De Rycke L, Saunders J. Congenital anomalies of the vertebrae in dogs. *Vlaams Diergen Tijds*. (2017) 86:105–18. doi: 10.21825/vdt.v86i2.16296

4. Westworth DR, Sturges BK. Congenital spinal malformations in small animals. *Vet Clin N Am Small Anim Pract*. (2010) 40:951–81. doi: 10.1016/j.cvsm.2010.05.009

5. Jeffery ND, Smith PM, Talbot CE. Imaging findings and surgical treatment of hemivertebrae in three dogs. *J Am Vet Med Assoc*. (2007) 230:532–6. doi: 10.2460/javma.230.4.532

6. Ryan R, Gutierrez-Quintana R, Ter Haar G, De Decker S. Prevalence of thoracic vertebral malformation in French bulldogs, pugs and English bull dogs with and without associated neurological deficits. *Vet J*. (2017) 221:25–9. doi: 10.1016/j.tvjl.2017.01.018

7. Gutierrez-Quintana R, Guevar J, Stalin C, Faller K, Yeamans C, Penderis J. A proposed radiographic classification scheme for congenital thoracic vertebral malformations in brachycephalic "screw-tailed" dog breeds. *Vet Radiol Ultrasound*. (2014) 55:585–91. doi: 10.1111/vru.12172

8. Wyatt S, Gonçalves R, Gutierrez-Quintana R, De Decker S. Outcomes of nonsurgical treatment for congenital thoracic vertebral body malformations in dogs: 13 cases (2009-2016). *JAVMA*. (2018) 256:768–73. doi: 10.2460/javma.253.6.768

9. Charalambous M, Jeffery ND, Smith PM, Goncalves R, Barker A, Hayes G, et al. Surgical treatment of dorsal hemivertebrae associated with kyphosis by spinal segmental stabilisation, with or without decompression. *Vet J*. (2014) 202:267–73. doi: 10.1016/j.tvjl.2014.08.011

10. Aikawa T, Kanazono S, Yoshigae Y, Sharp NJ, Munana KR. Vertebral stabilization using positively threaded profile pins and polymethylmethacrylate, with or without laminectomy, for spinal canal stenosis and vertebral instability caused by congenital thoracic vertebral anomalies. *Vet Surg*. (2007) 36:432–41. doi: 10.1111/j.1532-950X.2007.00289.x

11. Dewey C, Davies E, Bouma J. Kyphosis and kyphoscoliosis associated with congenital malformations of the thoracic vertebral bodies in dogs. *Vet Clin N Am-Small Anim Pract*. (2016) 46:295–306. doi: 10.1016/j.cvsm.2015.10.009

12. Ryan R, Gutierrez-Quintana R, Ter Haar G, De Decker S. Relationship between breed, hemivertebra subtype, and kyphosis in apparently neurologically normal French bulldogs, English bulldogs, and pugs. *AJVR*. (2019) 80:189–94. doi: 10.2460/ajvr.80.2.189

13. Elford J, Oxley B, Behr S. Accuracy of placement of pedicle screws in the thoracolumbar spine of dogs with spinal deformities with three-dimensionally printed patient-specific drill guides. *Vet Surg*. (2019) 49:347–53. doi: 10.1111/vsu.13333

14. Mavrides D, Charalambous M, Freeman P. Long-term follow-up of spinal segmental stabilization for surgical treatment of dorsal hemivertebrae associated with kyphosis in brachycephalic dogs. *Can Vet J*. (2021) 62:1323–7.

15. Kornberg ST, Brisson BA. Stabilization of the thoracolumbar spine In: A Shores and BA Brisson, editors. Advanced techniques in canine and feline neurosurgery. Hoboken, NJ: Wiley (2023). 109–28.

frontiers | Frontiers in Veterinary Science

TYPE Case Report
PUBLISHED 13 February 2025
DOI 10.3389/fvets.2025.1551567

OPEN ACCESS

EDITED BY
Andy Shores,
Mississippi State University, United States

REVIEWED BY
Gabriel Antonio Garcia,
University of Florida, United States
Richard Filgueiras,
Southwest Veterinary Center CVS, Brazil

*CORRESPONDENCE
Marc Kent
✉ mkent1@uga.edu

†PRESENT ADDRESS
Jeffery Smith,
Colorado Animal Specialty & Emergency (CASE), Iris Ave,
Boulder, CO, United States

RECEIVED 25 December 2024
ACCEPTED 21 January 2025
PUBLISHED 13 February 2025

CITATION
Smith J, Kent M, Glass E and Davis G (2025) Case report: Resolution of lameness via compartmental resection of a malignant nerve sheath neoplasm of the median nerve in a dog.
Front. Vet. Sci. 12:1551567.
doi: 10.3389/fvets.2025.1551567

Case report: Resolution of lameness via compartmental resection of a malignant nerve sheath neoplasm of the median nerve in a dog

Jeffery Smith[1†], Marc Kent[2*], Eric Glass[1] and Garrett Davis[1]

[1]Red Bank Veterinary Hospital, Red Bank, NJ, United States, [2]Department of Small Animal Medicine and Surgery, College of Veterinary Medicine, University of Georgia, Athens, GA, United States

A 7-year-old golden retriever was evaluated for a 6-month history of progressive right thoracic limb lameness. A lameness (grade 3 out of 5 on visual gait analysis) and pain with palpation of the medial aspect of the brachium proximal to the elbow were identified on exam. Magnetic resonance imaging of the right thoracic limb revealed a well-delineated, ovoid mass arising from the median nerve just proximal to the elbow. Compartmental resection of the mass with limb preservation was performed. Microscopically, the mass was a malignant nerve sheath neoplasm. One week postoperatively, the lameness was mild (grade 1). Three months postoperatively, the lameness had resolved (grade 0). One year postoperatively, the dog's gait remains normal. Malignant nerve sheath neoplasms commonly arise in the brachial plexus or cervical spinal nerves, often affecting the innervation provided by the radial nerve. Given its role in providing weight support, dysfunction of the radial nerve significantly impacts the gait. Conversely, dysfunction of the median nerve should not impair the gait. In the present case, compartmental resection of the neoplasm affecting the median nerve resolved the dog's lameness. The return of normal limb function supports the contention that the lameness was consequent to general somatic afferent dysfunction, neuropathic pain, rather than general somatic efferent function (paresis).

KEYWORDS

neuropathic pain, median nerve, malignant nerve sheath neoplasm, lameness, dog

Introduction

Causes of lameness in dogs are broadly divided into orthopedic and neurological etiologies. In orthopedic disorders, lameness occurs secondary to mechanical disruption of the limb movement, pain, or a combination of both. In neurological disorders, lameness occurs secondary to paresis, pain, or a combination of both. Regardless of the cause, the resultant lameness may look similar on visual gait analysis. In most cases, determining the underlying etiology requires physical examination and diagnostic imaging; however, it can be challenging if an apparent site of pain, mechanical dysfunction, or paresis is not readily identified on physical examination.

The following report details the diagnostic investigation and treatment of a dog with a chronic thoracic limb lameness. Examination alone failed to identify an orthopedic or neurologic etiology of the lameness. Clinicopathologic investigations and diagnostic imaging identified a malignant nerve sheath neoplasm (MNSN) involving the median nerve. With compartmental resection of the neoplasm, long-term resolution of the lameness and control

of the neoplasm were achieved. The authors suggest that the dog's lameness reflected neuropathic pain related to involvement of the median nerve. Compartmental resection with limb preservation was possible given the functional neuroanatomy provided by the median nerve and associated innervation.

Case report

A 7-year-old, 35-kg, female spayed golden retriever presented for evaluation of a 5-month history of progressive right thoracic limb lameness. At the onset, the primary veterinarian appreciated a mild lameness on visual gait analysis (grade 1 out of 5) (1). No other abnormalities were identified on physical examination. A complete blood count and a serum biochemistry panel were normal. Radiographs of the right elbow disclosed mild sclerosis of the trochlear notch. Treatment with omega fatty acid supplements (Vetoquinol Triglyceride Omega, Fort Worth, TX, USA) failed to improve the lameness. At re-evaluation 6 weeks later, the lameness had worsened. Physical examination remained normal except for the right thoracic limb lameness. Point-of-care serology (SNAP 4Dx Plus Test, IDEXX Laboratories, Inc., Westbrook, ME, USA) for *E. canis* was positive; serology for *D. immitis*, *B. burgdorferi*, and *A. phagocytophilum* was negative. Follow-up PCR testing for *E. canis* was negative. Treatment with meloxicam (0.1 mg/kg orally q 24 h for 7 days) and doxycycline (10 mg/kg orally q 24 for 14 days) failed to improve the lameness. Two months after the onset of lameness, repeat radiographic evaluation of the right elbow was unchanged. Additionally, radiographs of the shoulder and carpus were obtained and were normal with the exception of mild antebrachiocarpal joint osteoarthritis. Four months after the onset of lameness, computed tomography (CT) of the right thoracic limb was performed at different referral hospital. Apart from sclerosis at the trochlear notch, no other abnormalities were reported. Injections of methylprednisolone acetate (20 mg per injection) into the tendon sheath of the biceps brachii tendon and into the area of the tendon of insertion of the supraspinatus muscle were performed. Despite methylprednisolone therapy, the lameness persisted. Five months after onset, the dog's lameness continued to worsen and she was referred to Red Bank Veterinary Hospital for further evaluation of the lameness.

On presentation, a grade 3 out of 5 lameness of the right thoracic limb was observed. Pain was elicited with palpation of the medial aspect of the brachium proximal to the elbow. There also was moderate atrophy of the right thoracic limb musculature. With the exception of muscular atrophy, the remainder of the orthopedic examination was normal. Likewise, neurological examination was normal.

At the time of evaluation, only the CT imaging report was available for review. Since prior diagnostic imaging failed to reveal the cause of the lameness, magnetic resonance imaging (MRI) of the cervical vertebral column, right shoulder, and elbow was performed. Prior to MRI, a complete blood count, serum biochemistry profile, and a 3-view thoracic radiographic study were obtained. The blood work and thoracic radiographs were normal. Using a 1.5 -Tesla MRI unit (GE Brivo MR355 Inspire, General Electric Medical Healthcare Milwaukee, WI) multiplanar images were obtained of the cervical vertebral column and right shoulder. For cervical vertebral column and shoulder, sequences acquired included T2-weighted (T2W) and T1-weighted (T1W) prior to and following intravenous administration of contrast medium (0.2 mL/kg of gadolinium based contrast medium [0.2 mL/kg IV, Dotarem, Guerbet Princeton, NJ]). In the craniocaudal plane, a short tau inversion recovery (STIR) sequence was obtained of the right brachium that included the elbow and shoulder joints.

In the right thoracic limb, a 1.5 cm × 5.0 cm ovoid subcutaneous mass was identified on the medial aspect of the distal brachium immediately adjacent to the brachial artery and vein. The mass was homogenously hyperintense on STIR images. (Figure 1) Subjectively, the right thoracic limb musculature was atrophied. The cervical vertebral column and right shoulder were normal. The imaging features were felt consistent with a neoplasm; however, a granuloma could not be excluded from consideration. Given the anatomic location, involvement of the median nerve was suspected. Muscular atrophy was considered secondary to disuse.

Having identified a mass on MRI, the prior CT study, which had been performed at a different institution, was obtained for review. At

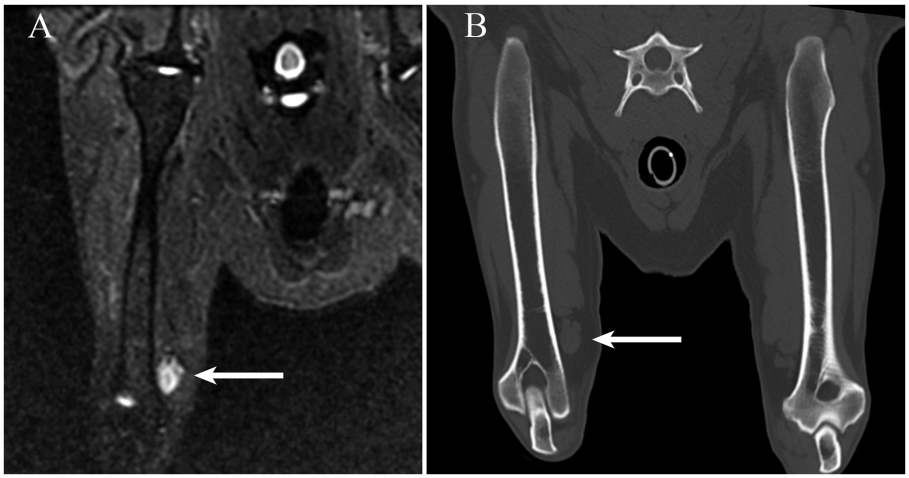

FIGURE 1
(A) On a short tau inversion recovery MRI sequence obtained in the craniocaudal plane, an ovoid hyperintense mass is readily identifiable adjacent to the medial aspect of the distal portion of the right humerus (arrow). **(B)** The mass (arrow) observed in panel **A** is visible on a multiplanar reconstruction CT image created along a plane similar to the short tau inversion recovery sequence.

the same location as observed on the MRI, there was a well-defined, a soft tissue attenuating, ovoid mass (Figure 2).

In consultation with the owner, surgical exploration with the intent of compartmental resection of the mass and limb preservation was pursued. The following day, the dog was anesthetized. The hair overlying the medial aspect of the distal brachium and elbow was clipped and the skin was aseptically prepared. A 10 cm incision was made over the medial aspect of the distal brachium just proximal to the elbow. Deep to the subcutaneous fat and deep fascia, a focal mass involving the median nerve was identified. The collateral ulnar artery was isolated and ligated at the point where it crossed the median nerve. The communicating branch of the musculocutaneous nerve was identified and transected. Compartmental resection of the mass was achieved in which the median nerve was transected approximately 5 cm proximal and distal to the mass. The fascia and skin were closed routinely.

The excised mass and median nerve were submitted for histopathology. Microscopically, the nerve was expanded and effaced by a neoplastic population of indistinct, spindle-shaped cells. In some areas, the neoplastic cells formed whorls and fascicles. The neoplastic cells had variable amounts of eosinophilic cytoplasm and elongated, oval nuclei. The nuclei contained stippled chromatin with a single nucleolus. Occasional nuclear atypia was observed. Areas of necrosis and invasion through the perineurium also were present. Throughout the mass, there were areas of positive immunoreactivity for myelin protein zero which confirms involvement of the nerve. The microscopic findings combined with the immunohistochemistry were consistent with a MNSN. At the proximal and distal cut ends of the nerve, the neoplastic cells blended with the normal nerve cells.

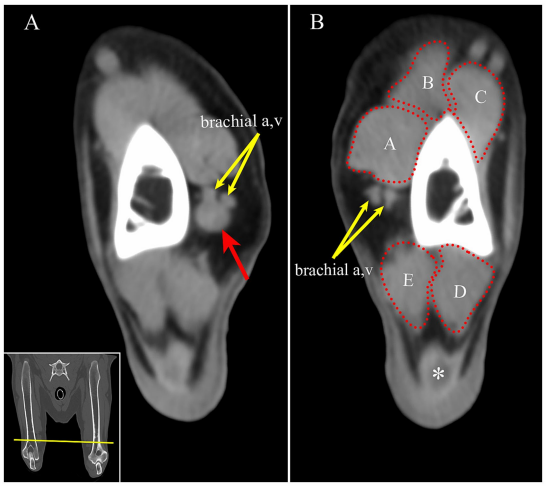

FIGURE 2
(A) On CT, the mass is identified as a round, soft tissue attenuating mass (red arrow) adjacent to the brachial artery and vein on the medial aspect of the right distal humerus (yellow arrows). **(B)** For comparison, the left brachial artery and vein are seen at approximately the same location on the left limb (yellow arrows). Transverse multiplanar reconstruction CT; acquired using a bone algorithm, window and level have been adjusted to make the mass most conspicuous. Inset: The yellow line is approximately the location of the transverse images in panel **A** and **B**. A-biceps brachii m. B-cleidobrachialis m. C-brachialis m. D- anconeus m. E- triceps brachii m, medial head, *- tendon of insertion of the triceps brachii muscle.

Consequently, radiation therapy was offered, however, the owner declined treatment.

Following surgery, the patient had a grade 2 out of 5 lameness on the right thoracic limb. The patient was discharged with carprofen (2.1 mg/kg orally q 12 h) and gabapentin (8.5 mg/kg orally q 12 h) for 14 days. One week post-operatively the owner reported improvements to the lameness.

At recheck 3 months and 8 months following surgery the dog's gait was normal. Neurologic exam also was unremarkable. Cutaneous sensory testing of the palmar aspect of the paw was not performed. Via telephone communication with the owner, the dog continues to walk normally at 12 months postoperatively.

Discussion

Lameness as a consequent to neurological dysfunction is the result of paresis/paralysis whereas lameness secondary to orthopedic disorders result in dysfunction of skeletal structures, muscles, tendons, ligaments, or joints. Neurologic and orthopedic disorders frequently are accompanied by pain which may further contribute to gait abnormalities. However, pain in the absence of an orthopedic or a neurologic disorder also may result in lameness.

Numerous classification schemes exist to categorize pain including those based on duration (acute or chronic), location, underlying disease (cancer pain), and mechanism involved (2). More broadly, pain can be classified as nociceptive or neuropathic (3). Nociceptive pain results from a noxious stimulus acting on a normal somatosensory nervous system (3). The somatosensory system, also known as general somatic afferent (GSA) system, is concerned with the perception of a noxious stimuli (nociception) as well as the perception of touch and temperature (4). In nociceptive pain, there is activation of normal receptors (nociceptors) in response to noxious stimuli. In short, nociceptive pain occurs secondary to damage or injury to non-neural tissue which evokes normal physiological activation of the somatosensory nervous system.

In contrast, neuropathic pain occurs secondary to disease or injury directly impacting either the peripheral or central nervous system components of the somatosensory system (3). In dogs, intervertebral disk herniation is commonly associated with neuropathic pain (2, 5). Persistent neuropathic pain may affect up to 15% of dogs following surgical treatment of intervertebral disk herniation (6). Moreover, neuropathic pain in dogs with intervertebral disk herniation may manifest as a nerve root signature (NRS) in which the affected dog is non-weight bearing in a standing position with possible concurrent lameness (7). In dogs with NRS secondary to caudal cervical spinal nerve root involvement, it is challenging to discern whether concurrent lameness is the result of neuropathic pain, general somatic efferent (GSE) dysfunction leading to paresis, or both.

In the present case, knowledge of the functional anatomy of the median nerve is imperative in understanding the etiology of the dog's lameness. The median nerve arises primarily from the C8 and T1 spinal nerves with occasional contributions from the C7 and T2 spinal nerves (8). The median nerve provides both GSE and GSA innervation (8). Median nerve GSE axons innervate the pronator quadratus, pronator teres, flexor carpi radialis, deep digital flexor, and superficial digital flexor muscles (8). GSA axons, via the palmar branches of the median nerve, innervate cutaneous areas of the palmar aspect of the

forepaw distal to the carpus (8). In the present case, GSE dysfunction can be excluded from playing a role in the cause of the lameness. Firstly, experimental transection of the median nerve in normal dogs does not produce an observable gait disturbance or lameness (9). Moreover, if GSE dysfunction contributed to the cause of the dog's lameness, a worsening lameness postoperatively would have been anticipated as the median nerve was transected during compartmental resection of the neoplasm. In fact, the opposite occurred; the lameness completely resolved following resection of the neoplasm and transection of the median nerve proximal to the neoplasm along with transection of the communicating branch of the musculocutaneous nerve. Therefore, it is most plausible that with transection of median nerve, loss of GSA function abolished neuropathic pain secondary to the neoplastic infiltration of the nerve.

Ultimately, neuropathic pain can be challenging to identify. While subjective and objective methods of establishing pain exist, differentiating neuropathic pain from nociceptive pain is difficult in noncommunicating species. In the present case, neuropathic pain, as a result of neoplastic infiltration of the peripheral somatosensory nervous system, alone remains the most plausible explanation for the lameness. The MNSN affecting the median nerve fulfills the definition of neuropathic pain in that the median nerve conveys GSA information.

While neuropathic pain is often treated with analgesic medications, compartmental resection of the MNSN not only resolved the neuropathic pain as evidenced by a return of a normal gait but also constituted a definitive treatment. Conventionally, treatment of MNSNs in dogs frequently consists of local surgical excision and transection of the involved innervation combined with limb amputation (10–16) Treatment also may involve radiation therapy alone or following surgery (10, 12, 14–17). Depending on the extent of proximal invasion by the neoplasm, laminectomy may be required to excise neoplastic invasion within the intervertebral foramen, vertebral canal, or into the spinal cord, in an attempt to obtain margins histologically clear of neoplastic cells. Despite excessive surgical excision including laminectomy, achieving clear histological margins is difficult. Survival times with surgical excision and amputation vary widely and most reports do not provide the specific anatomic location of neoplasm along the course of the affected nerve(s). In general, dogs treated with local excision and amputation with or without radiation therapy, the median survival times vary from 120 days to 1,303 days with most studies reporting approximately 1 to 2 years (10, 12, 14–16, 18). In dogs with neoplastic extension into the intervertebral foramen, vertebral canal, or the spinal cord, the median survival time may be as short as 5 months, suggesting histological margins are important (14). In other studies, the influence of obtaining histologically clear margins is uncertain as clear margins did not significantly affect survival times (10, 12, 18). It is possible that such survival data is confounded by adjuvant radiation therapy (12).

In the present case, knowing the median nerve GSE function does not contribute to maintaining a normal gait, compartmental resection of the neoplasm with limb preservation was able to be performed. Conceptually, compartmental resection entails excision of the anatomical "compartment" that contains the neoplasm (19). In the setting of soft tissue sarcoma, the muscle or muscle groups containing the neoplasm are excised in an attempt to remove the neoplasm within the robust anatomic borders provided by the normal tissue rather than making arbitrarily sized borders (19). Compartmental resection with limb preservation may offer survival times similar to, if not longer, than excision and amputation (10, 12). Median survival time for dogs undergoing compartmental resection and limb preservation may be as long as 1,303 days (10). In the context of a MNSN, the "compartment" is likely considered the nerve itself. Consequently, neoplastic infiltration outside the epineurium may be an important determinant in considering compartmental resection with limb preservation. Neoplastic infiltration may confer higher recurrence rates and shorter survival times than non-infiltrative neoplasms (median survival time of 487 days vs. 2,227 days, respectively) (10). To date, the histologic diagnosis of MNSN can be difficult given variation in histological features of MNSN, histological similarities shared with other mesenchymal neoplasms, and the lack of specific immunohistochemical markers unique to MNSNs (20). Moreover, histological features do not impact survival following surgical resection (12).

Importantly, compartmental resection with limb preservation offers the potential of return of normal limb function. With compartmental resection, restoration of normal limb function occurs in approximately 60% of dogs with the remainder of dogs having residual lameness. Given the importance of the radial nerve to the maintenance of the gait, compartmental resection of neoplasms involving the radial nerve should be carefully considered as postoperative gait deficits are likely (10).

To the authors' knowledge, four cases of MNSN involving the median nerve have been well documented (10, 11, 21, 22). The exact anatomic location of the neoplasm along the course of the median nerve was reported in three dogs (10, 11, 22). In two dogs the neoplasm was located at the level of the elbow; however, excision with amputation was performed in both dogs making comparison to the present case difficult (11, 21). In one dog, the neoplasm was located adjacent to the carpus and compartmental resection with limb preservation was performed (22). One month postoperatively, lameness was considered minimal (22). Further description of the dog's gait was not provided. Limb amputation was performed at 26 months postoperatively due to recurrence (22). In the fourth case, the anatomic site of the neoplasm affecting the median nerve was not reported and the dog underwent compartmental resection with limb preservation (10). Although lameness improved postoperatively, the dog maintained a persistent weight-bearing lameness, experienced recurrence, and survived for 306 days (10). In contradistinction to the present case, reports of dogs treated with compartmental resection for MNSN of the median, lameness persisted postoperatively (10, 22).

Results achieved in the present case combined with previous reports suggest that compartmental resection of MNSN involving the median nerve with limb preservation is an acceptable treatment strategy providing survival times comparable to resection and limb amputation. Microscopic assessment of the proximal extent of the neoplastic involvement of the nerve should be performed to assess completeness of resection. Although experimental transection of the median nerve in normal dogs does not produce lameness, residual lameness may remain in dogs treated with compartmental resection for MNSN involving the median nerve (10, 22). While GSE dysfunction may play a role in postoperative lameness, new or persistent neuropathic pain may also contribute to the clinical signs. Future studies should investigate additional therapeutic interventions for the treatment of neuropathic pain in dogs having undergone compartmental resection that demonstrate residual neuropathic pain or lameness.

The present case report has several limitations. Chiefly, it is challenging to infer broad conclusions from a single case. Comparison to previously reported cases is hindered by differences in preoperative patient assessment,

surgical techniques, and means of follow-up. While follow-up in the present case was collected via direct examination and telephone communication, imaging was not performed to assess the potential for recurrence at the surgical site. While recurrence may be present, maintenance of a normal gait suggests otherwise. Likewise, thoracic radiographs were not performed to assess for metastasis. Despite such drawbacks, the successful resolution of lameness postoperatively supports the notion that neuropathic pain may solely underlie the lameness observed in dogs with MNSN. Ultimately, the present case adds to the growing body of literature supporting the role of compartmental resection with limb sparing in providing long term survival for the treatment of MNSN in dogs.

Conclusion

Dogs with malignant nerve sheath neoplasms frequently are presented for lameness as a result of paresis alone or in conjuction with neuropathic pain. Knowledge of the functional neuroanatomy of both the GSE and GSA innervations helps guide clinicians with treatment options. Although conventional treatment for MNSN involves excision combined with limb amputation, in cases involving innervation that has a limited impact on the ability to bear weight and walk, such as those involving the median nerve, compartmental resection with limb preservation may be considered. Even in cases involving radial nerve innervation in which residual deficits are expected, compartmental resection may improve lameness through alleviation of neuropathic pain (10). Postoperative care directed at control of neuropathic pain may result in additional improvement in limb function.

Data availability statement

The original contributions presented in the study are included in the article/Supplementary material, further inquiries can be directed to the corresponding author.

Ethics statement

Ethical approval was not required for the studies involving animals in accordance with the local legislation and institutional requirements because it was a retrospective analysis. Written informed consent was obtained from the owners for the participation of their animal in this study.

Author contributions

JS: Writing – original draft, Writing – review & editing. MK: Writing – original draft, Writing – review & editing, Supervision. EG: Conceptualization, Writing – original draft, Writing – review & editing. GD: Conceptualization, Writing – original draft, Writing – review & editing.

Funding

The author(s) declare that no financial support was received for the research, authorship, and/or publication of this article.

Conflict of interest

The authors declare that the research was conducted in the absence of any commercial or financial relationships that could be construed as a potential conflict of interest.

Generative AI statement

The author(s) declare that no Gen AI was used in the creation of this manuscript.

Publisher's note

Supplementary material

The Supplementary material for this article can be found online at: https://www.frontiersin.org/articles/10.3389/fvets.2025.1551567/full#supplementary-material

SUPPLEMENTARY VIDEO 1
Visual gait analysis at the time of presentation, a grade 3 out of 5 lameness of the right thoracic limb is present.

SUPPLEMENTARY VIDEO 2
3-month after compartmental resection of a malignant nerve sheath neoplasm of the median nerve, the dog's gait is normal.

SUPPLEMENTARY VIDEO 3
An incision has been made on medial aspect of the right thoracic limb just proximal to the elbow. The median nerve has been isolated and retracted out of the surgical field using DeBakey hemostats. The closed tips of a Brown-Adson forceps trace the nerve from proximal (left side of the video) distally into a mass involving the median nerve. The smaller nerve that enters the mass is the communicating branch of the musculocutaneous nerve. In the second segment of the video, curved mosquito hemostats are used to grasp the proximal transected end of the median nerve to aide in the dissection of the mass distally (the elbow is toward the top left corner of the video).

References

1. Duerr F. Canine Lameness. Newark, NJ: John Wiley & Sons, (2020);3–13.

2. Moore SA. Managing neuropathic pain in dogs. *Front Vet Sci*. (2016) 3:12. doi: 10.3389/fvets.2016.00012

3. Merskey H, Bogduk N. Part III: pain terms: a current list with definitions and notes on usage In: H Merskey and N Bogduk, editors. Classification of chronic pain. Seattle: IASP Press (1994)

4. de Lahunta A, Glass E, Kent M. General sensory systems: general proprioception and general somatic afferent, (Eds): LahuntaAlexander de, Eric Glass and Marc Kent, de Lahunta's veterinary neuroanatomy and clinical neurology. Philadelphia, PA: Elsevier, (2020);246–266.

5. Fenn J, Olby NJ. Classification of intervertebral disc disease. *Front Vet Sci*. (2020) 7:579025. doi: 10.3389/fvets.2020.579025

6. Zidan N, Medland J, Olby N. Long-term postoperative pain evaluation in dogs with thoracolumbar intervertebral disk herniation after hemilaminectomy. *J Vet Intern Med*. (2020) 34:1547–55. doi: 10.1111/jvim.15800

7. Schachar J, Bocage A, Nelson NC, Early PJ, Mariani CL, Olby NJ, et al. Clinical and imaging findings in dogs with nerve root signature associated with cervical intervertebral disc herniation. *J Vet Intern Med*. (2024) 38:1111–9. doi: 10.1111/jvim.16982

8. Hermanson JW, DeLahunta A, Evans HE, et al. Miller and Evans' anatomy of the dog. St. Louis, MO: Elsevier, (2020);704–756.

9. Worthman RP. Demonstration of specific nerve paralyses in the dog. *J Am Vet Med Assoc*. (1957) 131:174–8.

10. van Stee L, Boston S, Teske E, Meij B. Compartmental resection of peripheral nerve tumours with limb preservation in 16 dogs (1995-2011). *Vet J*. (2017) 226:40–5. doi: 10.1016/j.tvjl.2017.07.002

11. Targett MP, Dyce J, Houlton JEF. Tumours involving the nerve sheaths of the forelimb in dogs. *J Small Anim Pract*. (1993) 34:221–5. doi: 10.1111/j.1748-5827.1993.tb02669.x

12. Stokes R, Wustefeld-Janssens BG, Hinson W, Wiener DJ, Hollenbeck D, Bertran J, et al. Surgical and oncologic outcomes in dogs with malignant peripheral nerve sheath tumours arising from the brachial or lumbosacral plexus. *Vet Comp Oncol*. (2023) 21:739–47. doi: 10.1111/vco.12938

13. Kerwin SC, Taylor AR. Neurologic causes of thoracic limb lameness. *Vet Clin North Am Small Anim Pract*. (2021) 51:357–64. doi: 10.1016/j.cvsm.2020.12.003

14. Brehm DM, Vite CH, Steinberg HS, Haviland J, van Winkle T. A retrospective evaluation of 51 cases of peripheral nerve sheath tumors in the dog. *J Am Anim Hosp Assoc*. (1995) 31:349–59. doi: 10.5326/15473317-31-4-349

15. Lacassagne K, Hearon K, Berg J, Séguin B, Hoyt L, Byer B, et al. Canine spinal meningiomas and nerve sheath tumours in 34 dogs (2008-2016): distribution and long-term outcome based upon histopathology and treatment modality. *Vet Comp Oncol*. (2018) 16:344–51. doi: 10.1111/vco.12385

16. Cooper-Khan RS, Frankovich AN, Thompson CA, Thomovsky SA, Lewis MJ. Clinical findings and outcome in 30 dogs with presumptive or confirmed nerve sheath tumors. *Vet Sci*. (2024) 11:11. doi: 10.3390/vetsci11050192

17. Dolera M, Malfassi L, Bianchi C, Carrara N, Finesso S, Marcarini S, et al. Frameless stereotactic volumetric modulated arc radiotherapy of brachial plexus tumours in dogs: 10 cases. *Br J Radiol*. (2017) 90:20160617. doi: 10.1259/bjr.20160617

18. Potamopoulou M, Petite A, Findji L. Combined forequarter amputation and hemilaminectomy for treatment of canine peripheral nerve sheath tumors of the brachial plexus invading the spinal canal: surgical technique and outcome in nine dogs. *Vet Surg*. (2024) 53:1477–84. doi: 10.1111/vsu.14166

19. Bray JP. Soft tissue sarcoma in the dog - part 2: surgical margins, controversies and a comparative review. *J Small Anim Pract*. (2017) 58:63–72. doi: 10.1111/jsap.12629

20. Tekavec K, Švara T, Knific T, Gombač M, Cantile C. Histopathological and Immunohistochemical evaluation of canine nerve sheath tumors and proposal for an updated classification. *Vet Sci*. (2022) 9:9. doi: 10.3390/vetsci9050204

21. Anderson O, Langley-Hobbs SJ. A peripheral nerve sheath tumour in the median nerve of a dog. *Vet Rec Case Rep*. (2022) 10:e323. doi: 10.1002/vrc2.323

22. Miyaho N, Mochizuki M, Honnami M. Forelimb lameness caused by malignant peripheral nerve sheath tumors of the median nerve in a dog: a case report. *J Vet Med Sci*. (2024) 86:860–5. doi: 10.1292/jvms.24-0038

frontiers | Frontiers in Veterinary Science

TYPE Case Report
PUBLISHED 14 February 2025
DOI 10.3389/fvets.2025.1512097

OPEN ACCESS

EDITED BY
Koen Santifort,
IVC Evidensia Small Animal Referral Hospital Arnhem, Netherlands

REVIEWED BY
Shinji Tamura,
Tamura Animal Clinic, Japan
Viktor Palus,
Neurovet, Slovakia

*CORRESPONDENCE
Yukiko Nakano
limetomint@gmail.com

RECEIVED 16 October 2024
ACCEPTED 23 January 2025
PUBLISHED 14 February 2025

CITATION
Nakano Y, Nozue Y, Hazeyama H, Matsunami T, Chambers J, Uchida K and Kobatake Y (2025) Case report: Successful surgical resection of an intracranial frontal lobe dermoid cyst in a cat.
Front. Vet. Sci. 12:1512097.
doi: 10.3389/fvets.2025.1512097

Case report: Successful surgical resection of an intracranial frontal lobe dermoid cyst in a cat

Yukiko Nakano[1]*, Yuta Nozue[2], Hiromi Hazeyama[3], Tokio Matsunami[3], James Chambers[4], Kazuyuki Uchida[4] and Yui Kobatake[2]

[1]Department of Neurosurgery, ER Hachioji Advanced Animal Medical and Critical Care Center, Hachioji, Japan, [2]Animal Medical Center, Gifu University, Gifu, Japan, [3]Matsunami Animal Hospital, Nagoya, Japan, [4]Laboratory of Veterinary Pathology, Graduate School of Agricultural and Life Sciences, The University of Tokyo, Tokyo, Japan

Introduction: Intracranial dermoid cysts (IDCs) are rarely observed in veterinary medicine, and reports regarding treatment strategies for feline IDCs are severely lacking. This report describes the surgical management of epileptic seizures caused by IDCs in a cat.

Case presentation: An 8-year-old, spayed, female American Shorthair cat presented with epileptic seizures. The epileptic seizures, which had developed at the age of 5 years, had been controlled by phenobarbital administration. At 8 years old, the cat contracted acute hepatitis, prompting a switch from phenobarbital to other antiseizure medications. This drug switch caused an increase in the frequency of epileptic seizures. Magnetic resonance imaging (MRI) revealed a dermoid cyst as a heterogeneous intensity mass on T2-weighted images, without falx cerebri displacement. The preoperative seizures occurred more than three times a day (cluster seizures), even though the cat was administered multiple antiseizure medications. The seizures ceased after surgical removal of the dermoid cyst. The cat did not experience seizures for 14 months after surgery, even with discontinuation of antiseizure medications.

Conclusion: In cats, surgical removal of frontal lobe IDCs may effectively control epileptic seizures without fatal complications, thus potentially leading to a great prognosis.

KEYWORDS

intracranial dermoid cyst, frontal lobe, epileptic seizure, surgical management, cat

1 Introduction

Intracranial dermoid cysts (IDCs) are rare in veterinary medicine, although they have been occasionally reported (1–3). IDCs are congenital lesions characterized as benign mass lesions in the cranial cavity containing keratinaceous debris and adnexa, which include hair follicles, sebaceous, apocrine, and sweat glands covered by squamous epithelium (3). Dermoid cysts originate from ectoderm and mesoderm remaining in the embryonic fusion plane (4). Intracranial extension of nasal dermoid cyst in a cat has been also reported (5). Reports of surgical management of a dog treated with ventriculoperitoneal shunt (3) and a cat treated with surgical removal (5) are available; however, to date, there are no reports of successful surgical treatment of IDCs in cats worldwide, and information on treatment strategies for feline IDCs is severely lacking. In this report, we describe the clinical symptoms, diagnostic

findings, surgical procedures, and outcomes of a cat with frontal lobe IDCs.

2 Case presentation

2.1 Signalment and history

A 5-year-old spayed female American Shorthair cat presented to a local veterinary hospital with a single epileptic seizure (day 1). Computed tomography revealed an intracranial 7.4 mm × 8.6 mm × 13 mm mass located in the frontal lobe region. The primary veterinarian suggested surgical intervention for the mass; however, the owners declined and elected to manage the seizures. Phenobarbital (3 mg/kg, PO, q12h, Phenobal tablets 30 mg, Daiichi Sankyo, Inc., Tokyo, Japan) was administered, and the patient was seizure-free for 3 years. However, 3 weeks before visiting the Animal Medical Center of Gifu University (day 872), when the cat was 8 years old, she developed acute hepatitis. The local veterinarian discontinued phenobarbital administration and switched to zonisamide (3 mg/kg, q12h, PO, CONSAVE tablets 25 mg, DS Pharma Animal Health, Osaka, Japan) due to the deterioration of hepatic function. After this switch, cluster seizures were observed, and levetiracetam (20 mg/kg, q8h, PO, E Keppra tablets 250 mg, UCB Japan, Tokyo, Japan) and gabapentin (5 mg/kg, q8h, PO, GABAPEN tablets 200 mg, Pfizer Japan, Tokyo, Japan) were administered. The additional antiseizure medications resulted in 3 seizure-free days. The acute hepatitis was treated with enrofloxacin (5 mg/kg, PO, q24h, Enroclear 50 mg tablet; Kyoritsu Seiyaku Corporation, Tokyo, Japan), amoxicillin (11 mg/kg, PO, q12h, Amoxiclear 100 mg tablet, Kyoritsu Seiyaku Corp.), and prednisolone (1 mg/kg, q24h, PREDONINE 5 mg; Shionogi Pharma Corp., Osaka, Japan). This treatment improved her condition and elevated hepatic enzyme levels.

The patient presented to the Animal Medical Center of Gifu University on day 889 for further examination and treatment of the intracranial mass and epileptic seizures. At presentation, the vitals were normal, and the physical examination was unremarkable. All items of the complete blood count were within the normal range, and serum biochemistry was mostly normal except for mildly increased alanine aminotransferase (ALT; 107 IU/L, reference interval: 22–84 IU/L). Thoracic and abdominal radiography was also normal. Neurological examination revealed the menace response reduced bilaterally. The clinical history and neurological examination suggested that the neurolocalization was forebrain. Magnetic resonance imaging (MRI; 3.0-T magnet, Achieva 3.0 T, Philips Japan, Tokyo, Japan) revealed a mass lesion (8.9 mm × 10 mm × 13 mm) in the left frontal lobe. Transverse, sagittal, and dorsal T1-weighted images (T1WI; TR, 2,000 ms; TE, 8) and T2-weighted images (T2WI; TR, 3,600; TE, 90) and T2-w fluid-attenuated inversion recovery (FLAIR; TR, 10,000 ms; TE, 100 ms) were obtained. Transverse T2*-weighted images (T2*WI; TR, 780 ms; TE, 18 ms) were also acquired. Postcontrast T1WI was obtained following intravenous administration of gadodiamide contrast medium (0.1 mmol/kg, Omniscan; GE Healthcare, Tokyo, Japan). Postcontrast T1WI was acquired in the transverse, sagittal, and dorsal planes. All slice thicknesses were 2 mm. The lesion showed heterogeneous signal intensity on T2WI, which was mainly isointense, and showed internal hyperintensity and hypointensity in the remaining part compared with the normal brain gray matter (Figures 1A,D,E). The margins were demarcated. The T1WI demonstrated hyperintensity at the margins and heterogeneous hyperintensity inside the mass (Figure 1B). The postcontrast T1WI revealed slight contrast enhancement at the margin of the mass (Figure 1C). The white matter adjacent to the mass appeared as the hypointense region in T2WI and T2*WI and isointense without contrast enhancement in T1WI. However, peripheral brain edema was not observed (Figures 1A,D,E). Although the lesion mildly compressed the brain parenchyma, displacement of the falx cerebri was not observed (Figures 1A,D). The abnormality of the cribriform and nasal cavity was not detected as well. The cerebrospinal fluid (CSF) could not be obtained. Considering the case signalment, the clinical history, and the MRI findings, the differential diagnosis included anomalous (such as dermoid cyst, epidermoid cyst, and subarachnoid cyst), infectious or inflammatory (such as cholesterol granuloma, toxoplasma gondii granuloma, brain abscess, and cryptococcal granuloma), and neoplastic diseases (meningioma and lymphoma). However, none of those diseases were completely consistent with the findings of this case.

Presumably, the epileptic seizures would be difficult to control with medical therapy despite the administration of multiple antiseizure medications hereafter because cluster seizures were observed again the day after the first presentation at the Animal Medical Center of Gifu University (day 875). Moreover, the cluster seizures were observed almost every day after day 875. The dose up of the antiseizure medications seemed to be required to control the seizures with medicine. However, the effect of increasing the dose of medicines would not be immediate. The owners decided to have the cat undergo surgical removal of the mass, which was performed on day 907.

2.2 Surgical procedure

The cat was induced with alfaxalone [2.5 mg/kg, intravenous (IV) to effect, Alfaxan multidose; Meiji Animal Health, Kumamoto, Japan] and maintained with sevoflurane with 40% 0_2 and alfaxalone, constant rate infusion (CRI) (3–4 mg/kg/h). She was also administered cefazolin sodium (20 mg/kg, IV, Cefamezin Alpha; LTL Pharma, Tokyo, Japan), maropitant citrate (1 mg/kg, SC, Cerenia, Zoetis Japan, Tokyo, Japan), famotidine (0.5 mg/kg, IV, Gaster injection 20 mg, LTL Parma), and prednisolone (1 mg/kg, SC, prednisolone injection; Kyoritsu Seiyaku, Tokyo, Japan) as pre-anesthetic medication. The patient was positioned in ventral recumbency on a vacuum bean bag. Adequate intraoperative analgesia was achieved with fentanyl (20–30 mcg/kg/h CRI, fentanyl injection 0.5 mg, Terumo, Tokyo, Japan). Dopamine hydrochloride (1–13 mcg/kg/h, CRI, dopamine hydrochloride 100 mg IV infusion, Nipro, Osaka, Japan) was used to control intraoperative blood pressure. Craniotomy was performed using a transfrontal sinus approach. After craniotomy, the dura mater was incised, and the mass was approached through a cortical incision in the left frontal lobe. When the hard mass covered by a capsule was visually recognized, the capsule was incised, and internal decompression of the mass was performed. A large amount of keratinized material, including hair, was collected from inside the mass (Figure 2). Some of the contents were subjected to bacterial culture testing. The mass was internally decompressed, and the capsule was separated from the surrounding brain parenchyma. The brain parenchyma around the mass seemed normal. The brain parenchyma

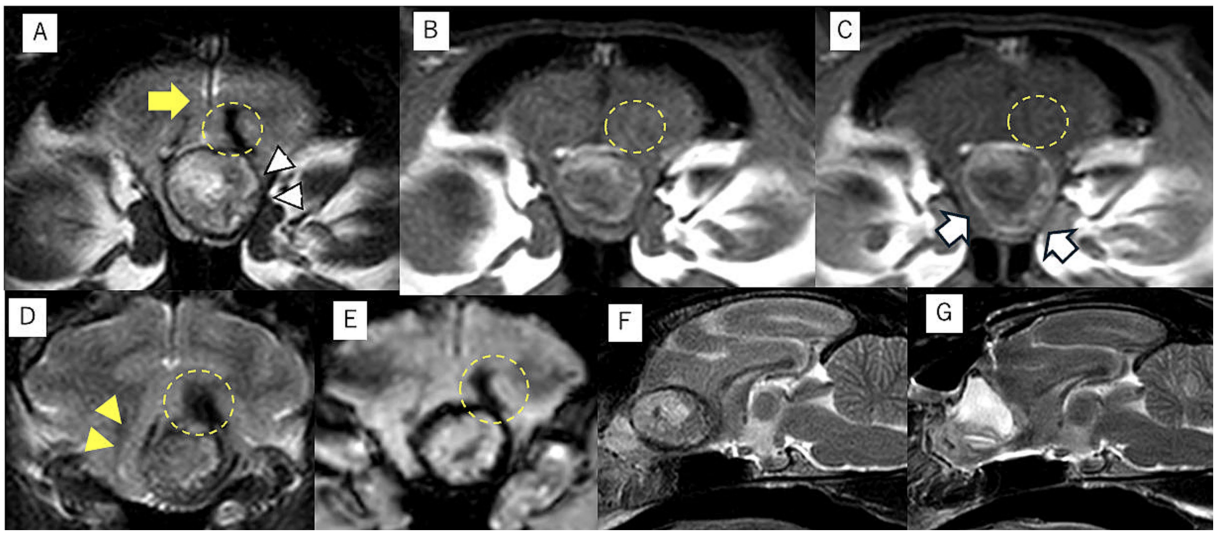

FIGURE 1
Magnetic resonance imaging of intracranial dermoid cysts (IDCs). The transverse T2-weighted image demonstrates a mass lesion with heterogeneous intensity at the midline. The center of the mass lesion is hyperintense, and the periphery is isointense to hypointense (white arrowhead) **(A)**. This transverse T1-weighted image shows the center is hypointense, and the periphery is isointense to hyperintense **(B)**. The edge of IDCs is mildly contrast enhanced in the transverse postcontrast T1-weighted image (white arrow) **(C)**. The falx cerebri midline shift is not observed at the middle level of the IDCs (**A**, yellow arrow). However, the brain parenchyma has shifted to the left side at the caudal slice of the IDCs in the transverse T2-weighted image (**D**, yellow arrowhead). The transverse T2-weighted images showed a hypointense area in the white matter adjacent to the IDCs without edema, and it was demonstrated as an isointense area without contrast enhanced in T1WI (yellow dotted circle) **(A–D)**. This lesion was also detected as a hypointense area on the T2* transverse image (**E**, yellow dotted circle). The preoperative **(F)** and postoperative **(G)** midsagittal planes of T2-weighted images demonstrated that IDCs have been completely removed after surgery, and the saline used during the surgery is accumulated in the extraction cavity **(G)**.

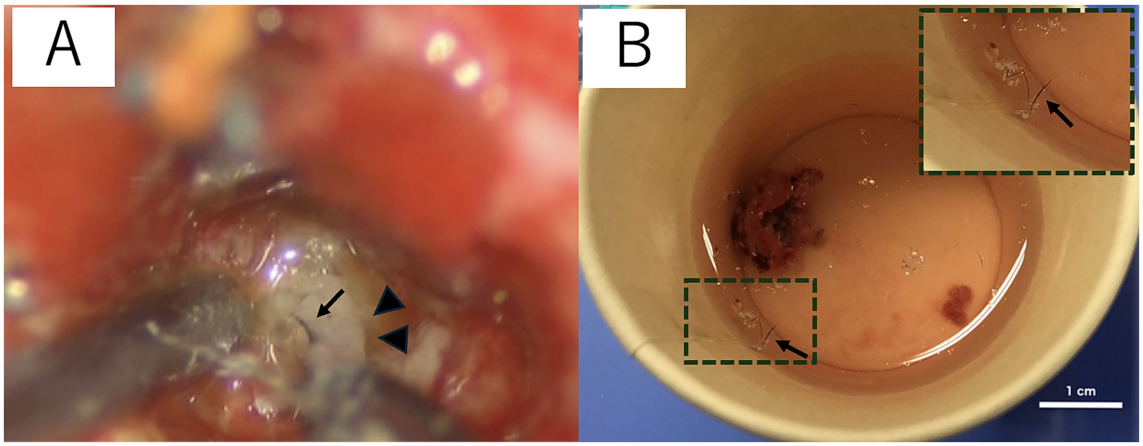

FIGURE 2
Surgical microscopic image **(A)** and the macroscopic image of the resected intracranial dermoid cysts (IDCs) soaked in saline **(B)**. IDCs contain hair (black arrow) and keratin (arrowhead) **(A)**. The hair is separated from the IDC contents and is floated in saline **(B)**. The image in the top right rectangular dashed frame is a magnified image of hair suspended in saline **(B)**.

and capsule were easily separable. As the capsule of the mass was completely continuous with the falx cerebri, the capsule of the mass was excised along with the falx cerebri. The rostral part of the mass was attached to the lamina cribrosa; therefore, it was cauterized and sectioned using bipolar on the rostral side as far as possible. After the irrigation of the extraction cavity with sterile saline, the dural replacement was performed using the fascia. The left temporal fascia was collected and divided into two pieces: one was attached to the cranial cavity side of the cribriform plate, whereas the other was used for dural reconstruction. Fibrin glue (Beriplast P Combi-Set Tissue adhesion, CSL Behring, Tokyo, Japan) was used to adhere the dura mater to the fascia graft. The skull was reconstructed using excised bone flaps, titanium screws (U-CMF AXS Self-drilling Screw 3 mm; Stryker, Tokyo, Japan), and titanium plates (Dynamic Mesh 0.6 mm, Stryker). The bone flap was returned to the originated location and stabilized with tiny, thin titanium plates and screws on four sides instead of

sutures. MRI examination was performed immediately after surgery, and complete removal of the mass was confirmed (Figures 1F,G).

The histopathological findings were the cyst wall was formed by the stratified squamous epithelium, and the cyst contained exfoliated keratin that was arranged concentrically, hair, and inflammatory cells such as lymphocytes and macrophages but did not include the skin adnexa (Figure 3). An epidermoid cyst was suspected by the postoperative histopathological examination; however, the finding that the mass contained hair was not consistent with the feature of epidermoid cysts. The bacterial culture test results were negative. The mass was made a diagnosis of IDCs based on the comprehensive evaluation of the clinical and histopathological findings.

2.3 Postoperative clinical course

No postoperative neurological deficits were observed, and the patient was discharged 1 day after surgery and administered an antibacterial drug (cephalexin, 17 mg/kg, PO, q12h, Cefaclor tablet 75; Kyoritsu Seiyaku Corp.) and antiseizure medications, including zonisamide (6 mg/kg, PO, q12h) and levetiracetam (15 mg/kg, PO, q12h).

Two weeks after surgery, the surgical wound became infected because the cat rubbed the surgical wound against the wall. Potassium clavulanate amoxicillin hydrate (15 mg/kg, PO, q12h; Augmentin Combination Tablets; GSK, Tokyo, Japan) was administered, which resulted in complete scar closure.

The epileptic seizures disappeared after surgery, and antiseizure medications were tapered off and completely discontinued on day 964. On day 1,337 (approximately 14 months after surgery), the cat presented to the local clinic for a health checkup. The patient was making good improvement without seizures and other neurological deficits, even after the discontinuation of the antiseizure medications. Radiographs showed no abnormalities in the titanium plates and screws as well (Figure 4).

3 Discussion

To our knowledge, this was the first report of a dermoid cyst in the frontal lobe of a cat that was successfully treated. Three case reports of IDCs have been presented in veterinary medicine (2, 3, 5). As clinical symptoms, a dog with IDCs in the fourth ventricle had head tilt, hind limb ataxia, aggressive behavioral change, and a 7-month history of progressive abnormal behavior such as avoiding exercise and bumping into obstacles (3). Another dog with IDCs in the left cerebellar peduncle presented head tilt and a 3-year history of episodes of hind limb weakness and ataxia (2). One case report described a cat with a nasal dermoid cyst that extended to the calvarium and contacted the left olfactory bulb and frontal lobe (5). In this case, the clinical signs were symptoms of the forebrain, including focal epilepsy. Reported clinical signs of infratentorial IDCs include hind limb ataxia and vestibular dysfunction (2, 3). Fourth ventricle IDCs can also present with signs involving the forebrain, including increased aggression and visual impairment, although these clinical signs suggest secondary obstructive hydrocephalus (3). The forebrain signs for fourth ventricle IDCs in the previous report did not

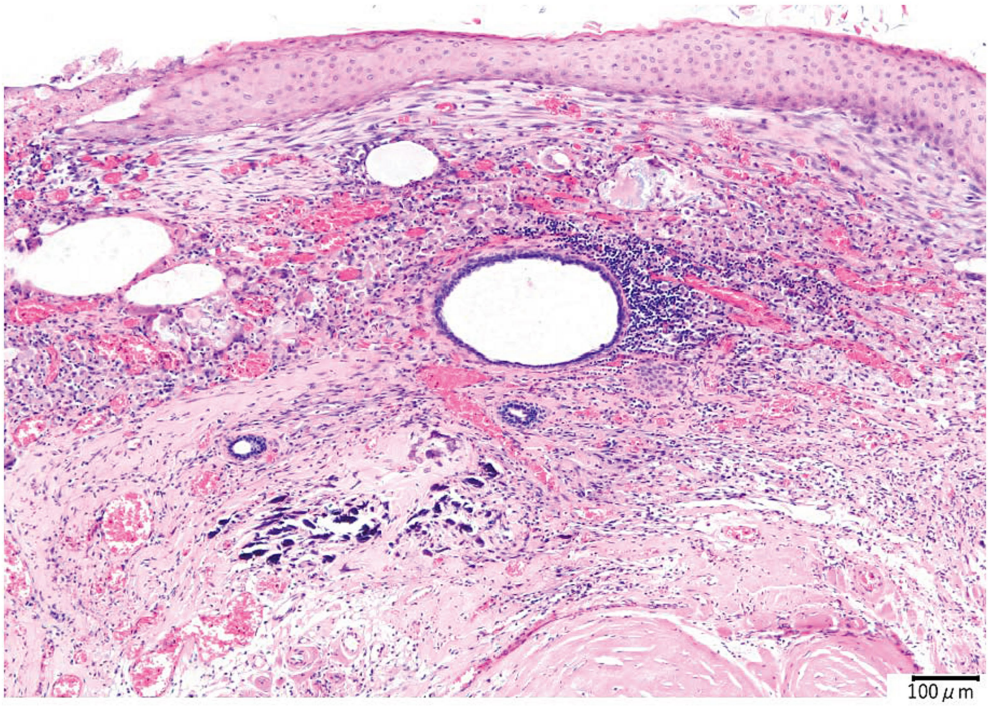

FIGURE 3
Histopathological image of the intracranial dermoid cyst. The cyst is lined by the stratified squamous epithelium. Concentric layers of exfoliated keratin are observed in the cyst. Lymphocyte and macrophage infiltrates around the cholesterol clefts and hair are also observed. Hemorrhage, hemosiderin-laden macrophages, and multinucleated giant cells are also observed in the inflammatory focus. At the edge of the inflammatory foci, the proliferation of collagen fibers, angiogenesis, and calcification is revealed.

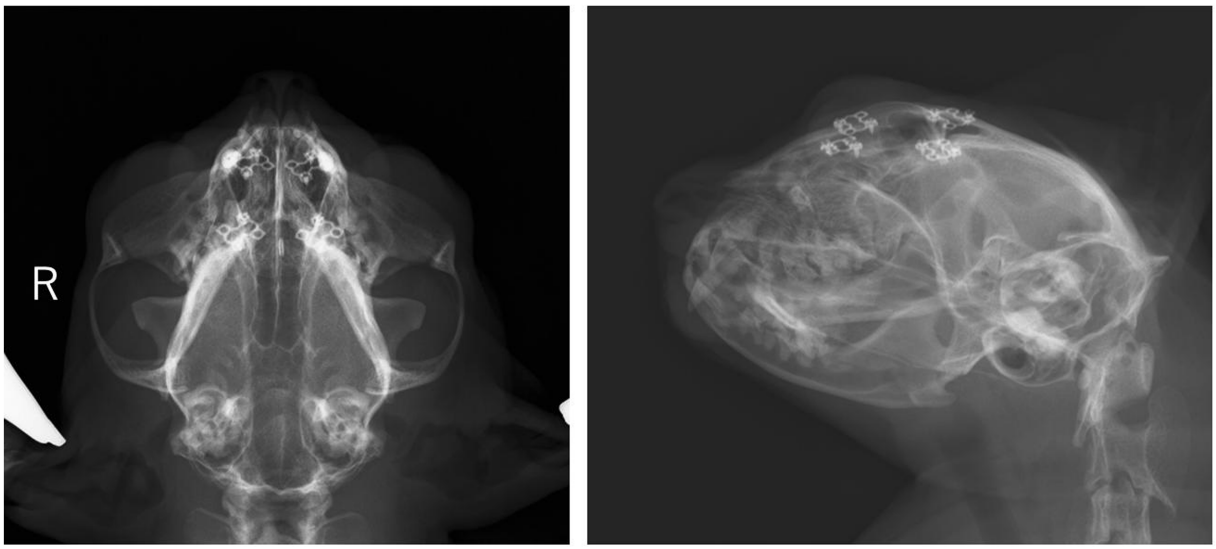

FIGURE 4
Radiographs of head on the day 1,377. Four titanium plates and eight screws are used to stabilize the outer plate of the frontal sinus. Alternation in opacity around the implants or implant migration is not observed.

include epileptic seizures but included mentation abnormalities, whereas those of IDCs affected the frontal lobe in both of the cases previously reported and our case included only epileptic seizures. The differences in forebrain signs between the secondary obstructive hydrocephalus and the fourth ventricle and frontal lobe IDCs may include increased aggression and behavior changes.

The intracranial cyst in this case contained not only the squamous epithelium but also a small amount of hair. Dermoid cysts have been reported as intracranial mass lesions which commonly contain hair in human medicine, whereas epidermoid cysts, which have similar pathological features to dermoid cysts, contain only the squamous epithelium. The difference between dermoid cysts and epidermoid cysts is the presence of not only hair but also the skin adnexa, including dermal elements such as hair follicles, sebaceous glands, and sweat glands in humans (6). IDCs sporadically have been reported in veterinary medicine, including one feline case (3, 5). The MRI findings of the previous feline case with dermoid cyst were heterogeneous hyperintensity on both T1WI and T2WI, rim contrast enhancement, located midline, and nasal cavity lesion extending through the cribriform plate and into the calvarium (5). These features are remarkably similar to our case; however, a nasal lesion connected to the intracranial mass was not detected by imaging modalities. The MRI findings and the presence of hair suggested it was a dermoid cyst, although the histopathological examination could not have detected the skin adnexa. Our case was eventually diagnosed with IDCs based on an MRI and the presence of hair in the cyst. The definitive reason for the cyst containing hair was unclear. One of the possibilities is that the intracranial mass connects to the invisible small nasal dermoid cyst resulting in the intracranial mass being made as the cyst that contains hair. Monitoring with imaging modalities such as CT and MRI may be necessary hereafter whether any nasal cavity lesions are detected.

Common intracranial mass lesions are accompanied by a mass effect (7). Usually, mass lesions are also unevenly distributed on either the left or right side (7). However, in this case, no obvious displacement of the falx cerebri was observed, whereas displacement of the brain parenchyma due to the mass effect occurred. This is consistent with the pathophysiology of this condition, in which the epithelial tissue remains in the neural tube when the brain is formed during neural tube closure in the embryonic period (8). In human medicine, IDCs are already known to be predominantly observed near the midline structure (8). The midline location of the mass and the absence of displacement of the falx cerebri might be one of the characteristic findings in frontal lobe IDCs in veterinary medicine as well. A mass effect in the brain parenchyma may be caused by IDC growth after birth, although there was no evidence of significant IDC size increase between the CT images on day 1 and MR images on day 889 in this case. The size increase might have been associated with the onset of the epileptic seizure, if it had occurred before the onset of the epileptic seizure. The alternation in the IDC size could not have been perceived because clinical symptoms other than epileptic seizures were not observed.

There was no significant change in the size of the IDCs between days 1 and 889. It seemed to be slightly larger in vertical and horizontal length; however, the difference is a minor change that is potentially affected by the difference in imaging modality. This finding suggested that the cause of increased seizure frequency was not IDC enlargement. The other possible cause could be withdrawal seizures. Administration of the initial antiseizure medication, phenobarbital, was discontinued rather than tapered off. This sudden change in antiseizure medication could result in withdrawal seizures. To prevent withdrawal seizures, the dose of the antiseizure medications is recommended to be decreased by 20% or less on a monthly basis (9). However, phenobarbital discontinuation was inevitable because of severe hepatic dysfunction in this case. Readministration of phenobarbital in this case also was not recommended, even though cluster seizures were observed with other antiseizure medications, such as zonisamide, levetiracetam, and gabapentin. The seizures eventually completely ceased after surgery; this result suggests that the cause of the seizures is potentially associated with the presence of IDCs. The remaining possibilities of the cause could be the inflammation and hemorrhage inside or outside the IDCs. Histopathological examinations revealed chronic inflammation and hemorrhage in the IDCs. T2WI and T2*WI

on MRI showed a hypointense region in the white matter adjacent to the IDCs, which could be a chronic hemorrhage outside of the IDCs (10). T2* WI hypointense lesions include hemorrhage, mineralization, gas, fibrous tissue, and iron deposits (10). Mineralization, gas, and fibrous tissue were hypointense in both T2WI and T1WI, which is not consistent with our case. Iron deposits including hemorrhage (deposits of hemosiderin) could be the lesion. However, intraoperative findings did not reveal hemorrhage in the white matter around the IDCs. It is possible that the lesion was small, chronic, and a mild change, and it was located inside the normal brain parenchyma, so the surgeon could not recognize the alternation. The IDCs may have elicited inflammation of brain tissue surrounding the IDCs; however, evidence could not be identified from preoperative MRI and intraoperative findings. CSF analysis could have been useful for detecting intracranial inflammation, although CSF was not collected in this case.

Surgical intervention for IDCs has been reported in a cat (5) and a dog (3). The neurological signs, including focal seizure activity, of the cat who had surgical resection of IDCs continuous with a nasal lesion at the frontal lobe temporarily improved, but rhinosinusitis with suspected local meningitis of the left olfactory bulb was observed as the complication more than 8 months after surgery, and the seizure activity relapsed (5). In our case, the mass lesion was found only in the cranial cavity, so the destruction of the cribriform plate was not observed even after surgery. It was suggested that the infection of the sinus and meninges was not observed because of the intact cribriform plate in our case. If the IDCs are connected to the nasal lesion, the complications of the infection of the sinus and meninges should be monitored, although the risk of such complications may be lower for the IDCs localized only to the frontal lobe. However, the skin adnexa, including hair follicle, was not observed in the pathological tissue of our case. This finding indicates the possibility that there is a residual lesion around the resection cavity. The prognosis of this case was excellent at 14 months after surgery, although longer follow-up and MRI scans are required because the possibility of recurrence and infection is still present. The dog with IDCs in the fourth ventricle and secondary hydrocephalus was treated with a ventriculoperitoneal shunt. The neurological deficit improved temporarily; however, the dog was euthanized because of the deterioration of neurological symptoms 4 weeks after surgery. To our best knowledge, there is no report of the resection of the medullary IDCs, although there are two reports of direct surgical intervention for the fourth ventricle of the intracranial epidermoid cyst, which has a similar pathology to IDCs. The medulla oblongata was injured by surgical invasion in the dog who underwent surgical resection of an intracranial epidermoid cyst in the fourth ventricle (11). In another previous report, a suboccipital approach for intracranial mass lesions and abnormal results on preoperative neurologic examination, including head tilt and abnormal mentation, were identified as risk factors associated with death (12). In addition, the odds ratio of death with a suboccipital approach increased in dogs with brain stem tumors in this report (12). Our feline case, which had frontal lobe IDCs, did not develop any fatal complications except for surgical wound infection as a minor complication. This result suggests that the risk factors associated with the surgical removal of IDCs are similar to other intracranial masses, including epidermoid cysts and brain tumors. The decision to perform surgical intervention ought to be made with caution if IDCs or epidermoid cysts are located in the infratentorial region, whereas the surgical resection of frontal lobe IDCs could be a relatively safe and reasonable treatment option.

Therefore, surgical resection of frontal lobe IDCs should be considered as a therapeutic option, especially if clinical symptoms are difficult to control with medicinal therapy. In our case, the macroscopic lesion of IDCs was completely removed, and the clinical signs have not recurred over 1 year after the surgery.

Data availability statement

The original contributions presented in the study are included in the article/Supplementary material, further inquiries can be directed to the corresponding author.

Ethics statement

The requirement of ethical approval was waived by the ethics committee for animal clinical research of Gifu University for the studies involving animals because the treatment methods including the surgical technique for the case are common in the veterinary medicine field. The studies were conducted in accordance with the local legislation and institutional requirements. Written informed consent was obtained from the owners for the participation of their animals in this study.

Author contributions

YNa: Writing – original draft, Writing – review & editing, Data curation. YNo: Data curation, Writing – review & editing. HH: Data curation, Writing – review & editing. TM: Data curation, Writing – review & editing. JC: Data curation, Writing – review & editing. KU: Data curation, Writing – review & editing. YK: Supervision, Writing – review & editing.

Funding

The author(s) declare that no financial support was received for the research, authorship, and/or publication of this article.

Acknowledgments

The authors are grateful to Hiroaki Kamishina and Masashi Terao for their useful advice and incisive comments.

Conflict of interest

The authors declare that the research was conducted in the absence of any commercial or financial relationships that could be construed as potential conflicts of interest.

Generative AI statement

The authors declare that no Generative AI was used in the creation of this manuscript.

Publisher's note

Supplementary material

The Supplementary material for this article can be found online at: https://www.frontiersin.org/articles/10.3389/fvets.2025.1512097/full#supplementary-material

SUPPLEMENTARY VIDEO S1
The video shows intracranial surgical manipulation for extraction of dermoid cyst. The capsule of dermoid cyst was observed after incision of the dura matter and the cerebral cortex of the left frontal lobe. The capsule was made incision, white keratinized material and hair were recognized in the capsule. Internal decompression of the cyst was completed, and the capsule was easily detached and removed from the normal brain parenchyma.

References

1. Platt S, Hicks J, Matiasek L. Intracranial intra-arachnoid diverticula and cyst-like abnormalities of the brain. *Vet Clin North Am Small Anim Pract*. (2016) 46:253–63. doi: 10.1016/j.cvsm.2015.10.004

2. Howard-Martin M, Bowles MH. Intracranial dermoid cyst in a dog. *J Am Vet Med Assoc*. (1988) 192:215–6.

3. Targett MP, McInnes E, Dennis R. Magnetic resonance imaging of a medullary dermoid cyst with secondary hydrocephalus in a dog. *Vet Radiol Ultrasound*. (1999) 40:23–6. doi: 10.1111/j.1740-8261.1999.tb01834.x

4. Paradis J, Koltai PJ. Pediatric teratoma and dermoid cysts. *Otolaryngol Clin N Am*. (2015) 48:121–36. doi: 10.1016/j.otc.2014.09.009

5. Brady S, Bell E, Courtman N, Chevoir ML. Nasal dermoid cyst with intracranial extension in a cat. *JFMS Open Rep*. (2019) 5:2055116919827404. doi: 10.1177/2055116919827404

6. Liu JK, Gottfried ON, Salzman KL, Schmidt RH, Couldwell WT. Ruptured intracranial dermoid cysts: clinical, radiographic, and surgical features. *Neurosurgery*. (2008) 62:377–84. doi: 10.1227/01.neu.0000316004.88517.29

7. Kraft SL, Gavin PR. Intracranial neoplasia. *Clin Tech Small Anim Pract*. (1999) 14:112–23. doi: 10.1016/S1096-2867(99)80009-7

8. Spallone A, Ivanova K, Ferrante L, Belogurov AA Jr. Atypical dermoid cyst of the corpus callosum: a case report. *Eur Rev Med Pharmacol Sci*. (2024) 28:1970–5. doi: 10.26355/eurrev_202403_35611

9. Bhatti SF, De Risio L, Munana K, Penderis J, Stein VM, Tipold A, et al. International veterinary epilepsy task force consensus proposal: medical treatment of canine epilepsy in Europe. *BMC Vet Res*. (2015) 11:176. doi: 10.1186/s12917-015-0464-z

10. Arnold SA, Platt SR, Gendron KP, West FD. Imaging ischemic and hemorrhagic disease of the brain in dogs. *Front Vet Sci*. (2020) 7:279. doi: 10.3389/fvets.2020.00279

11. De Decker S, Davies E, Benigni L, Wilson H, Pelligand L, Rayner EL, et al. Surgical treatment of an intracranial epidermoid cyst in a dog. *Vet Surg*. (2012) 41:766–71. doi: 10.1111/j.1532-950X.2012.01010.x

12. Kohler RJ, Arnold SA, Eck DJ, Thomson CB, Hunt MA, Pluhar GE. Incidence of and risk factors for major complications or death in dogs undergoing cytoreductive surgery for treatment of suspected primary intracranial masses. *J Am Vet Med Assoc*. (2018) 253:1594–603. doi: 10.2460/javma.253.12.1594

frontiers | Frontiers in Veterinary Science

TYPE Case Report
PUBLISHED 19 March 2025
DOI 10.3389/fvets.2025.1563798

OPEN ACCESS

EDITED BY
Koen Santifort,
IVC Evidensia Small Animal Referral Hospital Arnhem, Neurology, Netherlands

REVIEWED BY
Martí Pumarola,
Autonomous University of Barcelona, Spain
Susan A. Arnold,
University of Minnesota Twin Cities, United States

*CORRESPONDENCE
Hee-Myung Park
✉ parkhee@konkuk.ac.kr

RECEIVED 20 January 2025
ACCEPTED 27 February 2025
PUBLISHED 19 March 2025

CITATION
Kang M-H, Jeong W-P, Nam C-S, Yoon J-W, Choi D-M, Lee G-S, Kim Y-J, Dan T-J and Park H-M (2025) Case Report: Ischemic brain infarction and cognitive dysfunction syndrome in an aged dog.
Front. Vet. Sci. 12:1563798.
doi: 10.3389/fvets.2025.1563798

Case Report: Ischemic brain infarction and cognitive dysfunction syndrome in an aged dog

Min-Hee Kang[1], Woo-Phil Jeong[2], Chan-Sik Nam[3], Jun-Won Yoon[3], Dong-Min Choi[3], Gwang-Seob Lee[3], Yeon-Jin Kim[3], Tae-Jung Dan[3] and Hee-Myung Park[3]*

[1]Department of Bio-Animal Health, Jangan University, Gyeonggi-do, Republic of Korea, [2]Gangnam Annie Animal Hospital, Gyeonggi-do, Republic of Korea, [3]Department of Veterinary Internal Medicine, College of Veterinary Medicine, Konkuk University, Seoul, Republic of Korea

This case report describes a rare occurrence of canine cognitive dysfunction syndrome (CDS) accompanied by ischemic brain infarction, providing insights into the relationship between neurodegeneration and cerebrovascular pathology in aged dogs. A 19-year-old neutered male miniature poodle exhibited progressive behavioral changes over three years, including nocturnal restlessness, inappropriate urination, and aimless wandering. Neurological examination revealed mild disorientation, decreased proprioception, and weakened postural reactions in the hind limbs, with a cognitive dysfunction rating (CDDR) score of 64 indicating severe cognitive impairment. Magnetic resonance imaging (MRI) revealed hallmark indicators of brain atrophy, such as widened cerebral sulci and ventricular enlargement, along with multifocal ischemic lesions in the right parietal and occipital area. Histopathological findings confirmed widespread neurodegeneration, including severe vacuolation and neuronal necrosis in the precentralis interna and anterior subcallosal regions. Congo Red-positive staining identified amyloid-like deposits in cerebral vessels, and Lewy bodies in the brainstem suggested concurrent vascular and amyloid pathology. This case provides evidence of a potential connection between cerebrovascular pathology and CDS, indicating that ischemic and hemorrhagic lesions may aggravate neurodegeneration and contribute to cognitive and neurological deficits. The coexistence of brain infarction and amyloid deposits in this dog resembles pathological processes observed in human conditions such as Alzheimer's disease and vascular dementia, highlighting the multifactorial nature of CDS. Advanced neuroimaging and histopathological analysis were critical in diagnosing and understanding this complex interaction. Further research is needed to clarify the mechanisms linking neurodegeneration and cerebrovascular disease in aging dogs.

KEYWORDS

dog, geriatric, cognitive dysfunction syndrome, brain infarction, cerebrovascular pathology

Introduction

Canine cognitive dysfunction syndrome (CDS) is a neurodegenerative disorder observed in aging dogs, often compared to Alzheimer's disease (AD) in humans due to similar clinical signs and neuropathological features (1, 2). CDS primarily affects dogs older than eight years, leading to progressive cognitive decline, behavioral abnormalities, and memory impairment,

closely resembling human dementia (3). These similarities have positioned CDS as a valuable translational model for studying neurodegenerative diseases, contributing to a better understanding of disease mechanisms across species (2, 4). However, CDS remains underdiagnosed, resulting in many untreated cases and significantly affecting the quality of life for both affected dogs and their caregivers.

Despite these similarities, significant pathological distinctions exist. While both CDS and AD involve neuronal degeneration and vascular changes, hallmark features of AD, such as neurofibrillary tangles and Hirano bodies, are absent in dogs with CDS (1, 2, 5, 6). Nevertheless, studies indicate that tau hyperphosphorylation and amyloid-β accumulation in the aging canine brain may contribute to cognitive impairment, reinforcing the need for further research into shared and distinct pathological mechanisms (6, 7).

Cerebrovascular pathology, including brain infarction, is uncommon in dogs and has rarely been documented alongside CDS (8). However, recent studies suggest that neuroinflammation, oxidative stress, and vascular dysfunction may contribute to both neurodegenerative and cerebrovascular diseases, underscoring the importance of evaluating their potential interplay (7, 9, 10). Investigating these connections may improve our understanding of their impact on aging animals and guide clinical management.

This case report presents a rare occurrence of CDS accompanied by brain infarction in a geriatric dog. Imaging and histopathological analyses were conducted to explore the potential relationship between cognitive dysfunction and cerebrovascular pathology, offering insights into similar conditions in aging animals.

Case description

Case presentation and diagnostic investigations

A 19-year-old neutered male miniature poodle, weighing 5.2 kg, was presented with progressive behavioral changes, including nocturnal restlessness, excessive barking, aimless wandering at night, and compulsive pacing. Additional clinical signs included inappropriate urination and intermittent oral bleeding. The owner reported a gradual progression of these clinical signs over three years, leading to concerns about the dog's overall health and the possibility of CDS.

On physical examination, the dog appeared lethargic and less responsive to environmental stimuli. Pale mucous membranes were noted, and a firm mass was palpable in the right maxillary region. Mild respiratory distress was observed, with a respiratory rate of 40 breaths per minutes. Additionally, a suspected mammary gland tumor was identified in the left fourth mammary gland. Other physical examination findings were unremarkable. The neurological status of the dog was evaluated. The dog showed mild disorientation and slightly decreased proprioception in all limbs. The cranial nerve examination was unremarkable, and postural reactions were mildly weakened in the hind limbs. The spinal reflexes were within normal limits.

An assessment for CDS was conducted based on the dog's medical history, clinical signs, physical examination and neurological findings. The dog scored 64 points on the canine cognitive dysfunction rating scale (CCDR) (11), indicating severe cognitive impairment.

Hematological evaluation revealed severe anemia [hematocrit (HCT) 13.5%, reference interval (RI) 37.3–61.7%; red blood cell count (RBC) 1.79 × 10^12/L, RI 5.65–8.87 × 10^12/L; hemoglobin (HGB) 4.1 g/dL, RI 13.1–20.5 g/dL] and marked leukocytosis [white blood cell count (WBC) 30.75 × 10^9/L; RI 5.05–16.76 × 10^9/L]. Reticulocytosis was significant (333.6 × 10^3/μL; RI 10–110 × 10^3/μL). Biochemical analyses showed mild elevations in symmetric dimethylarginine (SDMA) levels (15 μg/dL; RI ≤ 14 μg/dL), alanine aminotransferase (57 U/L; RI 0–50 U/L) and alkaline phosphatase (1,036 U/L; RI 23–212 U/L), alongside markedly elevated C-reactive protein (50.8 mg/dL; RI 0–10 mg/dL). Electrolyte levels were within normal limits.

Diagnostic imaging was performed to assess the maxillary and mammary masses and evaluate systemic involvement. Computed tomography (CT) of the head revealed a 2.4 × 0.8 × 4.5 cm mass in the right maxilla, with extensive alveolar bone resorption affecting the maxillary premolars and molars, while the medial cortical bone remained intact. CT of the left mammary region identified a calcified mass (1.9 × 2.9 × 3.0 cm) suggestive of a subcutaneous mammary gland tumor. No evidence of metastasis was observed.

Neurological signs prompted magnetic resonance imaging (MRI), which revealed widened cerebral sulci and ventricular enlargement, consistent with brain atrophy. The ventricle-to-brain height ratio (VBHR) was 24–25%, exceeding the normal threshold (< 15%), indicating ventricular dilation. The interthalamic adhesion (ITA) measured 5.41 mm, which is lower than the normal range (6.09–7.49 mm) but thicker than the range typically observed in dementia (3.03–4.61 mm) (25). (Figure 1). T2-weighted and diffusion-weighted imaging (DWI) demonstrated multifocal hyperintensities in the right parietal and occipital area, located in the dorsolateral regions of the cerebrum, consistent with ischemic lesions. Apparent diffusion coefficient (ADC) mapping confirmed restricted diffusion, indicative of brain infarction (Figure 2). These findings were suggestive of cerebrovascular abnormalities contributing to cognitive dysfunction and neurological deficits.

Given the severity of the clinical conditions, including advanced CDS and cerebrovascular disease, humane euthanasia was elected. A limited post-mortem examination focusing on the central nervous system was performed to confirm the imaging findings and obtain a comprehensive understanding of the underlying pathology.

Histopathological analysis revealed extensive neurodegeneration, with widespread vacuolation and neuronal necrosis prominently affecting the precentralis interna and anterior subcallosal regions (Figures 3A,B). In addition, the right parietal regions, corresponding to the hyperintensity areas observed on MRI, revealed intravascular microthrombi distributed in the perivascular spaces and microhemorrhagic infarcts in the surrounding cortical areas, consistent with ischemic brain injury (Figures 3C,D). Numerous microglia and astrocytes were closely associated with neurons, indicating reactive gliosis (Figure 3E). Pyknotic neurons and structures resembling neurofibrillary tangles were observed in the hippocampus (Figure 3F) and brainstem (Figures 3G–I). Lewy body-like structures were identified in the brainstem (Figure 3J), suggesting the possibility of abnormal protein aggregation. Additionally, vascular abnormalities included hemorrhagic infarcts in the inferior frontal gyrus (Figure 3K) and subcallosal regions (Figure 3L). Congo Red-positive staining confirmed amyloid-like vascular deposits in the frontal (Figures 4A,B), prefrontal (Figures 4C,D), and cerebellar

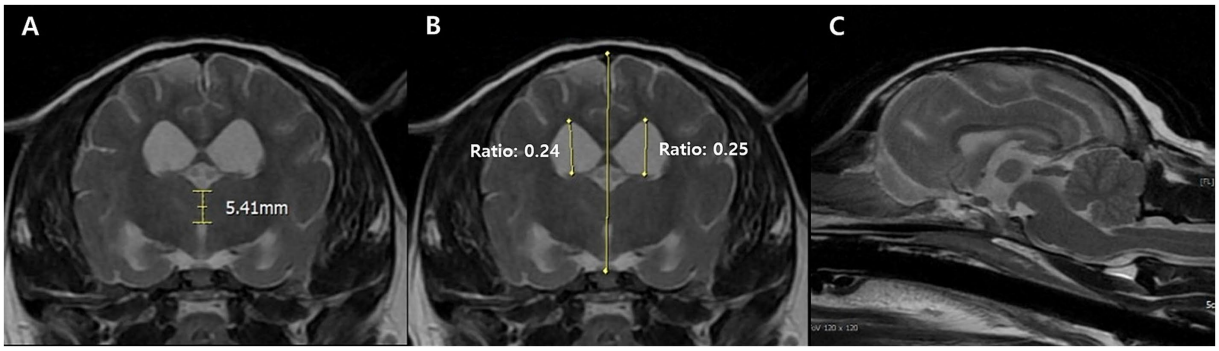

FIGURE 1
Transverse T2-weighted magnetic resonance images of CDS dog at the level of the interthalamic adhesion. The measurement of the interthalamic adhesion was 5.41 mm and heights of the right and left ventricles (ventricle to brain height ratio) is measured at 24–25% in the transverse view **(A,B)**. Generalized broadened and deeply observed cerebral sulci, along with ventricular enlargement was also prominent at the sagittal view **(C)**.

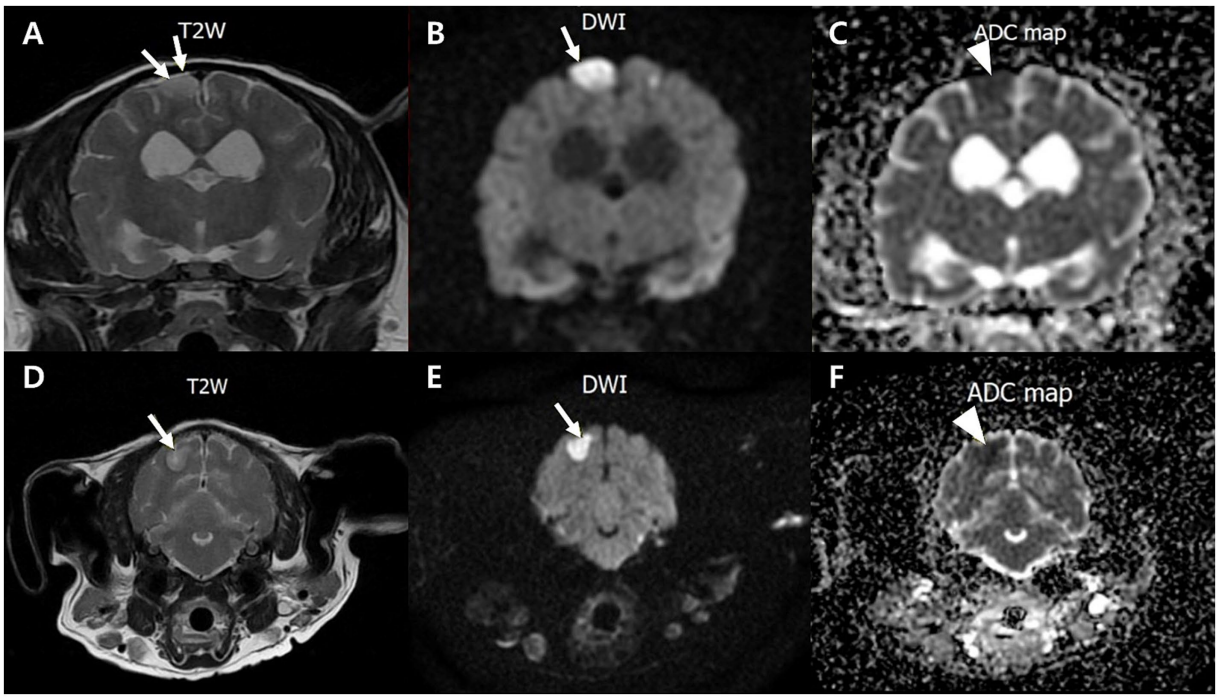

FIGURE 2
Transverse T2-weighted, diffusion-weighted imaging (DWI) and an apparent diffusion coefficient (ADC) magnetic resonance images of a dog with multifocal brain infarcts. Lesion locates in the right parietal **(A–C)** and occipital area **(D–F)** appears hyperintense with peripheral hypointensity (arrows) on T2 **(A,D)** and DWI **(B,E)**, and hypointensity (arrowhead) on an ADC map **(C,F)**.

cortices (Figures 4E,F). Reactive gliosis, with increased astrocytes and microglia, was observed in the frontal gyrus near the caudate nucleus (Figures 4G,H). These findings supported a diagnosis of advanced neurodegenerative disease with concurrent cerebrovascular pathology.

Discussion

This case report describes a rare presentation of CDS accompanied by ischemic brain infarction, providing insights into the relationship between neurodegeneration and cerebrovascular pathology in aged dog. While neurodegenerative diseases such as CDS and AD share several clinical and pathological features, this report emphasizes the distinctive aspects of CDS and its association with brain infarcts.

Over three years, the dog exhibited hallmark signs of cognitive dysfunction, including nocturnal restlessness, inappropriate urination, and behavioral changes. These clinical features aligned with a severe CDS diagnosis, confirmed by a CDDR score of 64. Canine CDS and human AD share common features, such as cognitive decline and behavioral changes (12, 13). However, significant pathological differences exist between the two. Prominent neurofibrillary tangles,

10.3389/fvets.2025.1563798

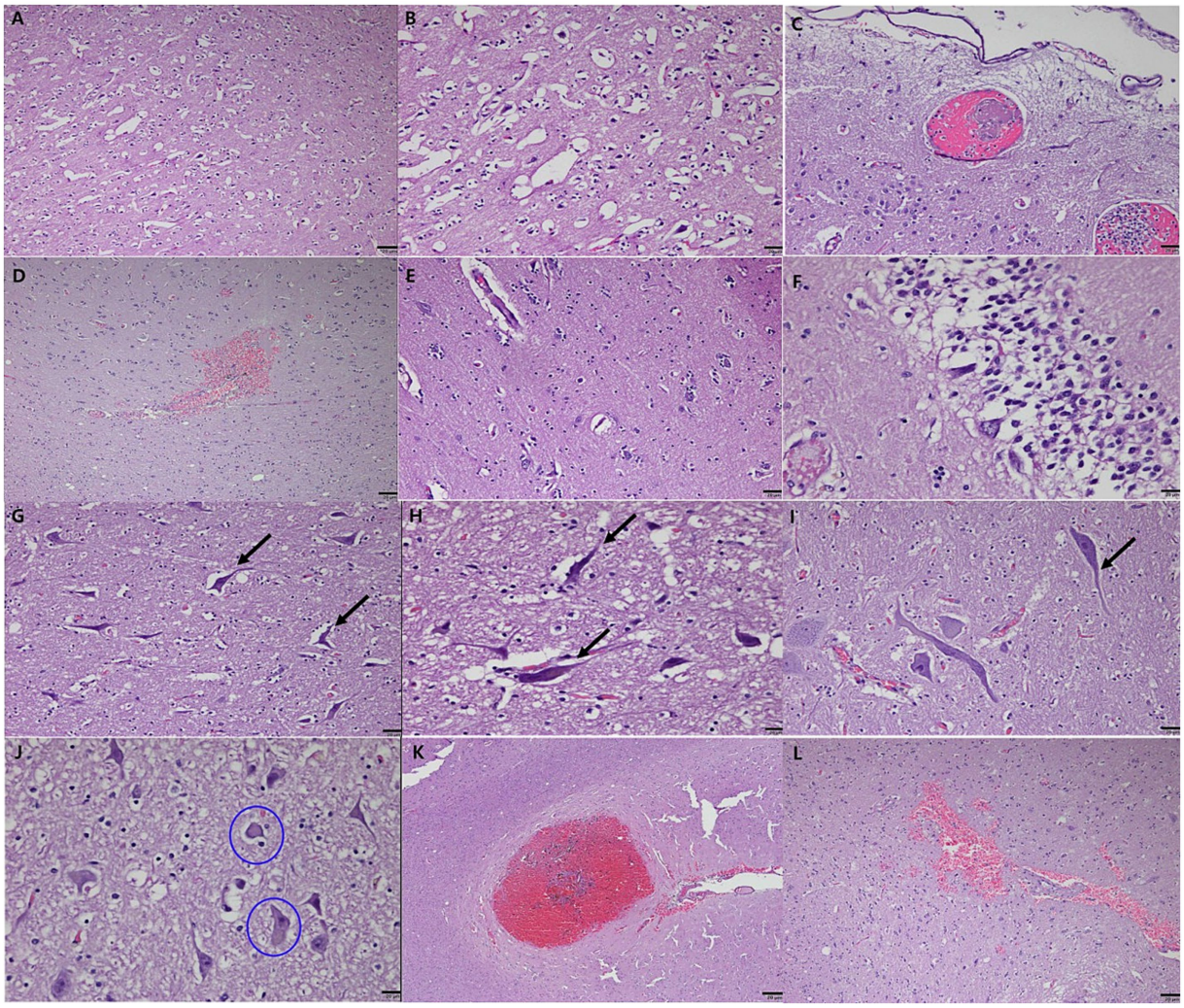

FIGURE 3
Histopathological features of neurodegeneration and cerebrovascular pathology in a geriatric dog with CDS. Severe vacuolation and neuronal necrosis in the precentralis interna and anterior subcallosal region of the cerebral cortex **(A,B)**. Low magnification view showing extensive vacuolation **(A)**. High magnification view highlighting pronounced neuronal necrosis **(B)**. Intravascular microthrombi distributed in the perivascular spaces **(C)** and microhemorrhagic infarcts **(D)** in the right parietal lobe, consistent with ischemic brain injury. Reactive gliosis with numerous microglia and astrocytes closely associated with neurons, observed in the surrounding cortical areas **(E)**. Pyknotic neurons and neurofibrillary tangle-like structures in the CA (Cornu Ammonis) 1 and CA2 regions of the hippocampus, resembling features of human neurodegenerative diseases **(F)**. Axonal degeneration and neurofibrillary tangle-like structures in the brainstem **(G)** and posterior cerebellum **(H,I)**. Lewy bodies (circled) identified within neuronal cells in the brainstem, indicative of abnormal protein aggregation **(J)**. Hemorrhagic infarcts in the inferior frontal gyrus **(K)** and subcallosal region of the anterior cerebral hemisphere **(L)**. Note: Scale bar = 20 μm for all panels.

a hallmark of AD, are notably less prominent in CDS, suggesting differences in the underlying mechanisms (12, 14–16).

The findings of this case provide evidence for the role of cerebrovascular pathology in the progression of CDS. MRI findings demonstrated hallmark indicators of brain atrophy, including widened cerebral sulci and ventricular enlargement, consistent with neural tissue loss due to aging and chronic disease (14, 17–19). In addition, diffusion-weighted imaging identified multifocal ischemic lesions in the right parietal and occipital areas, emphasizing the role of cerebrovascular events in the disease progression (8, 20, 21). These ischemic changes, combined with hemorrhagic infarcts, created a complex pathology exacerbating the dog's cognitive and neurological deficits (6). Similar observations have been reported in dogs with brain infarcts, indicating significance of vascular alterations in neurodegenerative conditions (4, 21). In particular, the presence of ischemic and hemorrhagic lesions has been shown to exacerbate neurodegenerative processes, further impairing cognitive function in both dogs and humans (10, 17). This case emphasizes the role of cerebrovascular pathology in the progression of CDS and reflects similarities with pathological processes seen in human conditions, such as vascular dementia and AD.

Histopathological findings confirmed widespread neurodegeneration, including severe vacuolation and neuronal necrosis in the precentralis interna and anterior subcallosal regions. Pyknotic neurons and structures resembling neurofibrillary tangle-like inclusions were identified in the hippocampus and brainstem. Although these inclusions were morphologically consistent with neurofibrillary tangles, definitive confirmation was not possible due to the absence of silver impregnation or immunohistochemical (IHC)

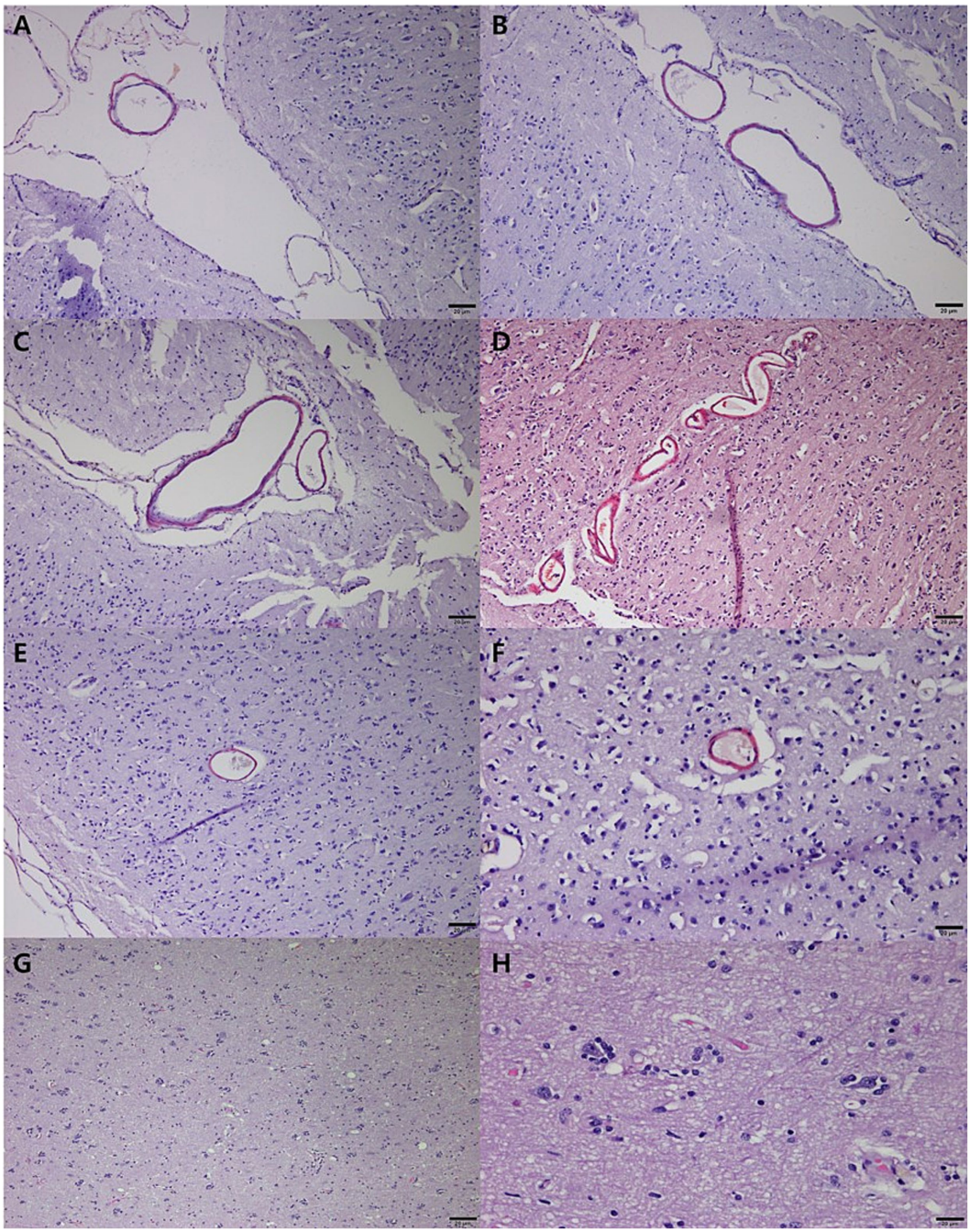

FIGURE 4
Congo red staining of neurodegeneration and cerebrovascular pathology in a geriatric dog with CDS. Congo Red-positive vascular deposits in veins within less folded sulci on the cortical surface of the frontal area **(A,B)**. Amyloid-like deposits in vessels of the prefrontal cortex, particularly in sulci on the cortical surface **(C,D)**. Congo Red positivity in vessels of the marginal gyrus in the anterior **(E)** and posterior **(F)** cerebral cortices, with thickened vessels surrounding neurons. Reactive gliosis in the frontal gyrus near the caudate nucleus, characterized by increased astrocytes and microglia **(G,H)**. Scale bar = 20 μm for all panels.

staining for phosphorylated Tau. Additionally, eosinophilic cytoplasmic inclusions resembling Lewy bodies were observed, suggesting the possibility of abnormal protein aggregation. However, the possibility of lipofuscin accumulation could not be excluded, highlighting the need for confirmatory IHC staining, such as ubiquitin or alpha-synuclein, in future studies (9, 14). Amyloid-like deposits in the vessels of the frontal, prefrontal, and cerebellar cortices, verified through Congo Red-positive staining, suggest a role for amyloid angiopathy in the development of CDS (1, 4). The identification of amyloid deposits and reactive gliosis supports the hypothesis that vascular amyloid pathology plays a contributory role in cognitive dysfunction (10, 22). Such findings are consistent with studies demonstrating that dogs with CDS frequently exhibit amyloid deposition in the brain parenchyma and vasculature, suggesting shared mechanisms with AD (1, 4, 22).

The vascular abnormalities observed in this case are particularly significant and provide valuable insights into the underlying mechanisms contributing to the dog's clinical deterioration. Hemorrhagic infarcts were identified in the inferior frontal gyrus and subcallosal regions in this dog, strongly indicating a substantial cerebrovascular component to the observed neurological and cognitive decline. These vascular lesions likely disrupted critical neural networks responsible for cognition and behavior by reducing regional cerebral perfusion and contributing to microvascular pathology, such as blood–brain barrier dysfunction and neuronal damage (9, 22). Neuropathological evidence suggests that cerebrovascular alterations, including silent brain infarcts, exacerbate pre-existing neurodegenerative processes, thereby accelerating cognitive and behavioral deterioration (9, 23). Silent brain infarcts, which are linked to increased dementia risk and accelerated cognitive decline in humans, may exert similar effects in dogs, underscoring the importance of vascular factors in CDS progression (23).

This case is distinguished by its integration of imaging and histopathological findings to demonstrate the relationship between cerebrovascular disease and neurodegeneration. While prior studies have documented microhemorrhages and brain atrophy in aging dogs (15, 18), few have explored the association between ischemic infarcts and CDS. In human dementia research, the link between silent brain infarction and AD is well established, but similar studies in dogs are rare (9, 10, 23, 24). This report contributes to the field by proposing a potential connection between brain infarction and CDS, using advanced diagnostic methods to support the findings.

However, several limitations should be noted. The absence of confirmatory IHC staining limited the definitive characterization of key neuropathological findings. Structures resembling neurofibrillary tangles were identified in the hippocampus and brainstem but could not be conclusively distinguished without silver impregnation or IHC for phosphorylated Tau. Similarly, eosinophilic cytoplasmic inclusions resembling Lewy bodies were observed in the brainstem, suggesting abnormal protein aggregation. However, the possibility of lipofuscin accumulation could not be excluded. Reactive gliosis was identified based on astrocytic and microglial proliferation observed on H&E staining. However, the absence of IHC markers such as GFAP for astrocytes and Olig2 for oligodendroglial lineage cells limited the precise characterization of gliosis and neuroinflammation. Additionally, the absence of serial imaging and longitudinal clinical monitoring limits the ability to establish a definitive temporal relationship between the vascular events and the progression of cognitive dysfunction.

These limitations emphasize the need for advanced diagnostic techniques, including IHC and special staining, to improve diagnostic accuracy and provide a more comprehensive understanding of neurodegenerative and cerebrovascular changes in CDS. Future studies employing these advanced methods are essential to clarify the relationship between neurodegenerative and vascular changes and to develop more effective diagnostic and therapeutic strategies for aging dogs with CDS.

In conclusion, this case illustrates the multifactorial nature of CDS, with both neurodegenerative and vascular factors contributing to the dog's clinical presentation. The coexistence of cognitive decline, ischemic infarcts, and amyloid deposits suggests that CDS may represent a complex interaction between neurodegeneration and cerebrovascular pathology.

Data availability statement

The original contributions presented in the study are included in the article/supplementary material, further inquiries can be directed to the corresponding author/s.

Ethics statement

Ethical review and approval was not required for the study involving animals in accordance with the local legislations and institutional requirements. Written informed consent was obtained from the owners for their animals' participation. Informed consent was obtained from the owner for publication of this case report and any accompanying images.

Author contributions

M-HK: Conceptualization, Investigation, Writing – original draft, Writing – review & editing. W-PJ: Data curation, Methodology, Writing – review & editing. C-SN: Data curation, Writing – review & editing. J-WY: Data curation, Writing – review & editing. D-MC: Data curation, Writing – review & editing. G-SL: Data curation, Writing – review & editing. Y-JK: Data curation, Writing – review & editing. T-JD: Data curation, Writing – review & editing. H-MP: Conceptualization, Methodology, Supervision, Writing – original draft, Writing – review & editing.

Funding

The author(s) declare that no financial support was received for the research and/or publication of this article.

Conflict of interest

The authors declare that the research was conducted in the absence of any commercial or financial relationships that could be construed as a potential conflict of interest.

Generative AI statement

The authors declare that no Generative AI was used in the creation of this manuscript.

Publisher's note

References

1. Landsberg GM, Nichol J, Araujo JA. Cognitive dysfunction syndrome: a disease of canine and feline brain aging. *Vet Clin North Am Small Anim Pract*. (2012) 42:749–68. doi: 10.1016/j.cvsm.2012.04.003

2. McKean NE, Handley RR, Snell RG. A review of the current mammalian models of Alzheimer's disease and challenges that need to be overcome. *Int J Mol Sci*. (2021) 22:13168. doi: 10.3390/ijms222313168

3. Neilson JC, Hart BL, Cliff KD, Ruehl WW. Prevalence of behavioralchanges associated with age-related cognitive impairment in dogs. *J Am Vet Med Assoc*. (2001) 218:1787–91. doi: 10.2460/javma.2001.218.1787

4. Vikartovska Z, Farbakova J, Smolek T, Hanes J, Zilka N, Hornakova L, et al. Novel diagnostic tools for identifying cognitive impairment in dogs: behavior, biomarkers, and pathology. *Front Vet Sci*. (2021) 7:551895. doi: 10.3389/fvets.2020.551895

5. Davis PR, Head E. Prevention approaches in a preclinical canine model of Alzheimer's disease: benefits and challenges. *Front Pharmacol*. (2014) 5:47. doi: 10.3389/fphar.2014.00047

6. Smolek T, Madari A, Farbakova J, Kandrac O, Jadhav S, Cente M, et al. Tau hyperphosphorylation in synaptosomes and neuroinflammation are associated with canine cognitive impairment. *J Comp Neurol*. (2016) 524:874–95. doi: 10.1002/cne.23877

7. Hines AD, McGrath S, Latham AS, Kusick B, Mulligan L, Richards ML, et al. Activated gliosis, accumulation of amyloid β, and hyperphosphorylation of tau in aging canines with and without cognitive decline. *Front Aging Neurosci*. (2023) 15:1128521. doi: 10.3389/fnagi.2023.1128521

8. Wessmann A, Chandler K, Garosi L. Ischaemic and hemorrhagic stroke in the dog. *Vet J*. (2009) 180:290–303. doi: 10.1016/j.tvjl.2007.12.023

9. Jellinger KA. Alzheimer disease and cerebrovascular pathology: an update. *J Neural Transm*. (2002) 109:813–36. doi: 10.1007/s007020200068

10. Elman-Shina K, Efrati S. Ischemia as a common trigger for Alzheimer's disease. *Front Aging Neurosci*. (2022) 14:1012779. doi: 10.3389/fnagi.2022.1012779

11. Salvin HE, McGreevy PD, Sachdev PS, Valenzuela MJ. The caninecognitive dysfunction rating scale (CCDR): a data-driven and ecologically relevant assessment tool. *Vet J*. (2011) 188:331–6. doi: 10.1016/j.tvjl.2010.05.014

12. Prpar Mihevc S, Majdic G. Canine cognitive dysfunction and Alzheimer's disease – two facets of the same disease? *Front Neurosci*. (2019) 13:604. doi: 10.3389/fnins.2019.00604

13. Dewey CW, Davies ES, Xie H, Wakshlag JJ. Canine cognitive dysfunction: pathophysiology, diagnosis, and treatment. *Vet Clin North Am Small Anim Pract*. (2019) 49:477–99. doi: 10.1016/j.cvsm.2019.01.013

14. Ozawa M, Chambers JK, Uchida K, Nakayama H. The relation between canine cognitive dysfunction and age-related brain lesions. *J Vet Med Sci*. (2016) 78:997–1006. doi: 10.1292/jvms.15-0624

15. Schutt T, Helboe L, Pedersen LO, Waldemar G, Berendt M, Pedersen JT. Dogs with cognitive dysfunction as a spontaneous model for early Alzheimer's disease: a translational study of neuropathological and inflammatory markers. *J Alzheimers Dis*. (2016) 52:433–49. doi: 10.3233/JAD-151085

16. Borras D, Ferrer I, Pumarola M. Age-related changes in the brain of the dog. *Vet Pathol*. (1999) 36:202–11. doi: 10.1354/vp.36-3-202

17. Burbaitė E, Gradeckienė A, Juodžentė D, Jankauskas M. MRI abnormalities in a severe cognitive impairment mimicking a forebrain lesion in a geriatric dog. *Braz J Vet Med*. (2022) 44:e001022. doi: 10.29374/2527-2179.bjvm00102

18. Dewey CW, Rishniw M, Johnson PJ, Davies ES, Sackman JJ, O'Donnell M, et al. Interthalamic adhesion size in aging dogs with presumptive spontaneous brain microhemorrhages: a comparative retrospective MRI study of dogs with and without evidence of canine cognitive dysfunction. *PeerJ*. (2020) 8:e9012. doi: 10.7717/peerj.9012

19. Hasegawa D, Yayoshi N, Fujita Y, Fujita M, Orima H. Measurement of interthalamic adhesion thickness as a criteria for brain atrophy in dogs with and without cognitive dysfunction (dementia). *Vet Radiol Ultrasound*. (2005) 46:452–7. doi: 10.1111/j.1740-8261.2005.00083.x

20. Pugliese M, Carrasco JL, Gomez-Anson B, Andrade C, Zamora A, Rodríguez MJ, et al. Magnetic resonance imaging of cerebral involutional changes in dogs as markers of aging: an innovative tool adapted from a human visual rating scale. *Vet J*. (2010) 186:166–71. doi: 10.1016/j.tvjl.2009.08.009

21. Rodrigues LL, Mesquita LP, Costa RC, Gomes RG, Biihrer DA, Maiorka PC. Multiple infarcts and hemorrhages in the central nervous system of a dog with cerebral amyloid angiopathy: a case report. *BMC Vet Res*. (2018) 14:370. doi: 10.1186/s12917-018-1700-0

22. Cory J. Identification and management of cognitive decline in companionanimals and the comparisons with Alzheimer disease: a review. *J Vet Behav*. (2013) 8:291–301. doi: 10.1016/j.jveb.2012.08.001

23. Vermeer SE, Prins ND, Heijer T, Hofman A, Koudstaal PJ, Breteler MMB. Silent brain infarcts and the risk of dementia and cognitive decline. *N Engl J Med*. (2003) 348:1215–22. doi: 10.1056/NEJMoa022066

24. Bir SC, Khan MW, Javalkar V, Gonzalez Toledo E, Kelley RE. Emerging concepts in vascular dementia: a review. *J Stroke Cerebrovasc Dis*. (2021) 30:105864. doi: 10.1016/j.jstrokecerebrovasdis.2021.105864

frontiers | Frontiers in Veterinary Science

TYPE Case Report
PUBLISHED 27 March 2025
DOI 10.3389/fvets.2025.1553617

OPEN ACCESS

EDITED BY
Susana Monforte,
University of Cambridge, United Kingdom

REVIEWED BY
Elena Scarpanre,
Dick White Referrals, United Kingdom
Oliver Marsh,
Linnaeus Veterinary Limited, United Kingdom
Beatrice Carletti,
Dick White Referrals, United Kingdom

*CORRESPONDENCE
Karen R. Muñana
krmunana@ncsu.edu

RECEIVED 31 December 2024
ACCEPTED 11 March 2025
PUBLISHED 27 March 2025

CITATION
Jackson E, Fefer G, Muñana KR and Hansen BD (2025) Case Report: Presumed cerebral salt wasting syndrome in a 10-week-old German Shorthaired Pointer. *Front. Vet. Sci.* 12:1553617. doi: 10.3389/fvets.2025.1553617

Case Report: Presumed cerebral salt wasting syndrome in a 10-week-old German Shorthaired Pointer

Elizabeth Jackson, Gilad Fefer, Karen R. Muñana* and Bernie D. Hansen

Department of Small Animal Clinical Sciences, College of Veterinary Medicine, North Carolina State University, Raleigh, NC, United States

This case report describes a rare presentation of cerebral salt-wasting syndrome (CSW) in a 10-week-old German Shorthaired Pointer following a traumatic brain injury. The patient presented stuporous and tetraplegic with advanced imaging revealing a depressed skull fracture and active brain hemorrhage. Following surgical intervention, the dog exhibited persistent hypovolemia and hyponatremia prompting treatment with intravenous hypertonic saline and enteral sodium supplementation. Positive response to sodium supplementation, coupled with elevated fractional excretion of uric acid (FEUA) despite clinical improvement, supported the diagnosis of CSW. This report contributes novel insights into CSW in veterinary medicine, emphasizing the distinctive features of its presentation, diagnostic considerations, and treatment responses. The clinical utility of FEUA as a diagnostic tool is highlighted for the first time in a canine patient, providing a valuable tool for differentiation. This information enhances veterinary practitioners' awareness, facilitating more accurate diagnoses and tailored treatment strategies for similar cases in the future.

KEYWORDS

canine, skull fracture, hyponatremia, traumatic brain injury, hypovolemia

Introduction

Cerebral salt-wasting syndrome (CSW), also known as renal salt-wasting syndrome, is a rare condition characterized by hyponatremia and extracellular volume depletion (1, 2). Although the most common cause of CSW in humans is primary central nervous system (CNS) disorders such as trauma (3–5), this syndrome has also been reported in people without any history of CNS disease (6–8). While the exact pathogenesis of CSW remains unclear, it is believed to result from complex interactions between the CNS and the kidneys, causing excess sodium excretion. The biggest challenge in diagnosing CSW is excluding syndrome of inappropriate antidiuresis (SIAD), however numerous criteria have been proposed to differentiate between the two diseases (9–11). Although well described in the human literature, CSW in canines has only been described in one other recent case report, despite historical reference as a differential for hyponatremia (12, 13). This case report describes the diagnosis, treatment, and outcome of presumed CSW in a 10-week-old German Shorthaired Pointer puppy.

Case description

A 10-week-old intact female German Shorthaired Pointer was presented for further evaluation of a traumatic brain injury (TBI). The dog was bitten on the head by another dog in the home, immediately becoming laterally recumbent and unresponsive. Prior to this, the dog was reportedly healthy, and up to date on her preliminary vaccines and anthelmintic series. No known familial diseases were reported prior to acquisition.

Upon evaluation by the primary veterinarian immediately following the incident, the dog was stuporous, hypothermic, and tachypneic. Serum chemistry panel, CBC, serum total T4, and full body radiographs did not reveal any significant abnormalities. Serum sodium was within the reference level at 148 mmol/L. The dog received a 20 mL/kg lactated ringer's solution (LRS) intravenous (IV) fluid bolus and supplemental oxygen. The dog was referred to a local specialty hospital for further care. Physical examination at that facility identified moderate asymmetry of the left caudal temporalis region attributed to a suspected depressed skull fracture. Neurologic examination revealed the dog to be stuporous and tetraplegic, with intact spinal reflexes in all four limbs, an absent menace response bilaterally with bilaterally miotic pupils that were minimally responsive to light, and bilateral ventral strabismus. Computed tomography (CT) of the head and cervical spine was performed, revealing a depressed left-sided temporal fracture (Figure 1). The dog received a single dose of mannitol (1 g/kg), hypertonic saline (2 mL/kg), and levetiracetam (30 mg/kg IV) followed by 60 mL/kg/day LRS IV, and a fentanyl continuous rate infusion, as well as continued oxygen supplementation. After a night at this facility with minimal neurologic improvement, the patient was then transferred to our facility approximately 48 h after the initial trauma.

On presentation, the dog was stuporous and laterally recumbent, with appropriate perfusion parameters and mild tachypnea, weighing 7.85 kg. Neurologic examination revealed tetraplegia with absent menace response bilaterally, absent facial sensation, and miotic pupils bilaterally. The Modified Glasgow Coma Score (MGCS) upon presentation was 9. The findings suggested injury to the brainstem, as the stuporous mentation and tetraplegia would not be explained by the depressed skull fracture alone. A peripherally inserted central catheter was placed; a venous blood gas analysis obtained was normal, with serum sodium of 141 mmol/L ([137-151 mmol/L]) and adequate ventilatory parameters. No osmotic agents were administered due to concern for intracranial hemorrhage. The dog was anesthetized for magnetic resonance imaging (MRI), which confirmed a left-sided calvarial depression fracture with compression and edema of the left temporal and parietal brain cortices. Additionally, there was a cavitary lesion in the pons and midbrain most consistent with active brain hemorrhage, which was the likely cause for the stupor (Figure 2). The dog was hospitalized and treated with conservative IV fluids due to concern for cerebral edema (0.45% NaCl +0.05 mEq KCl at 50 mL/kg/day), ampicillin-sulbactam (30 mg/kg IV every 8 h), dexamethasone sodium phosphate (0.15 mg/kg IV every 24 h), pantoprazole (1.02 mg/kg IV every 12 h), ondansetron (0.52 mg/kg IV every 8 h), and acetaminophen (10 mg/kg IV every 8 h). In the first 24 h of hospitalization, the dog lost approximately 0.5 kg of body weight and appeared hypovolemic based on physical examination (persistent tachycardia, tachypnea, hypotension, and marked polyuria) and thoracic point-of-care ultrasound (POCUS) evaluation. The half strength NaCl IV fluids were replaced with LRS with physiologic KCl supplementation, and the rate of administration was incrementally increased up to 100 mL/kg/day over the next 12 h. Multiple fluid boluses were administered due to persistence of apparent hypovolemia, with no change appreciated in the dog's volume status.

Improvement in the dog's mentation was noted after 36 h of hospitalization, MGCS 14, and a left sided rostrotentorial craniectomy with removal of a 1.5 cm long fracture fragment to decompress the brain was performed. Pre-operative bloodwork was largely unremarkable, with a serum sodium concentration of 146 mmol/L. The patient recovered uneventfully from general anesthesia and was soon able to eat a small amount of puppy food slurry. Two days post-operatively, the dog was eating more consistently but not meeting caloric demands. A nasogastric (NG) tube was placed, and a calorically dense liquid nutrition (NutriDapt™, Canine Biologics, Denver CO) was administered to supplement voluntary food intake. The ampicillin-sulbactam was discontinued and oral amoxicillin-clavulanate (Clavamox™, Zoetis, Parsippany NJ) was initiated. Additionally, dexamethasone was discontinued in favor of oral prednisone (0.6 mg/kg/day). The IV fluids were discontinued due to financial constraints, and enteral water was administered at a rate of 20 mL/h. Later that day, the dog had a generalized tonic–clonic seizure and therapy with levetiracetam was initiated (loading dose of 60 mg/kg IV, continuation at 30 mg/kg IV every 8 h).

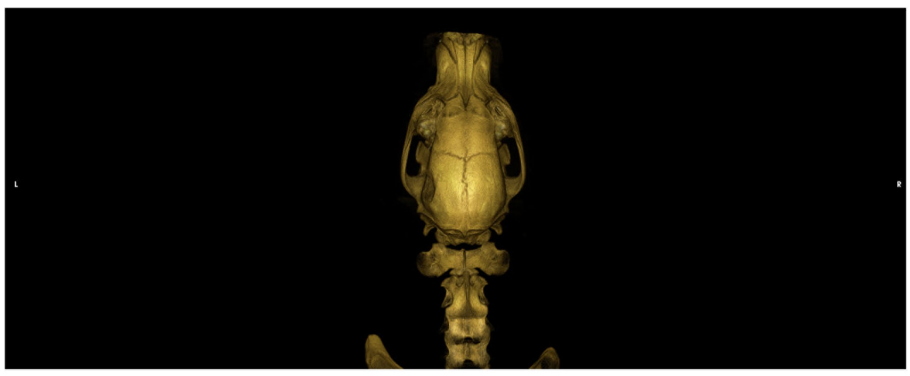

FIGURE 1
Dorsal view of a CT 3D reconstruction showing a depressed skull fracture of the left temporo-parietal bone.

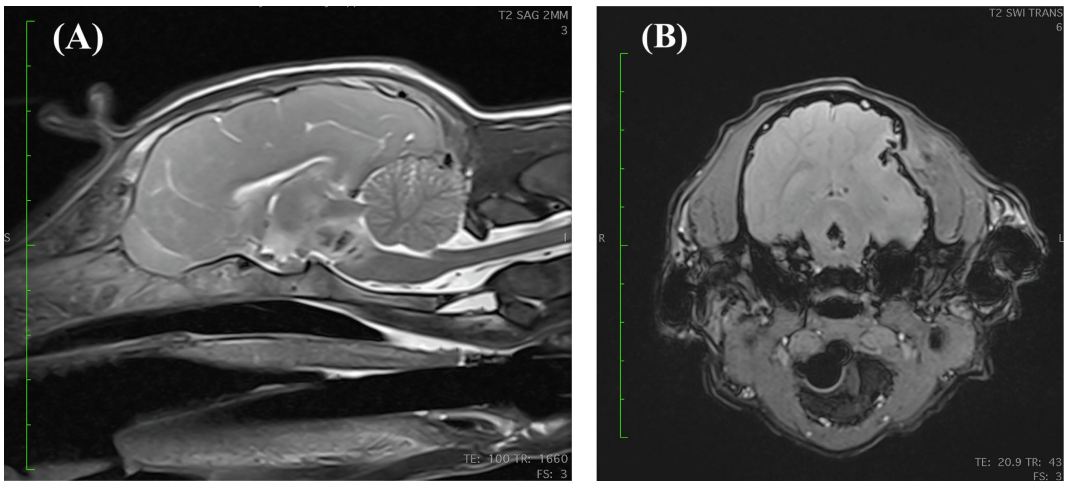

FIGURE 2
(A) Mid-sagittal view of a T2 weighted MRI revealing a heterogenous, potentially cavitated lesion within the pons and caudal midbrain that is centrally T2 hypointense and peripherally hyperintense. **(B)** Transverse susceptibility weighted imaging (SWI) view at the level of the caudal midbrain revealing a bone fragment being displaced medially into the cranial vault creating a concave skull defect. Additionally, there are multiple ill-defined intra-axial abnormalities with moderate susceptibility artifact at the left temporal and parietal lobes, likely representing smaller bone fragments. There is an irregularly shaped, possibly cavitated lesion within the caudal midbrain with a strong central and peripheral blooming susceptibility artifact which is highly suggestive of hemorrhage. The falx cerebri is slightly deviated toward the right side and the left lateral ventricle is compressed.

On day 6 of hospitalization (day 3 post-operatively), due to continued weight loss (6.80 kg) (Figure 3), and persistent physical examination findings consistent with hypovolemia despite enteral fluids and feeding, a serum biochemistry was obtained. Abnormalities included marked hyponatremia (122 mmol/L) with hypochloremia (87 mmol/L, corrected to 104 mmol/L) and normokalemia (4.5 mmol/L). Calculated serum osmolality was 258 mOsm/kg. To address the sodium deficit, with a rate not exceeding 0.5 meq/L/h, LRS supplementation (130 mEq Na/L) via the NG tube was reinstated at 60 mL/h. Serum sodium concentration was measured a few hours later, and marked hyponatremia was confirmed (119 mmol/L). The dog was administered 2 mL/kg of 7% hypertonic saline IV, with no improvement in hydration status appreciated afterward.

Despite gradual improvements in mentation and appetite, the dog remained polyuric with tacky mucous membranes and tachycardia. On day 7 of hospitalization, hyponatremia persisted (120 mmol/L) and two additional 2 mL/kg boluses of 7% hypertonic saline were administered. Approximately 8 h later, the dog remained hyponatremic (120 mmol/L) and a 7% hypertonic saline CRI IV (initially 2 mL/h for 5 h then tapered to 1.3 mL/h for 9 h) was initiated to correct the persistent volume depletion and marked sodium derangement. Administration of LRS at a rate of 60 mL/h via the NG tube was continued.

On day 8 of hospitalization, following 14 h of the hypertonic saline CRI, hyponatremia and hypochloremia had improved to 138 mmol/L and 103 mmol/L, respectively. Potassium remained within the reference interval at 4.5 mmol/L. Additional testing revealed a markedly elevated urine sodium concentration (310.5 mmol/L). Urine creatinine, urine uric acid, and serum uric acid were measured to calculate the fractional excretion of sodium (FENa 1.6% [0–0.5%]) and of uric acid (FEUA 19.71% [0–11%]). Despite the hyponatremia, the urine was moderately concentrated at 914 mOsm/kgH2O. The urine uric acid to urine creatinine ratio (uUA:uCr) was 0.20, which may further support the clinically presumed volume depletion (14). Pro-brain natriuretic peptide (proBNP) concentration measured 614 pmol/L ([0-900 pmol/L]).

The next morning (day 9), serum sodium concentration was higher than desired (157 mmol/L), and the hypertonic saline was discontinued. A CRI of enteral water (40 mL/h) via the NG tube was added to the LRS enteral supplementation. The following day, serum sodium concentration decreased to 141 mmol/L.

To facilitate discharge from the hospital, a saltwater-food slurry supplement was devised; ½ teaspoon of salt was mixed with 1,500 mL of water to create a 35 mmol/L sodium solution. The dog was given ½ cup of this saline solution with food every 4 h, therefore supplementing approximately 4 mEq Na per feeding. The following morning (day 11), serum sodium was normalized at 146 mmol/L and enteral LRS supplementation via the NG tube was discontinued. Over the next 2 days of hospitalization, supplementation with the salt solution was reduced to ⅓ cup with every meal. Water was offered free-choice, and the saline mixture was administered with food, with no NG tube supplementation. Serum sodium concentration remained at 146 mmol/L on days 12 and 13, and the dog's clinical hydration status markedly improved. Figure 4 depicts the complete serum sodium concentrations for the dog while hospitalized. At the time of discharge, the dog was ambulatory with significant proprioceptive ataxia in all four limbs, and occasional support necessary to prevent falls. She was blind with an absent menace bilaterally and no other cranial nerve deficits. She was discharged with prednisone (0.15 mg/kg/day) for 3 days, levetiracetam, and amoxicillin-clavulanate. The owners were instructed to continue the saline solution at ⅓ cup (~2.5 mEq Na) added to the dog's food every 4–6 h.

The dog was evaluated by the primary veterinarian weekly for electrolyte evaluation. Figure 5 shows the serum sodium concentrations at follow up as well as the tapering instructions for the saline solution. The saline supplementation was discontinued 6 weeks after discharge. The dog was re-evaluated by our neurology

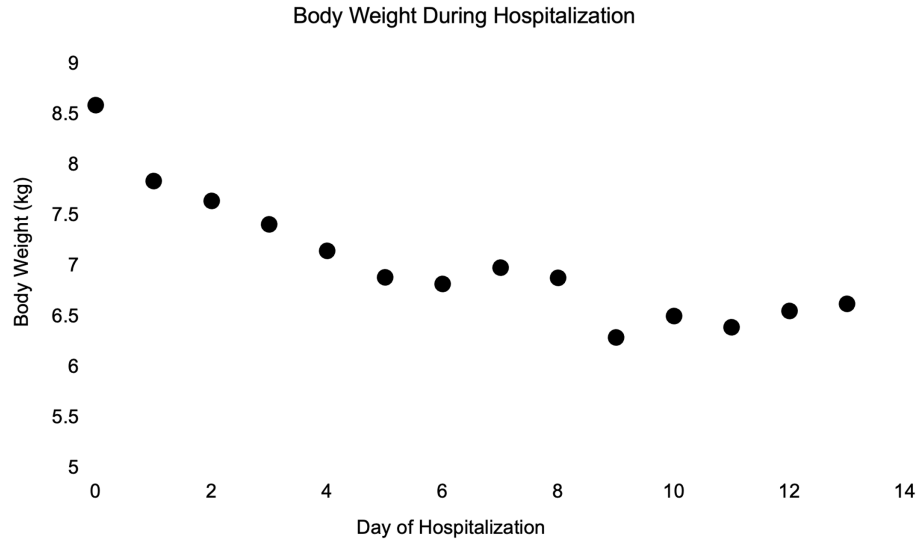

FIGURE 3
Simple dot plot depicting patient body weight in kilograms over time while hospitalized.

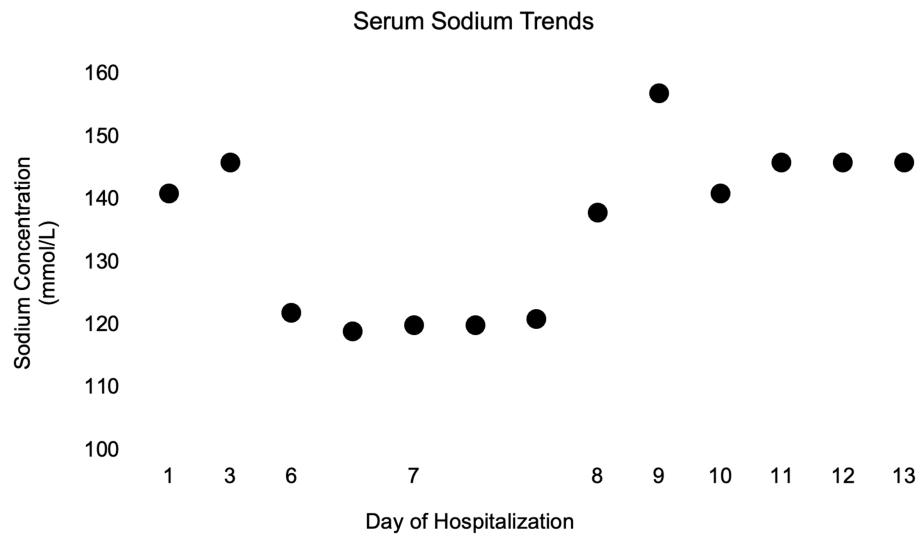

FIGURE 4
Simple dot plot depicting patient serum sodium concentrations in millimoles per liter over time while hospitalized.

service 1 week later (8 weeks post-operatively), at which time the dog was strongly ambulatory with no obvious proprioceptive ataxia. A mildly hypermetric gait was noted, most prominent in the forelimbs. Menace response remained absent bilaterally, but the dog appeared to visually track moving objects and was able to avoid stationary obstacles. Additional testing revealed a FENa of 0.7%, FEUA of 13.4%, BNP of 697 pmol/L, and urine osmolality of 999 mOsm/kgH2O.

Approximately 5 months post hospitalization, and 4 months after discontinuing all sodium supplementation, re-evaluation of the dog's laboratory values revealed persistent derangements. Although serum sodium concentration (146 mmol/L) and FENa (0.6%) were normal, her FEUA was 45.25%, her BNP was 758 pmol/L, and urine osmolality was 1,676 mOsm/kgH2O.

Discussion

Two syndromes have been associated with hyponatremia in humans with brain injuries, namely the syndrome of inappropriate antidiuresis and cerebral salt wasting (12, 15). The SIAD is characterized by excessive release of antidiuretic hormone (ADH) with water retention that promotes mild hypervolemia, triggering compensatory sodium excretion in order to maintain euvolemia (16). CSW is characterized by increased renal sodium excretion causing hypovolemia, with compensatory water retention to maintain extracellular fluid volume. The treatment of each is disparate, therefore distinguishing between the two is essential; however, the clinical findings are very similar and reaching a correct diagnosis is challenging. Both syndromes are most often associated with CNS

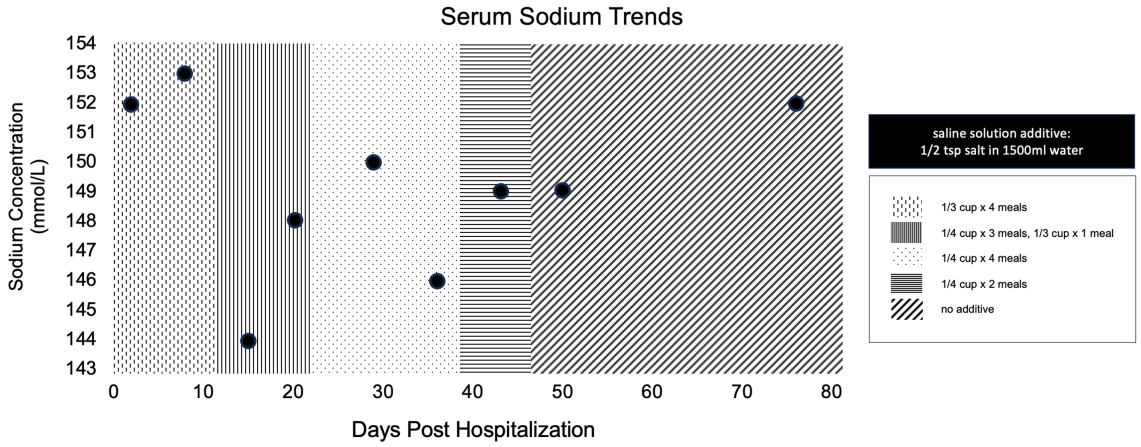

FIGURE 5
Simple dot plot depicting patient serum sodium concentrations in millimoles per liter over time at all recheck examinations post discharge. Overlaying patterns indicate amount of saline solution supplementation at the time of evaluation.

disease, resulting in hypotonic hyponatremia with an increased urine sodium concentration, and normal underlying renal, adrenal, and thyroid function (15).

CSW is clinically very similar to SIAD, but in this disorder ADH is appropriately secreted in response to volume depletion (17). Since its initial description, CSW has been most commonly reported as a sequential complication of CNS diseases in humans (3–5). More recently, some reports have described the same clinical syndrome without any concurrent CNS disease, which has prompted some to recommend renaming of the disease to renal salt wasting syndrome (8, 9). Precise definition of the syndrome is fairly controversial as the pathogenesis is poorly defined (18). Nevertheless, there is agreement that with this syndrome the kidneys are unable to conserve sodium, resulting in variable reductions in extracellular fluid volume (1).

As reviewed by Yee et al. (1) the two most widely cited theories regarding the pathogenesis of CSW implicate decreased renal sympathetic nervous system activity and increased natriuretic peptide secretion. Sympathetic innervation of the kidney plays a role in sodium absorption at the level of the proximal tubule as well as the release of renin by the juxtaglomerular cells (1, 2). Theoretically, decreased sympathetic tone would prevent the kidneys from mounting an adequate renin-aldosterone in response to decreased circulating volume. Yet, some humans with CSW are reported to have normal to elevated plasma concentrations of renin and/or aldosterone (1, 19). Renin and aldosterone concentrations were not measured in this dog.

Another theory implies excessive natriuretic peptide secretion induces natriuresis through an increased GFR and sodium excretion (1). Natriuretic peptides also have a potent effect on renal tubular function via antagonization of ADH activity and inhibition of sodium resorption (20). Identification of high serum concentrations of natriuretic peptides, particularly BNP, has been suggested as a method to differentiate CSW from SIAD. In CSW, the serum levels of BNP are elevated, whereas in SIAD, they remain within the normal range (21). However, this theory has not been easily corroborated in human CSW patients as some do not have elevated BNP concentrations, diminishing the accuracy of BNP as a diagnostic test (1). In the case described, concentrations of serum NT-proBNP, an inactive fragment of BNP with a long half-life, levels were measured at the initial onset of hyponatremia (9 days from the initial injury) as well as 1 month and 4 months after discharge; they remained at the upper end of the reference level at each measurement. One group has proposed that a proBNP cutoff of 125 pg./mL (or 458 pmol/L) can be used to distinguish between human SIAD and CSW (22). However, this was a pilot study and a definite distinguishing value of proBNP has yet to be confirmed (22, 23). The use of pro-BNP in dogs outside of cardiac diseases is extremely limited; therefore, although the high normal pro-BNP values in this case may support a diagnosis of CSW, this should be interpreted with caution.

In short, it is impossible to distinguish SIAD and CSW based on preliminary serum and urine laboratory analysis alone (24). Traditional guidelines emphasize the evaluation of patient volume status in classifying hypotonic hyponatremia and narrowing the list of differential diagnoses (18). However, the diagnostic assessment of volume status in human patients with hyponatremia has been reported to be low in sensitivity and specificity, with a wide range of subjectivity between evaluating clinicians, especially in neurologically inappropriate patients (17). Recent research has shown that diagnostic performance has improved when using an algorithm that includes both urine osmolality and urine sodium concentrations rather than overt volume status (25). The persistent elevation of FENa in this dog suggests that the hyponatremia was due to urinary excretion of sodium, but does not differentiate between etiologies of renal sodium loss.

Urine osmolality can be utilized to measure the tonicity of urine, revealing both solute output and concurrent ADH influence. A low urine osmolality indicates suppression of ADH activity, which is a normal response to low serum osmolality and allows excretion of excess free water (12, 18). Contrarily, an elevated urine osmolality indicates a response to ADH that impairs urine dilution. The dominant mechanism underlying hypotonic hyponatremia is impaired urinary dilution due to increased ADH activity, which can be physiologically appropriate

or inappropriate depending on the patient's volume status (18). In the case described, the dog consistently had a moderate elevation in urine osmolality, indicating an ADH dependent cause of hyponatremia but did not further distinguish the underlying etiology.

Recently, fractional excretion of uric acid (FEUA) has been used in differentiation of human SIAD from CSW (9). Uric acid is a product of purine metabolism that is freely filtered at the renal glomerulus and co-transported with sodium at the proximal tubule. The FEUA quantifies the percent excretion of the filtered load of uric acid across the glomerulus (7, 9). Multiple tubular uric acid transporters, have been identified that couple uric acid reabsorption to that of sodium (9).

A normal value for FEUA is <11% in humans, whereas patients with untreated SIAD and CSW have consistent elevations of FEUA >11% at the onset of hyponatremia (7, 9). After correction of the hyponatremia, the FEUA normalizes (<11%) in patients with SIAD but will remain persistently elevated (>11%) in patients with CSW (7). Thus, FEUA has been proposed as a more quantifiable measure to differentiate SIAD from CSW. In the case described, the FEUA was persistently elevated despite the resolution of hyponatremia and clinical volume status, as well as normalization of uUA:uCr at subsequent recheck evaluations.

The dog described in this report had markedly increased urinary sodium excretion occurring concurrently with findings suggesting hypovolemia, consistent with a diagnosis of CSW. The dog's hyponatremia rapidly corrected after initiation of a hypertonic saline CRI. The positive response (i.e., increased mucous membrane moisture, skin turgor, normalization of heartrate and blood pressure, and reduction in weight loss) to sodium supplementation and continued isotonic enteral supplementation also supports the diagnosis of CSW (2).

There are several limitations to this case report. First, the patient was never directly screened for hypoadrenocorticism. Hypoadrenocorticism may also present with marked hyponatremia and either euvolemia or hypovolemia depending on the severity of the clinical signs. However, the dog's hyponatremia resolved without mineralocorticoid supplementation. Another limitation to this report is the relative subjectivity of evaluating the dog's volume status. The traditional guidelines for distinguishing SIAD from CSW rely heavily on whether the patient is euvolemic or hypovolemic, a challenging prospect unless physical examination changes are pronounced. The uUA:uCr was also quantified in this case to aid in volume status estimation.

Furthermore, the fractional excretion measurements utilized are only evaluating a single point in time. These values can be influenced postprandially, although the dog being fed the same diet after discharge will limit this variability. Ideally, pooled urine samples collected over 24 h should be utilized to acquire a more accurate fractional excretion of sodium, however this would not have been feasible to perform on an outpatient basis during recheck examinations. Finally, the interpretation of FEUA was made based solely on reference ranges in people; further investigation is required regarding normal FEUA in domestic animals.

In conclusion, we have described a juvenile dog with persistent hypotonic hyponatremia and clinical findings consistent with CSW secondary to a TBI. The dog lost weight and appeared dehydrated while developing marked polyuria and remained severely hyponatremic and hypovolemic despite replacement fluid administration. The hyponatremia resolved only with administration of hypertonic sodium chloride and oral sodium supplementation. Urine osmolality and urine sodium concentrations were markedly elevated in all measurements, suggesting an ADH dependent process and renal specific sodium loss. The elevated FENa (>0.5%) despite clinical evidence of hypovolemia and an elevated uUA:uCr also supports these assumptions (26). Subsequent testing revealed an increased FEUA, which remained persistently elevated despite the resolution of her hyponatremia, which aided in the differentiation of CSW from SIAD. This additional diagnostic evaluation expands the knowledge base on this condition in canine patients as previously described in the recent report from Chromiak et al. (13).

Data availability statement

The original contributions presented in the study are included in the article/supplementary material, further inquiries can be directed to the corresponding author.

Ethics statement

Ethical approval was not required for the studies involving animals in accordance with the local legislation and institutional requirements because the dog detailed in the case report was presented at the North Carolina State University Small Animal Veterinary Hospital for evaluation and care. The owners signed a consent form to permit the diagnostic procedures, therapeutic interventions, and to use the collected clinical data. Written informed consent was obtained from the owners for the participation of their animals in this study. Written informed consent was obtained from the participants for the publication of this case report.

Author contributions

EJ: Conceptualization, Data curation, Formal analysis, Investigation, Methodology, Project administration, Resources, Software, Writing – original draft, Writing – review & editing. GF: Conceptualization, Data curation, Formal analysis, Funding acquisition, Investigation, Methodology, Project administration, Resources, Writing – original draft, Writing – review & editing. KM: Conceptualization, Data curation, Formal analysis, Investigation, Methodology, Project administration, Supervision, Writing – review & editing. BH: Conceptualization, Data curation, Formal analysis, Investigation, Methodology, Project administration, Supervision, Writing – review & editing.

Funding

The author(s) declare that financial support was received for the research and/or publication of this article. Funding for ancillary

diagnostic testing was provided by the CREATE fund of the North Carolina Veterinary Medical Foundation.

Acknowledgments

The authors would like to thank all house officers, faculty members, and veterinary nurses involved in the intensive management of this case.

Conflict of interest

The authors declare that the research was conducted in the absence of any commercial or financial relationships that could be construed as a potential conflict of interest.

Generative AI statement

The authors declare that no Gen AI was used in the creation of this manuscript.

Publisher's note

References

1. Yee AH, Burns JD, Wijdicks EF. Cerebral salt wasting: pathophysiology, diagnosis, and treatment. *Neurosurg Clin N Am*. (2010) 21:339–52. doi: 10.1016/j.nec.2009.10.011

2. Momi J, Tang CM, Abcar AC, Kujubu DA, Sim JJ. Hyponatremia-what is cerebral salt wasting? *Perm J*. (2010) 14:62–5. doi: 10.7812/TPP/08-066

3. Sorkhi H, Salehi Omran MR, Barari Savadkoohi R, Baghdadi F, Nakhjavani N, Bijani A. CSWS versus SIADH as the probable causes of hyponatremia in children with acute cns disorders. *Iran J Child Neurol*. (2013) 7:34–9.

4. Jiménez R, Casado-Flores J, Nieto M, García-Teresa MA. Cerebral salt wasting syndrome in children with acute central nervous system injury. *Pediatr Neurol*. (2006) 35:261–3. doi: 10.1016/j.pediatrneurol.2006.05.004

5. Hardesty DA, Kilbaugh TJ, Storm PB. Cerebral salt wasting syndrome in post-operative pediatric brain tumor patients. *Neurocrit Care*. (2012) 17:382–7. doi: 10.1007/s12028-011-9618-4

6. Maesaka JK, Miyawaki N, Palaia T, Fishbane S, Durham JH. Renal salt wasting without cerebral disease: diagnostic value of urate determinations in hyponatremia. *Kidney Int*. (2007) 71:822–6. doi: 10.1038/sj.ki.5002093

7. Maesaka JK, Imbriano LJ, Miyawaki N. Determining fractional urate excretion rates in hyponatremic conditions and improved methods to distinguish cerebral/renal salt wasting from the syndrome of inappropriate secretion of antidiuretic hormone. *Front Med*. (2018) 5:319. doi: 10.3389/fmed.2018.00319

8. Bitew S, Imbriano L, Miyawaki N, Fishbane S, Maesaka JK. More on renal salt wasting without cerebral disease: response to saline infusion. *Clin J Am Soc Nephrol*. (2009) 4:309–15. doi: 10.2215/CJN.02740608

9. Bardanzellu F, Marcialis MA, Frassetto R, Melis A, Fanos V. Differential diagnosis between syndrome of inappropriate antidiuretic hormone secretion and cerebral/renal salt wasting syndrome in children over 1 year: proposal for a simple algorithm. *Pediatr Nephrol*. (2022) 37:1469–78. doi: 10.1007/s00467-021-05250-1

10. Assadi F, Mazaheri M. Differentiating syndrome of inappropriate ADH, reset osmostat, cerebral/renal salt wasting using fractional urate excretion. *J Pediatr Endocrinol Metab*. (2021) 34:137–40. doi: 10.1515/jpem-2020-0379

11. Deslarzes T, Turini P, Friolet R, Meier P. Cerebral salt wasting syndrome versus SIADH. *Rev Med Suisse*. (2009) 5:2281–4. doi: 10.53738/REVMED.2009.5.225.2281

12. Burton AG, Hopper K. Hyponatremia in dogs and cats. *J Vet Emerg Crit Care (San Antonio)*. (2019) 29:461–71. doi: 10.1111/vec.12881

13. Chromiak AE, Finstad J, Cooper E. Suspected cerebral salt wasting syndrome secondary to traumatic brain injury in a dog. *J Vet Emerg Crit Care*. (2024) 34:285–90. doi: 10.1111/vec.13375

14. Troia R, Gruarin M, Grisetti C, Serafini F, Magna L, Monari E, et al. Fractional excretion of electrolytes in volume-responsive and intrinsic acute kidney injury in dogs: diagnostic and prognostic implications. *J Vet Intern Med*. (2018) 32:1372–82. doi: 10.1111/jvim.15146

15. Sherlock M, O'Sullivan E, Agha A, Behan LA, Owens D, Finucane F, et al. Incidence and pathophysiology of severe hyponatraemia in neurosurgical patients. *Postgrad Med J*. (2009) 85:171–5. doi: 10.1136/pgmj.2008.072819

16. Rivkees SA. Differentiating appropriate antidiuretic hormone secretion, inappropriate antidiuretic hormone secretion and cerebral salt wasting: the common, uncommon, and misnamed. *Curr Opin Pediatr*. (2008) 20:448–52. doi: 10.1097/MOP.0b013e328305e403

17. Chung HM, Kluge R, Schrier RW, Anderson RJ. Clinical assessment of extracellular fluid volume in hyponatremia. *Am J Med*. (1987) 83:905–8. doi: 10.1016/0002-9343(87)90649-8

18. Diringer MN, Zazulia AR. Hyponatremia in neurologic patients: consequences and approaches to treatment. *Neurologist*. (2006) 12:117–26. doi: 10.1097/01.nrl.0000215741.01699.77

19. Sterns RH, Rondon-Berrios H. Cerebral salt wasting is a real cause of hyponatremia: con. *Kidney360*. (2023) 4:e441–4. doi: 10.34067/KID.0001412022

20. Harris PJ, Thomas DMorgan TO. Atrial natriuretic peptide inhibits angiotensin-stimulated proximal tubular sodium and water reabsorption. *Nature*. (1987) 326:697–8. doi: 10.1038/326697a0

21. Youmans SJ, Fein MR, Wirkowski E, Maesaka JK. Demonstration of natriuretic activity in urine of neurosurgical patients with renal salt wasting. *F1000Res*. (2013) 2:126. doi: 10.12688/f1000research.2-126.v2

22. Tobin G, Chacko AG, Simon R. Evaluation of NT-ProBNP as a marker of the volume status of neurosurgical patients developing hyponatremia and natriuresis: a pilot study. *Neurol India*. (2018) 66:1383–8. doi: 10.4103/0028-3886.241401

23. Cui H, He G, Yang S, Lv Y, Jiang Z, Gang X, et al. Inappropriate antidiuretic hormone secretion and cerebral salt-wasting syndromes in neurological patients. *Front Neurosci*. (2019) 13:1170. doi: 10.3389/fnins.2019.01170

24. Maesaka JK, Imbriano L, Mattana J, Gallagher D, Bade N, Sharif S. Differentiating SIADH from cerebral/renal salt wasting: failure of the volume approach and need for a new approach to hyponatremia. *J Clin Med*. (2014) 3:1373–85. doi: 10.3390/jcm3041373

25. Spasovski G, Vanholder R, Allolio B, Annane D, Ball S, Bichet D, et al. Clinical practice guideline on diagnosis and treatment of hyponatraemia. *Intensive Care Med*. (2014) 40:320–31. doi: 10.1007/s00134-014-3210-2

26. Decaux G, Musch W. Clinical laboratory evaluation of the syndrome of inappropriate secretion of antidiuretic hormone. *Clin J Am Soc Nephrol*. (2008) 3:1175–84. doi: 10.2215/CJN.04431007

frontiers | Frontiers in Veterinary Science

TYPE Case Report
PUBLISHED 09 April 2025
DOI 10.3389/fvets.2025.1543611

OPEN ACCESS

EDITED BY
Koen Santifort,
IVC Evidensia Small Animal Referral Hospital Arnhem, Neurology, Netherlands

REVIEWED BY
Shinji Tamura,
Tamura Animal Clinic, Japan
Julien Guevar,
AniCura Tierklinik Thun, Switzerland

*CORRESPONDENCE
Hao Shi
haoshi@cau.edu.cn

†These authors share senior authorship

RECEIVED 12 December 2024
ACCEPTED 25 February 2025
PUBLISHED 09 April 2025

CITATION
Shi H, Wang Q, Shao Z, Xu H, Yang Y, Zhang Y, Ren R and Weng J (2025) Case Report: Endoscope-assisted single-incision double-channel mini-open hemilaminectomy for the treatment of acute thoracolumbar intervertebral disc disease in 11 dogs. *Front. Vet. Sci.* 12:1543611. doi: 10.3389/fvets.2025.1543611

Case Report: Endoscope-assisted single-incision double-channel mini-open hemilaminectomy for the treatment of acute thoracolumbar intervertebral disc disease in 11 dogs

Hao Shi[1,2*†], Qi Wang[3†], Zhurui Shao[1,2], Haojie Xu[1,2], Yufei Yang[1,2], Yiwen Zhang[1,2], Ruizi Ren[1,2] and Jieen Weng[1,2]

[1]The Clinical Department, College of Veterinary Medicine, China Agricultural University, Beijing, China, [2]China Agricultural University Veterinary Teaching Hospital, Beijing, China, [3]Babara Veterinary Hospital, Shanghai, China

This study aims to explore the feasibility and efficacy of an endoscopic-assisted mini-open hemilaminectomy technique for spinal cord decompression in thoracolumbar intervertebral disc extrusion. A total of 11 dogs with acute thoracolumbar intervertebral disc disease were included in the study, preoperative magnetic resonance imaging (MRI) and computed tomography (CT) were used for precise localization. The surgery was performed using a lateral approach with a skin incision approximately 2 cm in length for a minimally invasive hemilaminectomy of the thoracolumbar spine. After separating the epaxial musculature below the articular process and exposing the tendon attachment of the accessory process, the endoscope and surgical instruments were placed. A nerve hook and nucleus pulposus forceps were used to remove the thoracolumbar intervertebral disc extrusions and relieve spinal cord compression. Postoperative MRI or CT confirmed complete removal of the disc extrusions with no significant complications observed, and all dogs exhibited normal gait and neurological examination results. This technique demonstrated advantages such as easy handling minimal incision, precise localization, and reduced iatrogenic damage, resulting in good postoperative recovery. This case series demonstrates that the endoscopic-assisted mini-open hemilaminectomy technique can safely be implemented to decompress the spinal cord in dogs. This novel technique adds onto the current growing surgical options for minimally invasive spinal surgery in veterinary neurosurgery.

KEYWORDS

dog, intervertebral disc disease, minimally invasive surgery, neurosurgery, mini-open hemilaminectomy

1 Introduction

Canine intervertebral disc disease (IVDD) is one of the most common spinal disorders in dogs, with a peak incidence typically occurring between 3 and 6 years of age. It primarily affects chondrodystrophic breeds, with a particularly high prevalence in short-legged, long-backed breeds such as Dachshunds and French Bulldogs (1–3). The core issue of this disease lies in the degenerative changes or injuries of the intervertebral disc, leading to the extrusion of the nucleus pulposus or annulus fibrosus, which compresses the spinal cord or surrounding

nerves. This results in pain, neurological disorder, and even paralysis (1, 3–7). Currently, MRI is the golden standard for diagnosing IVDD.

The treatment of canine intervertebral disc disease can be categorized into conservative and surgical approaches. The choice of treatment largely depends on the severity of the neurological signs. According to the study by Crawford et al., conservative treatment (a combination of analgesic medication and restricted exercise) had been found suitable for dogs with mild disc extrusion and less severe spinal cord compression, achieving a success rate of 29% (8). Surgical treatment is indicated for dogs with more severe disc damage. Statistics had shown that open surgical procedures (a hemilaminectomy with anulectomy or with a partial discectomy) had achieved a success rate of 71% (8).

Currently, common techniques for thoracolumbar spinal cord decompression include hemilaminectomy and mini-hemilaminectomy. Those techniques are typically performed using an open approach (the muscle are disinserted from the bone extensively) allowing the surgeon to visualize the anatomical landmarks. Minimally invasive techniques have emerged in recent years in veterinary neurosurgery. This shift has been possible via the use of magnification and illumination technique. Endoscopic spinal surgery is gaining a lot of traction in human minimally invasive spine surgery (MISS) but little is known about the technique in veterinary medicine. Compared to traditional open surgeries, endoscopic surgeries offer smaller incisions, less tissue trauma, improved visibility, and a lower complication rates (9). Reports on the use of endoscopy for treating intervertebral disc disease in veterinary medicine had been limited (10–16). Moon et al. had demonstrated the feasibility of percutaneous endoscopic thoracolumbar mini-hemilaminectomy via a uniportal approach in small dogs. Although their study had simulated intervertebral disc extrusion using an injected barium and agarose mixture, the findings had indicated that this surgical technique was effective in alleviating spinal compression. It had provided a good view during the operation, required only a small skin incision (<1 cm), and had a relatively short operation time (58 min) (11). Hwang et al. had performed percutaneous endoscopic thoracolumbar pediculectomy on five healthy dogs at the thoracic spine and five healthy dogs at the lumbar spine. Postoperatively, only one dog had exhibited a transient, slight ipsilateral hind limb weakness, which had resolved within 4 days. The gait and neurological examinations of the other dogs had been normal. Two dogs had showed high signal intensities within the spinal cord on T2-weighted (T2W) magnetic resonance imaging (MRI), suspected to have been spinal cord edema or gliosis, which had improved after 4 weeks. These findings suggest that percutaneous endoscopic pediculectomy might have been an effective surgical method for decompression and removal of disc material in canine intervertebral disc disease (13).

Currently, there have been no reports on the use of the "single-incision double-channel mini-open" technique for treating thoracolumbar intervertebral disc disease in dogs. The uniqueness of this technique lies in achieving double-channel operation through a single incision, which not only retains the advantages of traditional endoscopic surgery, such as less intraoperative injury and rapid recovery, but also significantly enhances operational flexibility and visibility. This represents an important innovation in the treatment of intervertebral disc disease in dogs.

This study aims to describe a minimally invasive surgical technique for endoscope-assisted single-incision double-channel mini-open hemilaminectomy in the treatment of acute thoracolumbar intervertebral disc disease in dogs. The study reports on 11 cases treated with this technique and evaluates its efficacy in removing herniated disc material and achieving spinal cord decompression. To assess potential postoperative complications, neurological examinations, MRI, and computed tomography (CT) scans were conducted, and the clinical outcomes of the cases were followed to evaluate the safety of the technique.

2 Materials and methods

2.1 Case information and preoperative examination

This study included 11 dogs diagnosed with thoracolumbar intervertebral disc disease. All cases were of acute onset. Information such as breed, age, weight, and sex was recorded for all cases in Table 1. Physical examinations and neurological assessments were performed on each animal. Neurological assessments for all cases were conducted by a senior surgeon, focusing primarily on evaluating mental status, gait analysis, spinal reflexes, palpation, and pain perception. The neurological grading of the case follows the published scoring system (17). The grading system was as follows: grade 0, normal gait; grade 1, thoracolumbar pain with no neurological deficits; grade 2, ambulatory paraparesis; grade 3, non- ambulatory paraparesis; grade 4, paraplegia with intact deep pain perception in at least one limb; and grade 5, paraplegia with loss of deep pain perception. "Ambulation" was defined as the ability to walk 10 consecutive steps without support as previously reported (18). Complete blood count and blood biochemical analyze were performed before surgery; MRI (1.5 Tesla, uMR580, United Imaging Medical Technology Co., LTD, Shanghai, China) and CT (uCT 768, United Imaging Medical Technology Co., LTD, Shanghai, China) were used to diagnose thoracolumbar intervertebral disc disease in all cases and to identify the location of the affected intervertebral discs.

Each dog was preoperatively administered butorphanol intravenously (0.2 mg/kg). Anesthesia was induced with intravenous propofol (6 mg/kg, administered to effect), followed by maintenance with inhalation of 1.5% isoflurane in oxygen via endotracheal intubation. During the surgery, dexmedetomidine was infused intravenously at a rate of 1 μg/kg/h for intraoperative analgesia, and lactated Ringer's solution was administered at 5 mL/kg/h. Additionally, ceftriaxone (25 mg/kg) was used intraoperatively, with doses repeated every 90 min. The dogs were placed in a sternal position, and the surgical site was aseptically prepared.

2.2 Surgical procedure

The lesion site was identified preoperatively using MRI (Figures 1A,B). After shaving and aseptically preparing the surgical area, the dog was transferred to the CT table. The spinous process of the vertebra on the cranial side of the affected disc was palpated and clamped with sterile drape forceps. A CT scan was performed to confirm the correct clamping position (Figures 1C,D). The dog was then transferred to the surgical table, and the surgical site was re-disinfected. Sterile drapes were applied, and a thin sterile film was

TABLE 1 Basic characteristics of dogs undergoing mini-hemilaminectomy assisted by endoscopy, including breed, sex, age, weight, neurological grading, and the location of the affected intervertebral disc.

Case	Breed	Sex	Age	Weight	Neurological grading*	Lesion location
1	French Bulldog	Male	4Y	13.2 kg	2	T13-L1
2	Pomeranian	Female	3Y	4.3 kg	3	T13-L1
3	Shiba Inu	Male	6Y	18 kg	3	L2-L3
4	Corgi	Female	5Y	16 kg	4	L2-L3
5	Chinese rural dog	Male	5Y	6.8 kg	4	T12-T13
6	Bichon Frise	Male	7Y	6.1 kg	5	L1-L2
7	Poodle	Male	7Y	9.6 kg	4	T12-T13
8	German Shepherd	Male	7Y	46 kg	2	L1-L2
9	Corgi	Male	9Y	14 kg	3	T13-L1
10	Corgi	Male	7Y	15 kg	4	T12-T13
11	Corgi	Male	5Y	13.7 kg	4	L1-L2

Y, years old; kg, kilogram.
* The grading system was as follows: grade 0, normal gait; grade 1, thoracolumbar pain with no neurological deficits; grade 2, ambulatory paraparesis; grade 3, non- ambulatory paraparesis; grade 4, paraplegia with intact deep pain perception in at least one limb; and grade 5, paraplegia with loss of deep pain perception.

placed over the drapes to prevent spillage of saline irrigation during the surgery from soaking the animal. Based on the position of the drape forceps, the adjacent articular processes near the affected intervertebral disc were palpated. A 2 cm incision was made just below the articular process, with the incision center aligned with the articular process. During surgery, a vital signs monitor (ePM 12 M Vet, Shenzhen Mindray Bio-Medical Electronics Co., Ltd., Shenzhen, China) is used to track the heart rate, oxygen saturation, blood pressure, and end-tidal carbon dioxide levels.

Using coblation system (ASC4250-01, ArthroCare Corporation, Texas, USA) and a periosteal elevator (3/3 mm, 155 mm; Puenhua, Jiangsu, China), the epaxial musculature below the articular process was separated to expose the lamina, and used a Gelpi retractor to secure the wound opening. The coblation system minimized bleeding and caused minimal thermal damage to tissues, promoting faster wound healing. During dissection, care was taken to note the tendinous attachment points of the accessory process, which served as navigation marker (Figure 2A). After sufficient exposure, an endoscope (30°viewing angle, diameter 2.4 mm, length 73 mm; Hangzhou VetLuc Co., Ltd., Zhejiang, China) with a sheath (diameter 2.9 mm, length 58 mm; Hangzhou VetLuc Co., Ltd., Zhejiang, China) was inserted on one side of the incision, surgical instruments were introduced on the other side of the incision (Figure 1E). The positions of the endoscope and surgical instrument can be interchanged depending on the specific situation. Using an infusion pressure bag (500 mL, Vega (China) Instrument Co., Ltd., Zhejiang, China), normal saline was continuously infused into the surgical site through the endoscopic channel. The pressure was set to 30 mmHg, with a flow rate of 0.4 L/min. A right-angle suction tip was placed at the edge of the wound, and a suction device (7A-23D, Yuwell Medical Equipment Co., Ltd., Jiangsu, China) was used to remove excess fluid from the wound. Under endoscopic visualization, the accessory process was breaked using the periosteal elevator and further ground down with a electric drill (TPS MicroDrill, Stryker, Michigan, USA). After grinding away the outer cortical bone and cancellous bone, advancing inward with the bur until the lamina was penetrated and epidural fat was visible (Figure 2B). A laminectomy rongeur (PC3260, 1 mm/210 mm, Shanghai Medical Instruments Co., Ltd., Shanghai, China) was used to enlarge the view. Bone debris was flushed out with saline irrigation. At this stage, the spinal nerve root could be observed (Figure 2C). Using a nerve hook (600,011, Byers, Jiangsu, China) and a nucleus pulposus forcep (2 mm/220 mm, Hongda Medical Equipment Co., Ltd., Jiangsu, China), the compressive intervertebral disc material was removed under endoscopic visualization (Figure 2D). This process continued until spinal cord decompression was achieved and no further disc material could be removed. The nerve hook was passed below the spinal cord and through the entire intervertebral disc space to confirm the absence of residual disc extrusion. The surgical site was flushed with saline, and the endoscope and instruments were removed. The surgical site was closed routinely. Bleeding during surgery was one of the challenges that needed to be addressed. We typically used coblation system, compression, or hemostatic sponges for hemostasis. The main surgical instruments were shown (Figure 1F).

2.3 Postoperative care

MRI or CT were performed immediately after surgery to evaluate the decompression of the spinal cord. If preoperative CT imaging clearly showed the lesion, CT was preferred. Then the patients were hospitalized for 1 week for closely monitoring. During hospitalization, the condition of animals was closely monitored to prevent recurrence of spinal cord compression and complications. Additionally, postoperative monitoring helps assess the recovery of neurological function. Postoperatively, nonsteroidal anti-inflammatory drugs (NSAIDs) and butorphanol were administered for pain control. Sutures were removed 10–14 days after the surgery. From the third postoperative day, rehabilitation and laser therapy were used for the patients until they got discharged.

3 Results

3.1 Surgical technique evaluation

All cases were successfully treated. During the procedure, the combination of an endoscope and an irrigation system was used to

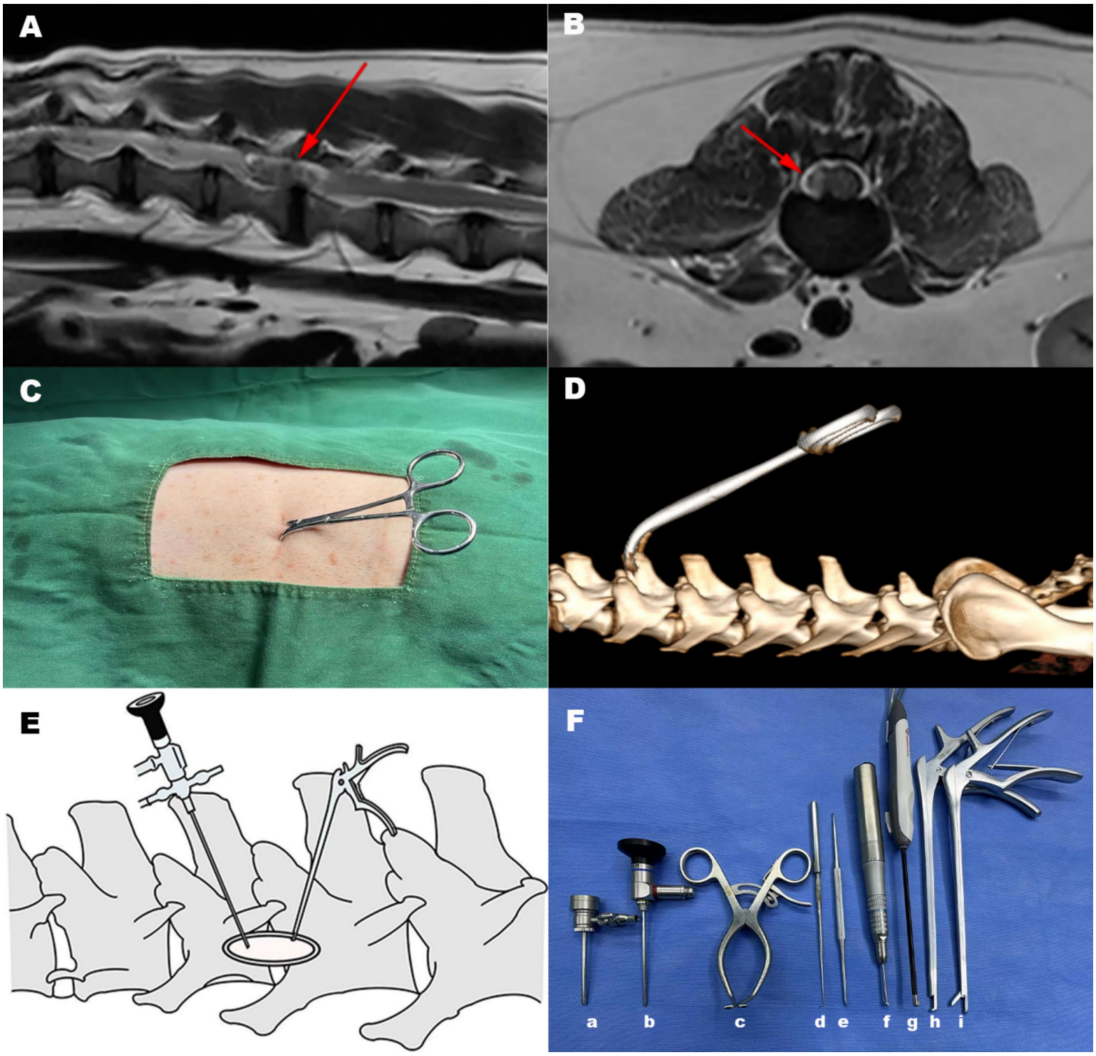

FIGURE 1
Surgical positioning and approach. **(A)** Locating the intervertebral disc for surgery using the MRI T2-weighted mid sagittal image. **(B)** Locating the intervertebral disc for surgery using the MRI T2-weighted transverse image. The arrow indicated the location showing the intervertebral disc lesion. **(C)** Palpation was used to secure the spinous process of the cranial vertebra at the lesion site with a sterile drape forceps. **(D)** After clamping the spinous process, the clamp position was confirmed via CT scan. **(E)** A modified unilateral biportal endoscopic surgical approach was adopted. A 2 cm incision is made just below the adjacent articular process to the damaged intervertebral disc, with the center of the incision aligned with the articular process. An endoscope with a sheath is inserted on one side of the incision, and surgical instruments are introduced on the other side of the incision. **(F)** Surgical instruments used in Endoscope-assisted single-incision double-channel mini-open hemilaminectomy, (a) Endoscope sheath (b) Endoscope (c) Gelpi retractor (d) Nerve hook (e) Periosteal elevator (f) Electric drill (g) Plasma cutter head (h) Rongeur (i) Nucleus pulposus forceps.

flush out debris from drilling, ensuring a clear surgical field. The muscle attachment point of the accessory process served as a navigation marker, providing critical reference for precise operations. Ultimately, the herniated disc material was precisely removed under endoscopic visualization, effectively relieving spinal cord compression. In all dogs, the affected intervertebral discs were clearly exposed, herniated disc material was successfully removed, and the nerve roots and blood vessels were systematically identified and preserved. As mentioned earlier, bleeding was one of the biggest challenges during the surgery. Sometimes, it was difficult to control and affected the surgical procedure. In such cases, we paused the irrigation and the surgery to focus on hemostasis first. The surgery duration was approximately 80–90 min.

3.2 Case outcome

All dogs received laser therapy and rehabilitation treatment postoperatively to promote healing and restore motor function, with no significant complications observed. By the fifth postoperative day, all dogs exhibited normal gait and neurological examination results (Olby score of 14) (19).

3.3 CT and MRI evaluations

All affected dogs exhibited varying degrees of neurological disorders before surgery, with neurological grades ranging from 2 to 5. Preoperative imaging revealed different degrees of nucleus pulposus

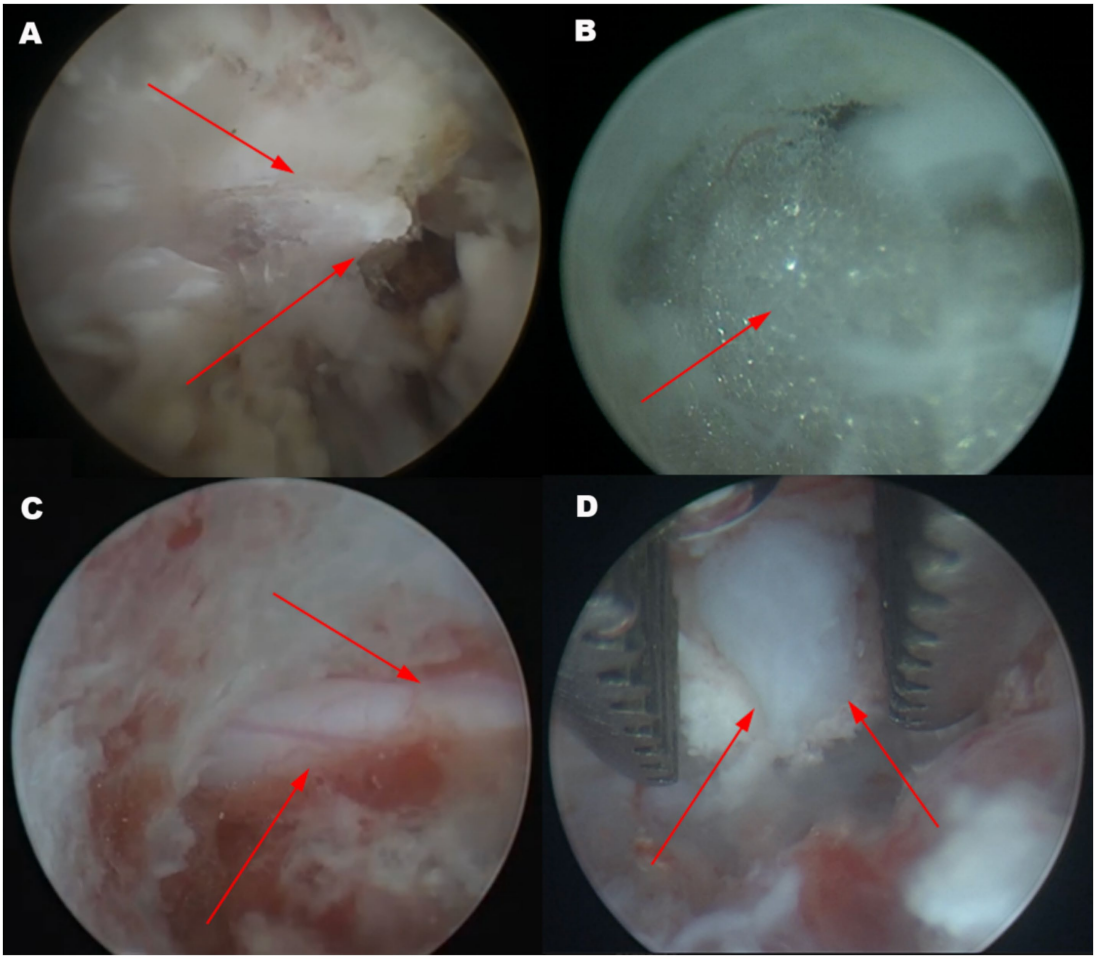

FIGURE 2
Endoscopic view of the surgical sites. **(A)** The tendinous attachment points of the accessory process can serve as a navigationa marker. The accessory process can be clearly observed (arrow). **(B)** Fat tissue inside the spinal canal becomes visible after drilling through the lamina with a bur (arrow). **(C)** Upon enlarging the approach, the spinal nerve root can be observed (arrow). **(D)** The compressed disc tissue is removed using a nucleus pulposus forceps. The arrow pointed to the herniated intervertebral disc.

extrusion and intervertebral disc degeneration in all 11 dogs, with the extruded nucleus pulposus spanning 1 to 2 vertebral segments and the area of spinal cord compression ranging from 30 to 50%. No significant spinal cord edema or hemorrhage was observed.

The 3D reconstructed image showed that after performing an endoscope-assisted single-incision double-channel mini-open hemilaminectomy, the surgical window was clearly visible (Figures 3A,B).

Due to the concern on anesthesia for postoperative MRI and CT evaluations, and in accordance with the owners' preferences, we collected postoperative MRI data for only two cases. In case 4, during the initial MRI scan, on the T2W (sagittal) image, a material with low to moderate signal was observed within the vertebral canal, compressing the spinal cord, while the signal of the spinal cord parenchyma showed no significant abnormalities (Figure 3C). On the third postoperative day, the loss of abnormal signal material in the vertebral cavity can be seen below the T2W (sagittal) image, with no significant abnormality in the spinal cord signal, while the muscles around the surgical site (accessory process) showed moderate to high signal intensity (Figure 3D). In case 11, during the initial MRI scan, on the T2W (sagittal) image, a material with low to moderate signal was observed in the vertebral canal, compressing the spinal cord (Figure 3E). In the follow-up MRI 16 months after surgery, on the T2W (sagittal) image, the surgical site segment of the spinal cord showed a localized high signal intensity, with mild disc protrusion, but no signs of spinal cord compression (Figure 3F).

4 Discussion

Minimally invasive treatment of intervertebral disc disease is generally considered challenging, primarily due to the complex anatomical structure of the spine, the presence of multiple muscle tissues, nerves, and blood vessels nearby, and the proximity of the surgical site to the spinal cord. This study presents a minimally invasive neurosurgical technique for treating canine intervertebral disc disease. The study included 11 dogs treated with this surgical technique, all of which showed favorable imaging results postoperatively. Physical and neurological examinations of all dogs were normal.

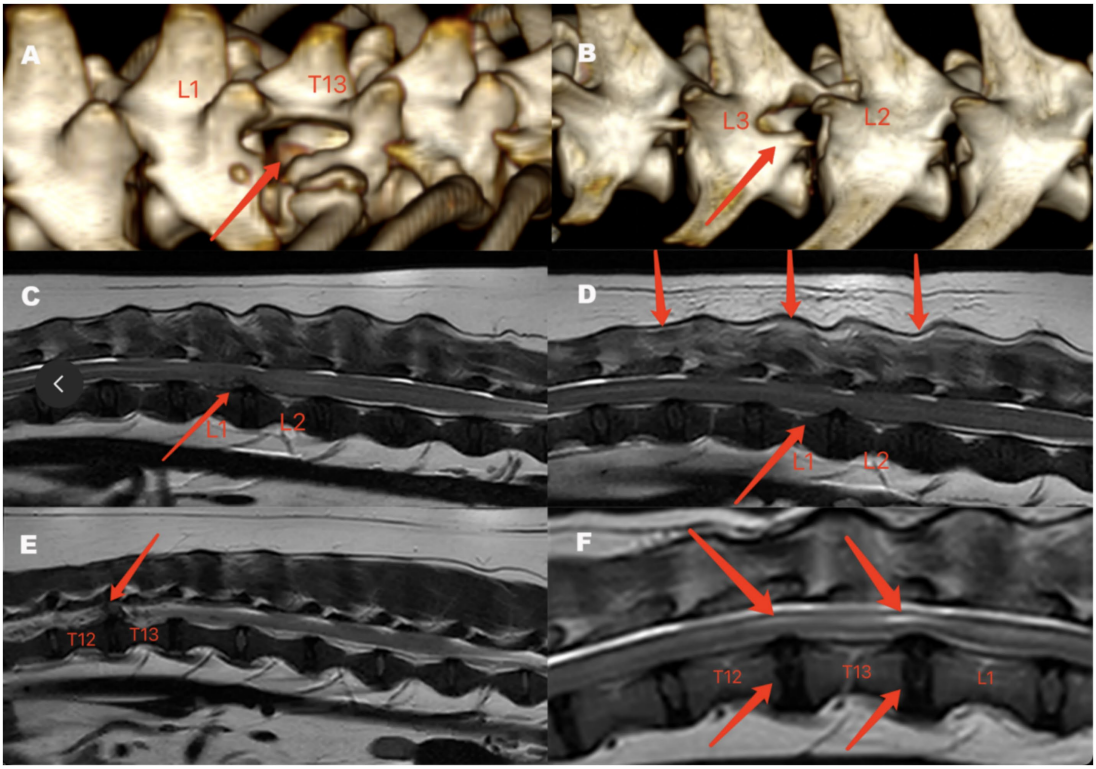

FIGURE 3
Postoperative 3D-reconstruction image of Case 1 **(A)** and Case 3 **(B)**, preoperative and postoperative MRI findings of Case 4 **(C,D)** and Case 11 **(E,F)**. **(A)** Lateral view of the 3D reconstructed image of Case 1, with surgery performed on the right side (arrow). **(B)** Lateral view of the 3D reconstruction of Case 3, with the surgery performed on the left side (arrow). **(C)** Preoperative MRI of Case 4 in the T2-weighted mid sagittal image shows low to moderate signal material within the spinal canal compressing the spinal cord, with no significant abnormality in the spinal cord signal. The arrow indicated the affected intervertebral disc. **(D)** Postoperative MRI of Case 4 on day 3 in the T2-weighted mid sagittal image shows the disappearance of the abnormal signal material in the spinal canal, no significant abnormality in the spinal cord signal (lower arrow), and a mixed moderate-to-high signal observed in the muscles surrounding the foraminal endoscopic surgery site (upper arrow). **(E)** Preoperative MRI of Case 11 in the T2-weighted mid sagittal image shows low to moderate signal material within the spinal canal compressing the spinal cord. The arrow indicated the affected intervertebral disc. **(F)** Postoperative MRI of Case 11 at 16 months in the T2-weighted mid sagittal image shows localized high signal intensity in the spinal cord at the surgical site segment (upper arrow), mild disc protrusion, and no signs of spinal cord compression (lower arrow).

The magnification and illumination functions of the endoscope can be achieved through the lens and cold light source or LED light source, enabling the magnified observation of small structures. This magnification and illumination capability helps veterinarians see fine details of the surgical site more clearly in darker or narrower surgical areas, which is particularly useful in surgeries involving the nervous system.

In human medicine, unilateral biportal endoscopy is a novel minimally invasive technique for treating thoracolumbar intervertebral disc herniation. The surgical approach involves making two incisions approximately 1 cm lateral to the dorsal midline, with saline infusion entering through one port and suction exiting through the other (20). In our preliminary stage of exploring the surgical approach, this technique was also tested on canine cadavers. The results showed that due to the looser skin in dogs and the larger space between the skin and muscle tissue, the infused saline would accumulate subcutaneously. Therefore, through modification and optimization, the approach was adjusted to use a single incision, with the suction device placed at the incision edge to effectively drain the fluid.

In other reports, the surgical site had been located and the working channel had been established under fluoroscopic guidance, using a Kirschner wire (K-wire) to locate the damaged intervertebral disc. After determining the position, a K-wire or spinal needle had been inserted and advanced medially to the pedicle until bony resistance had been met. Then, a series of gradually increasing dilators had been placed over the K-wire, and finally, a tubular retractor had been used to establish the working channel. Some studies had also employ a articulated arm to hold the retractor for the working channel (11, 13, 14). The positioning in this study was achieved using CT imaging, with surgical localization assisted by palpation and visual inspection, eliminating the need for fluoroscopy and simplifying the procedure.

In the reported surgical techniques, most had used a single-incision approach, where both the endoscope and other surgical instruments had been placed within the tubular retractor, with the surgical incision being approximately 1 cm in length (11, 13). In contrast, this study used a single-incision, double-channel approach for surgery. Although the surgical incision was relatively longer (about 2 cm), the double-channel surgical path provided more operating space. Tanaka et al. reported a lateral muscle-separating approach similar to the surgical approach in this study. The extent of the skin incision was from the posterior border of the articular process to the rostral vertebra and from the anterior border of the articular process to the caudal vertebra, with an average incision length of 2.7 cm. The incision length was correlated with the size of

the dog. In this study, the surgical incision was made as a 2 cm cut below the articular process, regardless of the dog's size (21). In our research, a 2 cm incision was sufficient to perform the surgical procedure. Spinal surgery is a technically demanding and challenging procedure and veterinarians must perform the surgery carefully and precisely, as even a slight error can damage nerves and lead to severe consequences. The single-incision, double-channel surgical approach was easier to perform, reducing the likelihood of iatrogenic injuries and improving the safety and stability of the surgery. Additionally, the surgical equipment and instruments used in this study were fewer and relatively easy to obtain.

Our study also has some limitations. For large dogs and obese dogs, where it was difficult to palpate the vertebral processes, drape forceps were not able to grasp the spinous processes. Additionally, the approximate surgical time was recorded in this study, which was around 80–90 min, longer compared to open hemilaminectomy (22). It should be noted that this surgical technique relies on endoscopic assistance, making the surgical costs higher than open surgeries that only require conventional spinal surgical instruments. Another limitation was that this surgical technique was suitable for cases where the prolapsed nucleus pulposus was located ventral to the spinal cord. For lateral or dorsolateral spinal extrusion or intradural extrusion, it might have been necessary to extend the laminectomy dorsally.

In our study, we reported a surgical technique using minimally invasive methods to treat canine intervertebral disc disease, which allowed for spinal cord decompression and removal of herniated disc material. Postoperative results indicated that the affected dogs recovered well without significant complications. Compared to traditional open surgery, this method offered advantages such as precise localization, reduced iatrogenic injury, and improved visibility. The use of a dynamic irrigation system during the procedure ensured a clear surgical field. Compared to the single-port approach, the double-channel design provided greater operating space, enhancing the safety and operability of the surgery. However, the sample size in this study was small, and there was a lack of long-term follow-up data to assess long-term efficacy. Further studies are needed to evaluate the application of this method in dogs with thoracolumbar intervertebral disc disease.

Data availability statement

The raw data supporting the conclusions of this article will be made available by the authors, without undue reservation.

Ethics statement

The animal studies were approved by the Institutional Animal Care and Use Committee (IACUC) of China Agricultural University for Laboratory Animal Welfare and Ethical Review of Animal Experiments. The studies were conducted in accordance with the local legislation and institutional requirements. Written informed consent was obtained from the owners for the participation of their animals in this study. Written informed consent was obtained from the participant/patient(s) for the publication of this case report.

Author contributions

HS: Writing – original draft, Writing – review & editing. QW: Resources, Writing – review & editing. ZS: Writing – original draft, Writing – review & editing. HX: Writing – review & editing. YY: Writing – review & editing. YZ: Writing – review & editing. RR: Writing – review & editing. JW: Writing – review & editing.

Funding

The author(s) declare financial support was received for the research and/or publication of this article. The research is supported by "The Talent Fund of China Agricultural University Veterinary Teaching Hospital." The fund code is 2223001.

Conflict of interest

The authors declare that the research was conducted in the absence of any commercial or financial relationships that could be construed as a potential conflict of interest.

Generative AI statement

The authors declare that no Gen AI was used in the creation of this manuscript.

Publisher's note

Supplementary material

The Supplementary material for this article can be found online at: https://www.frontiersin.org/articles/10.3389/fvets.2025.1543611/full#supplementary-material

References

1. Brisson BA. Intervertebral disc disease in dogs. *Vet Clin North Am Small Anim Pract*. (2010) 40:829–58. doi: 10.1016/j.cvsm.2010.06.001

2. Sharp W. Small animal spinal disorders diagnosis and surge. Missouri: Mosby Ltd. (2005).

3. Bergknut N, Egenvall A, Hagman R, Gustås P, Hazewinkel HAW, Meij BP, et al. Incidence of intervertebral disk degeneration–related diseases and associated mortality rates in dogs. *J Am Vet Med Assoc*. (2012) 240:1300–9. doi: 10.2460/javma.240.11.1300

4. Bray J, Burbidge H. The canine intervertebral disk. Part two: degenerative changes--nonchondrodystrophoid versus chondrodystrophoid disks. *J Am Anim Hosp Assoc*. (1998) 34:135–44. doi: 10.5326/15473317-34-2-135

5. Jeffery ND, Levine JM, Olby NJ, Stein VM. Intervertebral disk degeneration in dogs: consequences, diagnosis, treatment, and future directions. *J Vet Intern Med*. (2013) 27:1318–33. doi: 10.1111/jvim.12183

6. Macias C, McKee WM, May C, Innes JF. Thoracolumbar disc disease in large dogs: a study of 99 cases. *J Small Anim Pract*. (2002) 43:439–46. doi: 10.1111/j.1748-5827.2002.tb00010.x

7. Coates JR, Wininger FA. Canine degenerative myelopathy. *Vet Clin North Am Small Anim Pract*. (2010) 40:929–50. doi: 10.1016/j.cvsm.2010.05.001

8. Crawford AH, De Decker S. Clinical presentation and outcome of dogs treated medically or surgically for thoracolumbar intervertebral disc protrusion. *Vet Rec*. (2017) 180:569. doi: 10.1136/vr.103871

9. Birkenmaier C, Chiu JC, Fontanella A, Leu HF, Ruetten S. Guidelines for percutaneous endoscopic spinal surgery. *Orthop Trauma Prosth*. (2014) 1:87. doi: 10.15674/0030-59872014187-95

10. Drury AG, Monnet E, Packer RA, Marolf AJ. Determination of surgical exposure obtained with integrated endoscopic thoracolumbar hemilaminectomy in large-breed cadaveric dogs. *Vet Surg*. (2019) 48:O52–8. doi: 10.1111/vsu.12968

11. Moon HS, Hwang YH, Lee HC, Lee JH. Operative techniques of percutaneous endoscopic mini-hemilaminectomy using a uniportal approach in dogs. *J Vet Med Sci*. (2017) 79:1532–9. doi: 10.1292/jvms.17-0148

12. Lockwood AA, Griffon DJ, Gordon-Evans W, Matheson JA, Barthélémy N, Schaeffer DJ. Comparison of two minimally invasive approaches to the thoracolumbar Spinal Canal in dogs. *Vet Surg*. (2014) 43:209–21. doi: 10.1111/j.1532-950X.2014.12098.x

13. Hwang Y, Lee H, Lee J. Operative techniques and preliminary outcomes following percutaneous endoscopic thoracolumbar Pediculectomy in dogs. *Vet Surg*. (2016) 45:O84–94. doi: 10.1111/vsu.12569

14. Guevar J, Olby N. Minimally invasive microsurgical decompression of an intervertebral disc protrusion in a dog. *Vet Surg*. (2020) 49:86–92. doi: 10.1111/vsu.13263

15. MacQuiddy B, Bartner L, Marolf A, Rao S, Dupont E, Adams T, et al. The use of a minimally invasive integrated endoscopic system to perform hemilaminectomies in chondrodystrophic dogs with thoracolumbar intervertebral disc extrusions. *Front Vet Sci*. (2024) 11:1296051. doi: 10.3389/fvets.2024.1296051

16. Kamishina H, Nakano Y, Nozue Y, Nakata K, Kimura S, Drury AG, et al. Microendoscopic Mini-Hemilaminectomy and discectomy in acute thoracolumbar disc extrusion dogs: a pilot study. *Vet Sci*. (2021) 8:241. doi: 10.3390/vetsci8100241

17. Langerhuus L, Miles J. Proportion recovery and times to ambulation for non-ambulatory dogs with thoracolumbar disc extrusions treated with hemilaminectomy or conservative treatment: a systematic review and meta-analysis of case-series studies. *Vet J*. (2017) 220:7–16. doi: 10.1016/j.tvjl.2016.12.008

18. Jeffery ND, Olby NJ, Moore SA. Canine spinal cord injury consortium (CANSORT-SCI). Clinical trial design—a review—with emphasis on acute intervertebral disc herniation. *Front Vet Sci*. (2020) 7:583. doi: 10.3389/fvets.2020.00583

19. Olby NJ, Risio LD, Muñana KR, Wosar MA, Skeen TM, Sharp NJH, et al. Development of a functional scoring system in dogs with acute spinal cord injuries. *Am J Vet Res*. (2001) 62:1624–8. doi: 10.2460/ajvr.2001.62.1624

20. Park DK, Weng C, Zakko P, Choi DJ. Unilateral Biportal endoscopy for lumbar spinal stenosis and lumbar disc herniation. *JBJS Essent Surg Tech*. (2023) 13:e22.00020. doi: 10.2106/JBJS.ST.22.00020

21. Tanaka N, Kitagawa M, Ito D, Watari T. A modified lateral muscle-separation approach for mini-hemilaminectomy. *Vet Rec*. (2013) 173:296. doi: 10.1136/vr.101369

22. Itamoto K, Itoh H, Sunahara H, Horikirizono H, Nemoto Y, Tani K, et al. Comparison of surgical invasiveness between micro-endoscopic discectomy/microscopic discectomy and conventional hemilaminectomy in dogs. *J Vet Med Sci*. (2023) 85:617–24. doi: 10.1292/jvms.22-0226

frontiers | Frontiers in Veterinary Science

TYPE Case Report
PUBLISHED 09 May 2025
DOI 10.3389/fvets.2025.1572808

OPEN ACCESS

EDITED BY
Bruno André Lopes,
Southfields Veterinary Specialists,
United Kingdom

REVIEWED BY
Sam Long,
Veterinary Referral Hospital, Australia
Daniel Sanchez-Masian,
Hospital Veterinario de Referencia Veterios, Spain
Virginia Crespo,
Southfields Veterinary Specialists,
United Kingdom

*CORRESPONDENCE
Nicholas Rancilio
✉ rancilio@iastate.edu

†These authors have contributed equally to this work

RECEIVED 07 February 2025
ACCEPTED 24 March 2025
PUBLISHED 09 May 2025

CITATION
Rancilio N, Drozd M, Donaldson L, Harm T and Murakami K (2025) Oligodendroglioma pseudoprogression after radiotherapy in a dog: a case report. *Front. Vet. Sci.* 12:1572808. doi: 10.3389/fvets.2025.1572808

Oligodendroglioma pseudoprogression after radiotherapy in a dog: a case report

Nicholas Rancilio[1*†], Mary Drozd[2†], Logan Donaldson[3†], Tyler Harm[4] and Keiko Murakami[1]

[1]Department of Veterinary Clinical Sciences, Iowa State University, Ames, IA, United States, [2]School of Veterinary Medicine and Biomedical Sciences, University of Nebraska-Lincoln, Lincoln, NE, United States, [3]VCA Midwest Veterinary Emergency & Referral Center, Neurology & Neurosurgery, Omaha, NE, United States, [4]Department of Veterinary Pathology, Iowa State University, Ames, IA, United States

Pseudoprogression is a clinical and imaging phenomenon characterized by an increase in the size and contrast enhancement pattern of a glioma lesion following treatment with radiotherapy. In human beings, a substantial body of literature describes the phenomenon of pseudoprogression in glioblastoma after radiotherapy. The occurrence of gliomas in the cranial nerves has been reported in human beings as a clinically rare entity. A 7-year-old spayed female French Bulldog was presented with left-sided craniofacial muscle atrophy for a duration of 3 months and episodes of compulsive circling to the left. After a neurological examination, a magnetic resonance (MR) imaging scan of the brain was performed. A T2-and T2 FLAIR-weighted hyperintense, non-contrast-enhancing, T1-weighted hypointense intra-axial suprasellar lesion was found. In addition, an extra-axial, T1-weighted hyperintense, contrast-enhancing mass was identified at the level of the left trigeminal nerve. The lesions were presumptively diagnosed as a glioma and a left trigeminal nerve sheath tumor based on their imaging characteristics and the breed of the patient. A course of stereotactic radiotherapy (SRT) was prescribed, and 3 months after treatment, there was significant progression in the size of the suprasellar mass, indicative of either true progression or pseudoprogression. The left trigeminal nerve mass remained stable in size. Treatment with glucocorticoids resulted in a reduction in the size of the suprasellar mass, as observed on MR imaging 7 months after treatment. The left trigeminal nerve mass remained stable in size. Progression in the size of the suprasellar mass and the left trigeminal nerve mass occurred 9 months after the first course of treatment, and a second course of stereotactic radiotherapy was administered. Sixteen months after the first course of radiotherapy, a necropsy was performed. The suprasellar lesion and the left trigeminal nerve lesion were diagnosed as oligodendrogliomas on histopathology. Trigeminal nerve oligodendrogliomas and pseudoprogression following radiotherapy have not been previously described in dogs. Pseudoprogression should be considered a differential diagnosis for the progression of presumed or confirmed glioma lesions after treatment with radiotherapy. Concurrent oligodendroglioma lesions in the trigeminal nerve are also possible and should be included in the list of differential diagnoses for dogs with concurrent brain lesions.

KEYWORDS

glioma, oncology, MRI, pseudoprogression, oligodendroglioma, brachycephalic, trigeminal nerve, cranial nerves

1 Introduction

Pseudoprogression is a clinical and imaging phenomenon in gliomas, where the size and contrast enhancement pattern of the lesion on magnetic resonance (MR) imaging increases within 1 to 6 months following treatment with radiotherapy. The incidence of pseudoprogression varies widely, ranging from 9 to 30% in humans with gliomas (1–4). Pseudoprogression is most likely induced by a pronounced local tissue reaction involving inflammation, edema, and abnormal vessel permeability, leading to new or increased contrast enhancement on MR imaging (5, 6). Some studies have found an association between the incidence of pseudoprogression and improved survival, potentially attributable to an active inflammatory response against the tumor (7).

A decline in neurological function may accompany the imaging changes observed in pseudoprogression, or these imaging changes may be clinically silent. Pseudoprogression is managed conservatively with supportive care, such as glucocorticoids, or, in severe cases, with hospitalization and medical management of clinical signs (seizure medications, hypertonic saline, and mannitol). Serial imaging demonstrates a reduction in the lesion following the initiation of supportive care. Pseudoprogression of gliomas is well described in humans and presents a diagnostic challenge for neuro-oncologists in terms of appropriate case management (8). In this report, we present the case of a dog affected with a suprasellar oligodendroglioma and a concurrent trigeminal nerve oligodendroglioma, which was treated with stereotactic radiotherapy. The dog developed pseudoprogression 3 months after completing treatment, as evidenced by serial MR imaging at regular intervals. A summary timeline of key clinical events in this case is presented in Table 1. Understanding the phenomenon of pseudoprogression is important for confirming that post-treatment gliomas in dogs may behave similarly to those in human beings. In addition, clinicians managing dogs affected with gliomas should consider pseudoprogression following radiotherapy, as it can mimic the clinical signs of true tumor progression. Oligodendroglioma lesions in the trigeminal nerve are also possible and should be included in the list of differential diagnoses for dogs with concurrent brain lesions.

2 Manuscript formatting

2.1 Headings

2.1.1 Case description

A 7-year-old spayed female French Bulldog was presented with left-sided masseter and temporalis muscle atrophy for a duration of 3 months and episodes of compulsive circling to the left. Diffuse atrophy of the muscles of mastication was present; palpation of individual muscle bellies was clinically impossible due to the degree of atrophy and the patient's conformation at the time of the initial presentation. A right head tilt and right-sided facial paralysis were also noted on clinical examination. Absence of left-sided facial sensation and corneal sensation was not detected. Neuroanatomical localization was multifocal in nature, with clinical signs localizing to the left trigeminal nerve (motor and sensory branches), the right vestibular system, the right facial nerve, the midbrain (mesencephalon), and the pons (metencephalon). Magnetic resonance imaging of the brain was subsequently performed. All MR images were acquired using a high-field GE Excite HDX 1.5 T magnet (Milwaukee, WI), and intravenous contrast was administered using gadolinium 0.2 mL/kg (Clariscan, GE Healthcare, Marlborough, MA), unless otherwise noted. Lesion measurements on MR imaging were performed by a board-certified radiologist and measured in mm at the widest diameter from the rostral-caudal (RC), medial-lateral (ML), and dorsal-ventral (DV) axes in all studies performed.

A T1-weighted hyperintense, extra-axial, contrast-enhancing mass was noted in the left trigeminal nerve at the level of the pons (metencephalon) (Supplementary Figures 1A, 6A). The lesion was T2-weighted and T2-weighted FLAIR hyperintense and was 7.5 mm at the widest diameter. A presumptive diagnosis of trigeminal nerve sheath tumor was made based on these imaging findings and the neurologic examination. A T1-weighted hypointense, non-contrast-enhancing intra-axial suprasellar lesion was also evident. This lesion was T2-weighted hyperintense and had a heterogenous pattern of T2-weighted FLAIR hypointensity and hyperintensity within and surrounding the lesion. The suprasellar lesion measured 17 mm x 12 mm x 14 mm (Figure 1A and Supplementary Figures 2A–D). Given the breed and imaging changes, this lesion was presumptively diagnosed as a glioma.

Computed tomography (CT) simulation was performed for radiotherapy treatment planning of the brain, and CT images of the abdomen were also acquired for staging purposes, in accordance with our institutional protocol for radiotherapy patients (Toshiba Aquillon LB 32 Slice, Canon, Tustin, CA). Computed tomography was performed with a 1-mm slice thickness, both prior to and following intravenous contrast administration (Omnipaque 240 mg/mL, 1 mL/lb., GE Healthcare, Chicago, IL). No planning target volume (PTV) was applied due to the size and proximity of each lesion to one another, as well as the sensitive location of the masses adjacent to the brainstem. For the suprasellar lesion, the gross tumor volume (GTV) was defined as all areas of abnormal T2-weighted FLAIR hyper/hypointensity and all areas of abnormal T1-weighted hypointensity. As the suprasellar lesion was poorly defined on CT imaging, CT was not used for lesion contouring. For the left trigeminal nerve mass, the GTV was defined as all abnormal T1 contrast-enhancing areas around the lesion. Any abnormal contrast-enhancing areas evident on CT imaging were also used to contour/define the GTV of the left trigeminal nerve mass. Stereotactic radiotherapy (SRT) was administered on consecutive weekdays using a linear accelerator, with 7 Gy × 3 fractions for a total dose of 21 Gy to both lesions. Treatment plans were developed using the Varian Eclipse treatment planning system, employing nine coplanar fixed gantry angle intensity-modulated radiotherapy fields (IMRT). The plan underwent a quality assurance check prior to delivery using the Varian portal dosimetry system and was calculated with the Varian Eclipse AAA v13.6 algorithm, utilizing a grid size of 1 mm. Prior to each fraction, a cone beam computed tomography (CBCT) scan was performed to verify patient positioning. All equipment used for administering and planning radiotherapy was

10.3389/fvets.2025.1572808

TABLE 1 Description of suprasellar oligodendroglioma lesion progression and interventions during treatment.

Time point	Suprasellar lesion longest diameter	% lesion longest diameter increase/ decrease	RECIST response	Radiotherapy prescription	Prednisone dosages
0 (pretreatment)	17 mm	-	-	SRT 7 Gy x 3 fractions	0.5 mg/kg/day
3 months	24 mm	41%	Progressive	-	0.14 mg/kg/day
7 months	18 mm	6%	Stable disease	-	0.14 mg/kg/day
9 months	20 mm	18%	Stable (clinically progressive)	SRT 8 Gy x 3 fractions	0.5 mg/kg/day

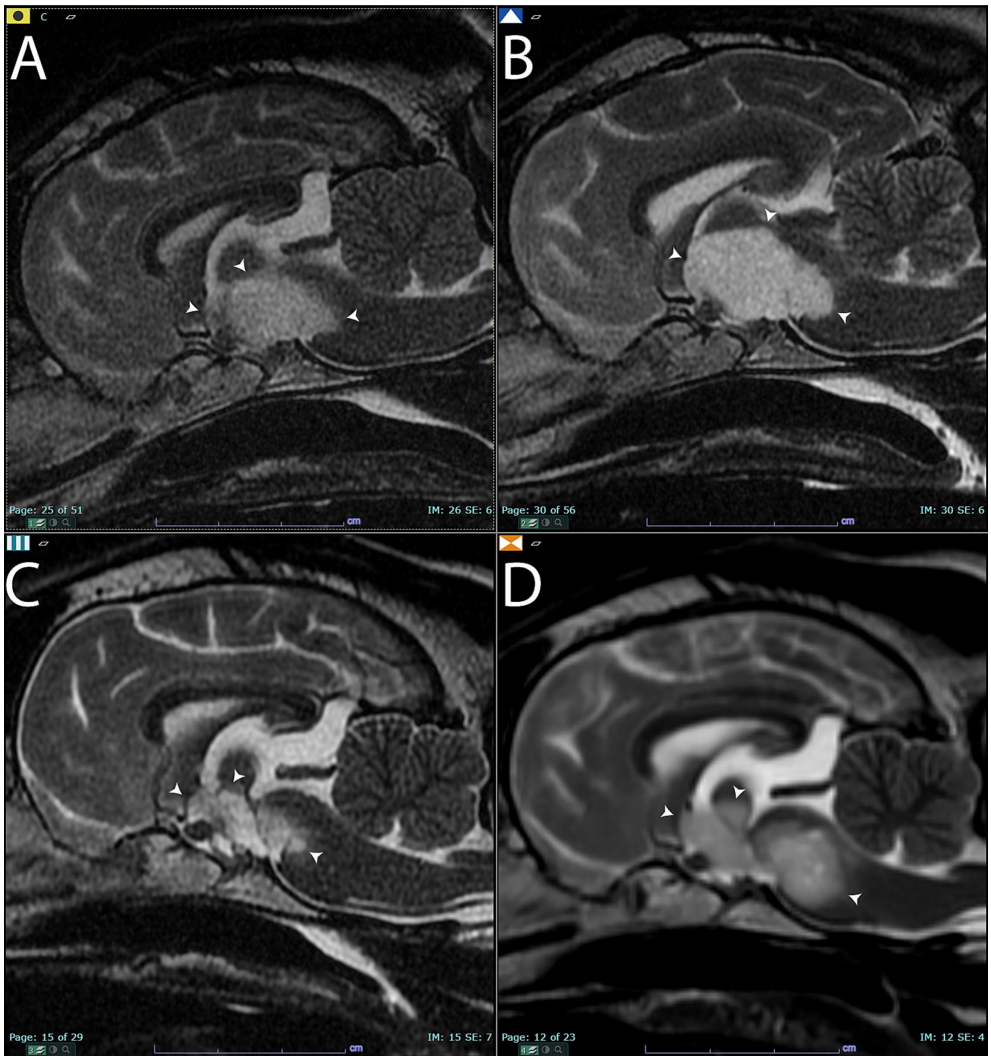

FIGURE 1
Sagittal T2-weighted images of the brain **(A)** before treatment. Arrowheads point to the T2 hyperintense lesion that was later diagnosed on histopathology as an oligodendroglioma. **(B)** Sagittal T2-weighted images of the brain 3 months after completing the first course of stereotactic radiotherapy. There was a qualitative and quantitative increase in the size of the mass (arrowheads) compared to panel **(A)**. Panel **(C)**, 7 months after completing stereotactic radiotherapy. The mass had significantly shrunk in size (arrowheads). Panel **(D)**, 9 months after completing stereotactic radiotherapy. Note the increased size of the mass (arrowheads) compared to panels **(A,C)**.

manufactured by Varian (Clinac Ix Linear Accelerator with 6MV photons, Eclipse, Portal Dosimetry-Varian Medical Systems, Palo Alto, CA). The patient was also prescribed prednisone (0.5 mg/kg once daily) by mouth to mitigate any potential intracranial inflammation that could result from radiotherapy (PrednisTab, Lloyd, Shenandoah, IA, USA). Table 1 provides additional details about the prednisone dosages throughout the management of this case.

Three months after completing SRT, the patient was presented for re-evaluation and follow-up MR imaging. The patient continued to exhibit intermittent circling behavior, and the masticatory muscle atrophy on the left side remained unchanged from previous

assessments. In the MR imaging, the lesion in the left trigeminal nerve was similar in size, shape, and T1-weighted post-contrast hyperintensity (Supplementary Figures 1B, 6B). However, the suprasellar lesion increased in size, measuring 24 mm x 15 mm x 10 mm at the widest diameters. The lesion appeared more T1-weighted hypointense than in the previous set of images, and a focal area of contrast enhancement was evident (Figure 1B and Supplementary Figure 3). The imaging changes were interpreted as either true progression of the presumed glioma or pseudoprogression, based on the response evaluation criteria in solid tumors v1.0 (RECIST) for dogs (9). The patient was continued on prednisone therapy but at a reduced dose due to reported clinical signs of anxiousness and panting at night (Table 1).

Six months after completing the first course of radiotherapy, the patient was presented with a ruptured corneal ulcer in the left eye. Enucleation and exenteration were performed, and the left globe was submitted for histopathology. No neoplasia was noted in the histopathologic examination of the left globe, and the diagnosis was characterized as perforating and ulcerative keratitis with corneal rupture and iris prolapse. Subacute fibrinosuppurative endophthalmitis with hyphema was also noted.

Seven months after the completion of the SRT course 1, the patient was re-evaluated. The circling behavior had resolved, and the MR imaging was repeated. The suprasellar mass lesion had decreased in size compared to previous imaging studies and measured 18 mm x 10 mm x 10 mm at the widest diameter. There was no contrast enhancement of the suprasellar mass, and it continued to have a similar pattern of heterogenous T2-weighted and T2-weighted FLAIR hyperintensity and hypointensity (Figure 1C and Supplementary Figure 4). Based on the RECIST criteria, the suprasellar mass was characterized as a stable disease compared to the pretreatment imaging. The left trigeminal nerve lesion remained unchanged in size and was also characterized as a stable disease based on the RECIST criteria at this same time point (Supplementary Figures 1C, 6C).

Nine months after the completion of SRT, the patient returned for evaluation due to the development of a right-sided head tilt and circling behaviors to both the left and right sides. A follow-up MR imaging study was performed using a 1.5 T high field magnet (GE Signa, Milwaukee, WI) both prior to and following the administration of 0.2 mL/kg of gadolinium (Clariscan, GE Healthcare, Marlborough, MA). Both the left trigeminal nerve (Supplementary Figures 1D, 6D) and suprasellar lesions were characterized as progressive disease based on the worsening clinical signs and an increase in size of the masses (Figure 1D and Supplementary Figure 5). The suprasellar lesion exhibited similar heterogenous T2-weighted and T2-weighted FLAIR hyperintensity and hypointensity, measuring 20 mm x 9 mm x 12 mm. Based on the clinical and imaging changes, a second course of SRT was prescribed using the same technique and equipment described above. A radiation prescription of 8 Gy x 3 fractions on consecutive weekdays was administered to both lesions, and the dose of prednisone was increased to 0.5 mg/kg per day by mouth. The increased prednisone dosage was chosen to limit the potential for radiotherapy-induced intracranial inflammation. The patient was euthanized 6 months after the second course of SRT due to the declining quality of life and worsening neurological clinical signs, as reported by the dog's owner. Additional in-clinic follow-up was not performed after the completion of the second course of radiotherapy. The overall survival time was 16 months following the initiation of the first course of SRT.

2.1.2 Necropsy findings

The left facial muscles were diffusely and markedly atrophied, and the left eye was absent. The left cranial nerves, including the maxillary and ciliary nerves, had ill-defined axonal margins compared to the contralateral nerves. The left ventral piriform lobe was enlarged and asymmetric, protruding (approximately 2 cm x 1 cm x 0.5 cm) along the ventral, medial, and rostral margins. The left half of the pons was similarly, mildly enlarged, and the adjacent meninges were dilated with watery, red fluid. On transection, the optic chiasm, fornix column, thalamus, third ventricle, and surrounding structures were effaced by necrosis. Proceeding caudally, transverse sections of the hypothalamus and ventral thalamus were severely to markedly effaced by a 9 mm x 6 mm, dark red to dark, indistinctly delineated neoplastic mass. The mass extended through successive sections of the mesencephalon and pons and infiltrated laterally toward the cerebellar peduncles (rostral and mid-cerebral peduncles). The areas of malacia extended through the center of the brain stem. The asymmetry of the gyri and sulci was occasionally associated with ill-defined areas of darker, softer neuropil (Figure 2).

Additional necropsy findings included acute, hemorrhagic typhlocolitis, lipid hepatopathy, and dermal hyperpigmentation and alopecia consistent with chronic corticosteroid treatment.

2.1.3 Histopathologic descriptions

Infiltrating the cranial nerves and ventral meninges and effacing the normal architecture of the hypothalamus and thalamus, the neoplastic mass extended into the brainstem and meninges of the cervical spinal cord. It was composed of polygonal cells arranged in sheets, cords, and pseudorosettes, interspersed with small, occasionally tortuous vessels. The surrounding neuropil was extensively effaced by abundant edema and mild to moderate glial inflammation, with occasional neuron degeneration. The neoplastic cells exhibited variable amounts of pale, eosinophilic to clear cytoplasm, with typically distinct cell borders. The irregular, round nuclei had coarse

FIGURE 2
A cross-section of the brain at the level of the mid-brain formalin-fixed section. The ventral midbrain was effaced by the neoplastic mass, with pallor and infiltration of the neoplasm toward the ventral right margin and right of the central mass (arrowheads). There was a similar mass in the left trigeminal nerve (asterisk).

to stippled chromatin and occasionally contained a small nucleolus. There was mild anisocytosis, anisokaryosis, and pleomorphic variation. A total of 16 mitotic figures were counted in 2.4 mm^2. The surrounding neuropil was extensively effaced by abundant edema, with mild to moderate glial inflammation and occasional neuron degeneration present. The neoplastic cells in the left trigeminal nerve and ganglion were similar to those in the primary mass (Figures 3A–C).

2.1.4 Immunohistochemical findings

The neoplastic cells in multiple areas of the neoplasm were moderately to strongly positive for Olig2 and consistent with oligodendroglioma. Oligo2 highlighted areas of neoplastic cell infiltration into the surrounding neuropil. While GFAP was negative within the neoplasm, the areas of neoplasm infiltration overlapped with glial inflammation at the neoplasm margins (Figures 3D,E) (10).

3 Discussion

To the best of our knowledge, this is the first report of a dog with histological confirmation of malignancy describing pseudoprogression of an oligodendroglioma, with serial follow-up imaging after stereotactic radiotherapy. In a series of dogs treated with radiotherapy for presumed gliomas, one dog was reported to have clinically silent lesion progression 620 days after the completion of radiotherapy (11). The authors in this series speculated that this silent lesion progression might be pseudoprogression, but no necropsy or other histological confirmation of malignancy was performed. Pseudoprogression and late radiation necrosis have overlapping pathological and imaging characteristics, and there is controversy regarding the temporality of these phenomena (6). Late radiotherapy-induced brain necrosis does not occur until 6 months or later after the completion of treatment; pseudoprogression has also been reported in some cases 6 months after treatment (12). Therefore, the overlap in temporality between late radiation necrosis and pseudoprogression can confound clinicopathologic categorization when a progressive lesion occurs at the 6-month time point. In our case, the presence of a progressive lesion within 3 months of treatment, followed by regression of the lesion on serial imaging, places the observed findings within the category of pseudoprogression.

Canine brain tumors are reported to have a molecular overlap with human pediatric brain tumors (13). Pseudoprogression after radiotherapy or chemoradiotherapy is reported at higher rates in humans with MGMT promoter methylation in glioblastoma multiforme (14). The present case involves a high-grade oligodendroglioma, not glioblastoma multiforme. MGMT methylation is not a commonly reported characteristic of human oligodendroglioma. However, in human beings, a common driving mutation in oligodendroglioma development is IDH-1 mutations, which may also be present occasionally in canine oligodendroglioma (13). Pseudoprogression in human oligodendroglioma is also reported to occur in both IDH-1 wild-type and mutant oligodendrogliomas (15). The IDH-1 mutation status of our patient is unknown since testing for this mutation is not widely available in dogs.

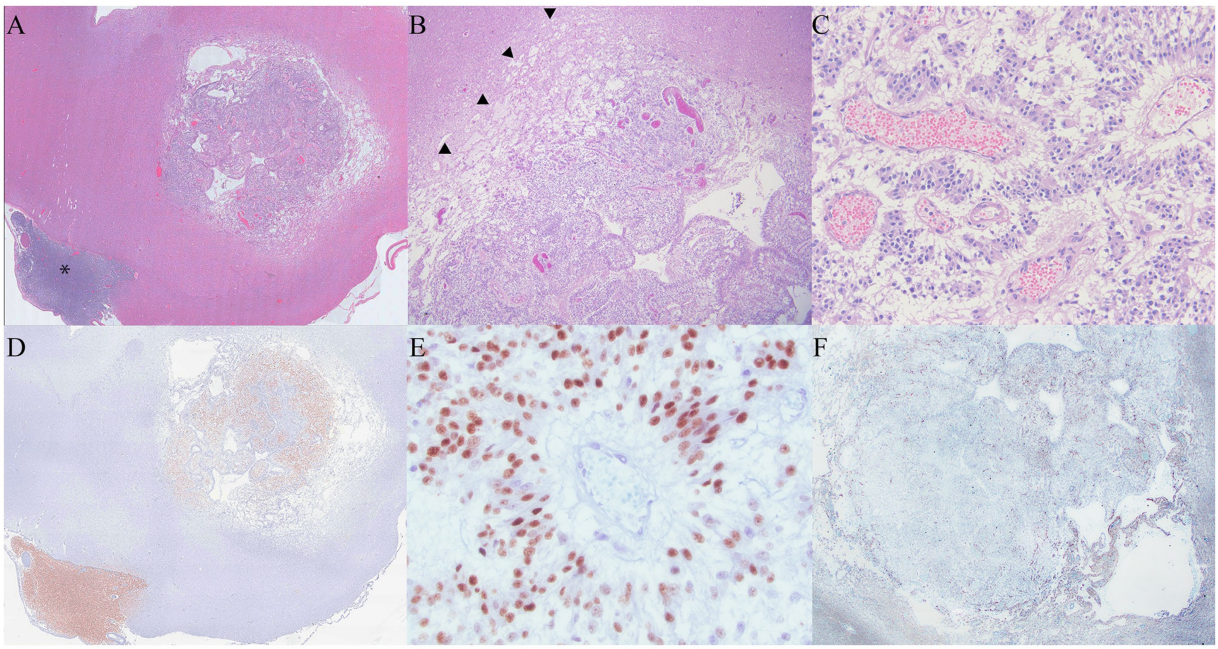

FIGURE 3
(A) At 1.5x magnification, the primary mass had a rim of pallor surrounding the neoplasm. The metastatic mass associated with the trigeminal nerve is identified with an asterisk. **(B)**: The rim of pallor (arrowheads) was composed of edema and necrosis consistent with pseudoprogression. **(C)**: Inset of 3c. The neoplasm was composed of polygonal cells arranged in the form of sheets and cords, infiltrated by tortuous, congested vessels. Pseudorossettes organized around congested vessels are features supportive of an oligodendroglioma diagnosis. **(D)** Neoplastic cells in both the primary mass and the mass overlying the trigeminal nerve were positive for Olig2 (Olig 2 immunohistochemistry). **(E)** At 400x magnification, Olig2 histochemistry staining was moderately to strongly positive within the neoplastic cells. **(F)** GFAP staining was negative within the primary neoplasm, and there was mild to moderate staining in the surrounding areas of necrosis.

This case presented a clinical challenge in determining recommendations for the owners regarding the next steps for continued management, as progressive lesions were found on serial MR imaging 3 months after the initial treatment. In our clinical experience, owners of brain tumor dogs with a progressive mass lesion on follow-up imaging often elect euthanasia due to the presumed lack of clinical response to treatment. However, the patient in the present case exhibited mostly mild clinical signs that were manageable on an outpatient basis, and euthanasia was discouraged. The finding of a progressive primary lesion and the likely diagnosis of a glioma required careful counseling of the owner regarding the need for serial follow-up imaging to characterize the behavior of the lesions. Therefore, this case highlights the importance of considering pseudoprogression in the differential diagnosis for dogs with a confirmed or strongly presumed glioma when progressive lesions are observed on the MR imaging after the completion of radiotherapy. Notably, despite the presence of pseudoprogression and true progression, the survival time in our patient is consistent with the survival time reported in the literature for presumed intracranial gliomas (11–21 months) (16–21).

While the patient in this report was treated with prednisone throughout the course of the disease, the inclusion of this medication is unlikely to have had much effect on the outcome. The dog was on the highest dose of prednisone before developing the pseudoprogressive lesion and was subsequently tapered to lower doses of prednisone when pseudoprogression was noted due to reported anxiousness and panting. Prednisone was initiated before radiotherapy with the intention of gradually reducing the dose to the lowest effective dose for controlling neurologic clinical signs. Until rather recently, prednisone dosing in veterinary radiotherapy for brain tumors has been anecdotal and not based on high levels of evidence. Prospective data that demonstrate the safety of rapidly tapering the dose of prednisone after the completion of radiotherapy for brain tumors have become available (22). The present case was treated prior to the publication of this data; therefore, the exact protocol from the aforementioned manuscript was not followed. Prednisone dosage was increased before starting a second course of radiotherapy, which was consistent with the findings of our clinical experience.

During treatment, the patient developed clinical signs consistent with a left corneal ulcer and rupture after the first course of radiotherapy. A subsequent neurological examination of this patient indicated no complete loss of corneal sensation or facial paralysis on the left side. It is possible that radiotherapy could have damaged the facial nerve due to the proximity of the treatment to the facial canal, and the presence of these clinical findings could indicate a late side effect of radiotherapy. No evidence of tumor extension into the left globe was found upon histological examination of the eye after enucleation.

The patient in the present case had a concurrent oligodendroglioma lesion in the left trigeminal nerve and ganglion. Trigeminal nerve oligodendroglioma has not been reported in dogs, and there are very few reports of its occurrence in human beings, with a total of 16 cases (23, 24). It is speculated that the extension of primary oligodendroglioma into the trigeminal nerve may occur through the infiltration of the tumor along the white matter tracts and through the root entry zone and proximal cisternal segments (23, 24). It is also well documented that oligodendrogliomas in dogs are capable of drop metastasis throughout the central nervous system. Drop metastasis is believed to occur when tumor cells seed through the ventricular system, leading to metastases distant from the primary tumor, appearing throughout the rest of the brain and spinal cord as the disease progresses (25–27). It is unknown in the present case whether the concurrent oligodendroglioma lesions represent drop metastasis, extension of one of the lesions to the other location, or simply concurrent primary tumors (independent events). We were unable to demonstrate antemortem or postmortem evidence for any of these scenarios.

In conclusion, pseudoprogression of oligodendrogliomas occurs in dogs and should be considered in the differential diagnoses of progressive masses and clinical signs following the completion of radiotherapy. Concurrent lesions in the cranial nerves, such as the trigeminal nerve, may also be oligodendrogliomas and should be included in the list of differential diagnoses.

Data availability statement

The raw data supporting the conclusions of this article will be made available by the authors, without undue reservation.

Ethics statement

Ethical approval was not required for the studies involving animals in accordance with the local legislation and institutional requirements because the work presented reports the outcomes for a client-owned animal that underwent treatment for a neurological condition as part of routine health care for oncologic conditions (brain tumor). Since this was conducted in the context of a veterinary-client-patient relationship no priori ethical approval was required. Written informed consent was obtained from the owners for the participation of their animals in this study. Written informed consent was obtained from the participants for the publication of this case report.

Author contributions

NR: Writing – original draft, Writing – review & editing. MD: Writing – original draft, Writing – review & editing. LD: Writing – original draft, Writing – review & editing. TH: Writing – original draft, Writing – review & editing. KM: Writing – original draft, Writing – review & editing.

Funding

The author(s) declare that no financial support was received for the research and/or publication of this article.

Acknowledgments

The authors wish to thank the client and pet described in this manuscript for their donation to science.

Conflict of interest

The authors declare that the research was conducted in the absence of any commercial or financial relationships that could be construed as a potential conflict of interest.

Generative AI statement

The authors declare that no Gen AI was used in the creation of this manuscript.

Publisher's note

Supplementary material

The Supplementary material for this article can be found online at: https://www.frontiersin.org/articles/10.3389/fvets.2025.1572808/full#supplementary-material

SUPPLEMENTARY FIGURE 1
Axial T1 weighted +C images at the level of the rostral pons **(A–D)**. Note the contrast enhancing T1 hyperintense extra-axial lesion at the left trigeminal nerve **(A)**. This lesion was diagnosed as an oligodendroglioma. **(B)** 3 months after treatment with radiotherapy the oligodendroglioma remains stable in size. **(C)** 7 months after treatment with radiotherapy. (D) 9 months after treatment with radiotherapy the lesion has progressed in size. Note also the left tympanic bulla in figure **(D)** contains effusion. This is likely due to dysfunction of the eustachian tube secondary to denervation of the tensor veli palatini muscle which is innervated by the mandibular branch of the trigeminal nerve.

SUPPLEMENTARY FIGURE 2
Axial images at the level of the pituitary gland demonstrating the pre treatment appearance of the oligodendroglioma. **(A)** T1 weighted images, **(B)** T1 weighted+Contrast images, **(C)** T2 weighted images, **(D)** T2 FLAIR weighted images. The tumor is delineated by the arrows in each panel.

SUPPLEMENTARY FIGURE 3
Axial images at the level of the pituitary gland 3 months after treatment with radiotherapy demonstrating pseudoprogression of the oligodendroglioma. **(A)** T1 weighted images, **(B)** T1+Contrast weighted images-note the area of new contrast enhancement (*), **(C)** T2 weighted images, **(D)** T2 FLAIR weighted images. The lesion is delineated by the arrows in each panel.

SUPPLEMENTARY FIGURE 4
Axial images at the level of the pituitary gland 7 months after treatment with radiotherapy demonstrating decrease in size of the oligodendroglioma lesion. **(A)** T1 weighted images, **(B)** T1 weighted +Contrast image, **(C)** T2 weighted images, **(D)** T2 FLAIR weighted images. The lesion is delineated by the arrows in each panel. The area of contrast enhancement around the lesion is no longer visible in panel **(B)** or any of the other planes examined.

SUPPLEMENTARY FIGURE 5
Axial images at the level of pituitary gland 9 months after treatment with radiotherapy demonstrating progression in size of the oligodendroglioma lesion. **(A)** T1 weighted images, **(B)** T1 weighted +Contrast image, **(C)** T2 weighted images, **(D)** T2 FLAIR weighted images. The lesion is delineated by the arrows in each panel.

SUPPLEMENTARY FIGURE 6
Dorsal T1 weighted + contrast images at approximately the level of the trigeminal nerve/trigeminal ganglion. **(A)** prior to treatment. **(B)** 3 months after treatment with radiotherapy. **(C)** 7 months after treatment with radiotherapy. **(D)** 9 months after treatment with radiotherapy. The arrow heads in each panel demonstrate the extra-axial lesion in the trigeminal nerve. It was not possible to image the trigeminal ganglion exactly at each time point due to differences in positioning, machines, and differences in size of the primary suprasellar lesion causing displacement of normal structures.

References

1. Wick W, Chinot OL, Bendszus M, Mason W, Henriksson R, Saran F, et al. Evaluation of pseudoprogression rates and tumor progression patterns in a phase III trial of bevacizumab plus radiotherapy/temozolomide for newly diagnosed glioblastoma. *Neuro-Oncol.* (2016) 18:1434–41. doi: 10.1093/neuonc/now091

2. Radbruch A, Fladt J, Kickingereder P, Wiestler B, Nowosielski M, Bäumer P, et al. Pseudoprogression in patients with glioblastoma: clinical relevance despite low incidence. *Neuro-Oncol.* (2015) 17:151–9. doi: 10.1093/neuonc/nou129

3. Balaña C, Capellades J, Pineda E, Estival A, Puig J, Domenech S, et al. Pseudoprogression as an adverse event of glioblastoma therapy. *Cancer Med.* (2017) 6:2858–66. doi: 10.1002/cam4.1242

4. Topkan E, Topuk S, Oymak E, Parlak C, Pehlivan B. Pseudoprogression in patients with glioblastoma multiforme after concurrent radiotherapy and temozolomide. *Am J Clin Oncol.* (2012) 35:284–9. doi: 10.1097/COC.0b013e318210f54a

5. Hygino da Cruz LC, Rodriguez I, Domingues RC, Gasparetto EL, Sorensen AG. Pseudoprogression and pseudoresponse: imaging challenges in the assessment of posttreatment glioma. *AJNR Am J Neuroradiol.* (2011) 32:1978–85. doi: 10.3174/ajnr.A2397

6. Brandsma D, Stalpers L, Taal W, Sminia P, van den Bent MJ. Clinical features, mechanisms, and management of pseudoprogression in malignant gliomas. *Lancet Oncol.* (2008) 9:453–61. doi: 10.1016/S1470-2045(08)70125-6

7. Gunjur A, Lau E, Taouk Y, Ryan G. Early post-treatment pseudo-progression amongst glioblastoma multiforme patients treated with radiotherapy and temozolomide: a retrospective analysis. *J Med Imaging Radiat Oncol.* (2011) 55:603–10. doi: 10.1111/j.1754-9485.2011.02319.x

8. Rossmeisl JH, Garcia PA, Daniel GB, Bourland JD, Debinski W, Dervisis N, et al. Invited REVIEW—neuroimaging response assessment criteria for BRAIN tumors in veterinary patients. *Vet Radiol Ultrasound Off J Am Coll Vet Radiol Int Vet Radiol Assoc.* (2014) 55:115–32. doi: 10.1111/vru.12118

9. Nguyen SM, Thamm DH, Vail DM, London CA. Response evaluation criteria for solid tumours in dogs (v1.0): a veterinary cooperative oncology group (VCOG) consensus document. *Vet Comp Oncol.* (2015) 13:176–83. doi: 10.1111/vco.12032

10. Koehler JW, Miller AD, Miller CR, Porter B, Aldape K, Beck J, et al. A revised diagnostic classification of canine glioma: towards validation of the canine glioma patient as a naturally occurring preclinical model for human glioma. *J Neuropathol Exp Neurol.* (2018) 77:1039–54. doi: 10.1093/jnen/nly085

11. Dolera M, Malfassi L, Bianchi C, Carrara N, Finesso S, Marcarini S, et al. Frameless stereotactic radiotherapy alone and combined with temozolomide for presumed canine gliomas. *Vet Comp Oncol.* (2018) 16:90–101. doi: 10.1111/vco.12316

12. Saito N, Hirai N, Sato S, Hayashi M, Iwabuchi S. Delayed Pseudoprogression in glioblastoma patients treated with tumor-treating fields. *Cureus.* (2024) 16:e55147. doi: 10.1093/nop/npad063

13. Amin SB, Anderson KJ, Boudreau CE, Martinez-Ledesma E, Kocakavuk E, Johnson KC, et al. Comparative molecular life history of spontaneous canine and human gliomas. *Cancer Cell.* (2020) 37:243–257.e7. doi: 10.1016/j.ccell.2020.01.004

14. Blakstad H, Mendoza Mireles EE, Heggebø LC, Magelssen H, Sprauten M, Johannesen TB, et al. Incidence and outcome of pseudoprogression after radiation therapy in glioblastoma patients: a cohort study. *Neurooncol Pract.* (2024) 11:36–45.

15. Bronk JK, Guha-Thakurta N, Allen PK, Mahajan A, Grosshans DR, McGovern SL. Analysis of pseudoprogression after proton or photon therapy of 99 patients with low grade and anaplastic glioma. *Clin Transl Radiat Oncol.* (2018) 9:30–4. doi: 10.1016/j.ctro.2018.01.002

16. Rohrer Bley C, Staudinger C, Bley T, Marconato L, Sabattini S, Beckmann K. Canine presumed glial brain tumours treated with radiotherapy: is there an inferior outcome in tumours contacting the subventricular zone? *Vet Comp Oncol.* (2022) 20:29–37. doi: 10.1111/vco.12703

17. Urso G, Boncu AG, Carrara N, Zaman DT, Malfassi L, Marcarini S, et al. Cranial spinal spreading of canine brain gliomas after Hypofractionated volumetric-modulated

arc radiotherapy and concomitant Temozolomide chemotherapy: a four-case report. *Vet Sci*. (2022) 9:541. doi: 10.3390/vetsci9100541

18. Debreuque M, De Fornel P, David I, Delisle F, Ducerveau MN, Devauchelle P, et al. Definitive-intent uniform megavoltage fractioned radiotherapy protocol for presumed canine intracranial gliomas: retrospective analysis of survival and prognostic factors in 38 cases (2013-2019). *BMC Vet Res*. (2020) 16:412. doi: 10.1186/s12917-020-02614-x

19. Moirano SJ, Dewey CW, Haney S, Yang J. Efficacy of frameless stereotactic radiotherapy for the treatment of presumptive canine intracranial gliomas: a retrospective analysis (2014-2017). *Vet Comp Oncol*. (2020) 18:528–37. doi: 10.1111/vco.12573

20. Trageser E, Martin T, Burdekin B, Hart C, Leary D, LaRue S, et al. Efficacy of stereotactic radiation therapy for the treatment of confirmed or presumed canine glioma. *Vet Comp Oncol*. (2023) 21:578–86. doi: 10.1111/vco.12920

21. Magalhaes TR, Benoit J, Necova S, North S, Queiroga FL. Outcome after radiation therapy in canine intracranial Meningiomas or gliomas. *In-Vivo*. (2021) 35:1117–23. doi: 10.21873/invivo.12357

22. Strasberg JR, Rossmeisl JH, Kelsey KL, Yoshikawa H, Gieger TL, Nolan MW. A prospective evaluation of succinct prednisone tapering after brain tumor irradiation in dogs. *J Vet Intern Med*. (2024) 38:2571–7. doi: 10.1111/jvim.17163

23. Ganapathy S, Baliga V. Primary oligodendroglioma of the trigeminal nerve – a very rare case report. *Interdiscip Neurosurg*. (2020) 22:100799. doi: 10.1016/j.inat.2020.100799

24. Mabray MC, Glastonbury CM, Mamlouk MD, Punch GE, Solomon DA, Cha S. Direct cranial nerve involvement by gliomas: case series and Review of the literature. *AJNR Am J Neuroradiol*. (2015) 36:1349–54. doi: 10.3174/ajnr.A4287

25. Bentley RT, Yanke AB, Miller MA, Heng HG, Cohen-Gadol A, Rossmeisl JH. Cerebrospinal fluid drop Metastases of canine glioma: magnetic resonance imaging classification. *Front Vet Sci*. (2021) 8:650320. doi: 10.3389/fvets.2021.650320

26. Vigeral M, Bentley RT, Rancilio NJ, Miller MA, Heng HG. Imaging diagnosis-antemortem detection of oligodendroglioma "Cerebrospinal fluid drop metastases" in a dog by serial magnetic resonance imaging. *Vet Radiol Ultrasound*. (2018) 59:E32–7. doi: 10.1111/vru.12474

27. Rancilio NJ, Murakami K, Harm T, Christensen N. Radiation therapy communication: retreatment of multiple histologically confirmed oligodendroglioma drop metastasis with stereotactic radiotherapy in a dog. *Vet Radiol Ultrasound*. (2025) 66:e13454. doi: 10.1111/vru.13454

Frontiers in Veterinary Science

Transforms how we investigate and improve animal health

The third most-cited veterinary science journal, bridging animal and human health with a comparative approach to medical challenges. It explores innovative biotechnology and therapy for improved health outcomes.

Discover the latest Research Topics

See more →

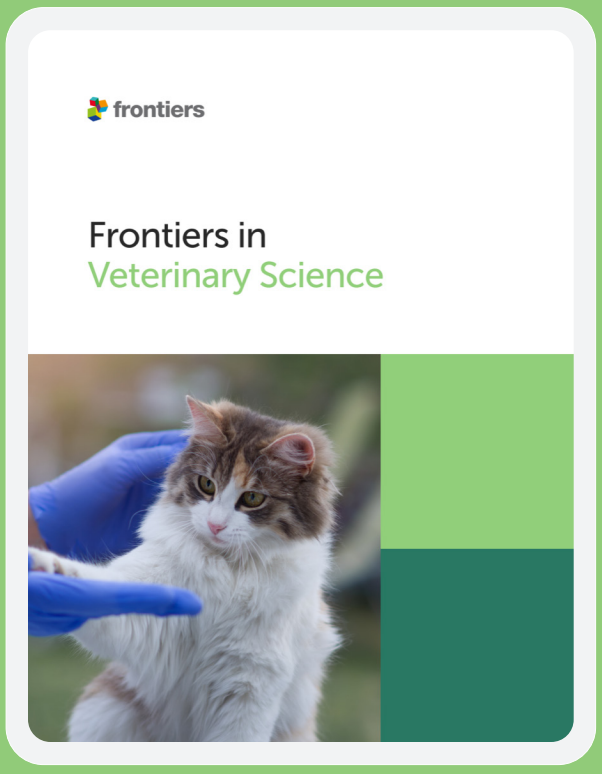

Frontiers

Avenue du Tribunal-Fédéral 34
1005 Lausanne, Switzerland
frontiersin.org

Contact us

+41 (0)21 510 17 00
frontiersin.org/about/contact